TM-86567

Research and Technology

Fiscal Year 1986 Annual Report

Marshall Space Flight Center

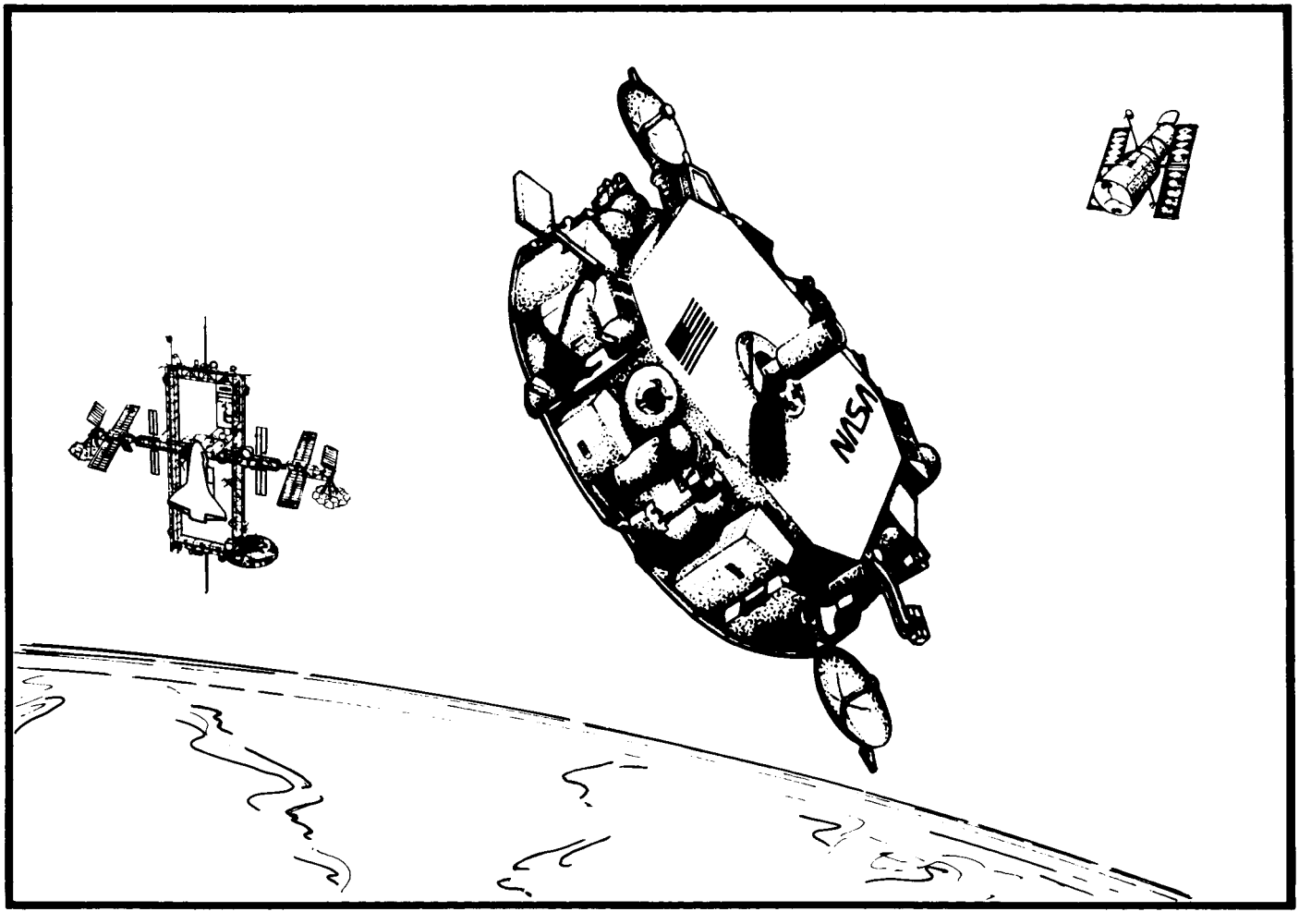

November 1986

(NASA-TM-86567) RESEARCH AND TECHNOLOGY, FISCAL YEAR 1986, MARSHALL SPACE FLIGHT CENTER Annual Report (NASA) 138 p CSCL 05A

N87-15034

Unclas
G3/88 43744

NASA

This artist's concept shows the Orbital Maneuvering Vehicle on its way from the U.S. Space Station to the Hubble Space Telescope for orbital maintenance.

INTRODUCTION

The Marshall Space Flight Center is continuing its vigorous efforts in space-related research and technology. Extensive activities in Advanced Studies have led to the approval of the Orbital Maneuvering Vehicle as a new start. Significant progress has been made in definition studies of new liquid rocket engine systems for future space transportation needs and the conceptualization of advanced launch vehicles. Our space systems definition studies have brought the Advanced X-Ray Astrophysics Facility and Gravity Probe-B to a high degree of maturity. Both are ready for project implementation.

MSFC's research effort continues in many directions relevant to the Center's assigned projects and advanced studies. As evidenced by this report, significant results have been obtained in low gravity sciences, solar terrestrial physics, high energy astrophysics, and atmospheric sciences.

Progress in MSFC technology programs has centered on propulsion systems, and on critical elements of the Space Shuttle Main Engine in particular. A variety of activities in the materials and processes area have worked toward the goals of improving the productivity of high-cost repetitive operations on reusable transportation systems, and extending the useful life of such systems. Increased emphasis was also placed on the structural dynamics and control dynamics of large space structures.

As Marshall enters its 27th year of space vehicle development, the research and technology highlighted in this report provides a foundation for progress on the Hubble Space Telescope, the Space Station, all elements of the Space Transportation System, and on the many other projects assigned to this Center.

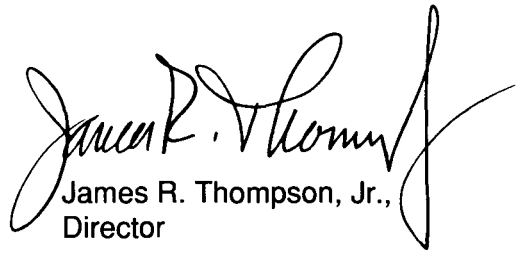

James R. Thompson, Jr.,
Director

PREFACE

The point of contact at Marshall Space Flight Center for this report is F. A. Speer, DS01 (544-3033), who provided overall supervision. He was assisted by an editorial committee consisting of W. Littles, S. Morgan, and T. Moorehead. Detailed editorial support was supplied by A. Howard and G. Campbell, with production assistance from W. Smith and J. Robinson. To assist the reader, the MSFC contact, office code, telephone number, and sponsoring agency are included at the end of each article. An alphabetical index of all authors is presented on page 127 of this report. The work at MSFC is a cooperative effort, but because of space restrictions, it is impossible to list all those involved in the projects described in this report.

TABLE OF CONTENTS

Advanced Studies

From its beginning NASA has looked to the future. Advanced studies are the building blocks that provide a pathway from the present and form the framework upon which the Nation's future in space is built.

With the realization of the Space Station on the horizon, MSFC is analyzing a wide range of activities to exploit both the enhanced capabilities and the potential for permanent human occupancy of space offered by this next major milestone of space flight. Current studies include space operations and advanced space transportation systems to meet the Nation's future needs and ensure the expansion of space exploration; science and application programs that will continue to utilize the unique space environment for the benefit of mankind and to extend our understanding of the Universe; and further development of the commercial use of space that will lead to new industries on Earth as well as in space.

Cost-effective space transportation systems with improved capabilities will provide the key to realizing the rewards of developing and exploring the vast frontier of space in the latter part of this century. New generation propulsion systems, launch vehicles, and inter-orbit vehicles are being studied to meet this challenge. Beyond low Earth orbit, increased activity in the valuable geosynchronous orbit realm and manned exploration of Mars are being analyzed.

Transportation Systems

Orbital Maneuvering Vehicle

With the advent of the Space Shuttle it is now possible to efficiently deliver a spacecraft to and from low Earth orbit. This payload performance can be further enhanced by using an Orbital Maneuvering Vehicle (OMV) which has been studied for several years. This activity originated with the Teleoperator Retrieval System, which was designed to reboost/deboost the Skylab, and has continued in an effort to optimize the OMV to accommodate a wide range of mission applications. The OMV will operate in orbits higher than the Shuttle or Space Station orbit and may also be used in geosynchronous orbit when delivered by high energy upper stages such as the Transfer Orbit Stage, Centaur, and Orbital Transfer Vehicles. Definition (Phase B) contracts were awarded to LTV, Martin Marietta, and TRW in August 1984, and the work was completed at the end of August 1985. An RFP for Phases C and D was issued November 1985 and proposals received in late December 1985. It is expected that a contract will be awarded to TRW in September, 1986.

The earlier conceptual and definition studies defined a highly efficient vehicle which can be used for a wide range of services. Figure 1 is a representative OMV configuration, and depicts the use of the vehicle to support the delivery, retrieval, reboost, viewing, and servicing of free-flying satellites. Advanced OMV missions visualized include on-orbit refueling functions, by addition of tanker kits; remote servicing using manipulator systems; and retrieval of spacecraft or collection of debris, accomplished with specialized docking systems and/or end effectors. The OMV will also be available for assembly and buildup of the initial Space Station, and will later augment the facility.

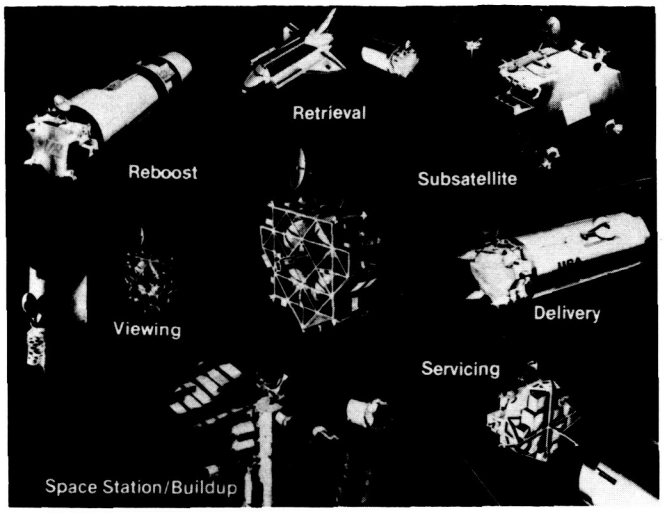

Figure 1. OMV Operational Missions.

Several configuration approaches are being defined, but the vehicle can generally be described as a relatively thin wafer, approximately 3 to 5 ft thick, and approximately 15 ft in diameter. This design allows it to be directly mounted to the Shuttle longerons and keel without the use of a cradle, thereby minimizing the need for airborne support equipment and maximizing the Shuttle payload manifesting flexibility.

The Shuttle-transported OMV will be based at the Space Station. Shuttle-supported operations will be utilized for high inclination orbits not accessible from the Space Station. The OMV Operations Control Center will be located on the ground; however, the OMV will be controlled from the Space Station when operating in its vicinity.

The OMV is being supported by concentrated MSFC development activities in the rendezvous and docking simulation areas, including the design, testing, and evaluation of various docking interfaces and docking/rendezvous aids. Primary areas of design deal with the remote rendezvous and docking sensors and aids needed by the pilot to ensure final approach and docking of the OMV to both stable and slowly rotating targets. In this category, the need for range and range rate radar is being investigated, in addition to television and lighting type and quality. Communication time delays and operator tolerance/capability are being studied and evaluated by having pilots fly high-fidelity demonstrations on both the OMV Robotic Flat Floor Facility (which has 6 degrees-of-freedom capability) and the Target Motion Simulator. Simulations are also being accomplished utilizing alternative docking interfaces. Primary efforts have been focused on the possibility of adapting the Remote Manipulator System end effector as the OMV docking interface.

Another area of concentration involves the requirements for a three-point docking system to interface with payloads equipped with three hard points, such as the Flight Support System currently being utilized by the Multi-Mission Spacecraft, the Hubble Space Telescope, and other large observatory spacecraft. MSFC activities are being closely integrated with the contractor simulations. These simulation activities, other supporting development work, and contracted definition studies have provided a sound foundation of knowledge on which to base the OMV development program. The OMV program will continue to rely on simulation support capabilities as the project moves into the development phase.

W. G. Huber/PF14
(205) 544-0550
Sponsor: Office of Manned Space Flight

Aeroassist Flight Experiment

The Aeroassist Flight Experiment (AFE) will simulate the atmospheric flight phase of an Aeroassisted Orbital Transfer Vehicle returning from geosynchronous orbit. The AFE (Fig. 2) will be composed of a carrier vehicle and the aerobraking system. The carrier vehicle will serve as the basic structure of the spacecraft and will house the avionics and propulsion system and provide integration support for the aerobraking system. The aerobraking subsystem will consist of the aerobrake structure, with instruments designed to measure the environmental parameters necessary for technological development. The first AFE flight is planned for 1992. The AFE, deployed from the Shuttle, will skim through the upper levels of the atmosphere and return to a preset orbit for Shuttle Orbiter retrieval.

The flight experiment will provide data concerning predicted nonequilibrium radiation and real gas aerodynamics which are unobtainable through ground tests or analyses. Environmental and vehicle design technology will also benefit from the experiment. Environmental technology includes nonequilibrium convective heating, wall

catalysis, and aerodynamics, while vehicle design technology involves enhanced flight performance, thermal protection system materials, avionics, guidance algorithms, and deployable devices. These technological designs are strongly influenced by atmospheric variations in the upper atmosphere.

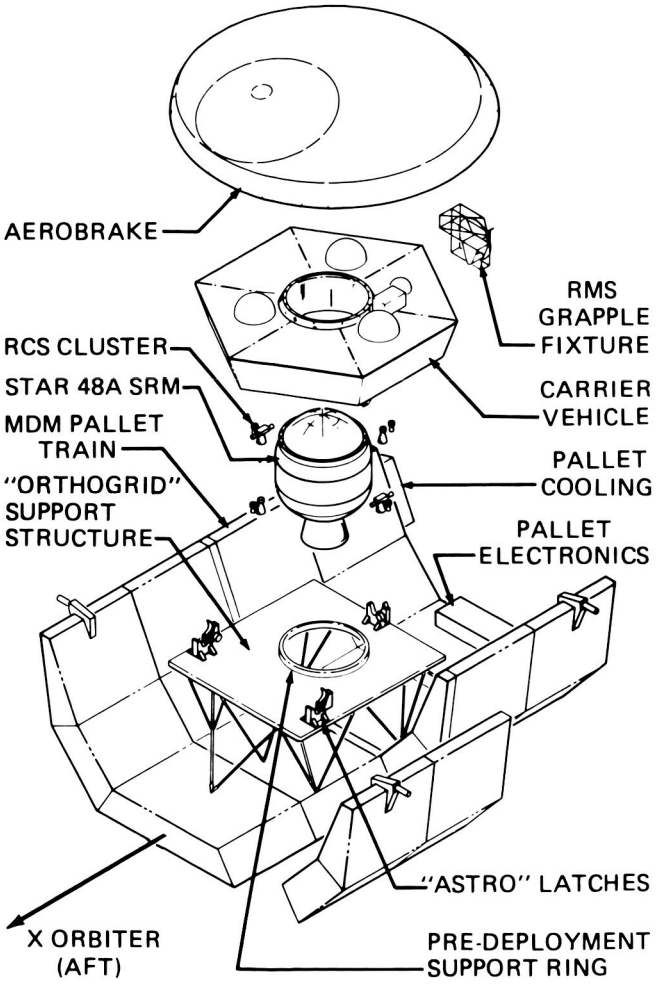

Figure 2. Aeroassist Flight Experiment.

In 1985/1986, the advanced development/definition activities accomplished substantial progress, with continued participation by MSFC and the Johnson, Langley, and Ames Centers. A Project Initiation Agreement developed in 1985 and early 1986 between these Centers and their Headquarters Program Offices has been finalized. The AFE Task Team was established at MSFC, the lead Center, in March 1986. Another major milestone, the AFE Definition Review, was conducted in May 1986. Future major milestones include the AFE New Start Review, establishment of the AFE Project Office at MSFC, and the initiation of AFE development as a new start program for FY88.

R. E. Austin/PF21
(205) 544-0633
Sponsors: Office of Space Flight
Office of Aeronautics and Technology

Orbital Transfer Vehicle

Transportation requirements have been identified from the analysis of NASA's long range planning in science, application, and technology, as well as from forecasts of future commercial activities in space. Analyses of these various sources resulted in the definition of a transportation system known as the Orbital Transfer Vehicle (OTV).

A broad spectrum of OTV concepts (Fig. 3) is being studied to determine the best method of meeting future mission requirements. These studies, conducted by three contractors (Boeing Aerospace, Martin Marietta, and General Dynamics Space Systems Division), are scheduled to be completed in mid-1987. Candidate OTV concepts have been developed and evaluated against a new mission model developed for the Space Transportation Architecture Studies. This new mission model provided significant changes in the system requirements for the OTV and in proposed flight rates. Candidate OTV concepts which are compatible with proposed new unmanned cargo launch vehicles have been defined and evaluated. During FY86 additional effort has been expended on refining the major trade studies previously initiated (particularly the basing trade and the aeroassist device comparison), and

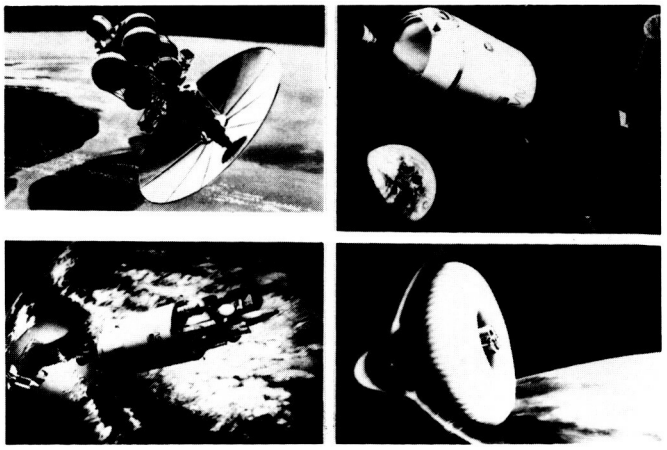

Figure 3. Orbital Transfer Vehicle Concepts.

on conducting sensitivity studies to determine the impact of major cost assumptions. The results of these studies will be combined with earlier studies and in-house NASA investigations to identify promising concepts or approaches, document alternative trade-offs, and determine areas requiring technological advancement.

D. R. Saxton/PF20
(205) 544-5035
Sponsor: Office of Space Flight

Advanced Launch Vehicles

Launch vehicles under consideration for the post-1995 time period are unmanned and manned vehicles, as well as expendable and fully reusable ones. The goal of MSFC is to determine the vehicle mix and appropriate options which meet the required missions, with the lowest life cycle costs.

In FY86, various missions being considered include commercial uses and emerging requirements from the Strategic Defense Initiative and the National Commission on Space. Each of the various missions being considered has a larger launch weight than current levels. Annual launch weights of the spacecraft, payloads, flight crews, and servicing materials to be orbited range from approximately 1.25 million pounds to 5 million pounds.

This year, vehicles which could potentially meet both the mission requirements and cost goals have been compared (Fig. 4). They are a partially reusable, unmanned Shuttle Derived Vehicle (SDV); a partially reusable, unmanned flyback booster vehicle; and a fully reusable, manned vehicle. The SDV and flyback booster would be available first, followed by the reusable manned vehicle. Payload capabilities will vary with the vehicle; the SDV may deliver from 80 to 160 thousand pounds, the flyback booster could deliver as much as 150 thousand pounds of cargo, and the fully reusable manned vehicle would be capable of delivering personnel and/or 5 to 80 thousand pounds of cargo to orbit.

Components of the SDV which were initially developed for the Shuttle Program are the solid rocket boosters, the core stage, and the liquid oxygen/liquid hydrogen (LOX/LH_2) main propulsion engines. This vehicle is partially reusable due to recovery and refurbishment of the solid rocket boosters and recovery of a module consisting of the core stage propulsion and the avionics. The flyback booster vehicle features a winged, fully reusable booster with advanced liquid oxygen/hydrocarbon engines. This booster could potentially be the same as that of the fully reusable vehicle. The second stage of the flyback booster would have advanced LOX/LH_2 engines which would be recovered in a module along with the avionics. Thus only the propellant tank and payload shroud would be expended on this vehicle. The fully reusable, manned vehicle would have LOX/LH_2 second stage propulsion and winged vehicle reentry. The payload shroud would be a new item for all three vehicles.

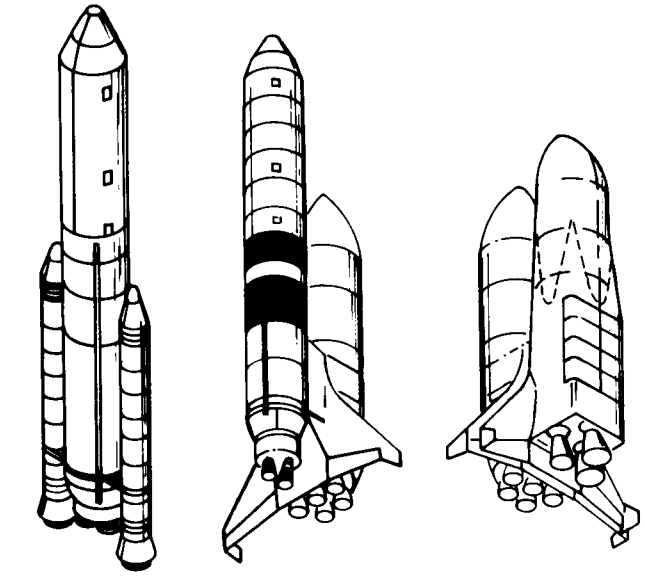

Figure 4. Potential Advanced Launch Vehicles.

Each vehicle is to be designed with major reductions in operating costs, achieved through technical improvements in avionics, data management, structures, propulsion, and aerothermodynamics. These improvements will lower vehicle mass, improve performance, increase onboard autonomy, reduce launch operations and turnaround time, and decrease ground control mission operations needs.

L. T. Spears/PF20
(205) 544-0464
Sponsor: Office of Space Flight

Space Transportation Main Engine

The Space Transportation Main Engine (STME) (Fig. 5) will provide Earth-to-orbit propulsion for the next generation launch vehicles. This high performance liquid rocket engine system will use liquid hydrogen (LH_2) fuel and liquid oxygen (LOX).

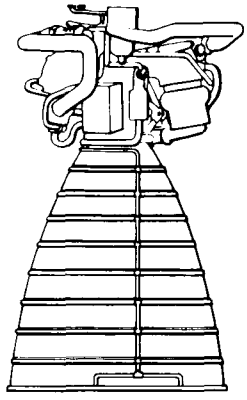

Figure 5. Space Transportation Main Engine.

The primary vehicle application for the STME will be the fully reusable cargo vehicle being defined by the Transportation Architecture Studies. This vehicle uses a flyback booster employing the Space Transportation Booster Engine and a core stage employing the STME. Since one of the key goals of these studies is to provide major reductions in the cost of transporting payloads to low Earth orbit, the STME will be designed for long life operation with very low maintenance. Also, vehicle safety, economics, and the high cost of some of these payloads dictate the need for engine-out capability. The STME will be designed for throttling up from its normal operating power level to an emergency power level to accommodate engine-out.

The STME studies are defining an engine system that will be simpler to manufacture, cheaper to operate, and more flexible than today's engines. Preliminary design requirements for the STME are:

- Maximum rated thrust = 580,000 lb
- Normal power level = TBD
- Design mission life = 100 missions
- Closed loop thrust/mixture ratio control

The STME will be used in a clustered configuration in the second stage of the cargo vehicle, as well as in various Shuttle II configurations. Each of these vehicle designs employs a Propulsion/Avionics (P/A) module to recover the main engines and expensive avionics. The STME design approach is to provide an engine that will operate from lift-off through orbit insertion, re-enter and land via the P/A module, and, with a minimum of maintenance and flight preparation, be ready for another flight. Operating characteristics of the STME are given in Table 1.

Table 1. STME Operating Characteristics.

• HIGH PERFORMANCE LOX/LH_2 ENGINE
• GAS GENERATOR OR STAGED COMBUSTION CYCLE
• HIGH EXPANSION RATIO, EXTENDABLE NOZZLE
• PRIMARY FOCUS IS HIGH RELIABILITY AT LOW OPERATING COST
• REQUIREMENTS TO BE BASED ON STAS VEHICLE NEEDS
• OPERATIONAL CAPABILITY BY LATE 1990's

J. E. Hughes/PS03
(205) 544-0455
Sponsor: Office of Space Flight

Space Transportation Booster Engine

The Space Transportation Booster Engine (STBE) will provide main boost propulsion for the Nation's next generation of launch vehicles (Fig. 6). This high performance liquid rocket engine system will use liquid oxygen (LOX) and a

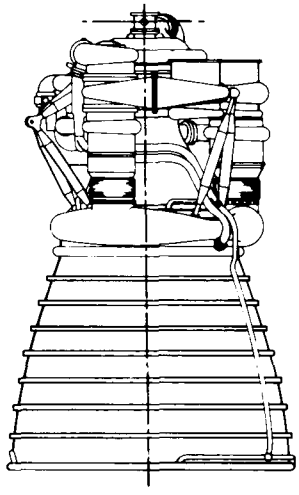

Figure 6. Space Transportation Booster Engine.

hydrocarbon fuel. Fuels under consideration are RP-1, methane (CH_4), and propane (C_3H_8). Cooling of the engine thrust chamber will be accomplished with either the fuel or with liquid hydrogen, which is subsequently burned in the main combustion chamber. The three different fuel options, each with a hydrogen cooling option, result in six different engine design approaches being studied by each of three study contractors. These studies have developed methodical evaluation plans which consider the relative importance of weight, envelope, performance, etc., on the life cycle cost of the system. These evaluation criteria will result in the selection of a single configuration to be carried into preliminary design.

The primary vehicle application for the STBE will be the fully reusable flyback booster being defined by the Space Transportation Architecture Studies. Since one of the key goals of these studies is to provide major reductions in the cost of transporting payloads to low Earth orbit, the STBE will be designed for long life operation with very low maintenance. In addition, vehicle safety, economics, and the high cost of some of these payloads will dictate the need for engine-out capability. The STBE, therefore, will include the capability to throttle up 20 percent above its normal operating point to provide engine-out from liftoff. Preliminary design requirements for the STBE are:

- Maximum rated thrust = 750,000 lb
- Normal power level = 625,000 lb
- Design mission life = 100 flights
- Thrust vector control: vehicle actuators, ±6° square
- Closed loop thrust/mixture ratio control

Table 2. STBE Operating Characteristics (LOX Oxidizer, 750-Klb Thrust).

DESIGN OPTIONS: • FUEL	RP-1		CH_4		C_3H_8	
• MCC COOLANT	RP-1	LH_2	CH_4	LH_2	C_3H_8	LH_2
OPERATING CHARACTERISTICS:						
• THRUST (SL), klbf	757	762	767	762	768	762
• THRUST (VAC), klbf	891	864	869	863	872	866
• AREA RATIO	25.7	48.2	48.2	48.2	49.0	49.0
• DEL SL I_{sp}, s	279.9	308.1	314.2	323.0	304.7	316.3
• ENGINE FLOW, lb/s	2705	2474	2441	2359	2521	2410
• ENGINE WEIGHT, lb	8150	7400	8200	8000	7700	7350

The STBE will operate at much higher combustion chamber pressures than any previous hydrocarbon-fueled engine. This higher pressure will provide significant performance improvement over earlier engines, as well as a much improved envelope, reduced vehicle base area, and benefit flyback characteristics. The operating characteristics of the STBE are given in Table 2.

J. E. Hughes/PS03
(205) 544-0455
Sponsor: Office of Space Flight

Advanced Recovery Systems

The development of advanced recovery systems for high-cost launch vehicle components is critical to a low-cost space transportation system. The ability to recover at selected sites, to refurbish rapidly, and to reuse certain vehicle components is needed to provide an efficient operating system with minimal overall program cost. Prior studies, as well as experience with the Space Shuttle Solid Rocket Boosters (SRBs), have shown the economic benefits of recovery and reuse of launch vehicle hardware. Materials and fabrication technologies have advanced since the selection of the SRB recovery method, necessitating further investigation of recovery concepts.

During FY86, MSFC studied two advanced recovery systems (Fig. 7). These studies, which will lead to a later demonstration program, will identify advanced recovery concepts, select the most promising one, and demonstrate in a scaled test program that the concept will perform as expected. Recovery systems identified must ensure minimal damage to the recovered components,

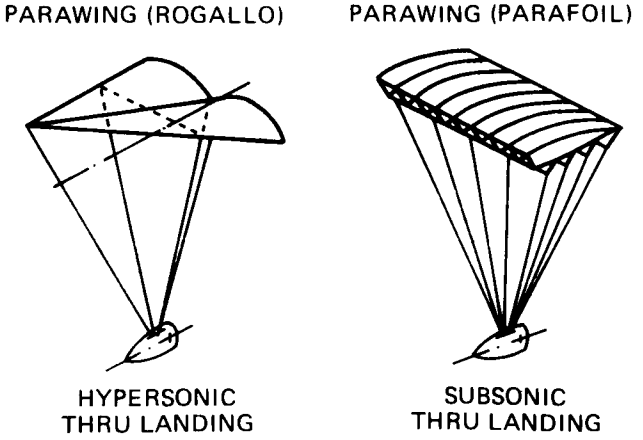

Figure 7. Advanced Recovery Systems - Basic Concepts.

and provide controls for precision landings either on land or in fresh water, with emphasis on land recovery. This approach should simplify the recovery process, minimize the requirements for complex cross country transportation, and avoid the effects of saltwater corrosion. Further beneficial effects of controlled recovery may be a shorter refurbishment cycle requiring a smaller reusable component inventory with fewer operations personnel, and therefore lower cost. A previous feasibility study identified some basic concepts which will be used as a starting point.

Recovery methods may vary, depending on the component to be recovered. Core stages and upper stage Propulsion/Avionics (P/A) modules attain orbit, and with controlled deorbit, can have soft touchdown on land. Booster stages and booster P/A modules are dropped during the ascent phase and therefore may require water landing or mid-air retrieval and tow by aircraft. These studies concentrate on launch vehicle components that attain orbit and therefore can have controlled landings at desired locations, such as the launch or refurbishment sites, but do not preclude fresh water landing.

This activity is an approximate 3-year total effort in two phases. The first phase will determine the feasibility and advanced development/technology requirements needed to improve recovery of large heavy-weight launch vehicle elements from Earth orbit and/or boost phase, while a second phase will plan and perform a scale model demonstration test.

G. W. Johnson/PF20
(205) 544-0636
Sponsor: Office of Space Flight

Propellant Scavenging

Requirements for consumables for extended space operations will be a major part of future scenarios using the Space Station and the reusable Orbital Transfer Vehicle (OTV). The OTV will be based at the Space Station and will require large quantities of cryogenic propellant on-orbit. The Orbital Maneuvering Vehicle (OMV) will also require on-orbit storable propellants. One method of supplying these cryogenic propellants to the space-based vehicles at a relatively low cost is by scavenging the residual and performance reserves from the Space Transportation System External Tank (ET) and propellant lines after the Shuttle flight requirements have been met, and scavenging residual storable propellants from the Orbiter Maneuvering System (OMS). Another method is to use "opportunity manifesting" of propellants as cargo on the unmanned cargo launch vehicle, taking advantage of excess payload-carrying volume and weight capabilities.

The feasibility of two scavenging concepts has been studied and an estimation of the amount of cryogenic and storable propellants that can be scavenged over a 10-year period (1993 to 2002) has been made, based on the current mission model. The two scavenging concepts are different in that one collects and stores the residual cryogenic propellant in tanks located in the Shuttle Aft Cargo Carrier (ACC), while the other concept collects residual cryogenic propellant in tanks located in the Orbiter's cargo bay. Each concept uses the OMV to transfer the tanks from low Earth orbit to the Space Station orbit. The storable propellants are scavenged into tanks located in the cargo bay. Tank sizes and configurations have been established and interface requirements for the tank to the Orbiter, OMV, etc., have been investigated.

The 1985/86 scavenging study identified a potential of 1.96 million pounds of cryogenic propellant in the 1993 to 2002 time frame for the ACC concept, and 1.5 million pounds of cryogenic propellant for the cargo bay concept. Approximately 1.0 million pounds of OMS storable propellants can be scavenged during the 1993 to 2002 time frame.

MSFC is sponsoring the ACC scavenging concept and JSC is sponsoring the cargo bay concept for cryogenic propellant scavenging and storable propellant scavenging. Both concepts are designed for system return to Earth for reuse via the Shuttle cargo bay. Conceptual interface concepts were developed in the 1985/1986 study efforts and basic test/development requirements were investigated. The study efforts to date have indicated that substantial propellants, both cryogenics and storables, can be made available for on-orbit application and use at a relatively low cost.

Technology required to initiate a scavenging system is primarily that of transferring propellants in

a zero-gravity environment from the ET into the transfer tanks and from the transfer tanks into the orbital holding/storage tanks in the Space Station vicinity. Another technology area that needs developing will be the measuring of the amount of cryogenic propellant in a tank in a weightless environment. Demonstrations will be required to test the concepts and systems to verify these technologies.

M. A. Page/PF20
(205) 544-0638
Sponsor: Office of Space Flight

Space Systems

Advanced X-Ray Astrophysics Facility

The Advanced X-Ray Astrophysics Facility (AXAF) is a free-flying observatory carrying a precision x-ray telescope for obtaining high resolution images and spectrographic data from x-ray emitting objects in space. The AXAF will be 50 to 100 times as sensitive as its predecessor, the High Energy Astronomy Observatory-2 (Einstein), due to the x-ray optical system which has twice the diameter and eight times the resolution, and also due the greater sensitivity of the science instrumentation selected for the AXAF mission. The AXAF program is managed by MSFC, with technical and planning support for x-ray systems from the Smithsonian Astrophysical Observatory. Figures 8 and 9 illustrate the concepts being studied by the two Phase B contractors, TRW and Lockheed Missiles and Space Company (LMSC).

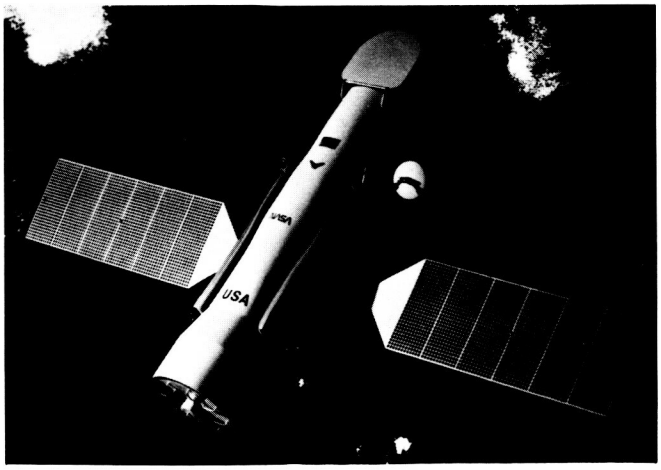

Figure 8. TRW Concept of the AXAF.

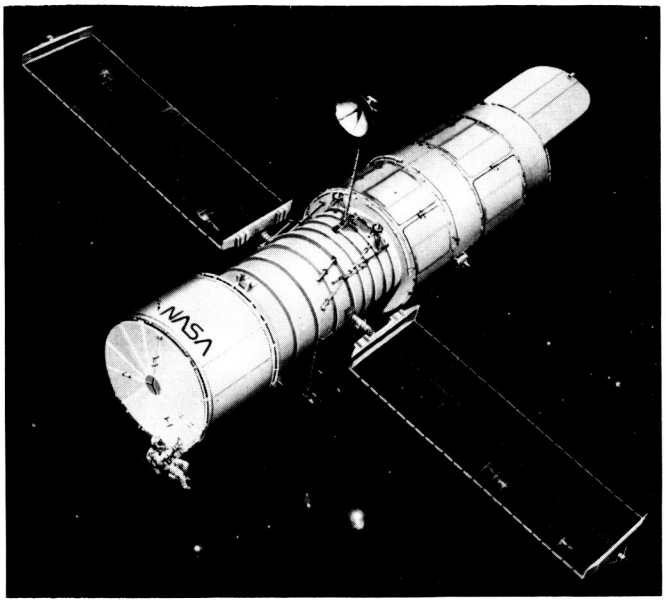

Figure 9. LMSC Concept of the AXAF.

During FY86, the AXAF program completed the second full year of the definition studies with TRW and LMSC, with their contracts extended to January 1987. The extension will permit the contractor teams to study in greater depth program issues such as interactions with the Space Station and OMV, and to perform additional analyses on the High Resolution Mirror Assembly (HRMA) and other critical observatory systems.

Programs for the science instruments (SI) are also in place and producing preliminary design information required for the overall observatory program. If the FY88 new start for AXAF is approved, the SI programs will culminate in the selection of three of the four focal plane investigations for development during the next fiscal year. Significant progress has been made in the high technology areas of the SI. The AXAF Charge Coupled Device (CCD) Imaging Spectrometer (ACIS) has experienced major simplification during FY86 as electronic techniques have been identified which permit elimination of costly mechanisms. Also, the continuing maturity of CCD technology has offered the potential of operation at much warmer temperatures than originally proposed (-30 °C to -50 °C as opposed to -70 °C). This latter development may permit significant simplification of the cooling system required for the ACIS. The other high technology instrument on the AXAF, the X-Ray Spectrometer (XRS), has seen a steady improvement in spectral resolution toward the goal of 10 electron volts (eV). Values of 33 eV are now

obtained, and modifications being implemented should further improve this value. If the 10-eV goal can be achieved in the full system, the XRS will represent a major step forward in x-ray instrumentation for space research.

Another key activity during FY86 was the successful completion of x-ray testing of the Technology Mirror Assembly (TMA) at MSFC, and the completion of data analysis. The test data showed that the TMA met or exceeded most of the performance goals established for the program, including the goal of 0.5 arc-second resolution. A goal which was not met, namely, the percentage of x-ray energy contained in a circle with a diameter of 1 arc-second at the shorter wavelengths, led to the conclusion that a low-level ripple in the mirror surface was responsible. This ripple was not detected by instrumentation in place during the polishing phase, and has led to a new program to ensure that such metrology is available in future flight fabrication activities, and to demonstrate that straightforward modifications to the TMA polishing tools will remove the ripple.

In support of definition studies performed by TRW and LSMC, several companion studies pertaining to the x-ray telescope were completed by the Smithsonian Astrophysical Observatory. Specifically, these special studies included the graphite-epoxy optical bench, the aspect camera system, and the HRMA. These systems are critical to the successful development of the AXAF. Independent studies of this kind provide a sound basis for assessing contractor effort in the corresponding systems areas and for ensuring that the requirements are met in the most cost-effective way.

D. C. Cramblit/PF19
(205) 544-0569
Sponsor: Office of Space Science and Applications

Gravity Probe-B

In March 1985, MSFC signed a contract with Stanford University for the first 24 months of engineering development of Gravity Probe-B (GP-B). The engineering development will consist of two distinct but complementary efforts. One effort concentrates on building a Shuttle Test Unit for flight on the Shuttle, while the other effort provides a similar unit for additional tests on the ground. The Shuttle Test Unit will consist of a full-scale flight dewar and an instrument with support electronics. The instrument, consisting of four gyroscopes mounted in a quartz block enclosed in a probe assembly, slides into the dewar (Fig. 10). Although the telescope will not be functional on the Shuttle flight, its inclusion is currently under consideration. Extensive operational and performance checks will be made on the gyroscopes as they fly on an approximate 7-day Shuttle mission.

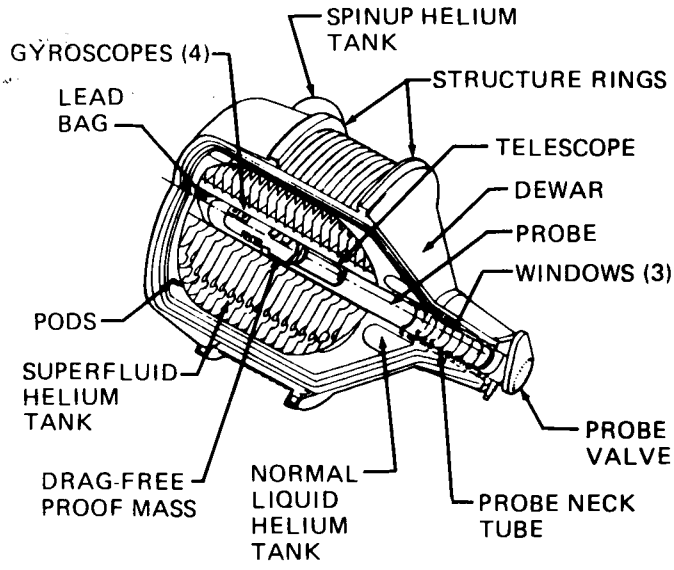

Figure 10. GP-B Experiment Module.

Certain portions of the GP-B instrument, in particular the reference telescope and fine pointing system, cannot be fully evaluated with the Shuttle Test Unit. For this and other reasons, a separate Ground Test Unit with a probe assembly essentially identical to that of the Shuttle Test Unit will be developed and tested on Earth in an inexpensive laboratory dewar. In addition, the Ground Test Unit will incorporate the telescope and fine pointing system. The design, building, and testing of these two units, coupled with analytical activities, should provide the experience, knowledge, and insight necessary to ensure a successful science mission that can be accomplished with reduced risks.

Technical development of various components has advanced significantly, and includes improved methods of lead bag expansion, rotor suspension system design and implementation, and gyro read-out ring development. During FY86, the tooling and jigs for expanding an 8-in. diameter lead bag were designed, built, and used successfully. One of these expansions resulted in

the largest reduction in magnetic field strength ever achieved in a single expansion. After multiple expansions, a field strength of 9×10^{-8} G was achieved inside the lead bag. The current thrust of lead bag technology is toward developing stiffening methods to ensure that the lead bag will remain securely in place during launch.

The rotor suspension system has been redesigned, built, and successfully tested. The system now operates at 2 kHz rather that 20 kHz, thus reducing induced rotor heating. In addition, a breakdown detection capability has been built into the system to prevent rotor damage in the event of a breakdown (i.e., arcing).

Technology that is being investigated for creating readout rings on the gyro housings includes laser milling. Niobium-coated flat quartz plates have been laser milled, and a scanning electron microscope has been used to study the trace profile. The impact of the milling on the superconducting properties of the remaining niobium has also been investigated. This technique has the potential of being able to create multiple loops which would greatly increase the signal-to-noise ratio from the superconducting quantum interference devices (SQUIDs). Various photolithographic techniques are also being investigated for their potential use for readout ring deposition.

Although technical development on various components will continue, the major thrust of the GP-B program in FY87 will be toward the integration of the various components into a functional system to meet an important milestone called the First Integrated System Test (FIST). The successful completion of FIST will be the last major technical hurdle prior to initiation of a flight program.

A. K. Neighbors/PF16
(205) 544-0565
Sponsor: Office of Space Science and Applications

Pinhole Occulter Facility

The Pinhole Occulter Facility (POF) is an observatory for solar coronal and hard x-ray studies. It will eventually be flown on the Space Station as part of the Advanced Solar Observatory, but will have at least one flight as a Spacelab experiment during the development process. A long (32 m) deployable boom is used to position an occulting mask to allow superior resolution of the coronal structure. The mask also contains a series of apertures which are used to form high resolution images of hard x-ray features on the solar disk. The same high-energy imaging concept will work equally well for studying celestial objects in spectral ranges never before possible.

The POF consists of the deployable boom, the occulting mask, and the base plane which contains the complement of imaging systems and coronal telescopes. The facility is mounted on the Instrument Pointing System, which points and stabilizes it (Fig. 11).

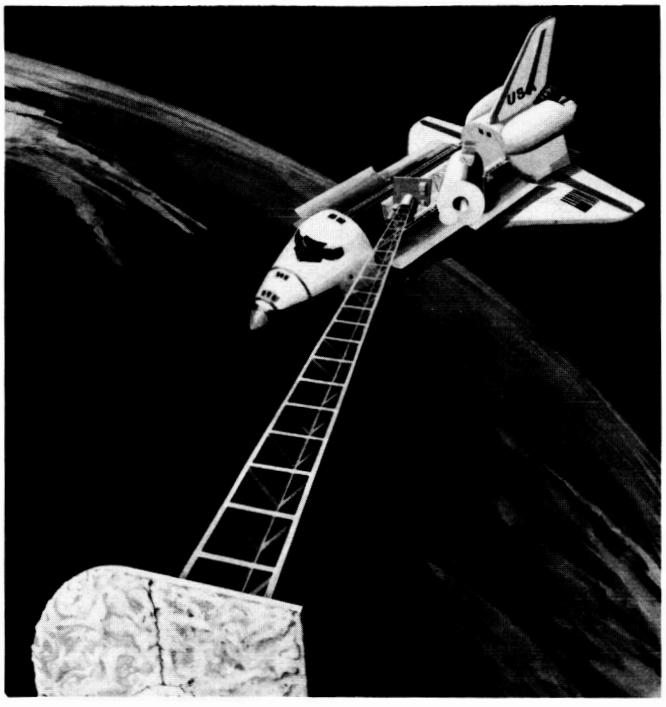

Figure 11. Pinhole Occulter Facility on the Shuttle.

Feasibility of concept has been accomplished by an internal MSFC study, and a science workshop was held, documented, and the findings distributed in the spring of 1986. Ongoing engineering efforts are directed toward development of science instrumentation concepts and preliminary designs. Concept verification and eventual breadboarding of the optical aspect and alignment system are also planned. In addition, studies are under way to identify Space Station integration requirements.

J. R. Dabbs/PS02
(205) 544-0623
Sponsor: Office of Space Science and Applications

Advanced Solar Observatory

To understand the physics of our nearest star, the Sun, we must begin by unraveling the basic enigmas of solar dynamics. These may be outlined by six fundamental scientific objectives to be addressed by the Advanced Solar Observatory (ASO):

- Magnetohydrodynamic structure and the behavior of the solar convection zone
- Solar activity cycle
- Structure and dynamic behavior of the solar photosphere, chromosphere, and corona
- Basic plasma processes
- Structure and dynamics of the solar corona and solar wind
- Three-dimensional structure of the heliosphere

These objectives may be addressed by the ASO comprehensive instrument complement which includes a Solar High Resolution Telescope Cluster, the Pinhole Occulter Facility, a Solar High Energy Cluster, and a Solar Low Frequency Radio Facility (Fig. 12).

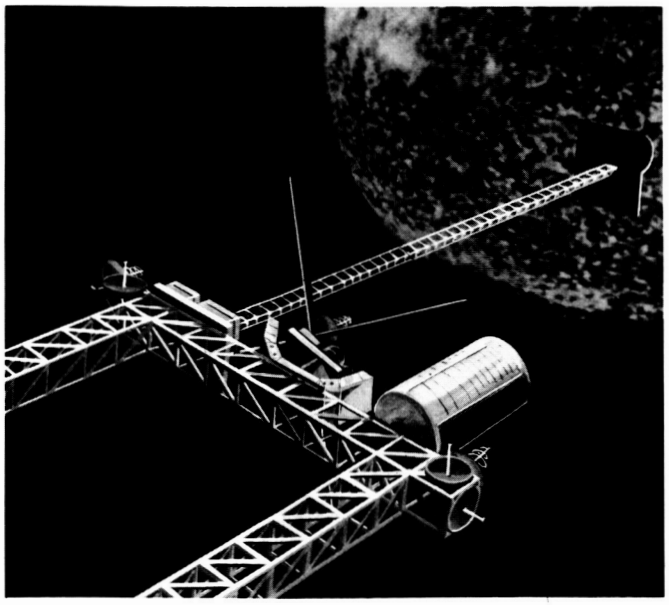

Figure 12. Advanced Solar Observatory on the Space Station.

A Science Study Group Report was published in early 1986. Technology issues which are to be addressed include the development of fine pointing systems to accommodate the High Resolution Telescope Cluster and the Pinhole Occulter Facility on the Space Station. These pointing systems must be capable of accommodating large instruments and providing arc-second accuracy. Data from the combination of ASO instruments could easily reach 50 Mb/s, and the handling, transmission, and display of this data is of particular importance. Finally, the dissipation of several kilowatts of thermal energy from instruments on a pointing system must be studied and resolved.

Walker, A. B. C.; Moore, R.; and Roberts, W. T.: The Advanced Solar Observatory. NASA/MSFC, January 1986.

W. T. Roberts/PS02
(205) 544-0621
Sponsors: Office of Space Science and Applications
Office of Space Station

Solar Terrestrial Observatory

The Solar Terrestrial Observatory (STO) is a combination of scientific instruments which provides information about the physical processes of solar terrestrial space. At this time the role of these processes in the variability of the solar terrestrial system is poorly understood. Although we have superficial knowledge of many relationships between the Sun, interplanetary space, and the Earth's magnetosphere and atmosphere, we have an incomplete understanding of the actual physical and chemical processes that underlie these relationships. This lack of understanding precludes a reliable predictive capability. The STO will be able to make unique measurements that will contribute to a better understanding of many of these processes.

The STO will be a major payload for the Space Station (Fig. 13), and initially will use instruments originally built for and flown on Shuttle/Spacelab

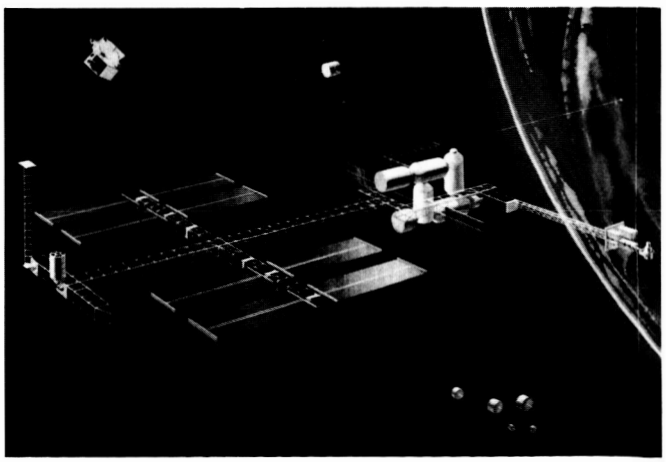

Figure 13. Solar Terrestrial Observatory on the Space Station.

missions. These Shuttle/Spacelab missions will be used to establish basic instrument and experiment techniques and capabilities.

A workshop on the STO was held in June of this year to review studies on the initial STO Space Station and to define the requirements for an evolutionary STO program, using the existing inventory of Spacelab experiments. The output of this study will be used to define the requirements for an initial STO.

Technological issues to be addressed include the evolution of energy storage systems (or direct electrical power from the Space Station) to provide high power (~60 kW) for the periodic operation of active instruments; the effects of contamination on instruments; the dynamic effects of the deployed tether; and the orientation requirements of active experiments. As the initial STO will consist mainly of instruments originally developed for Shuttle/Spacelab missions, the primary requirement is to develop a technological bridge across which the transition to the Space Station can move.

Solar Terrestrial Observatory Space Station Workshop Report. NASA CP-2411, 1986.

W. T. Roberts/PS02
(205) 544-0621
Sponsors: Office of Space Science and Aeronautics
Office of Space Station

Superconducting Gravity Gradiometer

Measurements and observations from space have stimulated a revolution in geophysics. Within NASA, both the Geopotential Research Program (GRP) and the Solar System Exploration Program have generated interest in gravity field measurements. One of the areas of investigation within the GRP is that of solid-Earth and ocean dynamics. This investigation includes analysis of existing data to produce models of fields, scientific interpretations of the models, and the development of instruments and missions that collect better data for improved models and enhanced knowledge of geophysics.

While one mission concept under active study involves the use of two spacecraft to obtain the Earth's gravity field by measuring the relative velocity changes between the spacecraft, other concepts would use gravity gradiometers. A promising instrument that would lead to greatly improved gravity measurements in the 1990's is the Superconducting Gravity Gradiometer (SGG).

The SGG program is designed to develop an instrument with a measurement sensitivity of 10^{-2} to 10^{-4} Eötvös (E) (1 E = 10^{-9} s^{-2}) with a time constant of 10 s. The sensitivity of room temperature gravity gradiometers is limited to about 1 to 10 E by the Brownian motion of proof masses. At liquid helium temperature (4.2 K and below), a sensitivity of 7 x 10^{-3} E (in 10 s) might be achieved by using a superconducting circuit and superconducting quantum interference device (SQUID, Josephson Junction) magnetometers. The properties of materials at low temperatures provide several other advantages. Construction materials are known to display greatly enhanced dimensional stability, together with reduced hysteresis and creep at low temperatures. These properties are expected to contribute to a large dynamic range and scale-factor stability of the device.

The basic components of the gravity gradiometer are superconducting accelerometers. The basic accelerometer is composed of a weakly suspended superconducting proof mass, a superconducting magnetic transducer, and a low-noise SQUID (Fig. 14). The magnetic field produced by the transducer coils is modulated by the motion of the proof mass and detected by the SQUID. These

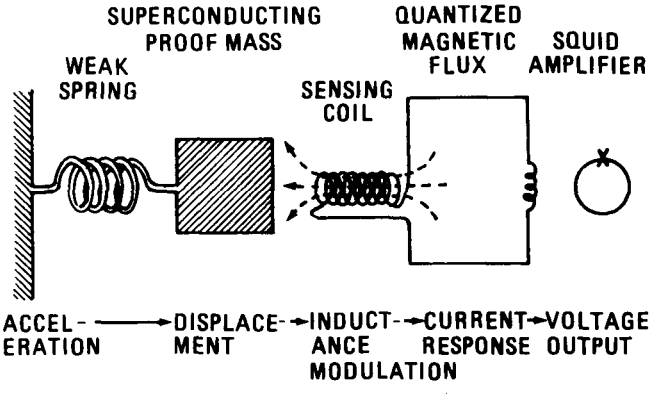

Figure 14. Superconducting Gravity Gradiometer Concept.

accelerometers may be combined to detect all three linear gravity gradient components and three angular accelerations — a six-axis superconducting accelerometer (Fig. 15).

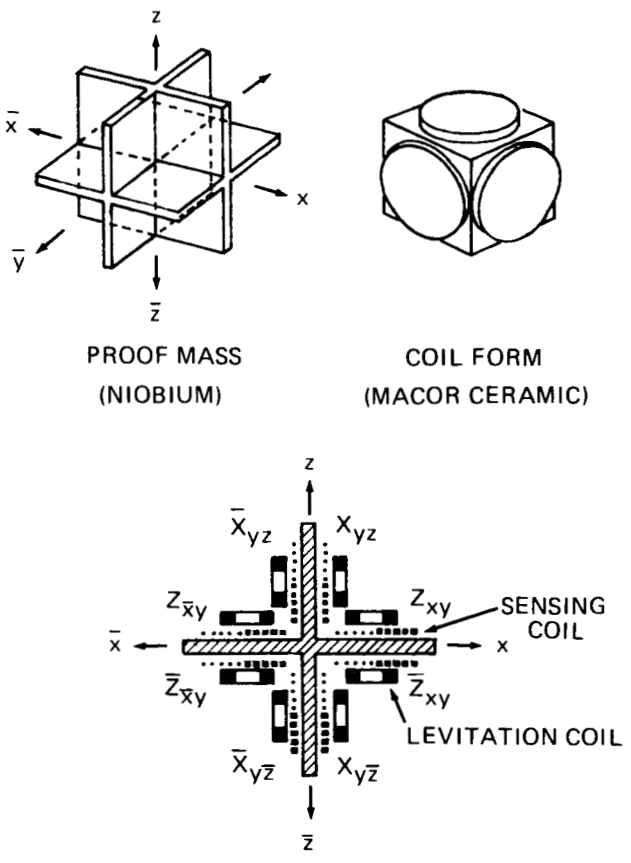

Figure 15. Design of a Six-Axis Superconducting Accelerometer.

Advanced research for the instrument is under way. Work is now focused on the design, proof of concept, and laboratory test of the instrument. Gradiometers are contaminated by accelerations and by gravity itself (nearby masses, vibrations, etc.). By placing the SGG in orbit, dramatic improvements are predicted in global gravity measurements. However, because of the sensitivity of the SGG, the instrument cannot be fully demonstrated in the laboratory. Beginning in FY86, MSFC headed a study team to investigate a test flight to enable the instrument to be tested and calibrated, either in the Shuttle cargo bay or on a recoverable platform. The flight mode recommended by the study team will depend on the results of various analyses.

A proof-of-concept SGG has been developed and tested. A three-axis engineering model gradiometer was designed during FY86, and is currently being assembled. Preliminary design of the flight support apparatus, which includes a suitable liquid helium dewar system and electronics, is also under way.

Paik, H. J.: A Spaceborne Superconducting Gravity Gradiometer for Mapping the Earth's Gravity Field. Digest of the 1981 International Geoscience and Remote Sensing Symposium, Washington, D.C., June 1981.

Wells, W. C. (ed): Proceedings of Spaceborne Gravity Workshop, Greenbelt, MD. NASA CP-2305, 1983.

Parker, J.; and Morgan, S. H.: Superconducting Gravity Gradiometer on the Space Shuttle. Proceedings of the 14th Gravity Gradiometry Conference, Colorado Springs CO, 1986.

S. H. Morgan, Jr./PS02
(205) 544-0614
Sponsor: Office of Space Science and Applications

Advanced UV/Optical Telescopes

Considerable advances in astronomical knowledge are confidently expected in the next decade, due to the imminent availability of the Hubble Space Telescope (HST) and the freedom from the effects of the Earth's atmosphere that it will provide. Just what new areas of astronomy will be exposed for research cannot be predicted, but it is clear that further increases in resolution and light-gathering power will still be requirements when the HST reaches the end of its projected performance period.

Concepts for advanced large space telescopes which will follow the HST have been investigated at MSFC during a technology study, with the major focus on optical configurations.Various concepts ranging from large filled-aperture systems to sparsely-filled phased arrays of linear and two-dimensional aperture configurations have been compared.

It is clear that resolution can be improved only by increasing aperture diameter. Light-gathering power, and hence sensitivity, are increased by added telescope collecting area and improved optical efficiency (reflectivity). Current technology, as demonstrated by the Multimirror Telescope, shows that it is possible to break up a normally circular telescope aperture and separate the parts to increase the effective aperture diameter, without increasing the expensive collecting area. Similar ideas have long been used in radio astronomy. Such approaches are now being examined in great detail for advanced ultraviolet (UV)/optical space telescopes with respect to reduction of weight and size of the subapertures, and assembly in space into complete telescopes. As our studies have shown, there are many

approaches to increasing the aperture and hence resolution and sensitivity. Figure 16 shows some of these optical concepts.

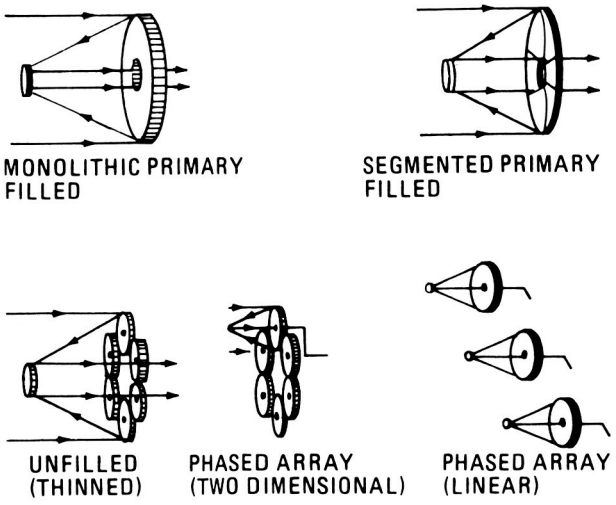

Figure 16. Aperture Options for Large Spaceborne Telescopes.

When "thinning" the aperture, there are some major optical considerations which must be addressed in order to ensure that the optical transfer function does not become zero anywhere at less than the highest spatial frequency corresponding to the diffraction limit of the circumscribed (full) aperture diameter. Otherwise, information at some spatial frequencies corresponding to zeros in the transfer function will not be passed by the system. The practical consequences of this are shown in a series of photos of a starburst pattern taken during the study on optical technology for large telescopes. The starburst pattern represents an object having a wide range of spatial frequencies increasing from the rim to the center in all possible orientations. Various aperture configurations representative of current and future telescope apertures have been used to produce photographs of this pattern. The photographs show clearly the consequences of zeros in the modulation transfer function or of

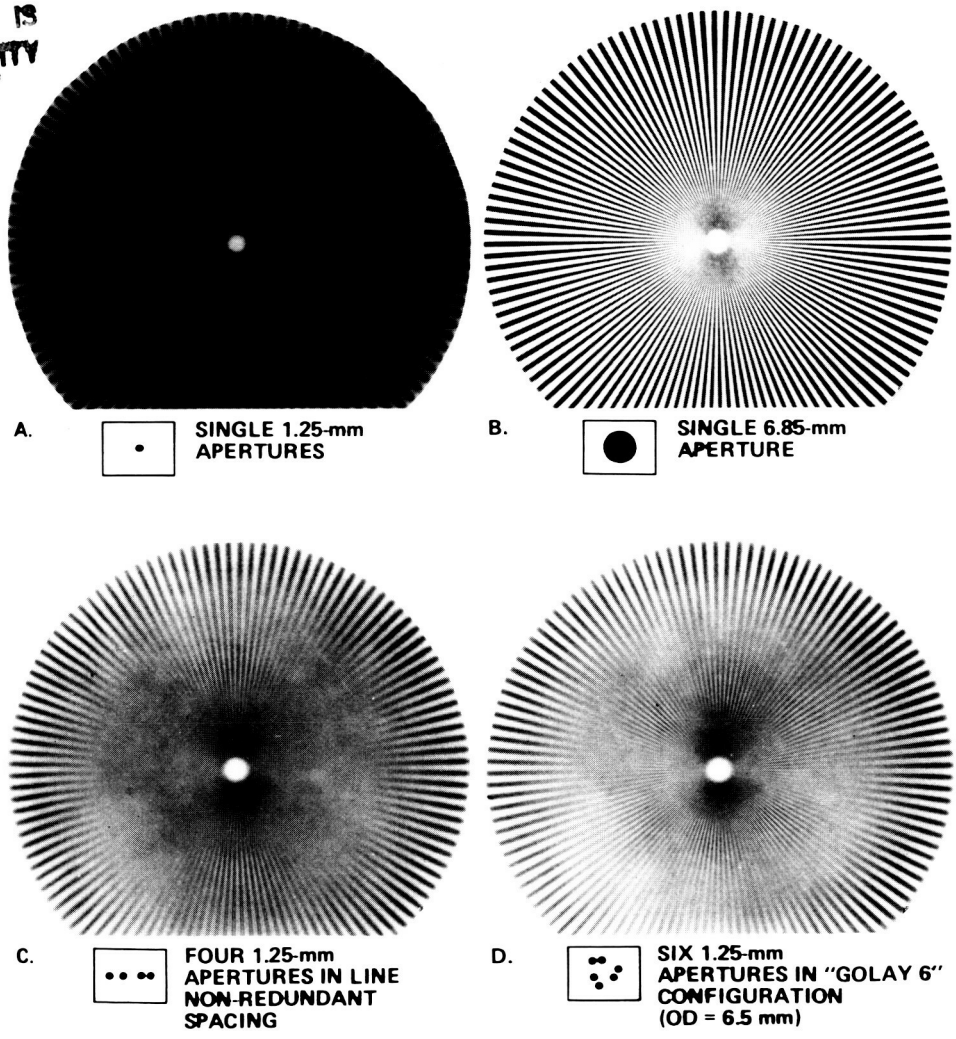

Figure 17. Imaging Performance of Various Aperture Configurations.

reduced amplification at particular spatial frequencies, and are indicative of the loss of optical performance which can be expected with different aperture configurations.

As can be seen in Figure 17, view A, a single, small, circular aperture provides resolution of only the lowest spatial frequencies (rim of starburst). Increasing the aperture to a large diameter (view B) results in excellent resolution of all but the highest spatial frequencies (center of starburst). The image formed by a non-redundant linear array of small subapertures (view C) provides high resolution in one direction, with a distinct loss in the intermediate spatial frequency content. However, the image formed by a two-dimensional non-redundant array of six subapertures (view D) results in virtually complete coverage of the spatial frequency plane resolvable by a single large circular aperture of the size spanned by the array. Areas of high and low contrast corresponding to the subaperture configurations are evident, as expected.

Results from these investigations are now being applied in concept studies of advanced telescopes. Aperture configurations selected for these telescopes will be based on these criteria and other considerations such as overall system performance, manufacturing complexity, orbital assembly and alignment, maintenance, launch capability, and cost.

During FY86, technology assessments of large-aperture UV telescopes have been completed, with several key enabling technology areas identified for further study. An important finding was that dimensional stability of large structures is primary among technological concerns.

M. E. Nein/PS02
(205) 544-0619
Sponsor: Office of Aeronautics and Space Technology

Advanced Gamma Ray Telescope

Gamma rays reflect the highest energy processes in the universe. Therefore, gamma ray astronomy is essential in understanding the evolution of stars and the universe, as well as the physical processes occurring in such exotic objects as pulsars and quasars, and in the vicinity of black holes. The galaxy and universe are essentially transparent to gamma rays in the energy range of 10^7 to 10^{15} eV, and most importantly, their directional information is unchanged. Thus, gamma ray observations directly provide spatial, spectral, and temporal information about the source.

The first significant results in high energy gamma ray astronomy were those from Orbiting Solar Observatory-3 (OSO-3, 1972). This detector had a sensitive area of 46 cm^2 with a large field of view to permit surveying. The next significant results came with the launching by NASA of the Small Astronomy Satellite-2 (SAS-2) in November 1972 and by the European Space Agency's launch of the Cos-B in August 1975. Both detectors were the same size, about 600 cm^2.

The next step will be the Gamma Ray Observatory (GRO), to be launched in the late 1980's aboard the Shuttle. The GRO will contain a spark chamber, as the earlier detectors did, but with a sensitive area of 6560 cm^2, ten times larger than the previous two satellites. Like its predecessors, it will also be performing an all-sky survey. Spark chambers are limited in size by their complexity and weight. Because of the positional uncertainties, many gamma ray sources are unidentifiable. The detection process is hampered by the difficulty of reconstructing the direction of the primary gamma ray, and by the very low fluxes involved. Thus a new gamma ray detector with greater sensitivity and resolution is necessary to follow up the survey work.

The telescope function can be visualized by following the sequence of processes necessary to identify a gamma ray event (Fig. 18). The first element used to mark the signature is the veto scintillator, S1, which is used to reject all charged

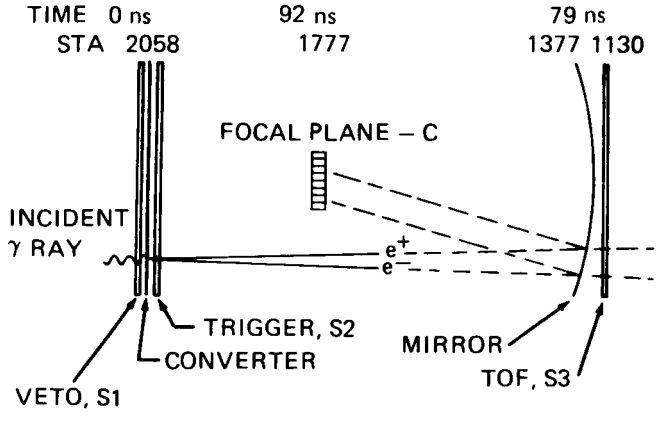

Figure 18. Gamma Ray Telescope Detection and Identification Sequence.

particles. The gamma ray, being neutral, will not be detected by S1 and the probability of its being converted within the scintillator is also small. Next, the gamma ray enters the converter, nominally of lead, where it will be converted into an electron-positron pair. The pair immediately enters the second scintillator, S2, where a pulse is produced. In fact, the pulse amplitude will be indicative of a two-particle event. Next the pair travels the length of the telescope, emitting Cherenkov light as it passes through the gas. This light is then imaged by the optical system onto an array of photomultipliers in the focal plane, C. Pulse height analysis of the array will enable reconstruction of the two rings of light and thus determine the incident gamma ray direction. After the pair continues through the mirror, it passes through a third scintillator, S3, which provides an additional time of flight (TOF) measurement and reduces the change coincident rate, particularly from backward-moving particles.

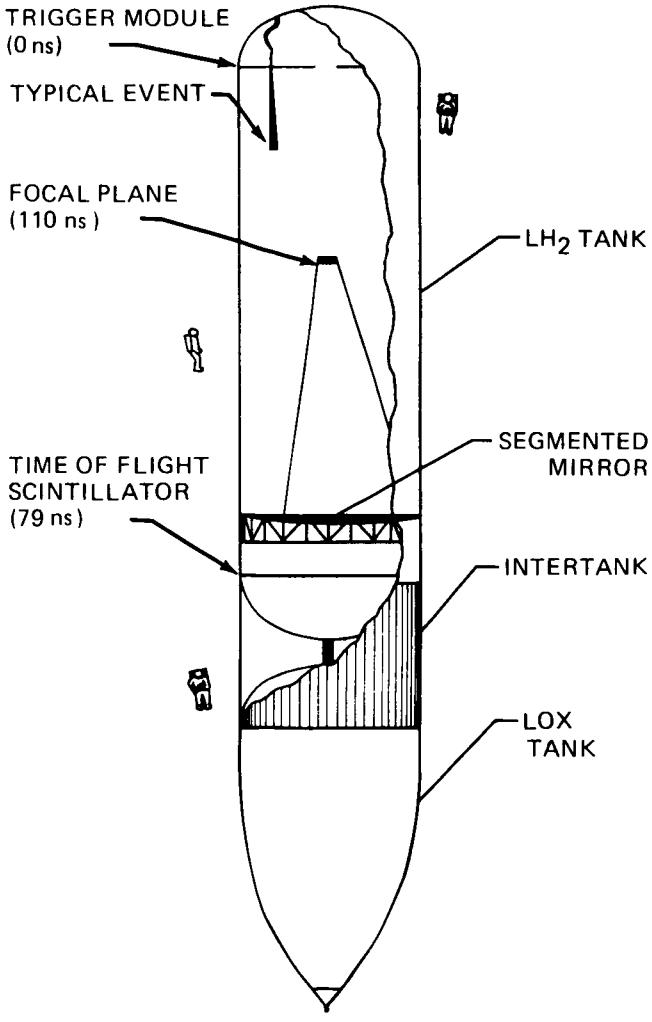

Figure 19. Gamma Ray Telescope in the Shuttle External Tank.

A telescope with high sensitivity and resolution was conceived by Professor Greisen in the early 1970's. It could be flown today with the existing Space Transportation System, although in an unconventional fashion. This telescope would have a collecting area of 2.5×10^5 cm^2 and make use of the Shuttle External Tank (ET) by appropriately instrumenting it once on-orbit (Fig. 19).

Currently, MSFC is conducting conceptual studies of this large gamma ray telescope. The investigations are directed toward defining the necessary instrumentation for the detection of gamma rays, and developing concepts for on-orbit assembly of the telescope components in the ET. Flight demonstration concepts are also being investigated and specific assembly tasks will be tested in the Neutral Buoyancy Simulator.

In FY86, a systems engineering study was initiated to investigate the technical and programmatic feasibility of the gamma ray telescope. The study included planning of neutral buoyancy simulations of orbital conversion of the ET to a gamma ray telescope.

Koch, David G.: A Large Area Gamma Ray Imaging Telescope System. Smithsonian Institution Astrophysical Observatory, Cambridge MA, 1983.

M. E. Nein/PS02
(205) 544-0619
Sponsor: Office of Space Flight

Tether Applications In Space

Tethers to be used in space are long, relatively thin, flexible cables which connect two or more masses moving together in parallel trajectories. The distance between the masses can be fixed or variable and the tether connections may be permanent or temporary, permitting the masses to be disconnected. Tethers may be conductive to carry electrical current, or nonconductive for the transmission of loads.

Two new developments supporting tether applications are in progress. The first involves the Small Expendable Deployment System (SEDS) to be used for flight demonstrations of critical areas in the tether applications program. Hardware design, production, assembly, and testing were begun in FY85. Testing continues through FY86, with a prototype system projected to be

available in FY87. The second development consists of a new type of conducting tether made by depositing conducting metal on Kevlar filaments, thus providing a unified, composite material with the combined characteristics of both strength and conductivity. A coating facility using this proprietary process to produce tether lengths up to 100 km (62 mi) is now under development.

A few concepts have reached the phase of demonstration mission definition, while the SEDS has become an approved flight experiment. A tethered remote docking experiment and a kinetic isolation tether experiment (KITE) are in the mission definition phase. This latter experiment is expected to provide data for assessing the feasibility of tethered Space Station platforms (Fig. 20).

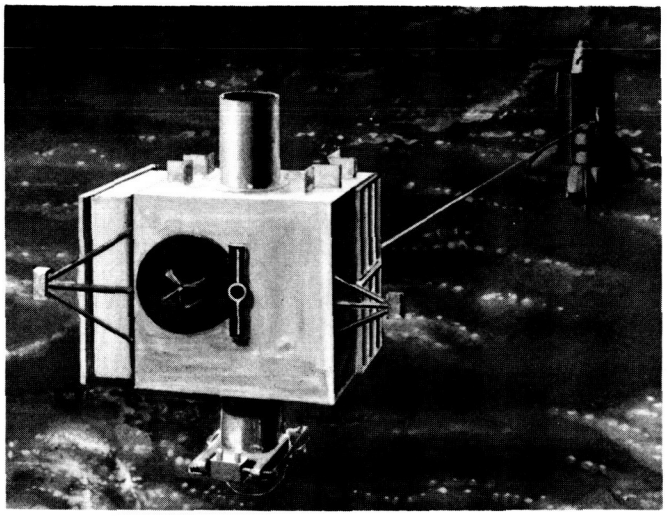

Figure 20. KITE Deployment Using the SEDS.

Present studies are defining how the Space Station could be accompanied by tethered platforms. These platforms would require no guidance mechanisms or propulsion systems, and little maintenance. The tethers could provide direct data relay and could also serve as power and communication links.

One of the currently studied applications of tethers is an engineering design and cost/benefit analysis of insertion of spacecraft into orbit from the Shuttle Orbiter. Such an insertion would transfer momentum from the Shuttle to the payload, and send the payload into a higher altitude without additional expenditure of propellant. As an added benefit, the Shuttle perigee would be reduced, making it easier for the Shuttle to reenter the Earth's atmosphere.

Other studies which advance into engineering design and economic analyses are in progress and involve the tethered deployment of various space vehicles from the Space Station. The tethered deployment of an Orbiter from a Space Station would transfer angular momentum from the Orbiter to the Space Station, thus accelerating the Station and decelerating the Orbiter. This would result in less orbit maintenance for the Space Station and considerable propellant savings for the Orbiter reentry.

Also under investigation at this time is the upward tethered launch of an Orbital Transfer Vehicle (OTV) from the Space Station. Such a launch would result in an increased OTV velocity and altitude, and an associated increase in payload capacity or propellant savings. The resulting altitude loss of the Space Station would be made up during the next Orbiter deployment.

Another study addresses the tethered deployment of small reentry capsules from the Space Station. This simple way to return materials processing or biological samples to Earth would make it unnecessary to wait for the next Orbiter flight. An early Shuttle-based flight demonstration is being defined using an available reentry capsule.

With regard to electrodynamic tethers, an Ultra-low Frequency/Extreme-low Frequency Antenna (ULF/ELF) is under study. This antenna would be self-powered and would emit electromagnetic radiation between 30 and 3 Hz. The definition of this system is in progress with the final goal of an Orbiter-based flight demonstration (Fig. 21).

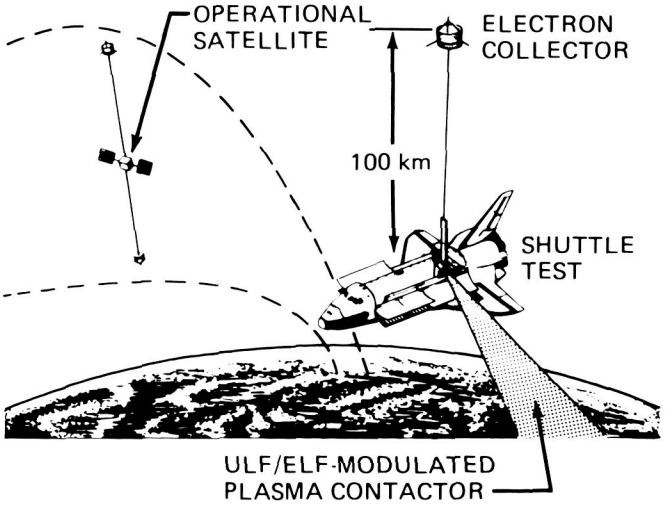

Figure 21. Ultra-Low Frequency/Extreme-Low Frequency Antenna.

Table 3. Tether Required Research and Technology.

REQUIRED RESEARCH AND TECHNOLOGY ADVANCEMENTS HAVE BEEN DERIVED FROM THESE STUDIES AND INVOLVE:

A. TETHER MATERIALS AND CONFIGURATIONS
- MEASUREMENT AND CATALOGUING OF TETHER MATERIAL PROPERTIES
- TETHER PROTECTIVE COATINGS
- ELECTRODYNAMIC TETHER INSULATION
- ELECTRODYNAMIC TETHER CONDUCTORS
- ON-ORBIT TETHER REPAIR CONCEPTS
- HIGH STRENGTH TETHER CONFIGURATIONS

B. TETHER APPLICATIONS ENGINEERING INSTRUMENTATION
- TETHER DAMAGE DETECTION
- DEFINITION OF EXISTING INSTRUMENTATION CAPABILITIES
- DEFINITION OF ADDITIONAL NECESSARY FLIGHT DATA FOR:
  - MISSION CONTROL
  - POST FLIGHT PERFORMANCE ANALYSIS
  - MISSION DESIGN VERIFICATION
- DEVELOPMENT AND DEMONSTRATION OF INSTRUMENTATION SYSTEMS
- DEVELOPMENT AND TESTING OF HOLLOW CATHODES

C. TETHER SYSTEM DYNAMICS/ORBITAL MECHANICS SIMULATION
- DEFINITION OF EXISTING CAPABILITIES OF SIMULATION PROGRAMS
- DEFINITION OF ADDITIONAL CAPABILITIES REQUIRED
- PROVISIONS FOR:
  - PROGRAM PORTABILITY
  - EASE OF USE
  - FLEXIBILITY
  - ECONOMY
- DEVELOPMENT OF REQUIRED PROGRAMS WITH AS UNIVERSAL AN APPLICATION AS ECONOMICALLY PRACTICAL

D. ATMOSPHERIC/AEROTHERMODYNAMIC TECHNOLOGY
- ANALYTICAL METHODS AND COMPUTATIONAL CODES DEVELOPMENT
- UPPER ATMOSPHERIC AEROTHERMODYNAMICS MODELING
  - STANDARDIZED DYNAMIC MODELING AND SIMULATION CAPABILITIES DEVELOPMENT

The above concepts will be candidates for a detailed engineering analysis during the next year. This will produce additional potential candidates for flight demonstrations. The required research and technology advancements which have been derived from the studies are listed in Table 3.

G. F. von Tiesenhausen/PS01
(205) 544-0617
Sponsors: Office of Space Flight
Small Business Innovative Research Program

Cryogenic Storage Facility

Long-term cryogenic fluid storage facilities will be required to support future space programs such as the space-based Orbital Transfer Vehicle (OTV), telescopes, and laser systems. The storage facility tanks will be required to permit fluid acquisition and transfer in low gravity and limit cryogen boiloff due to environmental heating. Boiloff management features, minimizing Earth-to-orbit resupply transportation costs, will include advanced multilayer insulation design concepts, vapor-cooled shields, low-conductance support structures, and refrigeration/reliquefaction systems.

A contracted conceptual design study is analyzing a liquid oxygen/liquid hydrogen (LOX/LH_2) orbital storage system with an approximate capacity of 90,800 kg (200,000 lb). The study concludes that a coupled tank design utilizing vapor-cooled shields, in conjunction with a reliquefaction system with approximately 1.6 cm (4 in.) of multilayer insulation, appears to be the preferred concept, if venting of tank boiloff is not permitted in the vicinity of an orbital facility (Fig. 22). This concept has the lowest estimated cost and is projected to represent the lowest safety risk, as there is no high pressure storage of boiloff. However, it presents a development risk due to the need for a long-life cryogenic refrigerator.

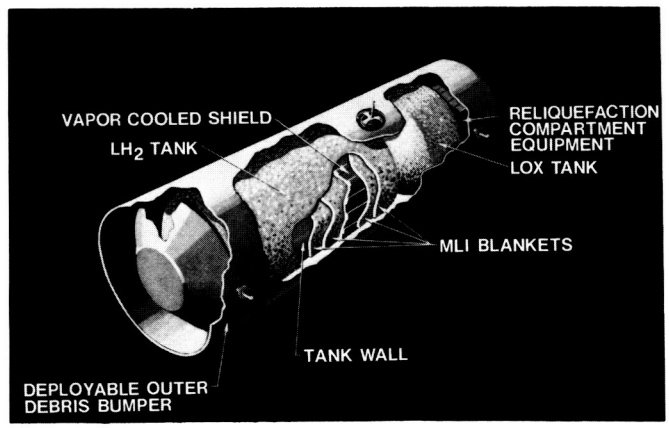

Figure 22. Orbital Cryogenic Storage Facility.

An all-passive concept (thermodynamically coupled tanks, multilayer insulation, vapor-cooled shields) is preferred for cost and reliability reasons if venting of boiloff is permitted, or if boiloff is used by an orbital facility. The all-passive design has a total boiloff of less than

0.2 percent per month for a 90,800-kg (200,000-lb) facility. Therefore, propellant resupply cost for the boiloff would be a relatively small penalty. The potential uses of hydrogen and oxygen aboard the Space Station or an orbiting platform could utilize boiloff while still satisfying the "no-vent" requirement. These potential uses would eliminate the boiloff disposal problems associated with an all-passive storage facility concept. In the area of fluid transfer, autogenous pressurization of the liquid storage tanks during tanking of an OTV can be performed using stored boiloff vapor. This appears to be practical for liquid oxygen, but not for hydrogen because high-pressure superheated hydrogen boiloff gains a high enthalpy which, when released back into the liquid tank, causes additional boiloff. Therefore, hydrogen is transferred using a heat exchanger and pump to produce saturated vapor for pressurant, which reduces heat loads.

A verification test article will be used for ground and flight testing (as required). The article will be a subscale version of the orbital storage facility. The purpose of the test article and subsequent testing will be to establish the thermal performance of the design, as well as long-term system exposure effects.

Contractors are continuing to develop a technology plan, establish test plan requirements for ground/flight testing, and develop a design of the test article. The detail design and development of the test article will be performed based on the results of the current study.

N. S. Brown/PD22
(205) 544-0505
Sponsor: Office of Space Flight

The Human Role In Space (THURIS)

Infrequent space tasks are becoming routine, automation is burgeoning, and crew sizes are increasing. Missions are becoming longer, vehicles larger, mission complexity greater, and in coming years both man and machine will be sent to niches in space that were previously inaccessible. Since real systems are usually complicated mixtures of humans and automated equipment, and since the space program is so dynamic, a means to objectively evaluate man/machine systems was needed. Although several techniques are capable of this, they require detailed design information and therefore are applied so late in the design process that many key decisions are already made.

In this context, The Human Role in Space (THURIS) study has examined how to quantify and define appropriate roles for humans in space by analyzing representative future missions. Prior work in the study organized and consolidated data on human capabilities and limitations, task performance times, relative costs, and technology readiness to support man/machine analyses. A data base was developed for relating cost, performance time, and technology criteria for 37 generic activities and 7 levels of automation. With this data base, complex scenarios could be analyzed to identify appropriate human roles. The data were expressed in relative terms and reduced to graphical formats to simplify analyses.

Work thus far has validated, refined, and extended THURIS techniques and data by applying them to mission elements that differ from the ones originally examined. Elements studied included refueling of an Orbital Maneuvering Vehicle, aerobrake replacement, vehicle assembly/disassembly, engine exchange, payload mating/demating for the Orbital Transfer Vehicle, and sample manipulation and product analysis in a space laboratory environment.

Validation involved ensuring that the data base contained the necessary and sufficient information and was properly defined to analyze new missions. It required that the accuracy, consistency, accessibility, and breadth of supporting data be verified, and finally, it involved reviewing the overall man/machine allocation approach to ensure that it is logical and that results are relevant.

Initially, THURIS cost relationships and basic data were limited to low Earth orbit (LEO) Space Station applications. The emphasis was on establishing a firm conceptual framework using predominantly available data. The current study will expand the range of applications to include Space Shuttle missions in LEOs and will examine the sensitivity of man/machine roles to various cost assumptions. It will also examine ways to implement technology readiness data more directly into the THURIS analysis scheme. Finally, it will examine the relationship between the cost effectiveness approach developed in THURIS, and the

non-economic factors which also influence the definition of human roles in space.

The results of the current study are being documented in formats that will permit effective treatment of key issues and rapid analysis of man/machine roles. They should be especially useful in the preliminary design phase of projects when man/machine tradeoffs are particularly difficult and the impacts of those trades are far reaching.

S. B. Hall/PD24
(205) 544-0517
Sponsor: Office of Space Flight

Geostationary Facilities

Geostationary Earth orbit (GEO) today is extensively utilized for domestic and international communications services, Earth science applications, and a variety of other services. Thus this Earth orbital location is becoming crowded. After the mid-1990's, it is projected that the practice of adding new satellites at unused orbital locations near the high-demand regions will no longer be possible. Replacement of existing satellites with larger, more complex platforms will become the only way to satisfy the large demand for public and consumer services. These platforms will alleviate the congestion problem primarily by "frequency reuse," via multiple narrow antenna beams, for some of the communications applications. The platforms will also be multipurpose, aggregating multiple services on a single structure. Commercial communications platforms have been studied extensively by NASA in the last 2 years. These studies have verified the "economy of scale" conclusions of past studies, and have shown that there are no insurmountable regulatory obstacles to such platforms.

Four of the commercial communications platforms defined and studied in FY85 and FY86 are shown in Figure 23. Contractor reports for the communications platforms studies were published in FY86. These platforms bracket the range of types of commercial communications platforms that could be built before the end of the century.

The demand for GEO slots will also increase because of the unique benefits of the GEO orbit. Astrophysics facilities would greatly benefit from this orbit because the facilities would be in constant view of the Earth operating station, and away from the Earth's background noise. Several astrophysics facility concepts have been produced by recent MSFC studies.

Another application of GEO which has already proven to be very beneficial to the public is Earth observation, especially for weather prediction. The GEO satellites have virtually revolutionized weather prediction by providing instantaneous global observations. Platforms will be ideal for this application because a much larger number of instruments can be operated from a single location. They continue to be the subject of intense study by MSFC.

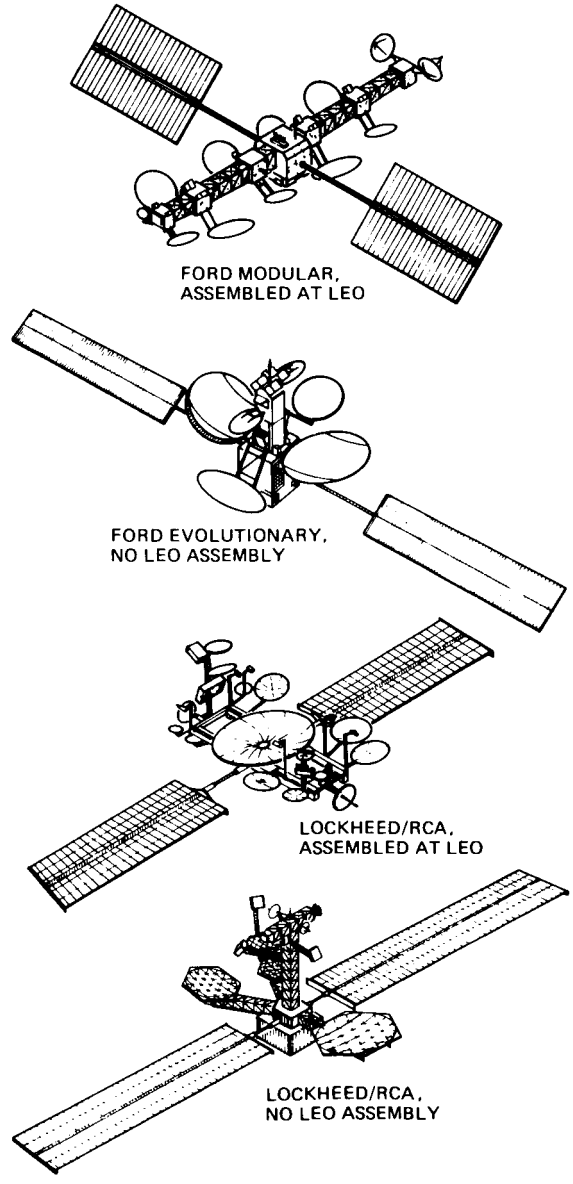

Figure 23. Commercial GEO Communications Platforms.

NASA has been studying manned and unmanned GEO facilities since the early 1970's. A typical GEO facility, defined in 1981/1982 and shown in Figure 24, was intended to demonstrate communications platform technologies. Now Earth science and Earth observation platforms are of greater interest because of the need for an operational U. S. government platform of this type by the late 1990's. Various versions of such platforms are currently being studied by MSFC.

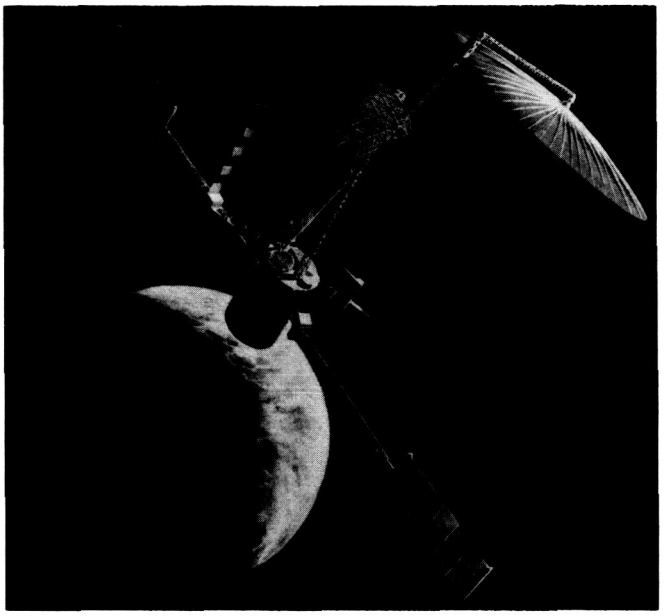

Figure 24. Typical Geostationary Facility.

A dominant consideration in the selection of specific technologies is economy. Low-cost methods for remote servicing, as well as for assembly/checkout, must be found. The planned facility will demonstrate low-cost GEO servicing and low Earth orbit assembly/checkout technologies.

R. H. Durrett/PS04
(205) 544-0628
Sponsors: Office of Space Flight
Office of Space Science and Applications

Manned Mars Missions

During the past year, MSFC has continued the studies of Manned Mars Missions (MMMs) which began in early 1985. Activities this year have been focused on two areas: (1) investigation of "combination" missions (visits to the surfaces of Mars and one of its moons on the same mission), and (2) definition and analyses of overall NASA space program options for the 1992 to 2035 timeframe which have a Mars "emphasis."

Landing on a moon of Mars is an easier mission than landing on Mars itself; it would offer some unique science opportunities, and in many respects might be a logical precursor to the Mars landing. On the other hand, a Mars landing would allow a wider variety of science activities as well as afford the prestige associated with setting foot on the planet. Both types of landings are highly desirable early in a Mars program. If both could be accomplished on a single mission, the value of the mission would increase significantly. Also, if only one mission could be flown per opportunity, use of a combination mission would prevent delay of the other type of landing by about 2.2 years. Study results to date indicate that combination missions would require about a 30 percent increase in low Earth orbit (LEO) weight compared to that required for a Mars-only landing. The weight of equipment which could be left on the surface of Mars by such a combination mission could be increased by about 30 percent over that left in a single-landing mission. Figure 25 depicts an early zero-gravity cryogenic chemical propulsion/aerobraking concept of a vehicle with two landers for combination missions (other options use non-identical landers, to save weight).

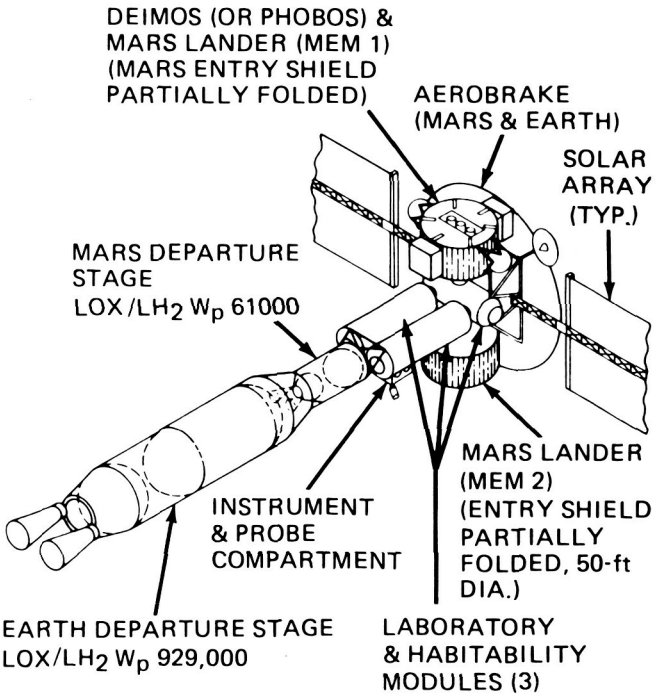

Figure 25. Mars Exploration Vehicle Concept, Combination Mission.

The activity in the area of analysis of overall NASA space program options, mentioned above, was done in support of the inter-center Advanced Missions Working Group, chaired by Ivan Bekey

of NASA Headquarters. In this activity, several overall NASA space program options have been generated, consisting of many individual missions in various "domains," such as LEO, geostationary Earth orbit (GEO), Moon, Mars, deep space, etc. The missions have been scheduled and costed to fit within a cost envelope defined by 2.4 percent real growth per year of the NASA budget. Figure 26 is a "relevance tree" from one of the program options, showing the major milestones in each of the domains. In this program option, Mars missions have been given preeminence over the GEO and lunar missions, but not over the early LEO missions. MMMs could begin earlier than the dates shown, by (1) providing a larger budget, (2) giving priority to MMMs over the early LEO missions, or (3) flying simpler Mars missions (such as flybys) initially, and delaying the more demanding Mars landing missions until later.

J. M. Butler/PS04
(205) 544-4833
Sponsor: Office of Space Flight

Commercial Materials Processing In Space

In orbit, the effect of gravity levels far below Earth ambient can be consistently obtained. Microgravity then becomes a parameter that can be used to optimize material processes, just as pressure and temperature parameters are routinely used to optimize such properties on Earth. Free from the influence of gravity, entirely new techniques for manipulating materials, investigating basic phenomena, and exploiting technologically important processes are possible.

Since the late 1960's, MSFC has conducted microgravity processing experiments utilizing both ground-based facilities and spaceflight research apparatus. This work is being done under the auspices of the Office of Space Science and Applications, Microgravity Sciences Division, and has resulted in a body of science and technology that forms the technical basis for the Commercial Materials Processing in Space (CMPS) program. The Office of Commercial Programs, supported by MSFC, has established policies and procedures for making business and legal arrangements with commercial firms and for providing technical assistance to their research and development work aimed at commercial applications of materials processing in space.

The overall approach of CMPS is shown in Figure 27, which depicts applications of CMPS to improve ground-based processes and to produce space products. For example, ground-based work on electronic materials indicates that weightlessness alters the fundamental interaction of heat flow, mass transport, and fluid mechanics during crystallization. Early flight experiments in space tend to confirm these expectations and have led to commercial research and development aimed at producing improved gallium arsenide crystals, semiconductor wafers, electro-optical crystals, and infrared sensors.

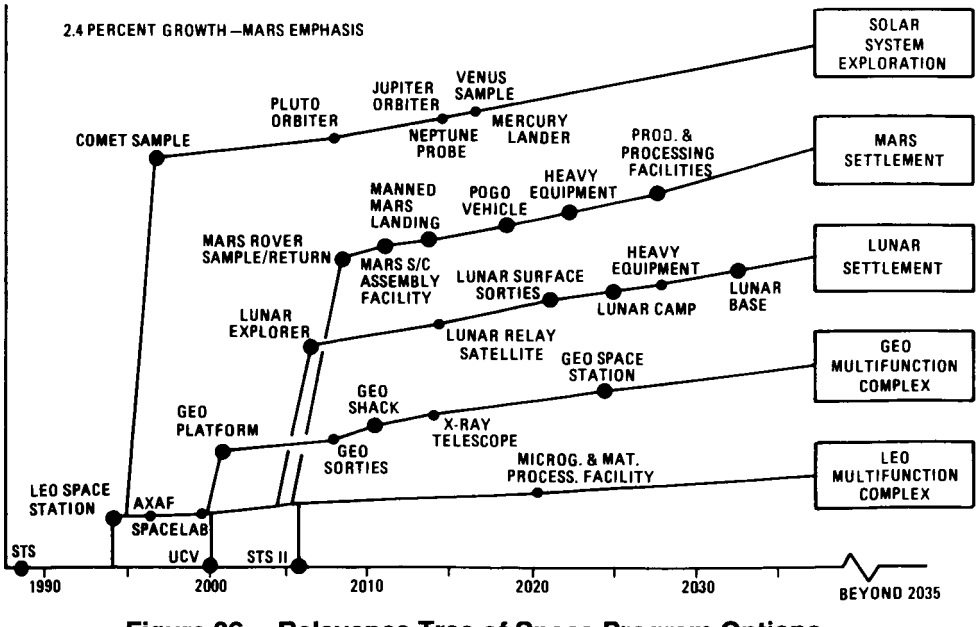

Figure 26. Relevance Tree of Space Program Options.

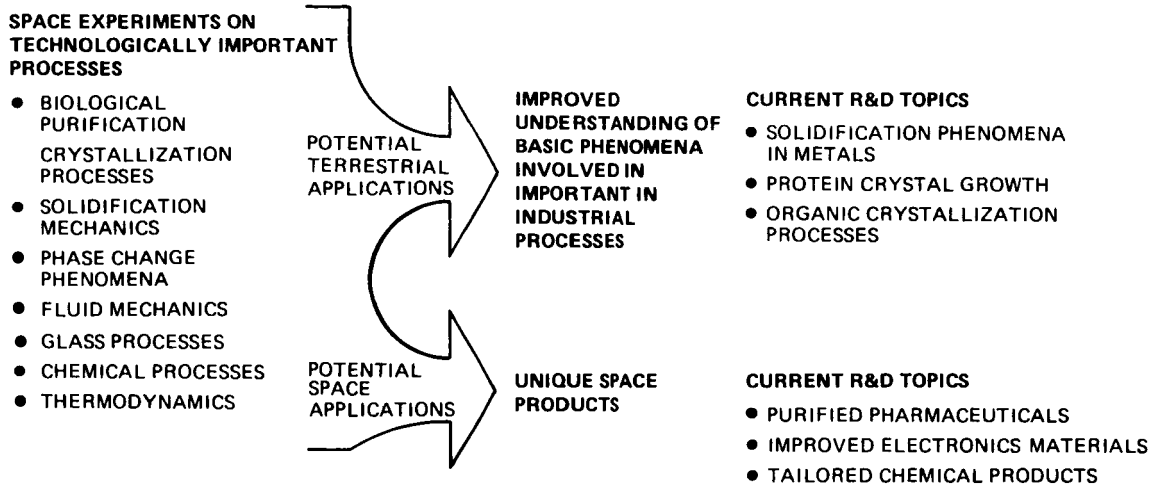

Figure 27. Current Applications of CMPS.

Another area of commercial interest is the control of the solidification of metals and alloys, which is basic to the entire field of metallurgy. Gravitational effects such as buoyancy-driven convection or sedimentation of various phases can greatly influence the macrostructure as well as the microstructure of metals and alloys.

Fluids and transport phenomena are the common denominators of the wide spectrum of materials processing on Earth. The supply of materials to the solidification process is controlled by heat and mass transport phenomena which are dominated by gravity-driven convection or sedimentation. Experiments in space simplify problems by eliminating the gravity-driven set of flows so the other phenomena can be isolated and analyzed.

A number of biotechnology processes are adversely influenced by gravity effects. These include electrophoresis, isoelectric focusing, phase partitioning, suspension cell culturing, and crystallization of proteins. In the case of electrophoresis, joint NASA-commercial work in space has shown large increases in both purity and throughput. Also, preliminary space experiments have already produced much larger protein crystals.

Glass and ceramic research typically takes advantage of the absence of gravity-driven convection and the ability to process samples without contacting a container. In space, materials can be heated, cooled, and manipulated while floating free of contact with container walls. Thus, deep undercooling is possible, corrosive materials are not contaminated by contact with containers, and surface tension tends to determine the shape of samples. Potential applications include novel glasses, fiber and laser optics, and fusion targets.

Research in space opens new opportunities for chemical processes. For example, seeded polymerization of latex has been used to grow monodisperse spheres that have become a commercial product. These spheres are sold as standards for calibration and are being considered for a range of biomedical applications.

MSFC's experience in low-gravity processing is used in the development of Joint Endeavor Agreements (JEAs), Technical Exchange Agreements (TEAs), and Industrial Guest Investigator's Agreements (IGIs). This capability has been instrumental in the development of JEAs with McDonnell Douglas, 3M, Microgravity Research Associates, Instrumentation Technology Associates, International Space Corporation, and Boeing. TEAs have been signed with Deere and Company, Rockwell Science Center, and Abex Corporation. This past year MSFC aided in the development and submission of JEA proposals from Deere, General Motors, Rockwell, and the Space Commercialization Consortium, a group of seven major U.S. industrial corporations. At present, 15 companies and institutions are participating as IGIs to the Protein Crystal Growth Experimental Program. In addition, 28 companies are participating in the program for commercial development of space through NASA Centers.

NASA has established groups at both NASA Headquarters and at NASA Centers dedicated to expediting technical and business arrangements with commercial users.

K. R. Taylor/PS05
(205) 544-0640
Sponsor: Office of Commercial Programs

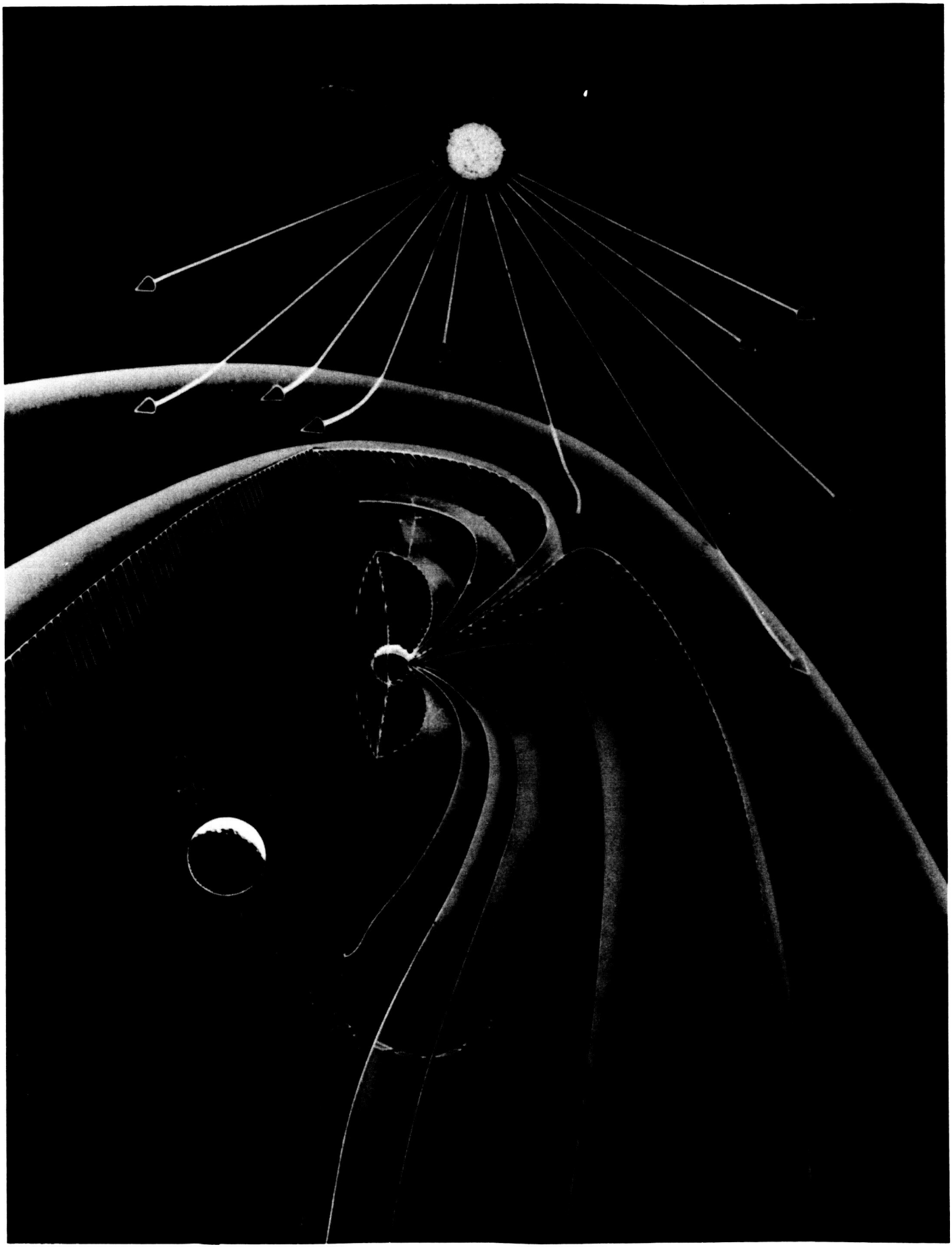

Research Programs

Several research programs have been developed at MSFC to support the many space missions managed by this Center. Scientists and engineers have created an exciting environment for research in all areas of interest to MSFC. As a result, considerable expertise resides in the areas of Microgravity Sciences, Space Sciences (including Solar, Magnetospheric and Atomic Physics, and Astronomy and Astrophysics), and the Atmospheric Sciences.

For the future, MSFC scientists and engineers are designing and building experiments, for both in situ and remote sensing, to take advantage of Shuttle and Spacelab flights, and especially for deployment on the Space Station.

Microgravity Sciences

Introduction

Experiments on materials in microgravity began with the Apollo lunar program. The Shuttle Program provided the opportunity to resume extended experiments in a microgravity environment. The first materials processing experiments were performed in the Orbiter mid-deck of flight STS-3 in March 1982. The mid-deck has proven to be an attractive place for small low-power experiments that require crew interaction. Larger experiments have been performed in the payload bay, either using the Materials Experiment Assembly (MEA), a self-contained package that provides power, cooling, control, and data acquisition, or in the Material Science Lab (MSL) carrier, which provides higher power by tapping into the Orbiter power and cooling systems. The Spacelab 3 and the German D-1 missions provided the opportunity for interactive microgravity science with payload specialists who were trained materials scientists.

Because of the temporary delay in the Shuttle program resulting from the Challenger accident, MSFC is making more use of short-duration low-gravity facilities, such as drop tubes, drop towers, and aircraft flying ballistic trajectories, to test new ideas and concepts in order to develop a new class of experiments when Shuttle flight operations are resumed. Significant ground-based experimental and theoretical investigations are also being performed to enhance scientific return from the future Shuttle/Space Station materials processing projects.

Crystal Growth

Crystal growth is currently of great interest due to its potential applications in electronics, optics, laser devices, and other areas of solid state, chemical, and biological science and technology. In most cases production of crystals with the desired composition and other properties is understood only quantitatively because of the complexity of the heat and mass transport, and the nucleation and growth phenomena involved. In a unit-gravity environment, the various phenomena are further complicated by natural convection driven by a density gradient. Such convection can readily lead to time-dependent variations in the pertinent heat and mass transport processes. The resulting growth rate fluctuations may significantly alter crystal compositional uniformity and defect density, leading to undesirable spatial variations in the electrical, optical and structural properties. In the presence of small gravitational accelerations, diffusive heat and mass transport may occur in the absence of surface tension gradient-driven convection. Thus, a low-gravity environment can

provide for better control of the dynamic and kinetic processes that affect growth interface stability, second phase segregation, line-defect generation, and the formation of dendretic and eutectic structures.

Considerable progress was made in FY86 in ground-based experimental and theoretical crystal growth studies as well as flight experimentation. The results from the vapor crystal growth experiment performed during the Spacelab 3 mission were especially gratifying. The measured gamma ray rocking curves revealed very narrow line widths, indicative of a high degree of internal order throughout the space-grown mercuric iodide crystals. Only small portions of the very best crystals grown on Earth showed similar line widths. The major parts of Earth-grown crystals showed significant line-broadening and multiple peaks, suggesting lattice strains or perhaps even low-angle grain boundaries. Space-grown crystals had measured electron and hole mobilities that were larger (by a factor of approximately two) than the highest values reported for Earth-grown crystals. This enhancement in electrical properties is additional evidence for the higher microstructural quality implied by the rocking curve data.

Significant advances were also made in hardware design and development leading to the crystal growth of electronic materials by directional solidification and vapor growth in low gravity. A comprehensive thermal model has been developed for an advanced automated directional solidification furnace and is used to predict spatial variations in the solidifying sample temperature distribution. The thermal model also serves as a design aid for the assessment of on-orbit power and heat rejection requirements.

Recently, solid solution semiconducting alloy systems have become of great scientific and technological interest because their electrical and optical properties and crystal lattice constants can be compositionally tuned to meet unique and exacting performance needs. Over the past several years the Bridgman-Stockbarger directional solidification method has been extensively used in the Space Science Laboratory at MSFC to grow mercury-cadmium-tellurium (HgCdTe) crystals and similar compound semiconducting alloys. The melt growth directional solidification technique has recently been extended to include additional growth methods, including traveling molten and solvent zone. A unique horizontal hot-wall zone growth apparatus based on high temperature heat pipe technology has been designed, built, and successfully used to grow HgTe, CdTe crystals by employing a Te solvent-zone method. However, the experiments indicate a high degree of correlation between the density of the Te second-phase dispersates being incorporated into the crystals and the growth rates employed. Growth rates required for dispersate elimination were typically found to be less than 0.2 cm per day. Thus, the growth time required to grow crystals 10 to 15 cm in length by this method is from 50 to 75 days. This growth time is beyond the on-orbit capability provided by the present Space Transportation System, and this activity must await the long-duration capability eventually provided by the Space Station.

An experimental magnetic field damping facility has been designed and is being assembled. Theoretical calculations have been performed to evaluate the effectiveness of magnetic field damping off of buoyancy-driven flow in semiconducting compound melts. The potential benefits of using magnetic field damping to supplement low-gravity effects in space are also being assessed. Preliminary calculations indicate that convective flows resulting from low-gravity residual acceleration in space can be reduced by nearly three orders of magnitude by application of magnetic fields that are within the capability of current superconducting magnet technology.

Continuing research on the casting, recrystallization, and characterization of solid solution semiconducting alloy systems focused on the $Hg_{1-x}Cd_xTe$ ($0 \leq x \leq 1$) alloys. HgCdTe alloys with $x = 0.2$ were quench-solidified in heat pipe furnaces in both the vertical and horizontal configurations, with well-defined thermal boundary conditions. The study results underlined the importance of gravitationally-driven convection in the development of large-scale compositional fluctuations during alloy solidification. A theoretical heat and mass transport model is being developed at the Oak Ridge National Laboratory to evaluate potential low-gravity casting benefits and to assist in the establishment of optimum casting parameters for future flight experiments. The model successfully deals with peculiarities arising from wide separation between solidus and liquidus in the $Hg_{1-x}Cd_xTe$ constitutional phase

diagram, as well as with variations in thermophysical properties with temperature and composition for alloys that are being developed as part of the ongoing research activities conducted at MSFC.

S. L. Lehoczky/ES75
(205) 544-7758
Sponsor: Office of Space Science and Applications

Directional Solidification Experiments

The effects of low gravity on the microstructure of directionally solidified metal alloys were studied, using a Bridgman-type automatic directional solidification furnace aboard a NASA KC-135 aircraft as it flew parabolic arcs and generated alternating periods of low and high gravity. In all three alloy systems studied (iron-carbon alloys, superalloys, and immiscible alloys), dramatic microstructural changes attributable to the gravity level during solidification were observed.

Results for iron-carbon (Fe-C) alloys (Fig. 28) show a refinement of the interlamellar spacing of the eutectic during low-gravity processing of metastable Fe-C eutectic alloys. Low-gravity processing of stable iron-carbon-silicon eutectic alloys (lamellar or spheroidal graphite) results in a coarsening of the eutectic grain structure. Secondary dendrite arm spacing of austenite increases in low gravity and decreases in high gravity. The effectiveness of low gravity in the removal of buoyancy-driven graphite phase segregation has also been demonstrated.

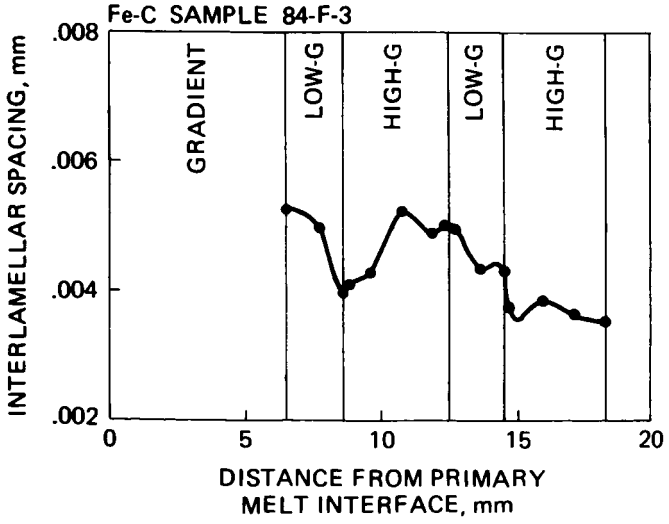

Figure 28. Interlamellar Spacing of the Austenite-Iron Carbide Eutectic.

Previous work with superalloys demonstrated the effect of gravity level during solidification on secondary dendrite arm spacing and on carbide shape, volume fraction, and composition for MAR-M246. Observations have been extended to primary dendrite arm spacing for the superalloy PWA-1480. The primary dendrite spacing was also found to increase in low-gravity solidified sections. This is the first experimental correlation of primary spacing to gravity level.

Electronic properties measurements have been made on sections of immiscible aluminum-indium-tin alloy solidified in high and low gravity. The superconducting transition temperature was found to be 1 K higher in low-gravity sections.

Stefanescu, D. M.; Curreri, P. A.; and Fiske, M. R.: Miscrostructural Variations Induced by Gravity Level During Directional Solidification of Near-Eutectic Iron-Carbon Type Alloys. Met. Trans. A, 17A, 1121-1130, 1986.

P. A. Curreri/ES74
(205) 544-7763
Sponsor: Office of Space Science and Applications

Physical Vapor Transport Crystal Growth

The prototypical crystal growth situation considered in this research is illustrated in Figure 29. A closed cylindrical ampoule is used, with source material at one (hot) end and a growing crystal at the other (cold) end. The interior of the cylinder contains the vapor phase of the crystal growth material (A) as well as an inert buffer gas. The growth process involves no chemical reactions, as it is due to evaporation at one end and deposition at the other end. Because the transport is due primarily to a diffusive process in a low density fluid, growth is relatively slow, and the resultant crystal is actually a thin film. Space flight experiments using such a method for organic crystal growth in the absence of Earth gravity were performed in FY85 by the 3M Company as part of a joint endeavor between NASA and 3M. Analysis of the results is still in progress.

Of interest in the research described here is the fluid flow in the vapor contained within the cylinder, and the effect of that flow upon the flux of component A at the cylinder's endwalls. The time scale in which this flow is established is very short compared to the time it takes to grow the

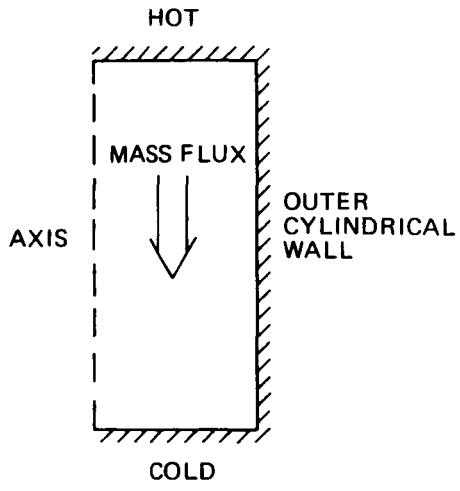

Figure 29. Prototypical Physical Vapor Transport Crystal Growth Model.

crystal. Thus we are considering steady-state flows. The equations upon which the model is based are the Navier-Stokes (viscous) fluid flow equations and conservation equations for heat and species. Because there is a flow from the hot end of the ampoule to the cold end due to the mass transport itself (the "Stefan wind"), there is a need for numerical modeling for microgravity as well as Earth gravity cases. In particular, the viscosity of the vapor causes the influence of the ampoule's side walls to be felt throughout the flow. The interior flow, on the other hand, influences the temperature and species concentration profiles within the vapor, and therefore affects the mass flux on the crystal interface.

Calculations have been performed with the parameters shown in Table 4 systematically varied in order to elucidate the effects of each of them upon the fluid flow. In the absence of Earth's gravity, the primary balance of forces is between the inertial effects of the Stefan wind and viscosity due to the presence of the sidewalls. The viscous effects cause significant effects to be felt by the mass flux through the crystal interface only in the case of extremely different partial pressures between the two endwalls, i.e., when the Peclet number is large. This would be the case when the buffer gas is present at a very small pressure. When enough buffer gas is used, there is very little variation of the crystal mass flux with radius, and a simple one-dimensional model describes the growth to a good approximation. One interesting fact is that the influence of the sidewalls is greater in a system with a short ampoule than with a long ampoule.

Table 4. Dimensionless Parameters Which Are Coefficients in the System of Equations.

• PECLET NUMBER (Pe)	INDICATES THE STRENGTH OF THE STEFAN WIND IN TERMS OF ITS EFFECTS UPON THE INTERIOR PROFILE OF SPECIES CONCENTRATION.
• PRANDTL NUMBER (Pr)	RATIO OF THERMAL DIFFUSIVITY TO VISCOSITY.
• SCHMIDT NUMBER (Sc)	RATIO OF SPECIES DIFFUSIVITY TO VISCOSITY.
• ASPECT RATIO (A)	RATIO OF THE LENGTH OF THE AMPOULE TO ITS RADIUS.
• RAYLEIGH NUMBER (Ra)	STRENGTH OF THE BUOYANCY EFFECTS DUE TO GRAVITY.
• REYNOLDS NUMBER (Re)	STRENGTH OF THE STEFAN WIND RELATIVE TO THE VISCOSITY OF THE GASEOUS MIXTURE.

When gravitational effects are considered, the vapor has buoyancy forces acting upon it, due to density variations in the fluid. Both temperature and species concentration affect the buoyancy. When buoyancy effects due to temperature are important, fluid motions (convection) occur in the vapor which are very dependent upon the exact nature of the furnace that is used to control the temperature on the ampoule's surface. For example, if adiabatic sidewalls are assumed, the convection in a case that is heated from below enhances the mass flux near the center of the crystal and suppresses it near the ampoule wall. When the sidewalls are maintained at a relatively warm temperature, the buoyant convection suppresses crystal growth near the center of the interface and enhances growth near the sidewalls. The information obtained as a result of this numerical modeling, along with the analysis of the experimental results, should provide a much firmer foundation upon which to design future crystal growth methods, for both ground- and space-based operations and experiments.

Miller, Timothy L.: Numerical Modeling of Physical Vapor Transport in a Vertical Cylindrical Ampoule, With and Without Gravity. NASA Technical Paper 2620, 1986.

T. L. Miller/ED42
(205) 544-1641
Sponsor: Office of Space Science and Applications

Solution Crystal Growth

A research effort is being carried out on the study of crystal growth from solution. This effort includes both ground-based laboratory studies and flight experiments. Until recently most of our efforts were concentrated on the study of triglycine sulfate (TGS) growth and applications. The highlight of this study was the May 1985 Spacelab 3 flight experiment in which single crystals of TGS were successfully grown, utilizing the Fluids Experiment Facility (FES) shown in Figure 30. Analyses of the results of that flight are still in progress. These include measurements of the physical properties of the crystals, analysis of the optical images of the interaction of the crystal-solution system during growth, fabrication of an infrared thermal detector element from one of the crystals, and a comparison of the growth data with a mathematical model for diffusion-controlled growth.

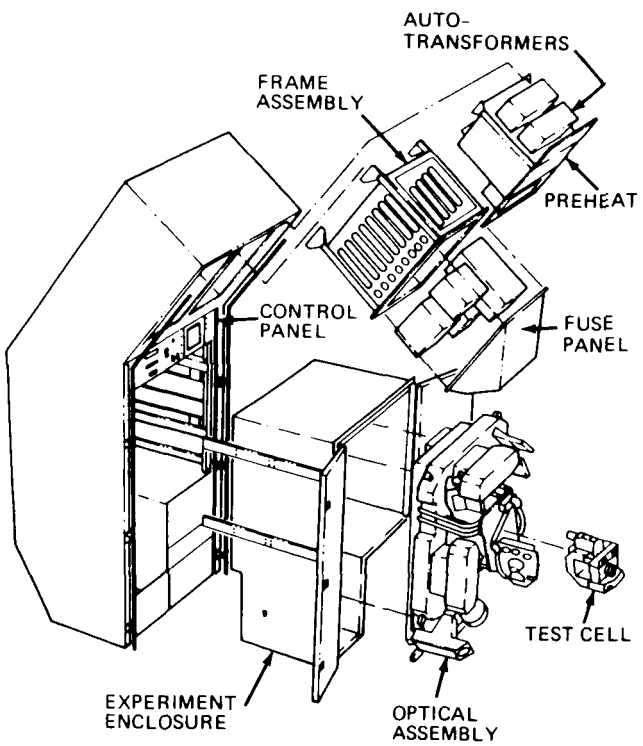

Figure 30. FES Rack Assembly.

Ground-based research has been expanded to include the identification and study of many other crystals that can be grown from solution and that have potential for space flight experiments due to the possible advantages of a low-gravity growth environment. Such materials are being identified and the research literature surveyed for their applications and physical properties. One example of such material is urea, which is of interest because of its non-linear optical properties, and which can be grown using several different techniques. At present these crystals are being grown from aqueous solution in the laboratory.

In addition to identifying materials of interest and determining their crystalline growth characteristics, the development and application of optical techniques for the study of the crystal growth process and for characterizing the defect structure of the grown crystals is being pursued. A unique technique of shadowgraph imaging is being used for the precise determination of the equilibrium temperature of a growing crystal in a given solution concentration. This information is used to generate solubility curves which are essential for controlled crystal growth. Holographic techniques are used to image crystals during growth, both in the lab and during spaceflight experiments on the FES. Their reconstructed images can be used to produce interferometric images which show the crystal-solution boundary layer during growth. A laser scattering technique used in conjunction with a microscope, a detector, and a computer system, and collectively termed the laser scattering ultra-microscope, has been developed. This instrument is being used to map in three dimensions the distribution of scattering centers such as inclusions within a crystal. Since this is a non-destructive technique, it is very valuable as a characterization tool. Etch pit counts from crystals give a quantitative measure of the density and distribution of dislocations within a crystal. An optical technique for partially automating this procedure is being developed, as it is a slow and laborious process when done manually.

Owen, R. B.; and Kroes, R. L.: Holography on the Spacelab 3 Mission. Optics News, 11 (7), 12-16, 1985.

Morgan, S. H.; Silberman, E.; Kroes, R. L.; and Reiss, D. A.: Raman Study of the Diffusion of Triglycine Sulfate in Aqueous Solutions. Appl. Spectro., 40 (1), 35-388, 1986.

Lal, R. B.; Aggarwal, M. D.; Bratra, A. K.; Kroes, R. L.; Wilcox, W. R.; Trolinger, J. R.; and Cirino, P.: Growth of Triglycine Sulfate (TGS) Crystal Aboard Spacelab 3. Science, submitted, 1986.

R. L. Kroes/ES76
(205) 544-7770
Sponsor: Office of Space Science and Applications

Protein Crystal Growth

Protein crystal growth in space has generated significant attention because of the potential applications for determining the three-dimensional structure of the proteins. Theoretical and experimental research indicates that density-driven convective flow patterns and sedimentation due to gravity can influence crystal growth. As part of a program to investigate the influence of gravity on protein crystal growth, ground- and Shuttle-based experiments are in progress, and suitable techniques and equipment for protein crystal growth in space are being developed. The research program includes several phases of hardware development, beginning with a simple prototype system and evolving to an automated protein crystal growth unit that will permit the major variables in protein crystallization to be monitored and controlled during the crystal growth processes. As part of the first step in hardware development, protein crystal growth experiments have been performed on four Shuttle flight missions.

Protein crystals are extremely fragile since they are stabilized by relatively weak crystalline interactions. Therefore, it might be expected that protein crystal formation would be especially affected by fluctuations in the growth environment, including those caused by sedimentation or convection in gravitational fields. Several laboratories around the world are involved in efforts to investigate gravitational effects on protein crystal growth. The first reported space experiments on Spacelab 1 indicated that space-grown protein crystals are considerably larger than crystals of these proteins obtained under the same experimental conditions on Earth. The results of the four recent Shuttle flights confirm some advantages to protein crystal growth in space.

In microgravity, it is expected that crystals will grow in isotropic environments completely surrounded by the growth medium. Growth in such isotropic environments may affect crystal morphology. Convection in solution growth is caused by density gradients that occur when solute is depleted from the solution at the growing crystal surfaces. Convection will force solution to flow past the crystal, thus bringing material to growing crystal surfaces at a rate that is significantly different from the steady-state diffusion rates that would be predominant in quiescent solutions. The flow patterns may generate significant variations in concentration at different parts of a crystal, thus leading to non-uniform growth rates. Also, convection may lead to significant physical stirring of growth solutions. In general, it is expected that such stirring effects might alter nucleation and growth processes. Contacts with vessel walls can lead to heterogeneous nucleation. In the absence of gravity, it is possible to form stable spherical droplets of crystallizing materials, without the extensive wall effects that generally accompany crystallization experiments on Earth.

The Shuttle experiments were designed to optimize the major variables in vapor diffusion protein crystal growth. Experiments related to drop stability established that in orbit large droplets (30 to 80 μl) are stable on blunt syringe tips even when Shuttle maneuvering rockets were fired. Although protein crystals have been grown in droplets as large as 80 μl, the experiments to date indicate that smaller droplets will ensure complete equilibration during the limited period (3 to 7 days) available for protein crystal growth on Space Shuttle missions. Ground-based and flight experiments also have provided qualitative information about equilibration rates within the vapor diffusion chambers. These studies have suggested that equilibration rates are significantly slower under microgravity conditions, presumably because of suppressed convection effects. The vapor equilibration chambers have been designed to accelerate these rates by increasing the surface area of wick exposed in the chambers and decreasing the distance between the protein drop and the wicking material.

During the most recent Shuttle experiments on STS-61C, crystals were grown of all proteins that were tested, including hen egg white lysozyme, human serum albumin, human C-reactive protein, bacterial purine nucleoside phosphorylase, canavalin, and concanavalin B. That particular Shuttle mission was prematurely shortened, and the protein crystal growth experiments were deactivated during the third day of the flight. Although many of the protein solutions had not completely equilibrated during that period of time, relatively large x-ray quality crystals were obtained for all of the proteins except lysozyme. In addition, photographic records of the crystallization solutions in the vapor diffusion apparatus were obtained while in orbit.

It appears that the elimination of density-driven sedimentation can affect crystal morphology. The best example of this is canavalin, which in space grew crystals that were dispersed through the droplets. Nearly all the space-grown canavalin crystals appear to have formed from separate nucleation sites, resulting in uniform morphologies. On the other hand, canavalin crystals grown by this method on Earth generally form as fused aggregates at the bottom of the droplets. Human C-reactive protein, an entirely new crystal form which had not previously been identified in ground-based crystal growth experiments, was obtained from Shuttle experiments. Crystallization of C-reactive protein has been studied extensively over the past 8 years at the University of Alabama in Birmingham, and only one crystal form has been obtained in these experiments. A new crystal form was first observed for C-reactive protein from experiments on STS-61B, and copious quantities of this crystal form were obtained on STS-61C. It diffracts to an appreciably higher resolution than the original crystal form. The new crystal form has now been obtained in ground-based experiments using the Shuttle hardware, so it may be influenced by altered equilibration rates or other experimental conditions that are hardware-dependent. It is not yet clear how microgravity affects the distribution of these two crystal forms of human C-reactive protein.

It is not clear whether the internal order or diffraction resolutions of space-grown protein crystals are significantly different from those of crystals grown on Earth. It will be necessary to do detailed comparisons involving large numbers of crystals grown under well-controlled conditions on Earth and in space before the potential effects of microgravity on protein crystal quality can be evaluated.

R. S. Snyder/ES76
(205) 544-7805
Sponsor: Office of Space Science and Applications

Crystal Growth of Organic and Polymeric Materials

Considerable interest has recently centered on organic molecular solids because of their nonlinear optical properties and their potential use in optical devices for optical information processing, telecommunications, and integrated optics. Of substances that possess nonlinear properties, polymeric materials consisting of parallel chains which serve as a delocalized π-electron system are one of the most promising. Examples of these materials are the polydiacetylenes. These materials not only have very large nonlinear optical susceptibilities but also very short response times.

The need for pure, defect-free single crystals of such materials makes the method and conditions for growing large single crystals a determinant factor. The growth of such crystals under Earth-gravity conditions invariably involves convection, which results in compositional variations and crystal imperfections. The reduction of such buoyancy-driven convections would require a low-gravity growth environment.

A ground-based investigation to explore the role of gravity in the processing of such technologically important materials has been initiated. The model diacetylene TCDU ($RC{\equiv}C{-}C{\equiv}CR$, where $R = -(CH_2)_4OCONHC_6H_5$) was studied, using the directional solidification technique. Several experiments were performed, varying the temperature gradient, speed of solidification, and shape of sample container. The results of the last trial were encouraging, as a single crystal several centimeters in length was grown. The crystals grown are currently under study by x-ray diffraction to determine their perfection and degree of polymerization. Other methods of crystal growth will also be used, as well as methods of controlling and measuring the effects of convection. This work was carried out in collaboration with GTE Corporation.

M. Vlasse/ES75
(205) 544-7781
Sponsor: Office of Space Science and Applications

Effects of Microgravity on Model Polymer Systems

The investigation exploring the effects of gravity on the crystallization of macromolecular systems has been completed. To optimize the procedure, over 100 samples were investigated in both ground and flight tests. Forty-three samples were judged suitable for statistical analysis, based upon the singularity of gravitational environments during both melt and crystallization processes.

Monodisperse linear polyethylene (molecular weight 52,000) was melted and recrystallized under three gravitational conditions: 0, 1, and 2 g. Two types of acceleration environments were imposed during the zero-gravity studies: non-quantified lateral accelerations, and no lateral acceleration. A cart was designed to allow optical microscopy of the melt-solidification processes. A Mettler hot stage apparatus with a video tape camera and recorder was used. An optical photometer, Leitz microscope, accelerometer, and chart recorder completed the cart. The samples were optically monitored during the melt phase transition; these data were later correlated to thermal and gravitational environments. The samples were then air-quenched in the various acceleration environments. Finally, the samples were characterized post-flight to determine morphology and, subsequently, gravity-induced defects.

The characterization effort for the samples involved correlating the following:

- Melt kinetics to gravity environment
- Crystallization time to gravity environment
- Sample thickness to crystallization environment
- Optical retardation to crystallization environment
- Relative birefringence to crystallization environment
- Spherulite type to crystallization environment
- Spherulite size to crystallization environment
- Degree of crystallinity to crystallization environment

The techniques used included:

- Low-angle light scattering
- Optical microscope (polarized visual mapping, measuring, Ehringhouse compensator waveplate, depth-of-focus measurements)
- Differential scanning calorimetry (DSC)
- Fourier transform infrared (FTIR)
- X-ray diffraction

The effects of gravitational accelerations were manifested both macro- and microscopically. Samples recrystallized in a microgravity environment were thicker (48 to 60 μm) than those fabricated in a high-gravity environment (20 to 37 μm). Those fabricated in a normal Earth environment fell between these extremes (39 to 49 um). The birefringence data were statistically correlated to crystallization gravity conditions.

These data indicated that either (1) a higher degree of order exists in either the crystalline or "amorphous" regions of the microgravity samples, or (2) the microgravity samples have a higher percent crystallinity than the high-gravity samples. Neither the x-ray data nor DSC data showed any correlation between degree of crystallinity and gravity environment during crystallization.

Semi-quantitative optical mapping of the samples provided data correlatable to the crystallization gravity environment. The samples crystallized in the zero gravity, negligible acceleration environment were distinctly more spherulitic, with larger spherulites and less variation sample-to-sample. No such trend was evident from the light scattering, FTIR, or DSC experiments; however, the data are complementary, not mutually exclusive. Finally, the orientation of the ordered regions of all samples was investigated. No correlation was noted for the high-gravity samples. The remainder of the samples was seen to have a majority of the largest, most distinctive spherulites in regions around the periphery of the slice. Further investigation revealed that the center portions of these samples were in some contact with the surfaces (both upper and lower) of the glass array (Fig. 31 and Fig. 32).

Two scenarios have been developed to explain the data and provide a probable, if unproven, interpretation. In the first scenario, under high-gravity crystallization conditions (Fig. 31), the surface tension of the molten polymer is insufficient to counteract the effects of the gravitational fields. The samples remain relatively flat and crystallize on the microscope slide (view B). The slide, though clean, provides numerous sites for heterogeneous nucleation. The samples crystallize

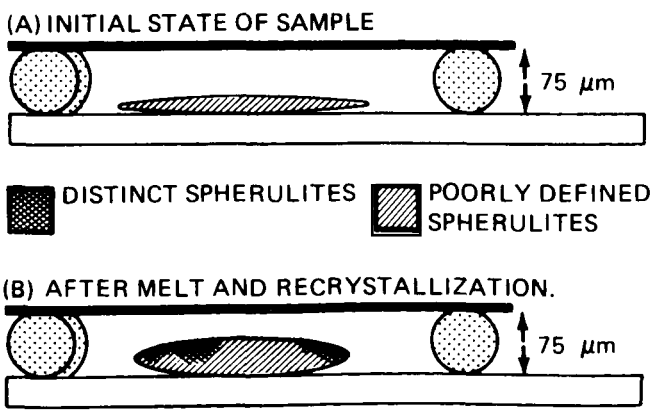

Figure 31. High-Gravity Scenario.

non-uniformly, with regions of optically distinct spherulitic ordering (very clean surface regions) and optically poor spherulitic ordering (surface areas providing multiple nucleation sites).

In the second scenario, under microgravity crystallization conditions (Fig. 32), the surface tension effects cause the molten polymer to "ball-up," the post-solidification thickness is increased, and surface contact with the glass slide is reduced (view B). For some samples, slightly negative g forces lead to contact with the cover glass. Thus, lateral accelerations cause additional surface contact, while under no accelerations, the sample solidifies with minimum contact (views C and D). Again, heterogeneous nucleation will occur most easily in the regions of the sample in contact with the surface. These regions will appear in the central portion of the samples after solidification, while the periphery will contain the majority of the optically distinct spherulites. Further, the edge sections do not solidify on a surface and are therefore free of the surface post-crystallization, as noted during the investigation.

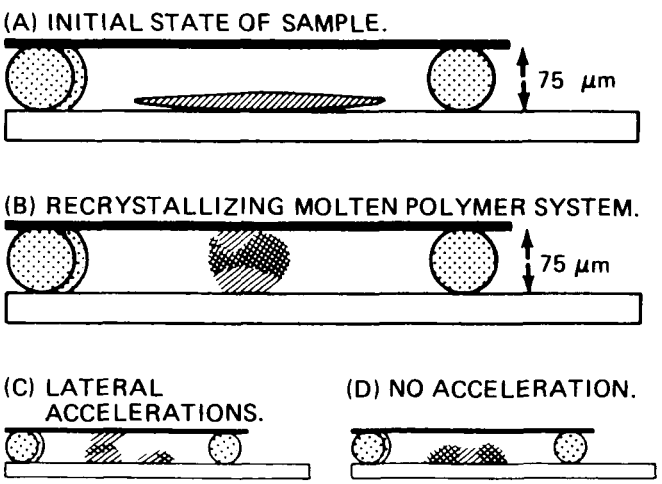

Figure 32. Microgravity Scenario.

These scenarios are fully compatible with all the data, and explain all but one of the observations. This observation, the birefringence results, required further investigation. This new investigation of the convective forces present during the solidification of the non-Newtonian liquid polymer system is currently under way.

B. E. Goldberg/EH34
(205)544-2683
Sponsor: Office of Space Science and Applications

Model Immiscible Systems

The study of transparent immiscible systems has been effective in aiding the study of solidification of metallic monotectic alloys. These systems provide the opportunity to observe processes during solidification. It is now known that preferential wetting and thermal migration contribute to phase separations during monotectic alloy production. Considerations on the nature of wetting phenomena include Cahn's critical-point wetting theory, which relates interfacial energies of liquid phases comprising a binary system in contact with a third component (e.g., container or vapor space) to the contact angle. Another theory is supported by work which shows that if a binary solution is cooled from above its consolute temperature (prior to reaching the consolute temperature while in the single phase region), critical adsorption of the phase having the highest chemical affinity for the container surface will occur. This observation is in agreement with the analysis of Fisher and DeGennes, who predicted that concentrations near a wall are perturbed by the wall. The result is that a layer of the preferentially wetting phase resides near the wall at temperatures immediately above the consolute temperature.

Comparison of phase distributions of liquid-nitrogen-quenched succinonitrile-water ingots in hydrophobic and hydrophilic containers is consistent with a critical wall layer concept. Isotopic adjustments at a temperature immediately above the monotectic temperature present the opportunity to freeze phase distributions in a solid matrix with minimal sedimentation. Varying surface wettability causes either phase to preferentially wet, depending on the nature of the surface. The nature of the container influences the average minority phase droplet size by affecting the droplet's bulk volume fraction. If a cylindrical container is preferentially wetted by the majority phase, a relatively high bulk minority phase volume fraction produces large droplets that move more quickly in a thermal gradient and, provided the discrete phase volume fraction is initially high enough, will produce an intact core column.

Homogeneous miscibility-gap type solutions are by definition nonideal. The direction of nonidealty (positive or negative) could, in part, influence the compositional nature of the "DeGennes" layer

adsorbed on a wall, which should vary with the temperature at which pre-quenching homogenization occurs. The evidence, from partial molal volume determination of hypomonotectic succinonitrile-water solutions at temperatures ranging from 20 to 55 °C, is that solution non-idealty crosses from negative, near the monotectic temperature and composition, to positive at about 30 °C. This variance could effect solidified ingot phase distributions, depending on the nature of the solution container.

Frazier, D. O.; Facemire, B. R.; and Fanning, U. S.: Surface Effects on Phase Distributions of a Fast-Quenched Miscibility Gap Type System: Succinonitrile-Water. Acta Metall. Vol. 34, 63-72, 1986.

D. O. Frazier/ES75
(205) 544-7528
Sponsor: Office of Space Science and Applications

Undercooling of Niobium-Based Peritectics

In order to improve present metals and alloys or to produce new alloys through space processing, it is necessary to understand the effect space processing has on the structure and properties of alloys. Niobium-based peritectics were selected for study for two main reasons. First, these alloys are important technologically in that they have superconducting phases, in particular the A15 phase at or near 75 atomic percent niobium in each system. Second, work on these alloys will provide a new dimension to materials processing in space because of their refractory nature. Presently, only lower temperature metals and alloys are studied in space and low-gravity processing. The alloys being studied are niobium-platinum (Nb-Pt), niobium-germanium (Nb-Ge), and niobium-silicon (Nb-Si). These systems represent a range of metastability of the superconducting A15 phase, in that the phase is present at correct composition in the equilibrium diagram of Nb-Pt, present but at off-stoichiometry in the Nb-Ge phase diagram, and completely absent in the Nb-Si equilibrium phase diagram.

The method selected for studying these alloys has been the low-gravity containerless environment of the MSFC 105-meter drop tube, shown in Figure 33. This environment allows the sample to cool in an environment conducive to undercooling. Undercooling is the cooling of a material below its normal solidification temperature without solidification or crystallization (i.e., the material remains in the liquid state). After undercooling, the alloy will solidify very rapidly. This could result in the formation of non-equilibrium phases in both composition and structure. It is thus the result of undercooling that is being studied in the selected niobium-based peritectic systems through the use of low-gravity containerless processing.

Previously, Nb-Ge alloys of compositions ranging from 13 to 35 atomic percent Ge were heavily undercooled. The microstructure and superconducting properties were extensively characterized. In the last year, effort has focused on

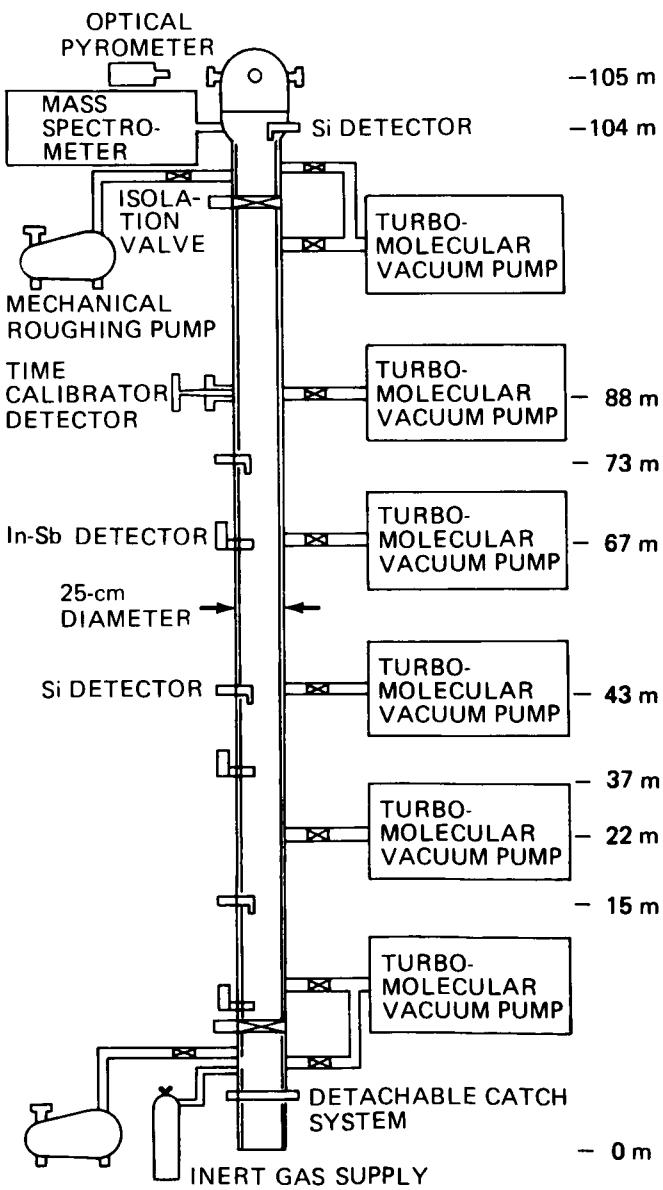

Figure 33. MSFC 105-Meter Drop Tube Facility.

studying this undercooled system using transmission electron microscopy (TEM). The TEM studies provided some interesting results. First, an α-γ eutectic was found instead of the normal β-γ eutectic. This indicates that the β phase was suppressed through undercooling, leading to formation of a hereto unseen metastable phase. Also found was an amorphous region, indicating that solidification was so rapid that no crystalline phase formed in these areas. The ongoing TEM effort will hopefully continue to offer insight into these heavily undercooled alloys.

Investigation of Nb-Pt and Nb-Si alloys was also begun during 1985/86. Samples of both systems have been heavily undercooled (~400 °C), using drop tube furnaces as well as a range of processing parameters. Analysis is under way to measure superconducting properties and to characterize the phases and microstructures present after undercooling. The effort to complete the study of all promising Nb-Si and Nb-Pt compositions continues.

In addition to the Nb-based peritectic studies, a wide variety of pure metals is being studied. At present, approximately 10 pure metals have been heavily undercooled. These pure samples will be used for research in nucleation theory.

Bayuzick, R.J.; Hofmeister, W. H.; and Robinson, M.B.: Review of Undercooling Experiments in Low-g Drop Tubes. Proceedings of 1986 Hume-Rothery Memorial Symposium,TMS-AIME Annual Meeting, New Orleans LA, March 2-6, 1986.

Evans, N.D.; Hofmeister, W.H.; Bayuzick, R.J.; and Robinson, M.B.: Solidification of Niobium-Germanium Alloys in Long Drop Tubes. Metallurgical Transactions A, 17A, 973-981, 1986.

Hofmeister, W.H.; Evans, N.D.; Bayuzick, R.J.; and Robinson, M.B.: Microstructures of Nb-Ge Alloys Processed in Inert Gas in the 100-Meter Drop Tube. Metallurgical Transactions A, 17A, 1421-1428, 1986.

M. B. Robinson/ES74
(205) 544-7774
Sponsor: Office of Space Science and Applications

Phase Partitioning

Two-phase separation is a method widely used in industry for the separation of organic compounds, and in research for the separation of biological cells and proteins. When polymers such as dextran and polyethylene glycol are mixed in water at low concentrations, two-phase systems form, each being enriched in one of the polymers. On Earth, phase separation proceeds rapidly in these systems due to density differences between the phases. A series of short-duration (20-second) experiments aboard KC-135 aircraft have demonstrated that in low gravity, phase separation still proceeds rapidly in spite of appreciable viscosities and low liquid interfacial tensions.

A Phase Partitioning Experiment (PPE) was successfully conducted on the Space Shuttle in April 1985. The object of the PPE was to determine whether the immiscible phases in a two-phase polymer aqueous phase system separated in the absence of density differences between the liquids (Fig. 34). The time course of the process was studied and initial observations made on the effects of particles (biological cells) on the separation. In addition, the effects of varying interfacial tension, phase volume ratio phase viscosity, polymer type, and phase wall-wetting behavior were studied (an oil/water mixing experiment performed on Skylab did not show separation in space). Comparison of laboratory and Shuttle flight data indicates that (1) the two polymer phases do separate in microgravity, (2) orientation of the separated phases is determined by which one best wets the cavity wall (the other phase forming an "egg yolk" near the center of the chamber), (3) the presence of cells does not dramatically alter the phase separation in microgravity, and (4) the rate of phase separation

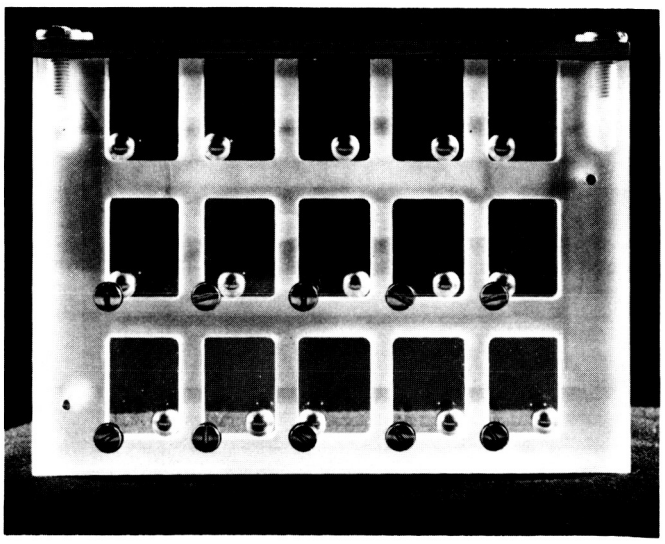

Figure 34. Two-Phase Partitioning Chambers.

was several orders of magnitude greater than predicted by current theories.

Many of the research interests of the NASA Microgravity Science and Applications program involve phase systems. Crystal growth, for instance, involves a solid phase in contact with a liquid or a vapor phase. Alloy production involves two or more metals in the molten liquid state being mixed and allowed to solidify by cooling. Protein electrophoresis involves protein-rich areas moving in protein-poor areas of a liquid. Analysis of phase separation in space should aid space and Earth materials processing, as it will allow us to distinguish between factors dependent and independent of gravity. These independent factors include interfacial tension, phase volume ratio, phase composition (polarity), and wall effects. Wall effects are very interesting, as they control which phase goes to the outside container wall. In space, the separated phases form one phase inside the other, rather than one on top of the other.

The objective of the Phase Partitioning Experiment program is to gain an understanding of the demixing behavior, both on Earth and in space, of liquid-liquid two-phase systems formed by mixing small quantities of two different polymers in simple water-salt solutions. This would lead to understanding the behavior of a number of different types of phase systems of interest and to improving the use of such polymer two-phase systems in laboratory and industrial-sized biotechnical separations of proteins and cells on Earth. Given current biotechnical interest in polymer two-phase systems, the latter goal is primary to the program. Finally, ground-based and space-based experiments have indicated that two-phase separations conducted in low gravity proceed by distinct mechanisms. These mechanisms may allow separations unobtainable on Earth to be carried out in space using polymer two-phase systems.

Related work being conducted at MSFC includes a patented coating to control electroosmosis, which hinders the separation efficiency of electrophoretic methods both on Earth and in space, and the development of a two-phase separation technique which utilizes the sensitivity and efficiency of immune system antibodies. This technique (immuno-affinity partition) greatly increases the potential of the polymer two-phase separation technique. Future objectives include practical application of this work to common separation challenges.

R. S. Snyder/ES76
(205) 544-7805
Sponsor: Office of Space Science and Applications

Rotary Reactor for Latex Production

The Monodisperse Latex Reactor Space Processing Experiment, flown on five space shuttle missions, has successfully produced large-particle monodisperse polystyrene latexes up to 30 μm in diameter with coefficients of variation of 2 percent or less. Additional monodisperse latex particles up to 100 μm in diameter are expected to be produced in space before the flight series ends.

Presently it is not possible to produce usable quantities of large-particle monodisperse polystyrene latexes with this uniformity on Earth using standard seeded emulsion polymerization techniques and equipment, because of buoyancy and sedimentation effects in a gravity environment. During the early stages of the polymerization reaction, the large monomer-swollen latex seed particles tend to rise to the surface of the mixture (cream) because the average density of the particles is less than that of the water medium in which they are suspended. During the later stages of the polymerization, the growing seed particles become heavier as more lower-density monomer is converted to higher-density polymer, and they tend to settle to the bottom of the reactor. As the particles are grown to sizes larger than about 3 μm, the rates of creaming and settling become so rapid that it is not possible to keep the particles in suspension using conventional paddle or propellor-type stirrers without resorting to excessive agitation rates. The growing particles are soft and sticky, and increasing the stirring rate causes more violent particle-particle collisions, resulting in flocculation. Since agitating the particles at rates high enough to prevent creaming or settling results in flocculation, a different method of agitation had to be developed to produce these large-size monodisperse latex particles.

To overcome this problem, a prototype rotating-cylinder reactor (Fig. 35), in which the entire

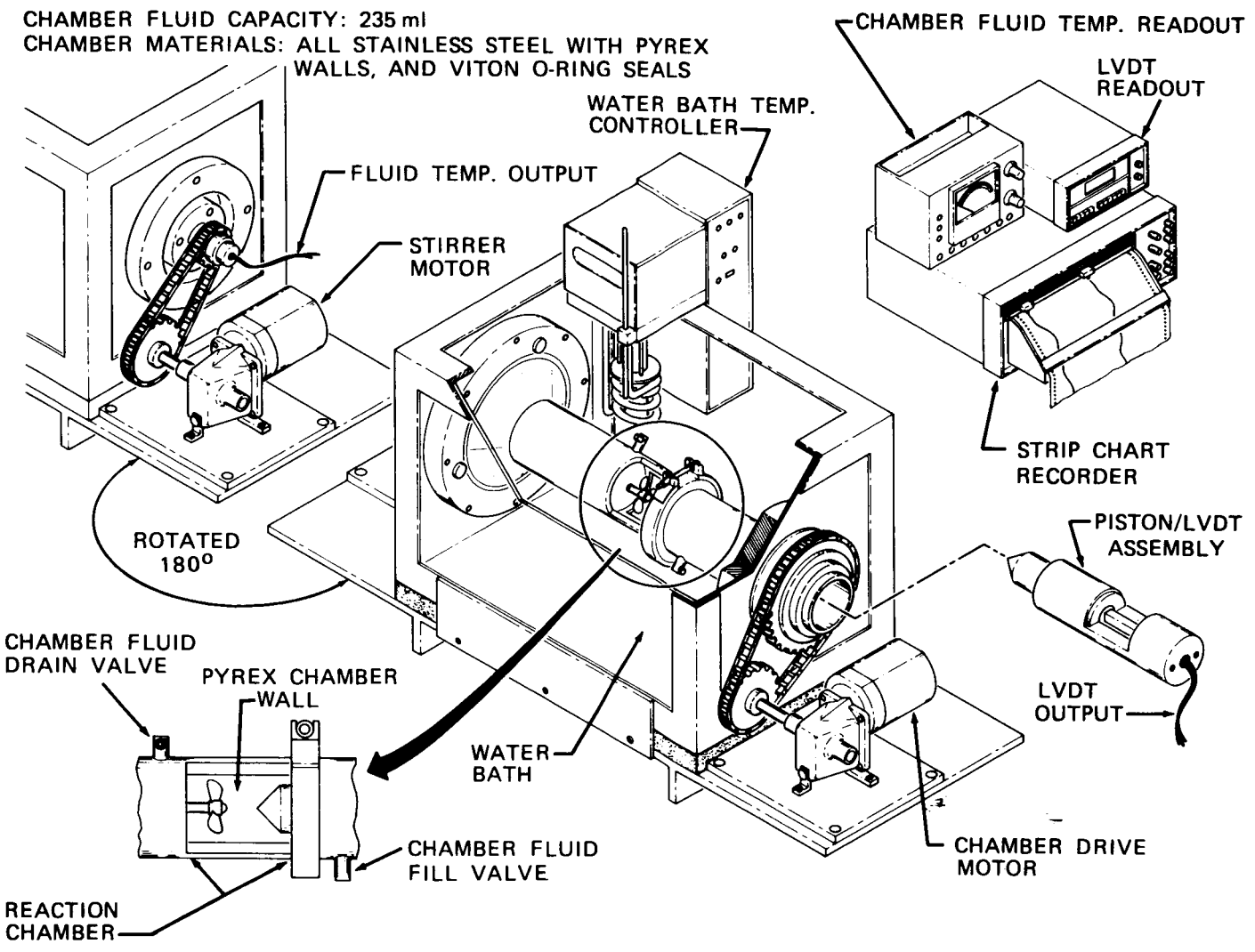

Figure 35. Rotary Reactor.

polymerization reaction chamber is rotated horizontally about its longer axis within a water bath, has been designed and constructed at MSFC. This rotary reactor, which can produce 235 ml of latex per batch, is designed to maintain uniformity in particle concentration and temperature profile with minimal or no stirring. The particles are kept in suspension through the rotation of the reactor. The reactor is basically a piston dilatometer. It is filled completely with the latex-forming mixture to eliminate a latex-air interface which would enhance flocculation by mechanical shear. The latex volume change is determined as a function of temperature and time by a linear variable differential transducer (LVDT) attached to the piston to give the variation of monomer conversion with time. The temperature of the reaction mixture is monitored with a thermocouple, and the temperature and volume-change data are recorded on a two-channel strip-chart recorder.

The objectives of this research effort are to determine whether the rotary reactor could be used to grow monodisperse polystyrene latex particles on Earth to sizes larger than are currently possible using the traditional stirred-tank reactors, and to determine the suitability of the new reactor concept in producing improved low-coagulum commercial (non-monodisperse) latexes of special interest to industry. It is expected that the slow rotation of the entire reaction chamber during the polymerization will prevent the growing particles from either creaming or settling, and the extremely gentle agitation caused by this type of motion will allow the particles to grow without the collisions that would result in flocculation.

Early results indicate that large-size latex particles up to 100 μm diameter can be successfully suspended and polymerized at low reactor rotation rates. Particles manufactured thus far have

exhibited coefficients of variation inferior to those produced on the Space Shuttle, but it is expected that latex quality will improve as latex recipes are optimized for this type reactor.

Plans have recently been approved for a larger version of the rotary reactor, and it should be completed and in operation before the end of FY86. Theoretical fluid dynamical studies have also been initiated to describe particle movement during operation of the reactor.

D. M. Kornfeld/ES76
(205) 544-7808
Sponsor: Office of Space Science and Applications

Mechanics of Granular Materials

Significant progress was made during the past year toward the development of the microgravity experiment, Mechanics of Granular Materials (MGM). After a successful Conceptual Design Review at MSFC in February 1985, ground-based studies continued in support of the forthcoming Preliminary Requirements Review. These studies have established that it is impossible to derive constitutive relations (load-deformation and strength characteristics) of cohesionless granular materials at very low confining pressures in a 1-g terrestrial environment. The inability of test specimens to sustain their own weight, and the action of gravity-induced stress gradients and particle convection within test specimens, render the results of tests per-formed in a 1-g environment meaningless.

Figure 36 shows a typical non-homogeneous deformation pattern of a dry, granular, cohesionless material specimen (3-mm spherical beads), subjected to strain-controlled triaxial compression testing in a 1-g environment and under 1.5 kPa (0.25 psi) confining pressure. The predicted lateral deformation mode of the same specimen in a 1-g as well as in a microgravity environment is shown in Figure 37. In the latter case, because of the absence of gravitational body forces, the predicted behavior is indicative of homogeneous stress and strain fields within the specimen during testing. Figure 38 shows the experimental results and predicted load-axial displacement of the same test specimen in a 1-g environment, as well as its predicted behavior in a

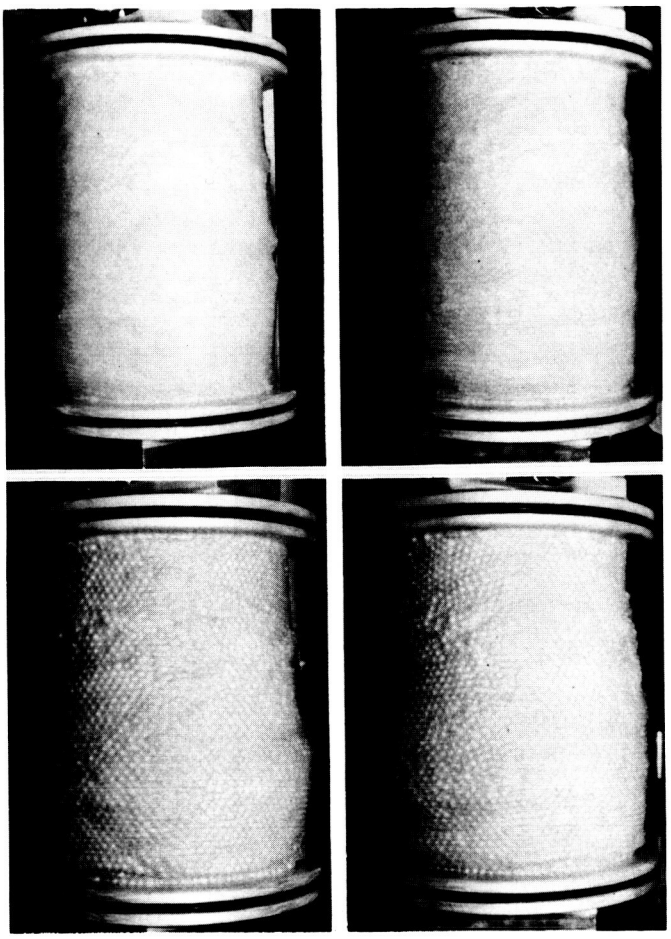

Figure 36. Testing Sequence of Granular Materials (3-mm Spherical Beads) in 1 g.

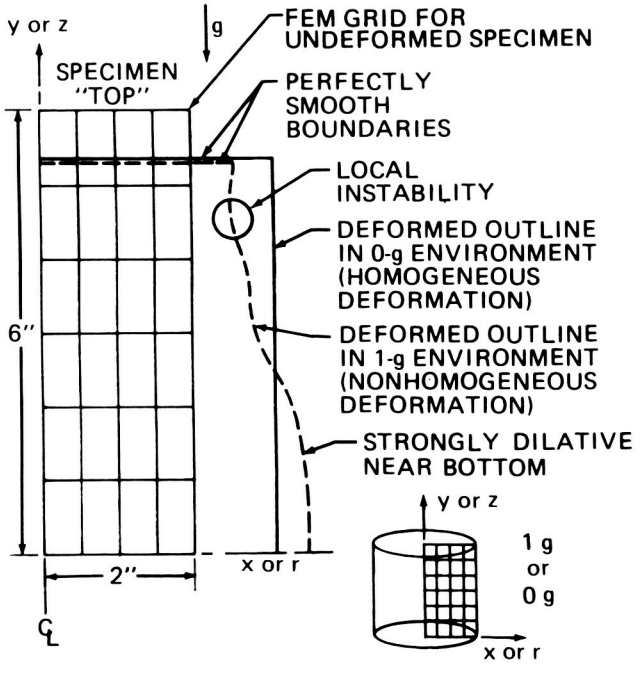

Figure 37. Theoretical Predictions of Specimen Deformation.

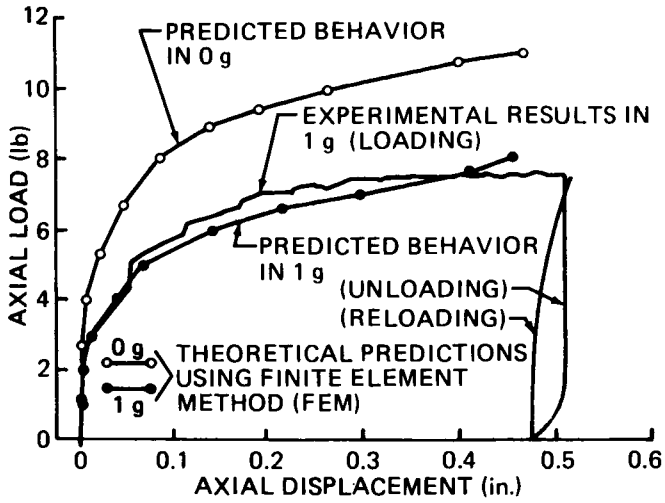

Figure 38. Comparison of Axial Load-Displacement Relations.

microgravity environment. The increased material stiffness of the same specimen under the same external loading conditions in a microgravity environment is attributed to homogeneous stress and strain fields developed in the absence of gravitational body forces.

Other tests, performed in environments of up to 10 g, have indicated that the test specimens under confining pressures of 60 kPa (10 psi) can withstand the dynamic environment of Space Shuttle launching and landing.

A presentation given at the 1986 PACE Symposium on the development status of the experiment was received very favorably by the Science Review Board of the Physics and Chemistry Experiments in Space program. Another milestone for the MGM microgravity experiment was the Preliminary Requirements Review this summer.

Sture, S.; and Costes, N. C.: Mechanics of Granular Materials (MGM). PACE Letter, Fall 1984.

Costes, N. C.; Sture, S.; and Janoo, V. C: Microgravity Experiments on Granular Materials. Symposium O, Materials Research Society, 1986 Fall Meeting, Boston MA (in preparation).

Costes, N. C.; French, K. W.; Janoo, V. C.; Parker, J. K.; and Sture, S.: Mechanical Behavior of Cohesionless Granular Materials at Very Low Intergranular Pressures. AIAA 25th Aerospace Science Meeting, Reno NV, to be presented January 13, 1987.

N. C. Costes/ED42
(205) 544-1637
Sponsor: Office of Space Science and Applications

Solar Physics

Introduction

The research activities of the MSFC Solar Science Branch cover the complete range of solar phenomena associated with the magnetic field. They include studies of the origin of the field through solar cycle studies; convection zone dynamics; the structure and evolution of the field in the observable solar atmosphere; and the major effects of the field, including heating of the solar atmosphere, production of flares and coronal mass ejections, and generation of the solar wind. Primary observational tools are the Vector Magnetograph and the Ultraviolet Spectrometer and Polarimeter on the Solar Maximum Mission (SMM). Data from these instruments are analyzed in combination with the complementary data from other instruments on the SMM, other solar space missions, and ground-based observatories. The results of these empirical studies are combined with theory and computer modeling to construct and test physical models of the observed magnetic phenomena. The results of instrument development, observations, and analysis complement both ongoing and future solar space missions. These include Sunlab, the International Solar Polar Mission, the High Resolution Solar Observatory, and the Pinhole Occulter Facility.

Solar Magnetic Fields

Knowledge of the Sun's magnetic field is vital to understanding solar processes, as the solar field plays fundamental roles in the physics of observed solar phenomena such as sunspots, prominences, explosive flares, and mass ejections into the solar wind. At MSFC there is a unique instrument for measuring the Sun's field, the MSFC Solar Vector Magnetograph. It is unique because it measures the total magnetic vector and not just the line-of-sight component measured with magnetographs at other U.S. solar observatories. The additional knowledge gained from making observations of the total magnetic vector has contributed immensely to our understanding of the magnetic Sun. As a consequence, research in solar magnetic fields at MSFC has produced many significant results.

A major highlight of the research program during FY86 was MSFC's collaboration on the solar

observations made during the Spacelab 2 Shuttle mission in the summer of 1985. Data were obtained jointly with the Spacelab solar instruments on all days except one during the 9-day mission (July 29 through August 6). A special MSFC Observatory Report providing information on our observations was issued and made available to the Spacelab principal investigators and to others in the solar community. The vector magnetic field of an active region studied by the Spacelab experimenters is shown in Figure 39. In the large panel a 5-by-5 arc-minute line-of-sight magnetogram is shown with field lines from a potential field calculation superimposed. Two smaller panels are enlargements of the line-of-sight fields in two separate areas. In each of these smaller panels, the transverse component of the magnetic field is represented by the line segments. The superimposed field lines were derived from a potential field calculation that was made shortly after the observations of the field were obtained. These data were then sent to the mission planners in Houston to aid in their selection of observing targets.

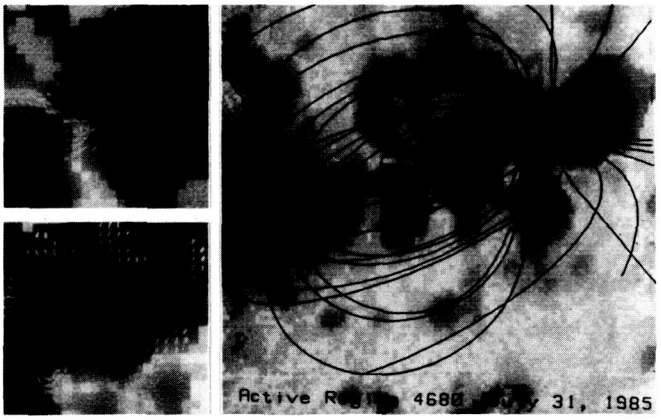

Figure 39. Vector Magnetic Field of Active Region 4680 (Boulder Number).

Analyses of the vector magnetic field data for many active regions show that the field sometimes exhibits a pronounced deviation from a configuration that would be expected if the field was in the lowest possible energy state, i.e., a potential configuration. This non-potential state of the magnetic field is characterized by the term "magnetic shear." These studies of magnetic shear indicate that it is strongly correlated with flare activity: where flares erupt, the field is almost always sheared. However, in some active regions there are areas with large magnetic shear where flares do not occur. It thus seems that large magnetic shear is a necessary but not sufficient condition for the onset of flares. With this in mind, three active regions have been studied to characterize the temporal development of magnetic shear, see how it builds up at known flare sites, and determine if flares can erupt only when one or more of the quantities of magnetic shear, field strength, and electric current exceeds a critical value. A summary of some of the initial findings is given in Table 5, which characterizes the three regions according to the degree of angular shear and field strength (with threshhold values of 80 degrees and 1000 G, respectively, for these two parameters).

Based on these data, two general statements can be made. First, flares did not erupt until the shear and field strength exceeded 80 degrees and 1000 G, respectively. Second, the combination of high angular shear and field intensity does not seem to have a critical value, based on the data for region #4474. The flare that occurred in region #4474 was one of the largest of this solar cycle, a 3B/X15 event that erupted only 2 hours after the data reported in Table 5 were acquired. The two points of emission at the initial onset of this flare were located next to the point of highest magnetic shear. Again this shows that the large shear is essential to the eruption of flares but, based on the data in Table 5, it is not the only factor, as some areas of high shear and high field strength were not the sites of flaring.

Table 5. Magnetic Shear Parameters.

REGION (DATE)	AREAS	MAXIMUM SHEAR (deg)	MAXIMUM FIELD (g)	FLARE ONSET ?
2776 (11-3-80)	NONE	< 80	< 1000	NO
2776 (11-4-80)	NONE	< 80	< 1000	NO
2776 (11-5-80)	1	88	1520	YES
2372 (4-6-80)	1	85	1300	YES
4474 (4-24-84)	1	85	1970	NO
	2	90	1725	YES
	3	89	1740	NO

To pursue this question further, a study of the electric currents flowing in these active regions has been initiated. Initial results have been obtained for the April 1980 region, #2372. In

Figure 40 the distributions of the vertical electric currents, calculated from the vector magnetic field, are shown in an area of repeated flare activity. The sites of flare onset are indicated for a flare that was in progress when the magnetograph data were obtained. The data in views A and B show that the flare initiated in areas of concentrations of the electric currents.

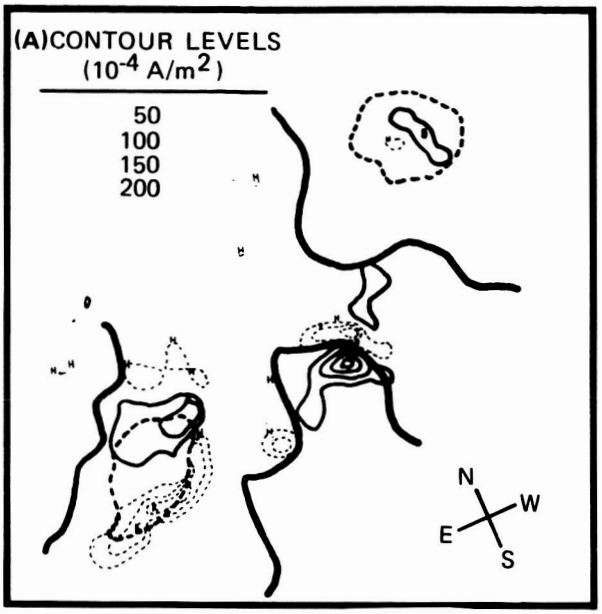

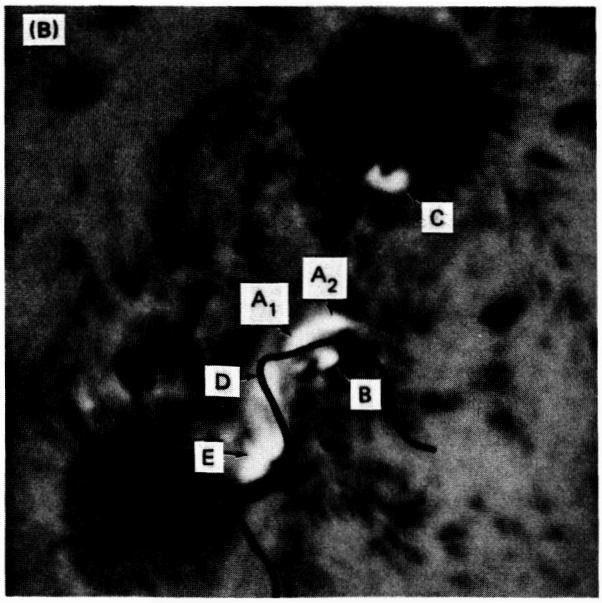

Figure 40. Initial Flare Points at Sites of Currents: (A) Electric Currents: Solid = Flowing Out, Dashed = Flowing In, Curves = Magnetic Neutral Line, Heavy Dash = Umbrae of Two Large Spots. (B) Initial Flare Points.

Taken together, these results suggest that while there is no critical value of shear or field strength that is a sufficient condition for the eruption of flares, the intensity of electric currents flowing in the surrounding atmosphere might be the critical factor — the 'missing' sufficient condition.

M. J. Hagyard/ES52
(205) 544-7612
Sponsor: Office of Space Science and Applications

Transition Region

The chromosphere-corona transition region of the Sun is the complex interface between the chromosphere and the corona. Through the transition region the temperature increases from 10^4 K in the chromosphere to 10^6 K in the corona. The heating of the transition region and corona is one of the long-standing fundamental puzzles of solar physics. The Sun's magnetic field strongly controls the structure of the transition region. Because the magnetic pressure greatly exceeds the plasma pressure, mass flow and thermal energy transport are channeled along the field lines. Consequently, understanding the physics of the transition region hinges on knowledge of the magnetic field threading it.

From the observed fine-scale structure of the transition region and of the photospheric roots of its magnetic field, Dowdy, Rabin, and Moore have proposed that the magnetic structure of the transition region is as shown in Figure 41. This picture

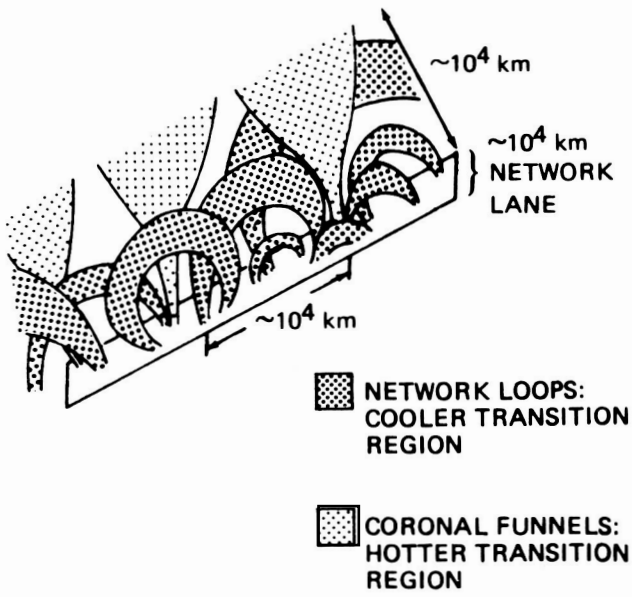

Figure 41. Proposed Magnetic Structure of the Transition Region.

Figure 42. High Resolution Magnetogram from Kitt Peak National Observatory.

was deduced from extreme ultraviolet spectroheliograms from Skylab, ultraviolet (UV) spectra from rockets and from Spacelab 2, UV filtergrams from rockets, and ground-based magnetograms, all with spatial resolution of a few arc-seconds or less. The magnetogram in Figure 42 from Kitt Peak National Observatory has 2 arc-seconds resolution. It shows that the magnetic network of the quiet Sun is a mixture of both polarities, with the patches of flux and separations between opposite polarities ranging in size from the limit of resolution (about 1,000 km) to about 10,000 km.

Because the transition region is observed to persist with height to 10,000 km, the magnetic structure seen in Figure 42 suggests that much of the transition region is contained in magnetic loops linking opposite polarities within the network lanes, as indicated in Figure 41. Models in which the transition region is heated by thermal conduction from the corona have much less than the observed amount of plasma in the cooler transition region at temperatures below 10^5 K. This suggests that most of the cooler transition region is contained in the small magnetic loops that do not reach into the corona. In this concept, the cooler transition region must be heated internally rather than by heat transfer from the corona.

Conduction models do match the observed distribution of plasma with temperature in the hotter transition region at temperatures above 10^5 K. This suggests that the hotter transition is contained in the legs of large coronal magnetic loops, i.e., in magnetic funnels that open into the corona, and that the hotter transition region is in fact sustained by heat transfer from the corona. However, in the new concept, the open funnels are much more constricted in the transition region than in previous models. For plausible shapes of the funnels, the greater constriction significantly reduces the flow of heat back from the corona, thus reducing the heating required to sustain the corona.

In addition to controlling the flow of energy and mass through the transition region, the magnetic field participates actively in the heating of the outer solar atmosphere. Convective motions in and beneath the photosphere move the feet of coronal magnetic loops, distorting them from their unstressed potential-field configurations. The energy stored this way can be released gradually, or in sudden, dramatic instabilities such as flares. These events, called magnetic reconnections because changes in field topology are required for the rapid energy release, are known to occur at magnetic neutral lines separating regions of opposite field polarity. Previous observations of reconnection events have been limited to flares, either in active regions or in x-ray bright points (XBP) in quiet regions. The XBP are the coronal signature of small magnetic bipoles, but not all such bipoles appear as XBP. This suggests that there should be some reconnection events in quiet regions at sites not marked by XBP.

This sort of activity is observable with the Ultraviolet Spectrometer and Polarimeter (UVSP) on the Solar Maximum Mission. Porter, Reichmann, Moore, and Harvey have examined UVSP observations of transition region (C IV) line intensity in the quiet regions and compared them with magnetograms and He I 10830 Å spectroheliograms from Kitt Peak National Observatory. They find that impulsive heating events are common at small bipoles, and that many of these are bipoles other than those that appear as XBP.

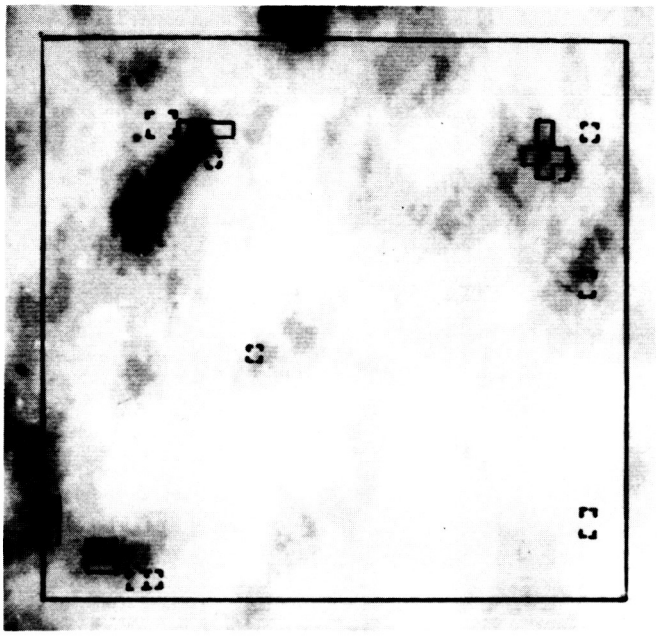

Figure 43. He I 10830Å Spectroheliogram,1 h after UVSP Observations in the 1548 Å Line of C IV.

Figure 44. Same He I Image as Figure 43, with the Magnetic Bipoles Observed at the C IV Sites.

Figure 43 shows a He I image marked with locations of bright C IV sites. Long-lived sites are shown as complete squares, and shorter-lived sites as corners only. The long-lived sites are in the darkest He I areas, which correspond to XBP. Most shorter-lived sites are apparently heated too sporadically to show a coronal signature.

In Figure 44, the magnetic bipoles found at the C IV sites have been outlined on the He I image. All but one of the C IV sites is an identifiable bipole, and the bipole areas correlate well with C IV brightness and He I darkness. These results suggest that the solar transition region and corona are heated mainly by microflare events.

Dowdy, J. F., Jr.; Rabin, D.; and Moore, R. L.: On the Magnetic Structure of the Quiet Transition Region. Solar Physics, Vol. 105, 35, 1986.

Porter, J. G.; Reichmann, E. J.; Moore, R. L.; and Harvey, K. L.: Magnetic Location of C IV Events in the Quiet Network. Space Science Lab Pre-Print, Series 86-134, 1986.

R. L. Moore/ES52
(205) 544-7613
Sponsor: Office of Space Science and Applications

Ultraviolet Spectrometer and Polarimeter

The repaired Solar Maximum Mission (SMM) has continued to furnish excellent data from a number of instruments, including the Ultraviolet Spectrometer and Polarimeter (UVSP). Polarimetric observations of the solar disk have been possible with the UVSP, and analyses of the first observations ever made of linear polarization in the wings of the MgII h and k spectral lines at 2800 Å show exciting results. The polarization is caused by scattering of solar radiation in the spectral lines and is affected by interactions between the energy levels in the magnesium ion. Observations near the solar limb show a trend toward positive polarization (i.e., electric vector parallel to the limb) longward of the h line and shortward of the k line, in agreement with theory. However, there does not seem to be any evidence for the negative polarization predicted between the lines. Thus, it may be necessary to modify to some extent the fairly complex theory of transfer of polarized line radiation in the solar atmosphere.

As the UVSP instrument observes spectral lines emitted from a plasma at temperatures around 10^5 K, studies have been made of how the emitting plasma moves around prominences. In this way insight can be gained into the complex dynamic behavior of the solar plasma and its interactions with the cool prominence material. By measuring the motions relative to the mean velocity at the solar limb it has also been possible to put the velocities on an absolute scale, and thereby deduce that the transition region near

disk center exhibits a downward motion of several km/s. Such results contribute toward understanding of energy and momentum transfer in the solar atmosphere.

E. A. Tandberg-Hanssen/ES01
(205) 544-7578
Sponsor: Office of Space Science and Applications

Coronal and Interplanetary Dynamics

The corona is the atmosphere of the Sun. Its temperature is more than one million degrees, causing the outer portion to expand supersonically and form the solar wind. Because of the Sun's magnetic field, the corona is also highly inhomogeneous. Magnetically confined portions are called coronal streamers and magnetically open regions are called coronal holes because of their relatively low density and brightness.

Physical processes in the solar corona and interplanetary medium are being studied through theoretical models and analysis of data. The motivation for this research is the opportunity to develop an understanding of the energetics and dynamics of processes involved in coronal expansion into the interplanetary medium. These include stationary and time-dependent phenomena, the characterization of the processes that heat and accelerate the solar wind, and the topological structure of the expansion in three dimensions. This work has proven extremely productive in motivating ideas on a variety of space projects.

Figure 45 shows a computer plot of the heliospheric current sheet (HCS), the surface which divides regions of predominantly opposite magnetic field polarity. These plots are unique and have been developed over the past year at MSFC. This particular plot shows the topology of the HCS at the time the European spacecraft Giotto encountered Halley's Comet on March 13, 1986. By chance, this encounter occurred at the time of a predicted intersection of Halley's Comet with the HCS, as illustrated by this figure. This coincidence greatly enhances the scientific value of the mission.

Plots such as Figure 45 are usually made assuming the solar wind speed is constant on the HCS. During the past year, this assumption has been critically examined using Voyager 1 and 2 data. It was found that the assumption is only marginally valid. Specifically, the overall topology of the HCS can sometimes be predicted approximately between the Sun and 1 Astronomical Unit (AU, the distance from the Sun to the Earth) when making the constant velocity approximation. However, beyond 1 AU this assumption becomes increasingly unusable in computing the actual HCS topology, and will have to be abandoned altogether beyond 5 AU.

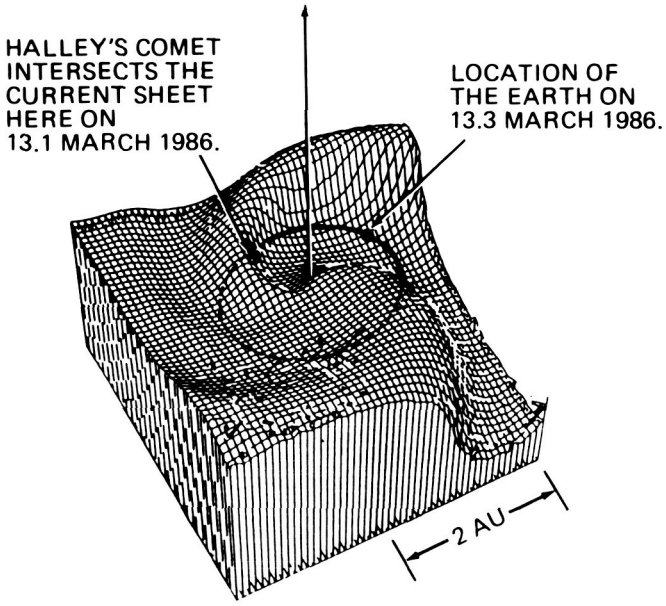

Figure 45. Topology of the Heliospheric Current Sheet.

In a second area of study, a magnetohydrostatic equilibrium simulation of a solar prominence has been developed. The model is used to study the influence of increasing magnetic shear on the equilibrium. Large shear has been found to be an important precursor to solar flares and active region prominence eruptions in MSFC Vector Magnetograph observational studies. Increasing shear initially causes a continuous change of the field from an arcade to an embedded loop inside an arcade. Then, as shear increases past a critical value, the field undergoes a discontinuous topological change to a new equilibrium with an extremely elevated loop. This new equilibrium is probably physically unreachable and therefore reflects the onset of time-dependent evolution and prominence eruption. Figure 46 illustrates three successive calculations of the magnetic field topology, with the shear increasing from top to bottom. The bottom panel shows only the footpoints of the elevated loops when the shear is sufficiently large to allow only the extremely elevated loop solution.

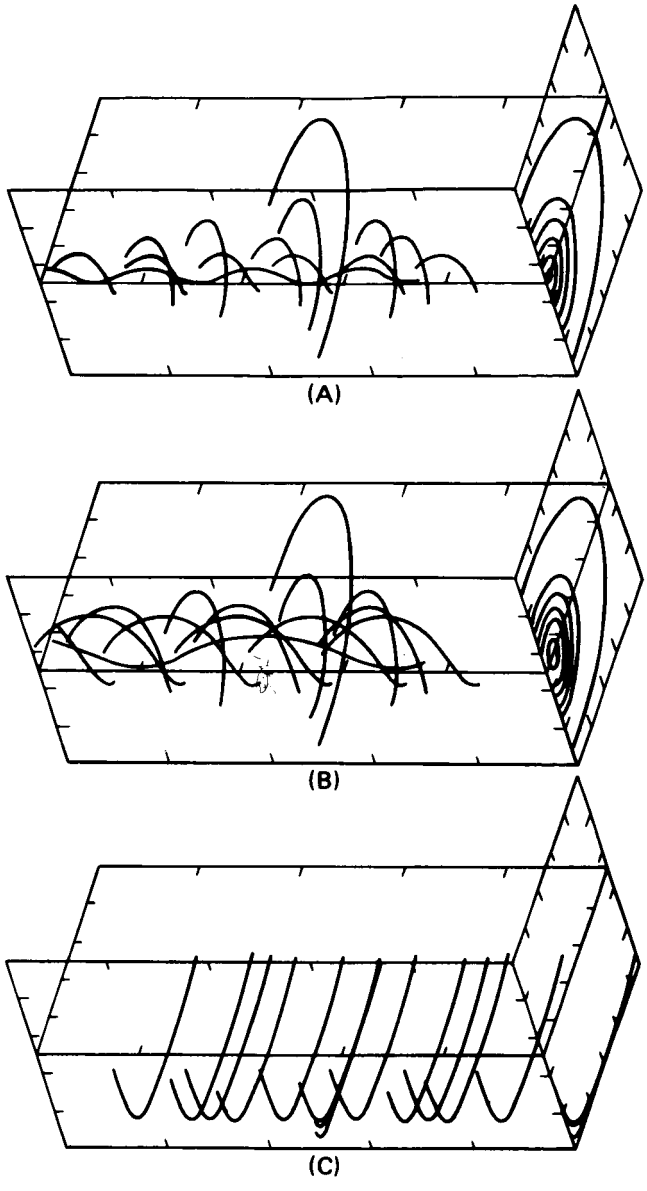

Figure 46. Successive Calculations of the Magnetic Field Topology (Shear Increasing from Top to Bottom).

An, C.- H.; and Suess, S. T.: Reconfiguration of a Prominence Magnetic Field in the Presence of Increasing Magnetic Shear. EOS, 67, 327, 1986.

Suess, S. T.; Scherrer, P. H.; and Hoeksema, J. T.: Solar Wind Speed Azimuthal Variation Along the Heliospheric Current Sheet. The Sun and the Heliosphere in Three Dimensions (R. G. Marsden, ed.), pp.275-280, D. Reidel Publishing Co., 1986.

Suess, S. T.; O'Farrell, J. M.; Hoeksema, J. T.; and Scherrer, P. H.: Topology of the Heliospheric Current Sheet at the Time of the Halley's Comet Giotto Encounter. Bulletin of the American Astronomical Society, 18, 678, 1986.

S. T. Suess/ES52
(205) 544-7611
Sponsor: Office of Space Science and Applications

Convection Zone Dynamics

Convective motions carry heat from the solar interior to its visible surface. These motions start at a layer about two-thirds of the way out from the center of the Sun, where radiative energy transport becomes inefficient, and continue up to the photosphere. In addition to transporting heat, these motions play a more interesting role in generating the Sun's magnetic field. In this role the convection zone dynamics are ultimately responsible for a broad range of solar activity and the structure of the solar atmosphere as well.

During the last year a technique has been developed for examining convective flows in the photosphere together with the large-scale global flows, including the Sun's rotation, differential rotation, and meridional circulation. This technique uses the properties of the spherical harmonic functions to represent each flow type and cleanly separate them for further study. Synthetic data have been constructed and used to test the technique. These data are similar in nature to data that will be obtained with instruments such as the Solar Oscillations Imager (SOI) on the Solar and Heliospheric Observatory. This technique will allow monitoring of the fluid flows on the solar surface on an hourly or day-to-day basis in much the same way that meteorologists monitor motions in the Earth's atmosphere.

The analysis technique may reveal the flows due to giant cells, large convective elements that span the convection zone. There is considerable theoretical support for the existence of giant cells, but observational evidence is still lacking. Giant cell convection is thought to be the prime driver of the solar differential rotation and magnetic dynamo, and to be responsible for organizing active regions and the large-scale solar magnetic field. Detecting and analyzing giant cell flows would be an important contribution toward understanding the solar dynamo and solar activity. A low amplitude giant cell flow pattern was embedded in the synthetic data and successfully extracted by this technique even though it was masked by other flows with amplitudes 10 to 40 times stronger. Data such as that obtained with the SOI will be processed by this analysis technique during the next year to determine the characteristics of the technique itself, as well as those of the large-scale solar velocity fields (Fig. 47).

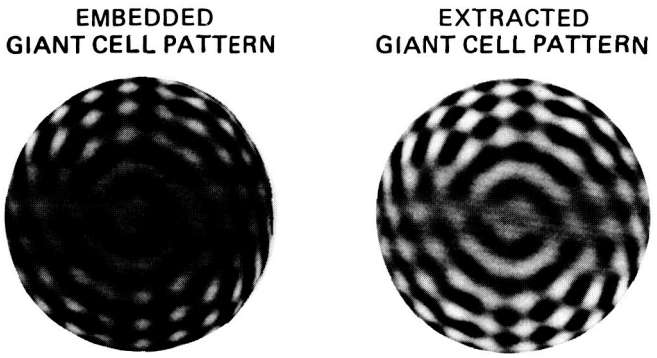

Figure 47. Giant Cell Analysis Results.

In an effort to better understand the solar dynamo, theoretical work has been completed on the nature of the interactions between convective motions and large-scale shear flows such as the solar differential rotation. Previous work has shown how convection, when influenced by solar rotation, can drive large-scale flows such as differential rotation and meridional circulations. In the absence of rotation, however, convection tends to destroy large-scale flows such as these. In the present work, three-dimensional and time-dependent numerical simulations of convection in flows with vertical or horizontal shear were carried out to examine how the influence of rotation alters the interactions between convection and shear flows. These simulations support the earlier work in showing how rotation and shear flows alter the convection in such a way that the convection can feed energy and momentum into the large-scale flows. However, the simulations also showed how rotation and shear flows can produce competing effects that weaken the convection or quench it entirely. Interactions such as these might lead to phenomena in which the convection and the shear flow strengthen and weaken in an oscillatory manner. Future work in this area will incorporate magnetic fields in the numerical simulations to aid and augment our understanding of the solar dynamo.

Hathaway, D.H.: Spherical Harmonic Analysis of Steady Photospheric Flow. Solar Physics, submitted 1986.

Hathaway, D.H.; and Somerville, R.C.J.: Nonlinear Interactions Between Convection, Rotation, and Flows With Vertical Shear. Journal of Fluid Mechanics, 164, 91-105, 1986.

Hathaway, D.H.; and Somerville, R.C.J.: Thermal Convection in a Rotating Shear Flow. Geophysical and Astrophysical Fluid Dynamics, submitted, 1986.

D. H. Hathaway/ES52
(205) 544-7610
Sponsor: Office of Space Science and Applications

Magnetospheric Physics

Introduction

The Earth's otherwise dipolar magnetic field is distorted by the outflow of ionized gas or plasma from the Sun, the solar wind. It is compressed on the upstream or dayside, and stretched out into a long tail on the downstream or nightside, forming a structure referred to as a magnetosphere. Magnetospheric physics is the application of continuum mechanics and plasma physics to obtain an understanding of the flow of matter, momentum, and energy near and within this structure. Such an understanding will enable better comprehension and anticipation of the interactions between solar events, interplanetary conditions, and terrestrial responses. Moreover, the solar terrestrial environment also serves as the laboratory of opportunity for in situ observations of processes which are of importance in other astrophysical plasma situations such as planetary and cometary magnetospheres and stellar atmospheres.

Magnetospheric plasma was initially thought to originate primarily in the solar wind, but measurements have shown that the Earth's atmosphere and ionosphere evaporate continuously into space, providing a dominant source of the plasma within the magnetosphere. With this has come the further realization that dissipation of solar wind energy into the ionospheric plasma enhances this outflow and influences its composition. The importance of this terrestrial plasma source and the processes by which ionospheric plasma is energized and transported within the magnetosphere have been basic motivations for the MSFC research in magnetospheric physics. This thrust has influenced the design of instrumentation, the analysis of data from multiple spacecraft, the laboratory study of flowing plasmas, the development of ionospheric and magnetospheric models, and the development of advanced data networking systems.

Magnetospheric Plasma Studies

Since the discovery of the Van Allen radiation belts by Explorer I, the existence of high-energy particles in the near-Earth environment has been thought to be due to the dominance of solar wind plasma in the Earth's magnetospheric system.

The basic assumptions of this argument were brought into question when a strong source of O^+ plasma from the Earth's ionosphere was observed to be streaming up into the auroral magnetosphere. Recent results from the Dynamics Explorer program have reinforced the significance of the ionosphere as the major source of plasma in the Earth's magnetosphere.

The magnetospheric consequences of these plasma sources have been a major thrust of the research carried out this year at MSFC. The results clearly indicate that there is more than enough plasma being lost from the Earth's ionosphere to account for all the plasma observed in the Earth's magnetosphere, including the energetic plasma components. Furthermore, the polar wind and cleft ion fountain sources found in the Dynamics Explorer/Retarding Ion Mass Spectrometer (DE/RIMS) data play a dominant role in supplying the magnetospheric plasma. This important realization has prompted the DE/RIMS science team to embark on a careful, systematic, statistical evaluation of the low-energy ion data in anticipation of better quantifying the strength of the ion outflow in the cleft ion fountain and polar wind, and of improving understanding of how this ionospheric plasma is initially energized. The results appear to suggest that the Earth supplies the plasma and the Sun the energy to drive the terrestrial magnetospheric system.

Once the low-energy plasma from the Earth's ionosphere is transported into the magnetospheric system it may become energized, thus forming part of the Earth's more energetic plasma populations. This energization takes place through particle acceleration by convective electric fields and by wave particle interactions. The low-energy plasma is an important moderator in wave growth processes. It can also serve as an excellent diagnostic tracer of energization processes due to its relatively small initial energy and correspondingly large perturbation from wave-particle energization processes. One such study of wave-particle processes that has been completed this year involves very low frequency micropulsations with wave periods from 2 to 10 min. Involving significant portions of the magnetospheric system, such low frequency waves have very long wavelengths. For these waves, the full three-dimensional behavior of RIMS-observed plasma has been studied, along with the wave polarization, eccentricity, and amplitude. Observations have been compared with theoretical descriptions of such large-scale events in a way never before possible due to the thorough characterization of the event from the low-energy ion measurements of RIMS. Study of these events helps us to better understand the transport of solar wind energy through the magnetospheric system on a global scale, and particularly in times of high magnetic activity.

Chappell, C. R.; Moore, T. E.; and Waite, J. H., Jr.: Is There Any Solar Wind Plasma in the Magnetosphere? J. Geophys. Res., submitted, 1986.

Giles, B. L.; Chappell, C. R.; Waite, J. H., Jr.; Moore, T. E.; and Horwitz, J. L.: The Auroral Ion Fountain: MLT, L-Shell, and Magnetic Activity Dependences. EOS, 67(16), 338, April 1986.

Waite, J. H., Jr.; Gallagher D. L.; Chandler, M. O.; Olsen, R. C.; Comfort, R. H.; Johnson, J. F. E.; Chappell, C. R.; Peterson, W. K.; Weimer, D.; and Shawhan, S. D.: Plasma and Field Observations of a Pc5 Wave Event. J. Geophys. Res., in press, 1986.

J. H. Waite, Jr./ES53
(205) 544-7635
Sponsor: Office of Space Science and Applications

Outer Planet Investigations

This year a new Research and Technology Objectives and Plans (RTOP) was initiated to study the upper atmospheres and ionospheres of the outer planets Jupiter, Saturn, and Uranus. Several interesting items are currently under study: the Jovian aurora, the effect of water from the Saturnian rings on the ionosphere of Saturn, and the analysis of the recent ultraviolet spectrometer measurements from the Voyager/ Uranus encounter.

One of the most exciting discoveries of the Voyager/Jupiter encounter was the existence of aurorae in the Jovian high latitude atmosphere and the possible magnetic connection of these auroral processes to the Io plasma torus. Subsequent analysis by energetic particle experiments aboard the Voyager spacecraft, as well as the analysis of x-ray emissions from the Jovian auroral zone observed by the Einstein Observatory, suggested that energetic sulfur and oxygen ions (as opposed to electrons in the Earth's auroral zone) were the source of the Jovian ultraviolet (UV) auroral emissions. To investigate this possibility, scientists from the University of Michigan and MSFC constructed a computer

model of the Jovian ion aurora. The results of this study indicated that if sulfur and oxygen ions were indeed responsible for the Jovian UV emissions, then characteristic sulfur and oxygen UV emission lines should also be present. Through participation in the International Ultraviolet Explorer (IUE) Guest Investigator program, an extremely high signal-to-noise ratio spectra of the Jovian aurora was obtained. Subsequent analysis puts a strong constraint on the limited role of sulfur and oxygen ions in producing the Jovian UV aurora and indicates that electrons as well as ions play a role in Jovian auroral processes. Figure 48 shows a plot of the IUE spectra of the Jovian aurora. The UV emission flux in units of erg cm^{-2} s^{-1} $Å^{-1}$ is plotted as a function of wavelength in Å. The H_2 Werner band system is clearly visible above 1320 Å. Note the complete absence of emissions near 1304 Å where emission from OI would be expected in the case of ion auroral precipitation.

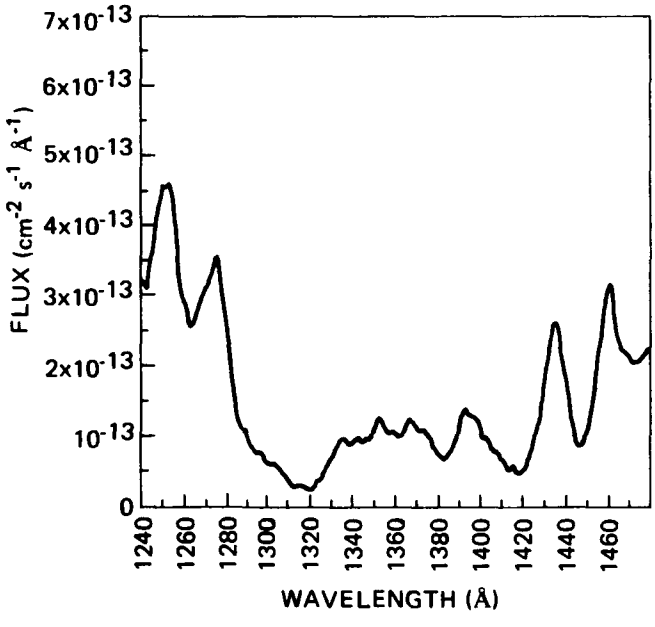

Figure 48. IUE Spectra of the Jovian Aurora.

The Voyager encounter with Uranus spurred considerable theoretical work on the nature of the atmosphere. Previous observations revealed the existence of strong (1 to 2 kilorayleighs [kR]) Lyman-alpha emissions from the planet. In preparation for the encounter, scientists from MSFC and the University of Alabama in Huntsville prepared a model of the neutral upper atmosphere and ionosphere.

Using the limited amount of data available, a temperature vs. pressure (or altitude above the 100-mbar level) profile was established. Drawing on knowledge of similar planetary atmospheres, reasonable estimates were made for the range of exospheric temperature. Based on this temperature profile, the altitude structure of the atomic and molecular hydrogen atmosphere of Uranus was calculated. A greatly extended atomic hydrogen atmosphere resulting from the low Uranus gravity and the high temperatures was shown. Column depths of atomic hydrogen above the methane layer were predicted to be greater than 10^{17} cm^{-2}. Figure 49 shows the density of atomic and molecular hydrogen as functions of altitude and pressure from model calculations for the atmosphere of Uranus. The temperature profile is a match to data from the Voyager infrared, radio, and ultraviolet wavelength observations at 4 degrees latitude.

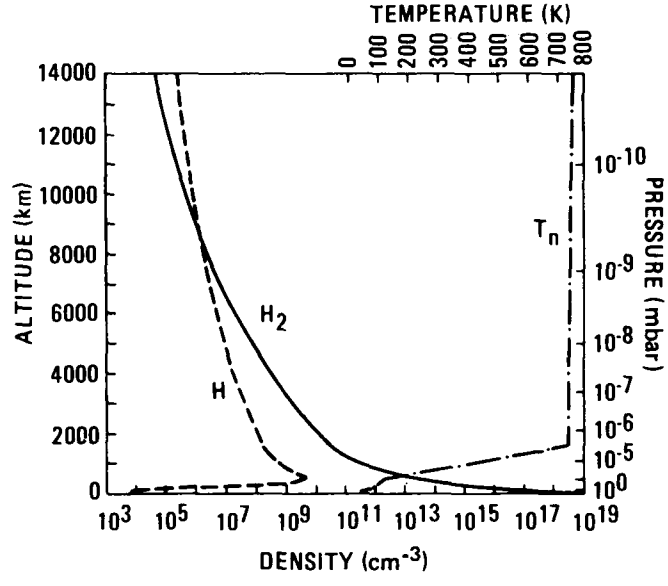

Figure 49. Density of Atomic and Molecular Hydrogen for the Atmosphere of Uranus.

The ionospheric model gave a maximum electron density near 10^5 cm^{-3} at a pressure level between 10^{-5} and 10^{-6} mbar. An influx of 10 keV electrons produced model densities up to 10^6 cm^{-3} while an influx of methane or water reduced the peak density to around 10^4 cm^{-3}. The electron precipitation also resulted in the direct production of approximately 1 kR of Lyman-alpha emission. An additional 400 R of Lyman-alpha was produced by resonance scattering of solar Lyman-alpha from the large column depths of atomic hydrogen.

These results were published prior to the Voyager/Uranus encounter. Recent work has centered on

updating the model and theoretical efforts to explain the observed UV emissions (e.g., the "electroglow"). Collaborative efforts have begun with scientists at the University of Arizona's Lunar and Planetary Laboratory in an effort to provide additional theoretical input for the interpretation of the UV observations.

Chandler, M. O.; and Waite, J. H., Jr.: The Uranus Ionosphere: A Myriad of Possibilities. Geophys. Res. Lett., 13, 6-9, 1986.

Horanyi, M.; Cravens, T. E.; and Waite, J. H., Jr.: An O^+ Ion Aurora Model for the Jovian Atmosphere. J. Geophys. Res., to be submitted, 1986.

Waite, J. H., Jr.; Clarke, J. T.; and Cravens, T. E.: The Jovian Aurora: Ion or Electron Precipitation? J. Geophys. Res., to be submitted, 1986.

J. H. Waite, Jr./ES53
(205) 544-7635
Sponsor: Office of Space Science and Applications

Ionospheric Heating and Transport

The terrestrial ionosphere, particularly in the auroral zones, is accelerated by stresses placed upon it by the solar wind and magnetospheric plasmas at high altitude. The stresses are communicated to low altitudes by the geomagnetic field and result in rapid horizontal flows of ionospheric plasma and strong shears within those flows. The electromagnetic transmission of shear stresses gives rise to electric currents and fields which accelerate ions and electrons in opposite directions along the magnetic field lines. A number of instabilities lead to the emission of plasma waves from this region. Part of the auroral energy dissipated in the ionosphere produces ion heating, which in turn gives rise to upward transport of ionospheric plasma into the magnetosphere. Magnetospheric Physics Branch studies in this area are based upon low-energy plasma instrument development efforts and the analysis and modeling of data from flight instruments.

Recent observations show preferential heating of the majority of heavy oxygen ions (O^+) of the ionosphere. Although preferential heating of heavy ion species has been anticipated theoretically, this is the first observation of such a process in the ionosphere. Ionospheric O^+ is generally at a temperature of approximately 2000 K. In observations obtained from the MSFC low-energy plasma instrument on the TOPAZ sounding rocket within the nightside auroral zone, approximately 1 percent of this O^+ was found to have an average energy about ten times higher than normal. The creation of such a hot population of O^+ will produce substantial transport to higher altitudes where further energization can take place.

Also, the discovery of ring-shaped ionospheric ion velocity distributions has been reported. Figure 50 shows an example of ring-shaped O^+ ion distribution functions observed by the Dynamics Explorer 1 Retarding Ion Mass Spectrometer. Each panel shows the tone-contoured distribution functions in the spin plane of the satellite. The white line through the origin indicates the magnetic field direction. Ordinarily, plasma ions are distributed in velocity with the greatest probability at low speeds, and the probability falling off in a Maxwellian (i.e., Gaussian) manner for higher speeds, regardless of direction. The greater the velocity of the ions, the greater their temperature. In a ring distribution, the most probable ion velocity lies along a ring encircling the local magnetic field direction, and there are relatively few ions at very low or very high speeds. Essentially all the ions have been accelerated to a particular speed perpendicular to the magnetic field, about which they gyrate. Such ions have been coherently accelerated rather than heated, and the occurrence of such a distribution implies a very special process for its creation. It is as if a natural cyclotron were operating in the upper ionosphere.

Observations capable of revealing such phenomena must be sensitive to the mass, energy, and direction of motion of the ions observed. Much of our instrument development effort is devoted to the quest for a sensor capable of scanning over a wide angular range, while responding differentially in energy and mass. A flat plate electrostatic energy analyzer and angle scanner system has been developed for use in a sounding rocket payload to be launched in FY88. The concept has been tested by numerical simulation and by prototype testing. A flexible sensor sequencer based upon state-of-the-art memory chip technology has been designed. All packing and payload interface design is complete, and fabrication, testing, and integration are under way. This angle scanning design has no moving parts, the scanning being accomplished by electrostatic deflection of the incoming ions.

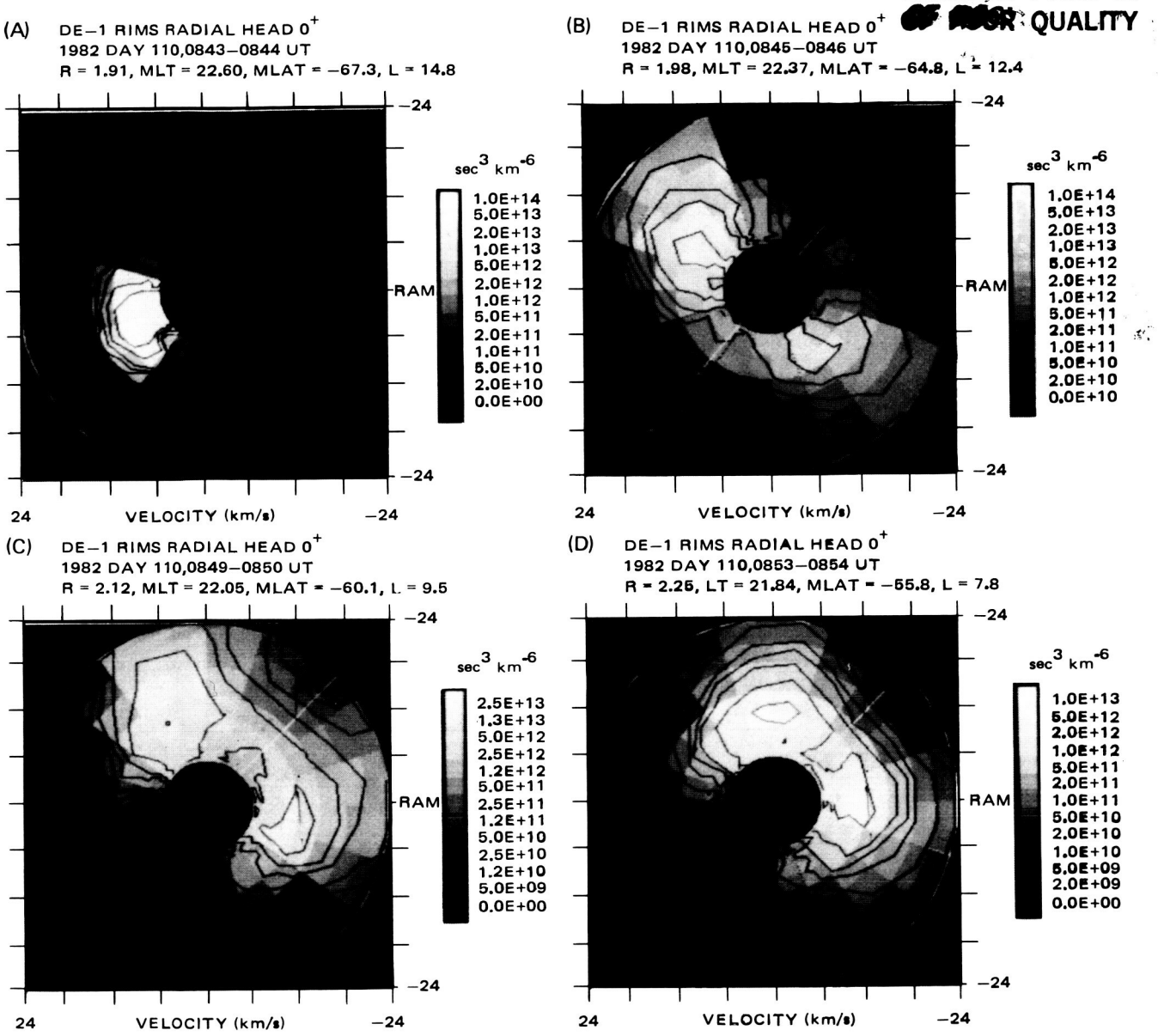

Figure 50. Example of Ring-Shaped O^+ Ion Distribution Functions.

A comprehensive and exhaustive study has been made of the response of the low-altitude collisional ionosphere to the imposition of a demand for plasma at an arbitrarily chosen upper boundary. The demand for plasma can be adjusted to reflect preferential demand for either hydrogen (H^+) or O^+ ions. Demand for H^+ ions exists normally, whereas demand for O^+ ions can be created by ion heating or electron heating. Ion-neutral chemistry creates sources and sinks of the ion species which are accounted for in the model. The neutral atom atmosphere can be adjusted to reflect varying neutral temperatures due to varying geomagnetic activity, solar extreme ultraviolet radiation (solar cycle effect), or illumination (seasonal effect). A number of interesting physical effects are found, including both solar cycle and seasonal variations, as well as a variation with the altitude at which the plasma demand is imposed.

Moore, T. E.; Pollock. C. J : Arnoldy, R. L.; and Kintner, P. M.: Preferential O^+ Heating in the Topside Ionosphere. Geophys. Res. Lett., submitted, 1986.

Moore, T. E.; Waite, J. H., Jr.; Lockwood, M.; and Chappell, C. R.: Observations of Coherent Transverse Ion Acceleration. Proceedings of the Chapman Conference on Ion Acceleration, Am. Geophys. Un., in press, 1986.

Barakat, A. R.; Schunk, R. W.; Moore, T. E.; and Waite, J. H., Jr.: Ion Escape Fluxes in the Terrestrial High Latitude Ionosphere. IAGA 5th Scientific Assembly, Prague, 1985.

T. E. Moore/ES53
(205) 544-7633
Sponsor: Office of Space Science and Applications

Plasma Instrumentation Development

The Retarding Potential Analyzer/Differential Ion Flux Probe (RPA/DIFP) was successfully flown on the Plasma Diagnostics Package of the third Space Shuttle mission (STS-3), and reflown on Spacelab 2. This instrument is shown in Figure 51. The primary scientific objective of the instrument is to study perturbed, nonequilibrium plasmas, including the plasma environment in the near vicinity of the Space Shuttle Orbiter. Particular emphasis was placed upon perturbations to the plasma environment produced by the Orbiter wake and sheath effects, by electron beam emissions from the Fast Pulse Electron Gun Experiment, and by neutral gas emissions from the Orbiter. The instrument performed perfectly in all respects, and approximately 64 hours of data were obtained. The data show that the Orbiter produces significant perturbations to the local plasma, including the creation of multiple ion streams and the ionization of neutral gas emissions out to a distance of 10 m from its surface in the forward direction, and a trailing plasma wake as shown in Figure 52 of the succeeding article, "Shuttle Orbiter/Ionosphere Interactions."

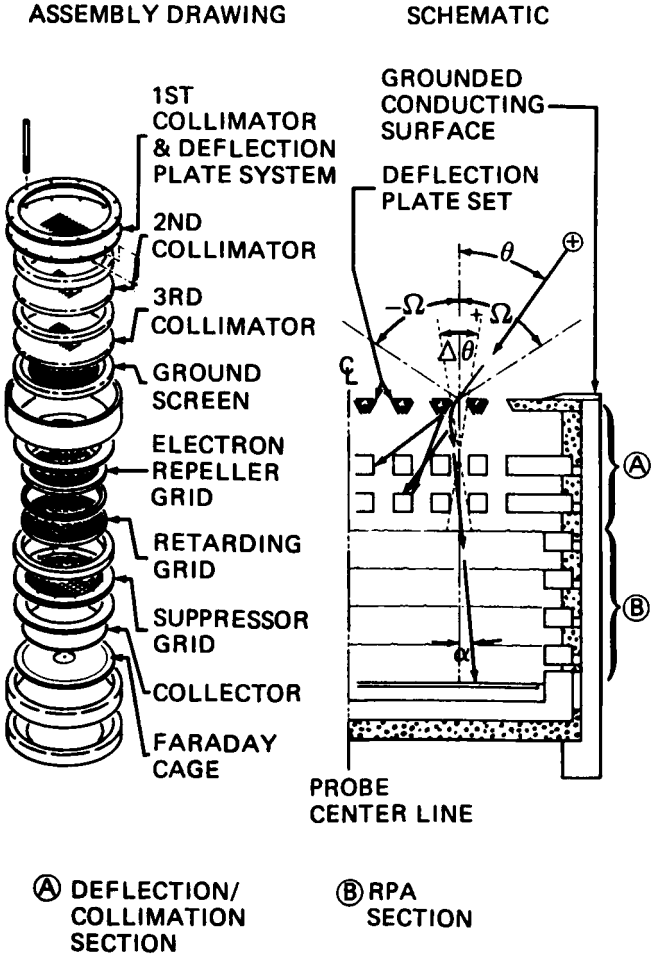

Figure 51. The Spacelab 2 DIFP Sensor Head.

Experience gained from this and other flights of the DIFP has been used to improve the instrument design and operation. These improvements were incorporated into flight instruments for two sounding rocket payloads (Centaur 2-A and Centaur 2-B). The purpose of the Centaur sounding rocket program is to investigate charged particle acceleration mechanisms in the polar regions of the ionosphere to altitudes of approximately 700 km. Significant ion flows, shears, and reversals were observed on the Centaur 1-A and 1-B missions, which passed through the polar cusp region. Unfortunately, the Centaur 2-A payload failed to deploy and no scientific data were obtained. The Centaur 2-B payload is tentatively scheduled for launch in the fall of 1988.

Future instrument development will incorporate a mass analysis capability into the DIFP to provide a Differential Ion Flux and Mass Analyzer (DIFMA) instrument. This instrument will provide the unique capability to separate complex, nonparallel plasma flows and analyze the ion energy and mass consistency of each independent ion stream. The results from Centaur 1-A and 1-B, STS-3, and Spacelab 2 have shown this capability to be essential to the diagnostics of highly complex and nonequilibrium plasma regions existing naturally in space, and in the perturbed near-plasma environment of the Space Shuttle Orbiter.

The suitability of a number of ion mass analysis techniques for coupling with the DIFP instrument, including a number of time-of-flight devices and the Bennet mass analyzer, was investigated this year. Flight instruments based on the resulting DIFMA design have been proposed for the Electrodynamic Tethered Satellite System Mission and as an option for the Air Force Geophysical Laboratory Interactions Measurement Payload for Shuttle experiment to be flown on a polar orbit Shuttle mission.

Hwang, K. S.; Stone, N. H.; Wright, K. H., Jr.; Samir, U.; and Gurnett, D. A.: Theoretical Investigation of Broadband Electrostatic Noise Associated with Secondary Ion Streams Near the Shuttle Orbiter. J. Geophys. Res., submitted, 1986.

Stone, N. H.; Wright, K. H., Jr.; Hwang, K. S.; Samir, U.; Murphy, G. B.; and Shawhan, S. D.: Further Observations of Space Shuttle Plasma-Electrodynamic Effects from OSS-1/STS-3. Geophys. Res. Lett., 13, 216, 1986.

Wright, K. H., Jr.; Stone, N. H.; Hwang, K. S.; and Samir, U.: A Preliminary View of the Orbiter Plasma Wake from Spacelab 2. EOS, 67, 347, 1986.

N. H. Stone/ES53
(205) 544-7642
Sponsor: Office of Space Science and Applications

Shuttle Orbiter/Ionosphere Interactions

Laboratory investigation of the electrodynamic interaction between a body and a flowing, rarefied plasma continues to be an area of investigation with potential applications to solar system plasma physics and to the spacecraft-space plasma electrodynamic interaction. A number of plasma phenomena and processes have been shown to occur over a wide range of conditions that encompasses both the laboratory and certain natural space plasmas. Thus, investigation of these phenomena in the laboratory can effectively contribute to our understanding of natural phenomena in solar system plasma physics and in the interpretation of in situ data. From the measurement technology point of view, the spacecraft-space plasma interaction creates a disturbed region in the ambient medium in which diagnostic instruments must operate to determine geophysical plasma characteristics.

The laboratory investigations have centered around the plasma dynamics of test bodies in collisionless plasma flows. In addition, we have studied specific plasma dynamic processes, including the focusing of charged particles into the wake by electric fields existing in the plasma sheath surrounding a body; the phenomena associated with the expansion of plasma across a strong density gradient, such as near the wake boundary; and the anomalous ionization of neutral particles near a positively-biased surface immersed in a "collisionless" plasma, such as is expected in the case of the first Tethered Satellite System mission.

The development of a streaming binary (two ion species) plasma source has been completed and the study of the effects of multiple species on the overall plasma dynamics of simple test bodies is in process. The investigation of the plasma expansion process continues and will include the effects of a binary plasma. Investigation of the anomalous ionization phenomena, discovered during the last reporting period, is being continued in order to find a physical explanation for the observed data.

The results of these laboratory investigations, along with theoretical treatments and the in situ results from the Ariel 1 and Explorer 3 satellites,

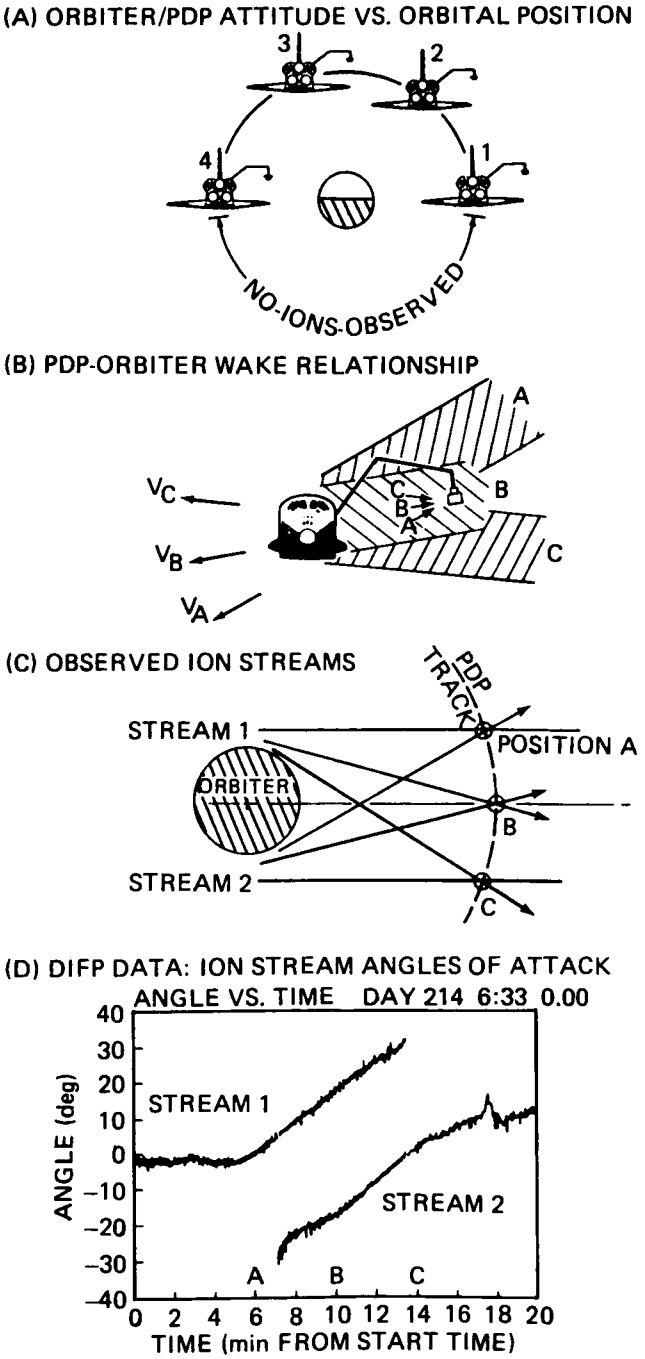

Figure 52. Ion Flow Directions in the Orbiter's Wake.

have formed the basis for early Shuttle-borne investigations, and have provided an invaluable insight into the meaning of the in situ data collected.

The Spacelab 2 Plasma Diagnostics Package (PDP) experiment included the Differential Ion Flux Probe (DIFP) to provide directional measurements of bulk ion motions in the disturbed plasma environment of the Orbiter. An example of the data obtained is shown in Figure 52. The Orbiter was in a fixed, inertial attitude during daylight portions of the orbit (view A), allowing observation of the Orbiter's wake region (views B and C). The measured angles of attack of the two ion streams observed by the DIFP to be deflected around the Orbiter are depicted in view D. Since the PDP was located upstream of the point at which wake closure would occur due to simple thermal motion, and both streams were always observed, it is concluded that the ions were accelerated into the plasma wake of the Orbiter by an electric field. Plasma theory, along with the results of our experimental studies of various plasma processes and phenomena, suggest that such a field could exist either in the plasma sheath of the Orbiter, or at the wake boundary as a result of the plasma expansion phenomenon.

A detailed comparison is being made between the ion streams observed during the STS-3 and Spacelab 2 missions, and the laboratory-measured characteristics of the two acceleration mechanisms. This effort should provide a new insight into the physics of spacecraft plasma dynamics and suggest what conditions are required for certain phenomena to become the governing process.

Wright, K. H., Jr.; Parks, D. E.; Katz, I.; Stone, N. H.; and Samir, U.: More On the Expansion of a Collisionless Plasma Into the Wake of a Body. J. Plas. Phys., 35, 119-123, 1986.

Samir, U.; Wright, K. H., Jr.; and Stone, N. H.: Ion Acceleration: A Phenomenon Characteristic of the Expansion of Plasma Into a Vacuum. Proceedings AGU Chapman Conference on Ion Acceleration in the Magnetosphere and Ionosphere, Wellesley MA, June 3-7, 1985.

Samir, U.; Stone, N. H.; and Wright, K. H., Jr.: On Plasma Disturbances Caused by the Motion of the Space Shuttle and Small Satellites: A Comparison of In Situ Observations. J. Geophys. Res., 91, 277, 1986.

N. H. Stone/ES53
(205) 544-7642
Sponsor: Office of Space Sciences and Applications

Waves In Space Plasmas

The first 30 years of instrumented space flight have brought a growing appreciation for the importance of the magnetospheric processes of our terrestrial environment, and of the various measurements necessary to understand those processes. Most recently, the MSFC Retarding Ion Mass Spectrometer (RIMS) on the Dynamics Explorer 1 spacecraft shed new light on the significance of terrestrial sources of magnetospheric plasma and on the formation of the multi-ion plasma of the magnetosphere.

The characteristics of naturally occurring plasma waves and the details of wave-particle processes are strongly influenced by the presence of both light and heavy ion constituents in space plasma. An example of the complexity of plasma waves in a multi-ion plasma is shown in Figure 53. Here, dispersion curves of cold plasma waves are sketched for a four-component ion plasma. Shaded areas are swept out as the angle of the wave vector is varied from 0 to 90 deg to the ambient magnetic field. Shading is used to indicate the ratio of the wave electric and magnetic fields. Vertical lines indicate the gyrofrequencies of the four ions present.

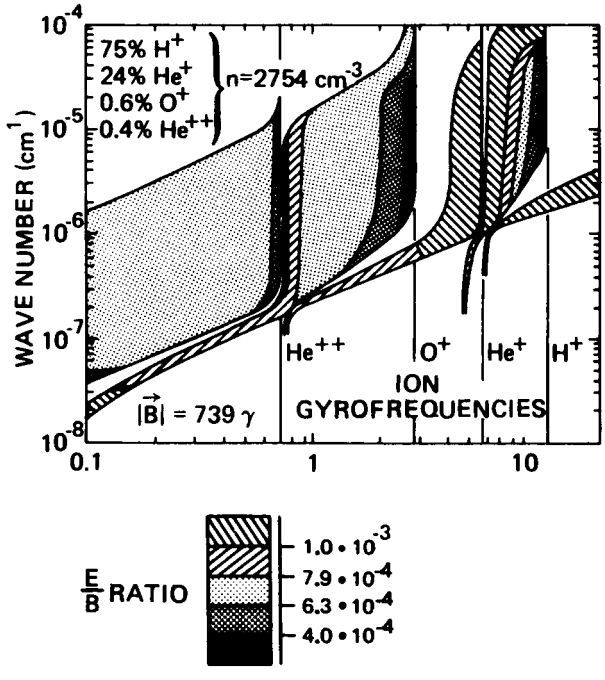

Figure 53. Cold Plasma Wave Dispersion Curves.

The use of RIMS measurements of plasma composition in 1986 has made it possible to explore several wave-particle processes. In the polar cap, plasma outflow of hydrogen and oxygen into the

magnetosphere at unexpectedly high densities has been found. To understand this event, natural wave emissions were used together with plasma measurements by MSFC's RIMS, and the High-Altitude Plasma Instrument. Our detailed understanding of this event is now being used with other observations by RIMS near the Earth's polar cleft and in the magnetotail to complete a picture of this significant plasma outflow.

Several other studies have been undertaken in the region near the plasmapause. One study is of phased bunched helium and hydrogen ions in connection with an ion-ion hybrid or Buchsbaum wave. Cold plasma wave dispersion characteristics have been used to identify the likely wave mode and test-particle simulations of the resonant interaction between the particles and the wave. This study details the first direct identification of phase resonant hydrogen and helium ions at the plasmapause. Because the wave frequency is between the helium and hydrogen gyrofrequencies and is the same as that found in the motions of the ions, the observed event is additionally interesting.

Near the magnetic equator and the plasmapause, hydrogen ions are almost always found trapped at the magnetic equator and coincident with two or more types of wave emissions between the hydrogen gyrofrequency and the lower hybrid resonant frequency. The observed waves have been tentatively identified as lower hybrid and Bernstein wave modes. The persistence of the particles and waves at the equator gives significance to the phenomenon, which may be involved in energy transport from the energetic ring current to the plasmaspheric particle populations, and may influence plasmaspheric filling.

Gallagher, D. L.; Menietti, J. D.; Burch, J. L.; Persoon, A. M.; Waite, J. H., Jr.; and Anderson, R. R.: Evidence of High Densities and Ion Outflows in the Polar Cap During the Recovery Phase. J. Geophys. Res., 91, 3321-3327, 1986.

Reinleitner, L. A.; Gallagher, D. L.; and Gurnett, D. A.: Ion Cyclotron Resonance With Thermal Helium Near the Plasmapause. EOS, 67, 349, 1986.

Olsen, R. C.; Shawhan, S. D.; Gallagher, D. L.; Green, J. L.; Chappell, C. R.; and Anderson, R. R.: Plasma Observations at the Earth's Magnetic Equator. J. Geophys. Res., submitted, 1986.

D. L. Gallagher/ES01
(205) 544-7587
Sponsor: Office of Space Science and Applications

Atomic Physics and Aeronomy

Introduction

Aeronomy is the study of the physics and chemistry of the upper atmosphere, and the ionized component of this region known as the ionosphere. The various processes taking place in the upper atmosphere all derive their energy from the Sun. This energy arrives at the atmosphere in the form of ultraviolet photons (light) and energetic particles (electrons and protons). A detailed understanding of both the interaction of the solar photons and energetic particles with the atmospheric constituents, and the rich array of photochemical and dynamical processes that result, is crucial to an understanding of the nature and balance of this part of Earth's environment. Many of the atomic and molecular interactions occurring in the upper atmosphere are unique to these regions and provide material for laboratory studies of atomic processes. Many of the processes have unknown or roughly estimated physical parameters which can be quantified if these processes can be made to occur in the laboratory. Once such parameters are measured in the laboratory, the results can be fed back into models of the upper atmosphere to provide information on yet other processes.

A study of the Earth's upper atmosphere involves gathering suitable data on these regions, combining these data with appropriate atomic and molecular parameters, and developing comprehensive numerical models which can reproduce and predict the detailed behavior.

Ultraviolet Spectroscopy of the Stratosphere

The stratospheric ozone layer plays a role of major importance to life on Earth, in that it filters out harmful ultraviolet radiation before it reaches the surface. It is thus essential to conduct the studies necessary to understand the processes that control the balance of ozone. Ozone is lost in reactions with constituents that are both naturally occurring in the atmosphere and others which are being introduced to the atmosphere as a result of man's industrial activities on the surface. Various chemically active molecules (for example, NO, OH, ClO, BrO) are very efficient in the

catalytic removal of ozone, and the concentrations of these molecules must be measured in order to correctly model the ozone. In order to understand the impact of man-made chemicals, an understanding of the role of the natural loss species is required. One of these natural loss species for which there is very little quantitative data is OH. A high resolution echelle-cross disperser imaging spectrometer, shown in Figure 54, has been developed to measure OH in emission in the sunlit stratosphere. The instrument images the OH electronic band at 3090 Å onto an intensified-CCD focal plane detector at a spectral resolution of 0.08 Å.

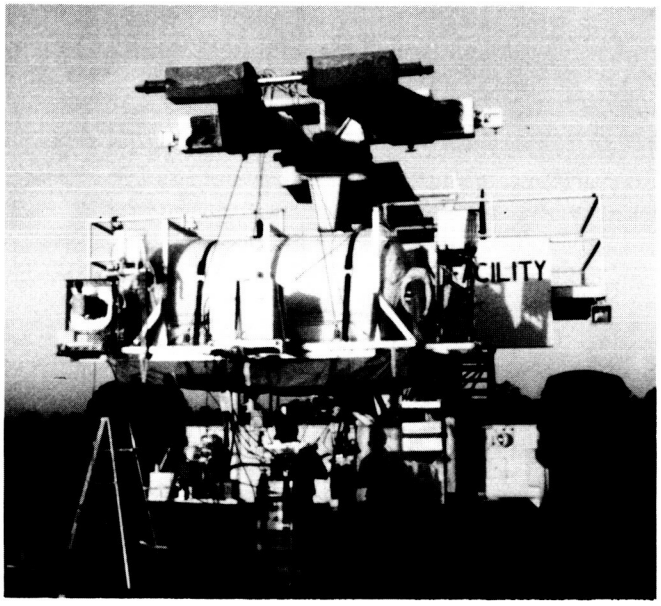

Figure 54. High-Resolution Imaging Spectrometer Onboard the Balloon Launch Vehicle.

This system was flown on a large high-altitude balloon on June 12, 1986, and operated at 40 km for 6 hours. Analysis of the data base thus acquired will provide information on the altitude and diurnal variations of the OH concentration.

M. R. Torr/ES55
(205) 544-7676
Sponsor: Office of Space Science and Applications

Spectroscopic Measurements from the Space Shuttle

The Spacelab 1 Shuttle mission was launched on November 28, 1983, carrying a multidisciplinary payload which included the Imaging Spectrometric Observatory (ISO), an array of five spectrometers for studying the emission spectrum of the upper atmosphere from the extreme ultraviolet to the near infrared. The five spectrometers operated simultaneously, imaging the spectrum in one dimension of a two-dimensional focal plane detector, and imaging spatial information in the other. This was achieved by using an intensified solid state array detector developed for this instrument. During the Spacelab 1 mission, almost 30 hours of observations were acquired with the instrument, much of which was devoted to testing the instrument's performance under a wide variety of operating conditions. These data are being used to compile a spectral survey of the upper atmosphere dayglow spectrum which will be used to define detailed studies to be made with the instrument on future Shuttle missions. In addition, the Spacelab 1 data have been used for studies on a number of specific features and processes.

A relatively bright feature near 2150 Å was noted in auroral spectra in the early 1970's, and was at first thought to be due to nitric oxide (NO). However, the spectra were not consistent with a NO identification, and it was suggested that the feature might be due to a spin-forbidden transition from $N^+(^5S)$ resulting in a doublet at 2143.45 Å and 2139.68 Å. Work in 1982 determined that this same feature should also be produced in the dayglow by solar photons at approximately $\lambda \leq 329$ Å, and might have contaminated measurements of the bright NO band at 2150 Å from which nitric oxide concentrations are inferred. The $N^+(^5S)$ and NO(1- 0) were spectrally resolved by the ISO (Fig. 55) and the brightness determined. The circumstances could be then identified under which the N^+ line would dominate the NO band.

The $O(^1S)$ green line at 5577 Å is produced in abundance near 100 km as a result of three-body recombination of atomic oxygen. Atomic oxygen is difficult to measure at these altitudes using in situ techniques. Thus, measuring the bright 5577 A feature offers (in principal) a straightforward way to remotely monitor atomic oxygen concentrations at these altitudes. However, despite the fact that the $O(^1S)$ green line has been studied longer than any other feature of the airglow, the details of the processes by which the $O(^1S)$ is produced in the mesosphere and lower thermosphere are still not fully understood. The various reactions occurring represent one of the most complex photochemical processes taking

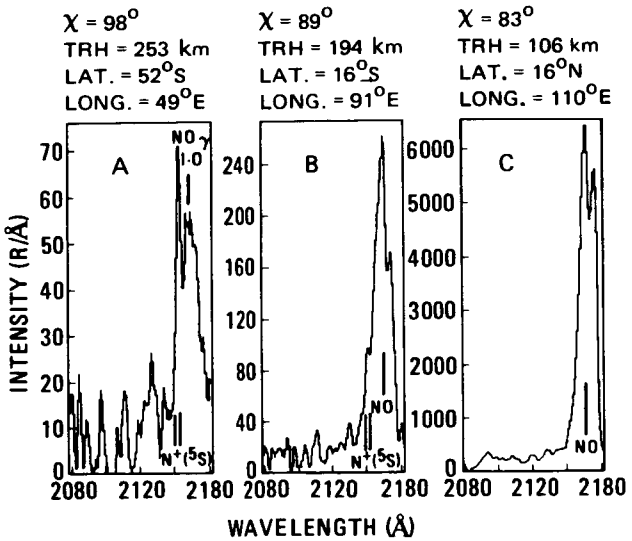

Figure 55. Illustration of the N^+ (^5S) and NO (1-0) Gamma Band Features for Profile 1 (TRH ≡ Tangent Ray Height).

place in the mesosphere. The O(^{1}S) is coupled to emissions from O_2(b $^1\Sigma$), various precursor states of O_2 from which the O_2(b $^1\Sigma$) and O(^{1}S) are formed by collisional deactivation, and also to other atoms and molecules involved in the photochemistry. One of the fundamental questions to be answered is the identity of the precursor state(s) from which the O_2(b $^1\Sigma$) and O(^{1}S) are formed. The ISO on Spacelab 1 obtained limb scans of several of these features. The data appear to best support the O_2(b $^1\Sigma$) arising from deactivation of the O_2 ($C^1\Sigma$) state, although an additional source of O_2(b $^1\Sigma$) is indicated. The O(^{1}S) data appear to favor the O_2 ($A'^3\Delta$) as the intermediate state. The information gathered to date will allow performance of an optimized experiment from the next flight of this instrument on the Shuttle.

The very strong 0-0 band of the O_2 atmospheric system at 7620 Å cannot be observed from the ground due to absorption by the O_2 in the stratosphere. While various rocket profiles have been obtained at night for mesospheric studies of the type described above, the ISO has provided spectra of the O_2 atmospheric bands in the visible dayglow, showing the 0-0, 1-1, 2-2, and 3-3 bands (Fig. 56). These data have revealed a new source of O_2(b $^1\Sigma$) in the upper atmosphere, namely $N(^2D) + O_2 \rightarrow N + O_2(b\ ^1\Sigma)$.

An example of one of the novel measurements made by the ISO on the Spacelab 1 mission is one in which the ISO views the atmosphere tangentially, from an orbital altitude of 250 km. In this

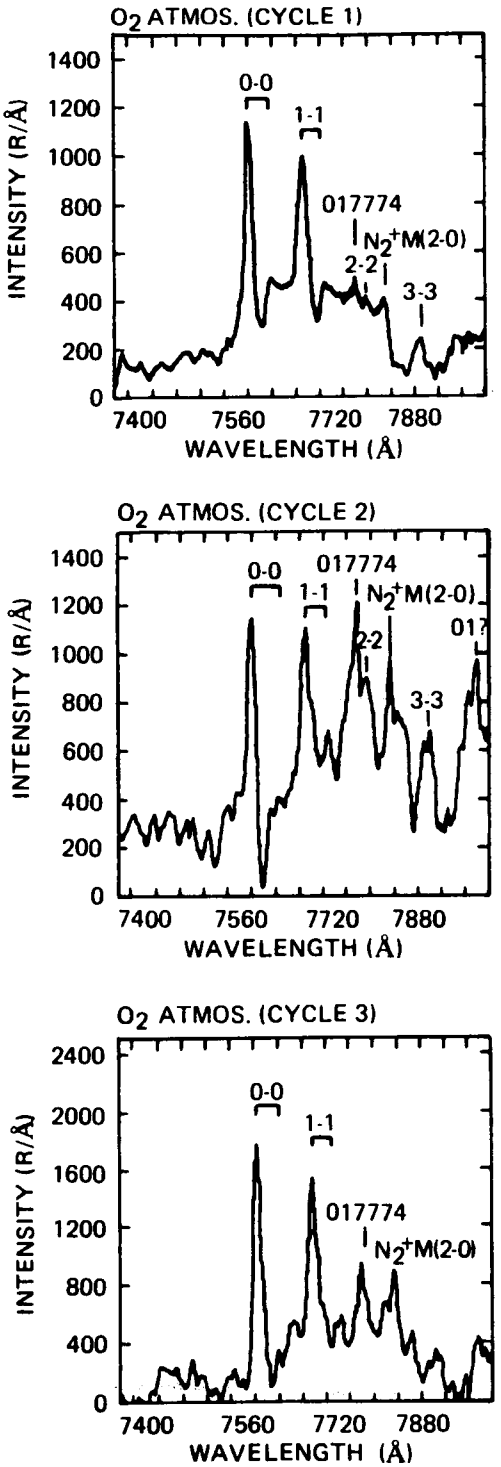

Figure 56. Segments of the Visible Dayglow Spectrum Measured from Spacelab 1.

sequence, the vehicle was oriented so as to place the spectrometer entrance slit perpendicular to the limb of the Earth, with the center of the slit at approximately 94 km. The 0.65-deg field-of-view of the instrument along the slit subtends approximately 20 km, resolved into eight adjacent 2.5-km altitude segments from 84 km to 104 km.

A preliminary analysis of the NO from these data confirms observations by an infrared instrument on Spacelab 1 which found the NO concentration to be much higher than anticipated. A detailed study is in progress.

The ISO will be flown on the ATLAS-1 mission. Measurement sequences will draw on the experience gained from the Spacelab 1 mission in order to optimize investigations of specific issues yet to be resolved.

Torr, M. R.; Torr, D. G.; Baum, R.; and Spielmaker, R.: Intensified-CCD Focal Plane Detector for Space Applications: A Second Generation. Applied Optics, Vol. 25, 16, 2768-2777, 1986.

Torr, M. R.; and Torr, D. G.: The N II 2143 Å Dayglow from Spacelab 1. J. Geophys. Res., 90, 6679, 1985.

Torr, M. R.; Torr, D. G.; and Laher, R. R.: The O_2 Atmospheric 0-0 Band and Related Emissions at Night from Spacelab. J. Geophys. Res., 90, 8525, 1985.

Torr, M. R.; Welsh, B. Y.; and Torr, D. G.: The O_2 Atmospheric Dayglow in the Thermosphere. J. Geophys. Res., 91, 4561, 1986.

M. R. Torr/ES55
(205) 544-7676
Sponsor: Office of Space Science and Applications

Studies of Vehicle-Induced Emissions

Early flights of the Space Shuttle revealed a very pronounced optical effect associated with passage of the vehicle through the ambient atmosphere. Any surface directed into the velocity vector was found to glow orange-red. These glows could be photographed with a hand-held camera and were on occasion visible to the naked eye. Despite extensive research into this phenomenon, its precise cause is as yet unknown. Clearly, unanticipated processes of interest to basic physics and chemistry are occurring. In addition to these surface glows, various measurements have indicated that there is a subtle halo extending out from the vehicle. This halo may be indicative of an interaction region surrounding the vehicle, in which collisions between ambient and induced gases are occurring.

To date, rather limited measurements have been made on these induced glows and halos, with the result that the causative mechanisms have not yet been identified. These unexplained atomic and molecular processes require study, as does their possible impact on investigations involving low light level measurements from the Shuttle or other large vehicles. In order to obtain the necessary information, an ultracompact imaging spectrometer is being developed which can operate from the end of the Shuttle Remote Manipulator System to scan various surfaces at various angles to the velocity vector and over a spectral range of several thousand angstroms.

M. R. Torr/ES55
(205) 544-7676
Sponsor: Office of Space Science and Applications

Astronomy and Astrophysics

Introduction

Space astronomy and astrophysics have been an important part of the space program since its beginning. Marshall Space Flight Center is engaged in theoretical and experimental research in astronomy and astrophysics closely related to scientific payloads and missions. Research areas include x-ray astronomy, gamma ray astronomy, cosmic rays, and infrared astronomy. Flight data obtained during past missions such as HEAO and Spacelab 2 are being analyzed, and new instruments and experiments for future space flight missions are under development. Ground-based astronomical observation and balloon-borne experiments are being carried out in support of space flight objectives and experiments.

X-Ray Astronomy

Investigation of time variability has proven to be a valuable tool for probing the physical nature of galactic x-ray sources. High time resolution data collected by the Time Interval Processor (TIP) of the Monitor Proportional Counter (MPC) on the High Energy Astronomy Observatory-2 (HEAO-2) are currently being studied for clues to the nature of these exotic objects. The recent discovery by the European Space Agency's X-Ray Satellite EXOSAT of quasi-periodic oscillations (QPO) from several bright galactic bulge and burst x-ray sources provides additional motivation for pursuing these studies.

Figure 57 shows a power spectrum obtained from TIP data for the galactic bulge x-ray source GX 5-1. The peak at 15 Hz arises from the quasi-periodic oscillations, while the shoulder rising at lower frequencies (described as red noise) is due to an underlying noise process. Power spectra with these characteristics follow naturally when the x-ray intensity is represented mathematically as shot noise with oscillating shots. Furthermore, several physical models for QPO x-ray sources can be represented mathematically as shot noise with oscillating shots. During the past year, analysis and interpretation of the TIP data has focused on QPO shot noise models.

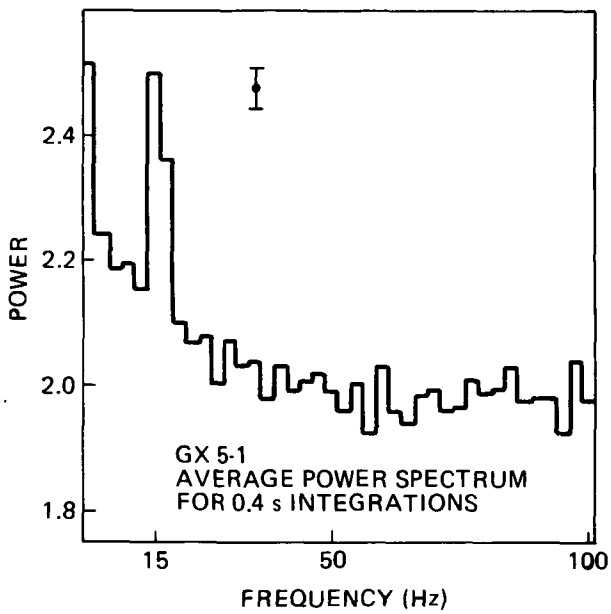

Figure 57. MPC/TIP Power Spectrum for GX 5-1.

Fits to power spectra do not completely determine the parameters of these models. It has been demonstrated that accurate measurement of the third and higher moments leads to additional constraints on the model parameters. If timing data are of sufficiently high statistical quality, then a complete solution for all parameters is possible under certain sets of assumptions. The capability of finding complete solutions for these parameters would greatly enhance the usefulness of shot noise models as probes of the physical processes in QPO x-ray sources.

The simplest model assumptions are not consistent with the power spectra obtained for GX 5-1. This does not mean that shot noise models are unsuitable representations for the data, only that the physical processes underlying the observed variability are complicated. The simplest model assumptions can be relaxed in several ways that lead to power spectra consistent with observations of GX 5-1. These include the adoption of more complicated waveforms for the oscillating portion of the shot profile (instead of a simple sine wave), various distributions for the random variables invoked in these models, and physically significant correlations among these variables. These and other possibilities are presently under investigation. The study of the QPO phenomenon offers a valuable opportunity for increased understanding of the physical processes occurring in galactic x-ray sources.

Associated with the data analysis and interpretation effort is a growing program of theoretical studies of physical processes occurring in the high temperatures and strong magnetic fields associated with compact galactic x-ray sources. Quite a few galactic x-ray sources are observed to pulse with very well-defined frequencies. These objects are widely believed to be strongly magnetized neutron stars with their radiation powered by the accretion of matter from a binary companion. The magnetic field channels the flow of the infalling plasma and creates hot spots on or near the surface; the observed radiation is thus modulated by the rotation of the neutron star. A major theoretical task now underway is the construction of theoretical model atmospheres for the sources, as in the case of the more normal optical stars, which can then be used to determine the relevant physical parameters and processes. Perhaps the most exciting part of these studies is the chance to examine extreme conditions totally inaccessible in terrestrial laboratories. For example, the magnetic fields involved are of the order of a million times stronger than those of the best superconductors on Earth. Furthermore, the atmospheric plasma must be very hot and dense to produce such a high x-ray luminosity.

Although these conditions present a unique opportunity, they also complicate the theoretical descriptions of the fundamental processes enormously. Recently, fully relativistic calculations of the radiation normal modes in a strongly magnetized plasma have been developed, and these have been used in a rather exhaustive study of photon scattering. One important result is that resonant double scattering (one photon in, two out) greatly dominates bremsstrahlung as a source of

radiation.The scattering rates are being incorporated into a Feautrier radiative transfer calculation, in collaboration with workers at Pennsylvania State University. In addition, these effects are being included in a calculation of the Rosseland mean opacity in the stellar surface layers. Since radiation pressure may play a dominant role in determining the structure of the surface, it is crucial to have reliable calculations of this quantity. Another aspect of the model atmosphere problem is the nature of the energy deposition of the accreting matter. At present, MSFC is working with a group at the University of Illinois to develop a Fokker-Planck description of the rate at which a beam of fast ions in a strongly magnetized plasma will thermalize. These results, which determine the heating of the atmosphere, will eventually be combined with the radiative transfer calculations to provide a self-consistent picture of the luminous atmospheres of the pulsing x-ray binaries.

An international symposium with the theme "Double Layers in Astrophysics" was sponsored by the X-Ray Astronomy Branch in March 1986. Participants from six different countries came together for 3 days to discuss their latest research efforts in the experimental, theoretical, and astrophysical studies of double layers. Hannes Alfvén delivered the keynote address at the symposium, outlining the historical and experimental status of studies of double layers, as well as citing several examples of their astrophysical applications. Two novel astrophysical applications of double layers have originated within the x-ray group and these were discussed at the symposium. First, double layers may form in the accretion column of an accreting neutron star and play an important role in decelerating the infalling material and producing high energy radiation. Second, formation of a double layer may lead to the critical velocity ionization phenomenon which prevents the velocity of a neutral gas beam from exceeding a critical velocity when passing through a magnetized plasma. Work is continuing in these two areas.

The thrust of our experimental effort has been directed toward the development of advanced instrumentation for x-ray astronomy. In particular, work has been concentrated in the area of imaging proportional counters, as these can provide the large collecting areas necessary for resolving x-ray sources in the 10 to 100 keV energy range. Two specific techniques have been developed that vastly improve the performance of these detectors. The first is a multistep technique wherein the charge liberated by an incoming x-ray photon is passed first through a gaseous preamplification region, from which the energy of the event is measured, and then into a conventional imaging section. In this way the usual conflict between high gas amplification for good image resolution and low amplification for good energy resolution is avoided by having two separate regions, one devoted to each parameter. Successful operation has been demonstrated in a wide variety of gas mixtures suitable for x-ray astronomy.

The second technique is that of fluorescent gating, which makes use of the fact that under certain circumstances valid x-ray events give characteristic signatures which distinguish them from the charged particle background against which they are measured. This signature arises from the photoelectric interaction between the x ray and the detector gas (xenon) which results in the production of a fluorescent photon. This photon is then reabsorbed elsewhere in the detector, producing a pair of separate, though correlated, events. Charged particles, conversely, have a very low probability of producing fluorescence, and looking only for pair events provides a very powerful technique for discriminating against them. Typical laboratory measurements have demonstrated an order of magnitude increase in signal-to-noise ratio over ungated detectors. Work is currently under way to combine these two techniques to provide an extremely versatile high resolution, low background x-ray detector.

In addition to this purely x-ray work, funding has recently been received for a joint x-ray/infrared project. The proposal here is to develop a large In/Sb array system for detailed study, in the 1 to 5 μm wavelength region, of celestial sources discovered at x-ray wavelengths. Currently an order has been placed for the array and work has started in-house on the data-processing electronics. It is anticipated that the system will be operational in the second half of 1987.

M. C. Weisskopf/ES65
(205) 544-7740
Sponsor: Office of Space Science and Applications

Nuclear Radiation Monitor

The Nuclear Radiation Monitor (NRM) was flown on Spacelab 2 from July 29 to August 6, 1985, to obtain quantitative measurements of background radiation in the Shuttle/Spacelab environment. The primary elements of the NRM are shown in Figure 58. The instrument operated continuously during the orbital portion of the mission. The data now being analyzed are expected to be useful to future experimenters using radiation-sensitive instruments in the Shuttle/Spacelab environment.

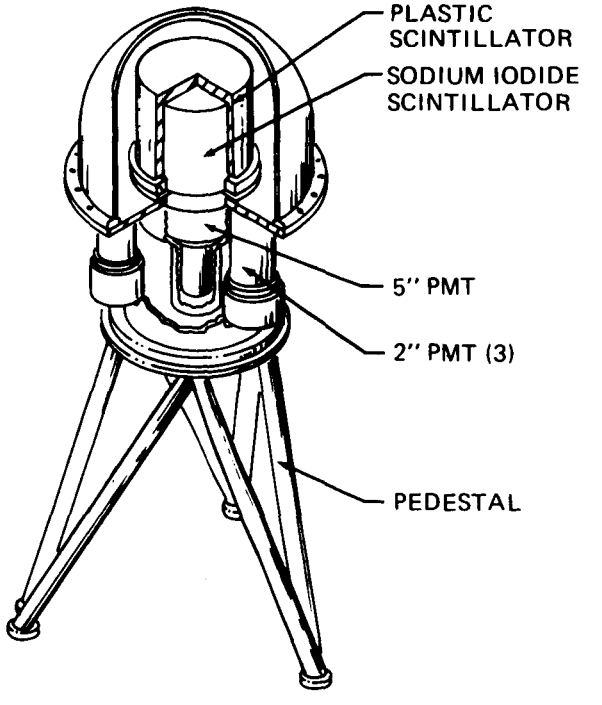

Figure 58. Detector Assembly, Nuclear Radiation Monitor.

Data that have already been analyzed indicate that a gamma ray burst was observed by the NRM. These enigmatic objects remain one of the most outstanding puzzles in high-energy astrophysics today. Their brief duration, random occurrence, and lack of identified optical, radio, or x-ray counterparts make them difficult to study. Most current models of gamma ray bursts are based on an explosive event near or on an isolated neutron star.

The burst occurred at 00:56:38 Universal Time (UT) on August 5, 1985, and was confirmed by observations of the same burst by instruments aboard the Pioneer Venus Orbiter, the International Cometary Explorer, and two other instruments aboard Spacelab 2. The NRM detector has a high data rate and a large central detector which allowed observation of this burst with unprecedented sensitivity at high energies. Previous burst detectors have been limited in their efficiency for gamma rays above ~1 MeV, and/or they have limited time resolution.

Figure 59 shows the time profile of the burst. The burst is dominated by a single peak ~2 s wide. At lower energies there are additional emission features for up to 20 s after the main peak. The emission above 1 MeV peaks ~0.3 s before that at lower energies. Above 10 MeV, there is evidence of emission ~3 s prior to the main peak. These observations may provide theorists with important new information on the gamma ray emission mechanism and energy source.

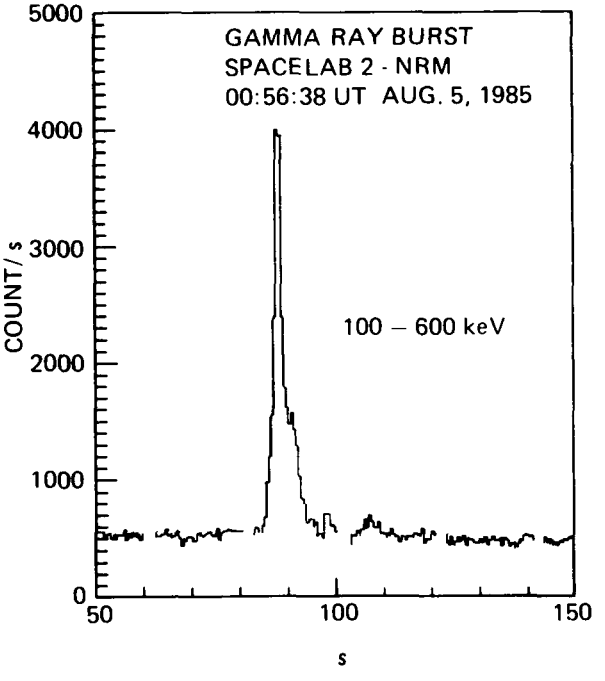

Figure 59. Time Profile of the Aug. 5, 1985 Gamma Ray Burst.

The NRM data will be searched extensively for other bursts. These burst observations will provide valuable data for the MSFC Burst and Transient Source Experiment on the Gamma Ray Observatory.

G. J. Fishman/ES62
(205) 544-7691
Sponsor: Office of Space Science and Applications

The Infrared Telescope Flight

The Infrared Telescope (IRT) operated in orbit for 8 days beginning July 29, 1985, as part of the Spacelab 2 payload. The cryogenic and mechanical apparatus worked very well, although infrared astronomical measurements were confused in the mid-wavelength channels by a high infrared background, probably due to the Orbiter's induced environment. In addition, a heat shield which broke during the mission caused some obscuration. However, continuing data analysis shows good quality and unique astronomical and zodiacal dust data.

The cryogenic system was crucial while infrared observations were in progress. For the first 6 days of the mission, cooling was used to meet the specific infrared system temperature requirements. During the final 2 days of the mission the cryogenic system was used to investigate the superfluid helium storage equipment.

The IRT cryogenic system includes a fixed storage dewar with control plumbing and a porous plug phase separator, all surrounded by three vapor-cooled shields (VCSs); an articulated cryostat containing the infrared optical apparatus and surrounded by four VCSs; and a set of flowmeters and valves for measuring and controlling the vent flows through the dewar and the cryostat. A number of thermometers measured the temperatures of the superfluid helium bath and critical components throughout the system.

By 36 hours mission elapsed time (MET), the liquid helium bath had stabilized at a temperature of about 1.95 K, well below the superfluid transition temperature of 2.17 K. The temperatures on the liquid and vent line sides of the porous plug phase separator measured about 1.90 K and 2.08 K, respectively, as expected from ground test data. Total mass flow rate through the porous plug averaged about 26 mg s^{-1}, or 15.5ℓ per day, divided between the dewar and cryostat components. Maximum flow was directed through the cryostat during the entire infrared observing period, but the dewar flow was periodically changed in order to maintain the dewar VCS at relatively warm temperatures, allowing the total boiloff rate and the bath temperature to remain high enough to ensure proper infrared system operation.

It was important that temperatures within the cryostat remain colder than certain preset specifications, in response to the cold vent gas flow from the dewar. The required maximum temperatures and the temperatures actually achieved are shown in Table 6. Although the detector temperature slightly exceeded the pre-mission requirement, it proved to be acceptable. The other temperatures were well below maximum requirements.

Table 6. Key Cryostat Temperatures.

COMPONENT	MAXIMUM TEMPERATURE REQUIREMENT (K)	TEMPERATURE ACHIEVED (K) MET DAY 0–5
INFRARED DETECTOR ARRAY	3	3.1
MIRROR AND LOWER TELESCOPE BAFFLE	8	6.5 – 7.0
UPPER TELESCOPE BAFFLE	60	50 – 55

After infrared observations were completed near the end of MET Day 5, special tests were performed on the cryogenic system. In one test, all of the vent valves were closed for time spans varying from seconds to hours, and then reopened. At no time was there any indication that a significant amount of liquid helium had passed through the porous plug. Consequently, recovery was always observed and the instabilities seen during some ground tests, in the form of strong flow and pressure oscillations, were totally absent.

Another performance check involved two tests in which the bath was permitted to warm to well above the superfluid transition of 2.17 K (up to a maximum of 2.34 K), and then was repumped to below the transition. Results indicated that the helium can be warmed to the normal phase and then be repumped to the superfluid phase without instabilities. This means that helium dewars do not have to be fully converted to the superfluid phase prior to launch. Later tests are planned for exploring the upper limit on this zero-gravity pumpdown.

In order to determine whether the heater on the downstream side of the porous plug could be used to increase vent flow, a small heater on the porous plug was energized several times in an attempt to draw additional liquid through the plug. In every

test the effect was to dry out the downstream side of the plug and reduce the vent flow rate. This result raises questions concerning the zero-gravity operation of the so-called fountain effect pumps for on-orbit transfer of liquid helium between two helium dewars.

The cryogenic system of the infrared telescope operated very well during the mission. The system tests conducted answered several important questions which affect the design of future cryogenic space systems.

E. W. Urban/ES63
(205) 544-7721
Sponsored: Office of Space Science and Applications

Infrared Astronomy And Cometary Research

This year witnessed the full commissioning of the MSFC infrared (IR) camera developed for astronomical observations at 8 to 30 μm. The key component is a spatial array of 20 gallium-doped germanium bolometers, which are extremely sensitive in the high thermal background environment of ground-based observatories. Astronomical observations at the Wyoming IR Observatory (WIRO) and the NASA IR Telescope Facility (IRTF) have shown that this camera provides a substantial improvement in observing capability. Because of its relatively large spatial coverage, the camera permits many types of observations that are not possible with smaller field-of-view, single channel IR photometers.

This capability was demonstrated at WIRO when the IR camera was used to map the 10-μm radiation from Comet Giacobini-Zinner (GZ). Figure 60 shows the first thermal-IR image of a comet ever obtained by a ground-based observatory. Detailed analysis of the IR image has provided insight into such properties as the rate at which particulates leave the comet nucleus, the types of particles, and their temporal behavior. Because relatively nearby comets rapidly change their appearance, the MSFC IR camera is uniquely suited to obtain an image in a short enough time period for the results to be meaningful.

About 1 month after the observations of GZ, the International Cometary Explorer (ICE) became the first spacecraft to encounter a comet when it

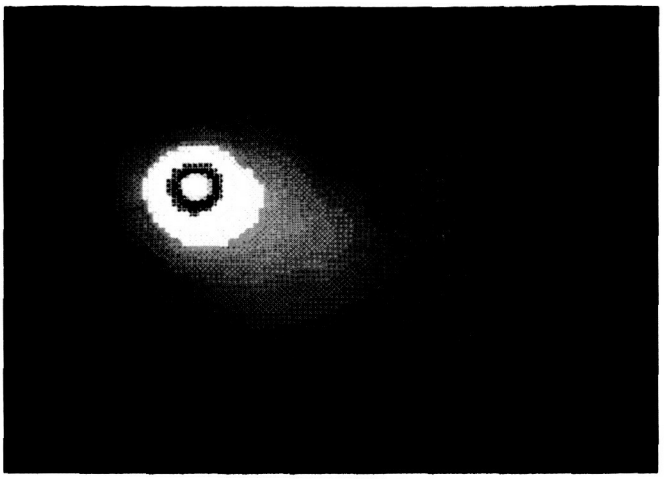

Figure 60. Comet Giacobini-Zinner, 10.8-μm Map (MSFC Mid-IR Camera).

passed through the tail and within 8000 km (4800 mi) of the nucleus of GZ. The ground-based thermal-IR image of GZ, combined with data regarding the impact rate of dust on the ICE antennae, has been especially useful for constraining the characteristic sizes of the dust grains.

The first thermal-IR image ever made of Comet Halley was obtained with the MSFC IR camera on November 18, 1985, at the IRTF on Mauna Kea. Images obtained on several successive nights in March 1986 showed that Halley's IR brightness varied greatly. The brightness variations have been tentatively attributed to exposure to the Sun during rotation of cometary nuclear surfaces having a range of properties.

In addition to its application to cometary research, the MSFC IR camera has been used to study IR radiation from galaxies detected by the Infrared Astronomical Satellite. The camera permits detailed maps to be made of these galaxies, which are strong IR sources. The efficiency of the IR camera is illustrated by the fact that it was used to map four galaxies in less than half an observing night, whereas only nine had ever been mapped previously.

In parallel with the observational program using the mid-IR camera, investigation is proceeding into the use of special light-collecting cones to concentrate 10-μm radiation onto an array of bolometers. These cones, which have never been used at wavelengths as short as 10 to 30 μm, should permit the development of more efficient

bolometer arrays than possible with field mirrors. In addition, work is ongoing on a unique survey camera for astronomical observations at 1 to 5 μm. The array device is now being procured and the design of the system is nearing completion.

Campins, H.; Telesco, C. M.; Decher, R.; Mozurkewich, D.; and Thronson, H.: Geophys. Res. Lett., 13, 295, 1986.

C. M. Telesco/ES63
(205) 544-7723
Sponsor: Office of Space Science and Applications

Radiation Environment Within Spacelab 1

When Spacelab 1 was launched, both active and passive radiation detector packages had been placed onboard by investigators from Marshall Space Flight Center, the University of Alabama in Huntsville, and the University of San Francisco. The two active packages consisted of a single integrating tissue-equivalent ion chamber and two small xenon-filled proportional counters, one of which was shielded by a copper sleeve. The active detector output was recorded once per second, giving a time history of both the dose accumulated and the flux of high-energy charged particles and bremsstrahlung x rays encountered during the flight.

There were four Verification Flight Instrumentation Program Passive Detector Packages flown, containing a number of different detector materials. Under experiment INS006, 30 passive packages were flown: 26 passive dosimeter packages and 4 thick plastic stacks, distributed inside the Spacelab module and the transfer tunnel. The packages contained types 200 and 700 thermoluminescent detectors (TLDs) and CR-39 plastic. The four thick plastic stacks contained silver chloride crystals, as well.

Because Spacelab 1 flew a low-altitude mission (236 to 260 km), doses were relatively low. Typical TLD mission doses accumulated over the 10 days were around 100 millirad in thinly shielded regions, with the pallet receiving around 40 to 100 percent more. The ion chambers measured 125 and 128 millirad over the mission. Most of the difference between the ion chamber and TLD measurements was due to the efficiency of TLD in responding to heavy cosmic ray nuclei.

By mapping the active detector response in time onto the orbital trajectory, a radiation map in geographic coordinates was constructed (Fig. 61 and Fig. 62). The South Atlantic Anomaly was well defined in both the ionization chamber and the proportional counter maps. Since the orbital inclination was 57 deg, the edge of the south horn of the outer trapped electron belt was seen in the proportional counter map. The horn was not seen in the ion chamber maps because the xenon-filled proportional counter was recording the secondary bremsstrahlung x rays which contributed little to the dose. The horn electrons were absorbed by the spacecraft structure. The accumulated dose during South Atlantic Anomaly passes was only 13 percent of the total for the mission. Most of the dose came from galactic ray nuclei, with a minor component due to horn electrons.

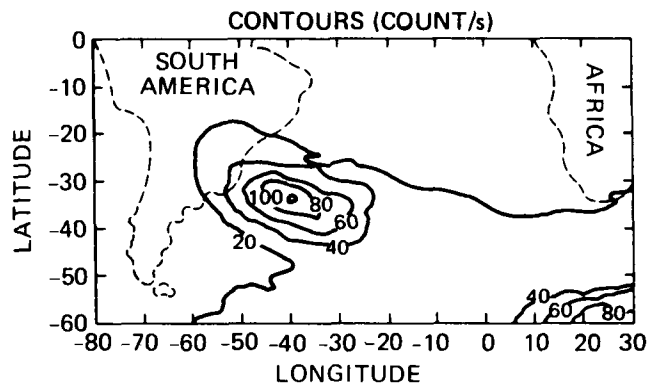

Figure 61. Count Rate Map from the Unshielded Proportional Counter.

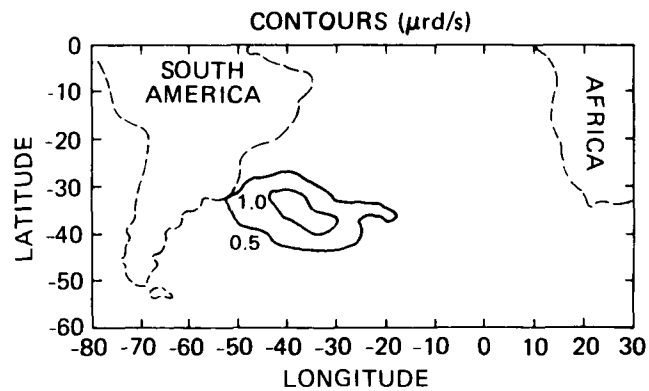

Figure 62. Dose Rate Map From the Ionization Chamber.

J. W. Watts/ES62
(205) 544-7696
Sponsor: Office of Space Flight

Atmospheric Sciences

Introduction

The goal of the NASA/MSFC atmospheric sciences program is to develop and utilize space technology to observe the Earth's atmosphere from space in order to gain basic understanding of atmospheric processes and the role they play in the interactions between various components of the Earth system (atmosphere, hydrosphere, cryosphere, biosphere, and solid Earth). The research program consists of theoretical/analytical model development, remote sensor development, flight payload analyses, and the laboratory and field experiments required in these activities. A major area of focus is the hydrologic cycle. Ground- and space-based measurements of atmospheric parameters are used to develop and verify analytical and theoretical models of global and mesoscale atmospheric processes and establish remote sensor requirements. Field experiments provide the data required to verify the operation of air- and spaceborne remote sensing instrumentation. Data derived from observations are used as input to atmospheric model computer codes. Extensive use is also made of interactive data display and access systems to study the time-dependent development of atmospheric systems of all scales.

Geophysical Fluid Flow Cell Experiment

The geophysical fluid flow cell (GFFC) experiment simulates a wide variety of thermal convection phenomena in spherical geometry. By applying an electric field across a spherical capacitor filled with a dielectric liquid, a body force analogous to gravity is generated around the fluid. The force acts as a buoyant force in that its magnitude is proportional to the local temperature of the fluid and in the radial direction perpendicular to the spherical surface. In this manner, cooler fluid sinks toward the surface of the inner sphere while warmer fluid rises toward the outer sphere. The value of this artificial gravity is proportional to the square of the voltage applied across the sphere and can thus be imposed as desired. With practical voltages, its magnitude is only a fraction of Earth's, and so requires a microgravity environment to be significant.

The experiment flew on Spacelab 3 and operated for over 100 hours. It has verified that dielectric forces can be used to properly simulate a spherical gravitational field to drive thermal convection. By controlling the relative importance of thermally driven buoyancy, an entire spectrum of convective motion was observed, from the initial onset of laminar convection to fully turbulent flow. Figure 63 shows a compilation of some of the photographic data taken during the experiment. In this series of photographs, the circular field of view of the camera shows a portion of the sphere in which the pole is at the top of the image and the equator is at the bottom.

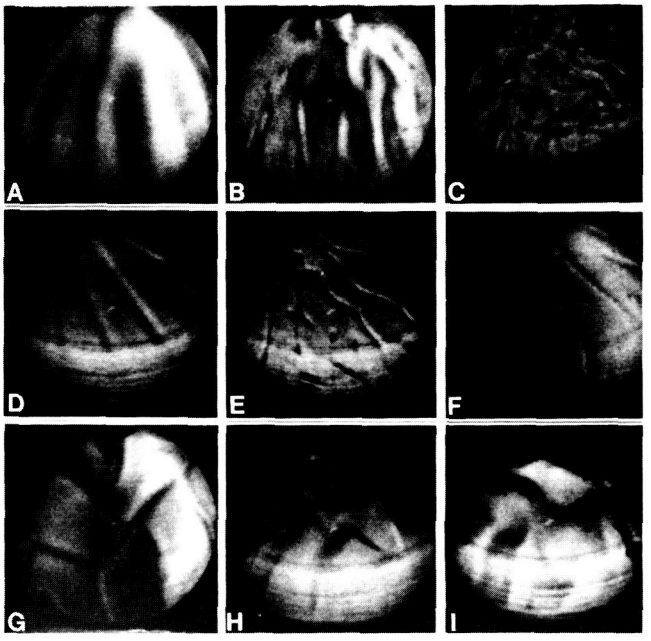

Figure 63. GFFC Convective Patterns.

Several experiments were performed in which the inner sphere temperature was uniform and higher than that on the bounding outer sphere. Thought to be analogous to the deep convection layers of the Sun, these experiments produced "banana cells" aligned with the rotation axis for fast rotation rates (view A). Some cases showed a prograde motion of the cells near the equator, while the mid-latitude cells were retrograde. These results may help explain the differential rotation of the Sun's equator. As the heating was increased, the flow became more concentrated (view B). Finally, with very high heating, the flow became turbulent and the banana cells were confined to a small region near the equator (view C). Numerical modeling of this phenomenon using a three-dimensional computer model showed good agreement with the observed wave number and phase speed.

Another series of experiments imposed a pole-to-equator temperature gradient in addition to the radial temperature gradient (i.e., the pole was hot relative to the equator). These flows are shown in views D through F. In these cases, the rotation was not as fast as in the above cases, and the instability became more spiral in nature. With relatively weak heating, the spiral waves were confined to mid-latitude (view D). With an increase in heating, the pattern branched out toward the equator, but retained a tilt toward the direction of rotation. A further increase in the heating caused the motion to become more chaotic, consisting of small scales of motion, although the tilt was still evident (view E).

View G shows a slowly rotating case without the meridional temperature gradient to drive a north-south circulation. The heating was also weak and the convective motion was organized into polygons reminiscent of Benard convection cells. In this case the motion was weak, with the upward motion confined to the narrow region between the polygons, while the descending motion occurred over the broad interior of the cell. View I shows the development of triangular waves resulting from the addition of a north-south temperature gradient while increasing both the heating and rotation. These motions were unexpected and much effort is being expended on analyzing them. The pattern persisted even when the heating and rotation were further increased (view H). The development of the banana cells appears evident near the equator and is coupled to the waves.

Spherical convection can be used to experimentally simulate the three-dimensional flows of planetary and solar atmospheres. Analytical theories incorporate simplifying assumptions and need experimental guidance for further improvements. Complete numerical solutions are beyond even today's supercomputers for modeling convective turbulence requiring high temporal and spatial resolution. The GFFC can easily generate these flows made relevant by dynamic similitude. With the capability of producing a wide range of experiment conditions, the GFFC offers a unique opportunity to investigate solar and planetary atmospheres as well as more fundamental fluid dynamics. Analysis of these flows using analytical, numerical, and experimental techniques is continuing while preparations are under way for the next flight of the instrument aboard the International Microgravity Laboratory.

Hart, J. E.; Toomre, J.; Deane, A. E.; Hurlburt, N. E.; Glatzmaier, G. A.; Fichtl, G. H.; Leslie, F.; Fowlis, W. W.; and Gilman, P. A.: A Laboratory Model of Planetary and Stellar Convection Performed on Spacelab 3. Science, in press, 1986.

Hart, J. E.; Glatzmaier, G. A.; and Toomre, J. : Space-Laboratory and Numerical Simulations of Thermal Convection in a Rotating Hemispherical Shell With Radial Gravity. Journal of Fluid Mechanics, submitted, 1986.

F. W. Leslie/ED42
(205) 544-1639
Office of Space Science and Applications

Geophysical Fluid Dynamics

Fluid dynamics is the study of flows which characterize fluid systems subjected to various forcing mechanisms and in containers of various geometries. The systems of interest are the Earth's atmosphere and oceans, and the atmospheres of other planets. To gain an understanding of the real systems, mathematical and laboratory systems which are simpler but which model the same essential, fundamental processes are studied. While ground-based experiments in cylindrical geometry can model certain aspects of large-scale atmospheric and oceanic flow, there are limitations to the relevance of these experiments, due to geometric differences. It would be desirable to conduct experiments in spherical geometry, with a radial body force similar to that felt by a planetary atmosphere or ocean.

One of the accomplishments of the past year was the development of a computer program to analyze in detail flows such as those seen in the Geophysical Fluid Flow Cell (GFFC), flown on Spacelab 3, or similar apparatus, as well as those in cylindrical geometry. A previous program used the full (Navier-Stokes) equations to predict the steady flow that is predicted when axisymmetry is assumed. The new program is also based upon these equations, but examines the linear stability of the previously computed, axisymmetric flow to three-dimensional disturbances. The two codes, when used in tandem, can accurately determine whether axisymmetric or wavy flow will be observed in the laboratory. Further, the new code computes the fastest-growing, three-dimensional eigenmode which destabilizes the axisymmetric flow. The structure and energetics of these eigenmodes, in combination with the examination of the axisymmetric flow, can help explain and/or predict the flow that would be observed in the

laboratory, shedding light on the process that is of interest in the atmospheric system.

The results of the codes have compared well with the GFFC Spacelab 3 experiment. One Spacelab 3 experiment of relevance to the Earth's atmosphere showed agreement with the prediction by the codes that no barolinic waves would be seen. Other calculations indicate that waves would have been present under slightly different experimental conditions (Fig. 64). The codes have also been applied to experiments in which a latitudinal temperature gradient was applied along with heating from the inner sphere (of relevance to Jupiter and Saturn), and the points of transition and the flow structures are consistent with the experimental data.

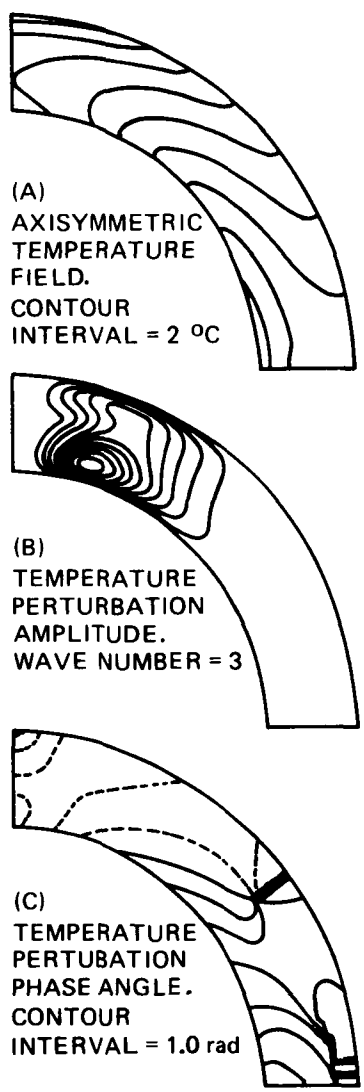

Figure 64. Results of the Numerical Calculations for a GFFC Baroclinic Case.

Laboratory experiments in cylindrical geometry are being conducted in Earth gravity to provide a broader basis for understanding the space-based experiments. In addition to the obvious geometrical difference between the space-based experiments and the previous experiments in cylindrical geometry, the spherical system allows the heat to enter and leave the fluid system through horizontal boundaries, rather than through vertical sidewalls. Experiments have been conducted at MSFC in a cylindrical annulus with thermally conducting horizontal boundaries. Flow regimes of a nature that is qualitatively different from those of the side-heated annulus can be observed in such a system. As a possible precursor to a design for a new spherical experiment, other experiments are now being conducted in a new cylindrical annulus with heating and cooling on the lower boundary only, the upper boundary being made of a thermally insulating material. This work, which will help elucidate atmospheric flow as well as assist in the design of future microgravity experiments, is just beginning.

Miller, T. L.; and Fowlis, W. W.: Laboratory Experiments in a Baroclinic Annulus with Heating and Cooling on the Horizontal Boundaries. Geophys. Astrophys. Fluid Dyn., 34, 283-300, 1986.

T. L. Miller/ED42
(205) 544-1641
Sponsor: Office of Space Science and Applications

Global Wind Measurement

During 1986, significant progress was made toward the goal of taking global wind measurements. Panels were formed to address both of the major recommendations of the NASA Workshop on Global Wind Measurement. These recommendations were that an aerosol backscatter survey experiment be conducted, and that the Doppler lidar (laser-radar) wind profiler be considered for participation in the Earth Observing System (EOS).

With MSFC as the lead Center, the Global Backscatter Experiment (GLOBE) panel has been formed and the first experimental data obtained. Plans have been made for a comprehensive experimental program to determine if the distribution of naturally occurring aerosol is sufficient to allow global wind measurement by a spaceborne Doppler lidar. The MSFC contributions to this effort

will include development of airborne and ground-based lidars, aerosol physics experiments, and modeling of global atmospheric backscatter at the wavelengths of lidar operation.

The EOS Laser Atmospheric Wind Sounder (LAWS) panel was also formed during 1986, with MSFC as the lead Center, to guide the preparation of a document to support the Doppler lidar in the EOS Announcement of Opportunity which is expected to be released during FY87. The LAWS panel report will be completed during FY86 and will define the EOS wind sounder and its relationships to the rest of the EOS instruments and data management system. Because of experience and leadership in this area, MSFC will be expected to obtain the responsibility to develop this important instrument on the Space Station/-EOS.

Significant progress was also made during 1986 in the area of laser development. Programs were set in motion to resolve the issues of laser lifetime and energy, scaling from current laser sizes up to the size needed for a spaceborne wind sounder. These efforts will take additional time and resources, as will the other activities mentioned, but all of the initial indications are that the Doppler lidar technique is a viable, cost-effective means to provide a much needed improvement in wind data. Such data will be essential for improved global weather forecasting and for the investigation of the complex interactions between the atmosphere, biosphere, and hydrosphere.

D. E. Fitzjarrald/ED43
(205) 544-1651
Sponsor: Office of Space Science and Applications

Global Aerosol Backscatter Assessment

One of the most exciting thrusts of space-based technology in the next decade will involve inclusion of a Doppler lidar (laser-radar) in the Earth Observing System (EOS) to determine global-scale wind fields from the Earth's surface to the lower stratosphere. The wind measurement principle involves the Doppler shift between the energy transmitted from a pulsed lidar and the energy backscattered from small atmospheric aerosol particles that move with the wind. The accuracy of the derived wind measurements will depend on the backscatter efficiency of the wind tracer particles at the wavelength of the lidar. Feasibility studies for this system therefore require information on the typical values and spatial/temporal distribution of aerosol backscatter efficiency on a global scale.

NASA has mounted a new program, the Global Backscatter Experiment (GLOBE), to improve understanding of aerosol backscatter properties. GLOBE participants include several universities and NASA centers, with MSFC as lead Center. The GLOBE activity involves a balanced program of literature reviews, theoretical modeling, reanalysis of existing data, and new measurements of aerosol optical and physiochemical properties. MSFC is developing the model framework, program plan, data center, short-range focused lidars, and one of several long-range pulsed lidars for the GLOBE effort.

The exploratory phase of GLOBE will extend from 1986 to 1989, when the information will be needed for the design of the Doppler lidar system. Intermediate milestones will be closely coordinated with the EOS schedule. The confirmatory phase of GLOBE will involve evaluation of aerosol data from early space-based lidar backscatter missions, and eventually from the performance of the EOS wind measurement system.

The most recent predictions of global backscatter values from GLOBE are generally promising for Doppler lidar wind measurements from EOS. Routine stratospheric wind measurements will certainly be possible for 2 to 4 years after major volcanic eruptions. Stratospheric wind measurement potential may be marginal during prolonged intervolcanic periods. Tropospheric aerosol backscatter efficiencies also appear to be high enough for accurate wind measurements from the surface to at least 8 or 10 km (26,000 to 33,000 ft). However, the predictions for the troposphere involve numerous uncertainties, many of which could reduce the estimated backscatter to below the projected design threshold.

Work is already under way to resolve many of these uncertainties. An MSFC-developed focused carbon dioxide lidar is operating in an airborne aerosol study program in Australia. Later this year, the same instrument will be deployed to the

Mauna Loa Observatory on the island of Hawaii. These new measurements will provide vital information on aerosol properties in the Pacific basin, where backscatter is expected to be quite low. They will also provide useful experience for future backscatter measurement programs that will begin in the Pacific in 1987 and 1988.

D. A. Bowdle/ED43
(205) 544-1682
Sponsor: Office of Space Science and Applications

Airborne Doppler Lidar Wind Measurement

MSFC has undertaken several measurement programs using an Airborne Doppler Lidar System (ADLS). The ADLS emits energy pulses from a carbon dioxide laser and determines the radial velocity of the air by measuring the Doppler shifted radiation scattered back along the line of sight by naturally occurring aerosols. Since the observations are made from a moving platform, the aircraft attitude and ground speed are subtracted from the raw radial velocity to obtain the desired ground-relative wind motion. Consequently, the degree to which the apparent Doppler velocities, corresponding to returns from the surface of the Earth, depart from zero is a measure of the accuracy of the wind measurements, since the Earth's surface must have zero velocity.

Prior to the first set of flights in 1981, a system was developed for calibrating and pointing a scanner which controls the attitude of the lidar beam as it exits the side of the aircraft. The scanner was programmed to direct the beam within a horizontal plane, at angles of 20 deg forward and aft of an imaginary line perpendicular to the left side of the aircraft. Analysis of data from the 1981 flights showed that the rate of data flow from the aircraft Inertial Navigation System (INS) was not adequate to ensure that the pointing of the lidar beam was independent of aircraft attitude. Accordingly, an INS dedicated to the lidar system was mounted directly onto the optical table. In order to use the attitude information, a new control system was developed which allowed the scanner to respond more rapidly to the aircraft roll and pitch. The new control system also provided much more flexibility in beam pointing, and increased system reliability. Up to 15 different scan angles, chosen from any plane within the 20-deg capability of the scanner, could be used in each scan pattern. The chosen angles remained fixed in space as long as the aircraft roll did not cause the scanner limits to be reached.

During subsequent flights in 1984, the scanner was programmed to direct the beam into several planes, at least one of which was tilted below the horizon. Analysis of Flight 6 data demonstrated that the addition of the dedicated INS and the more flexible scanner control system improved the effective accuracy of the measurements. Whereas the ADLS used in 1981 could only sample the winds within a horizontal plane, the improved scanner system permitted three-dimensional measurements. Maximum apparent Doppler velocities were less than half of those noted in 1981, the error source being within the INS itself. Errors of less than 1 deg were determined for the scanner elevation angle; moreover, the errors were found to be sensitive to calibration factors used by the INS to control the attitude of the lidar beam.

A consequence of this analysis has been to suggest methods of improving the effective accuracy of the wind measurements. One approach to minimizing wind measurement errors during post-processing would be, first, to apply smoothing to the apparent Doppler velocities and, second, to subtract the smoothed results from the raw radial velocity measurements. The existence of a continuous record of ground returns (obtained during Flight 6) provides the means to eliminate these errors almost completely. Finally, knowledge of errors in the lidar beam attitude permits a more accurate determination of the three-dimensional wind structure of the atmosphere.

Bilbro, J. W.; DiMarzio, C. A.; Fitzjarrald, D. E.; Johnson, S.; and Jones, W. D.: Airborne Doppler Lidar Measurements. Applied Optics, submitted, 1986.

Bilbro, J. W.; Fichtl, G. H.; Fitzjarrald, D. E.; Krause, M.; and Lee, R. W.: Airborne Doppler Lidar Wind Field Measurements. Bulletin of the American Meteorological Society, 65, 348-359, 1984.

McCaul, E. W., Jr.; Bluestein, H. B.; and Doviak, R. J.: Airborne Doppler Lidar Techniques for Observing Severe Thunderstorms. Applied Optics, 25, 698-708, 1986.

J. Rothermel/ED43
(205) 544-1685
Sponsor: Office of Space Science and Applications

Coherent Lidar Research and Development

Research and development in coherent lidar (laser-radar) systems have continued to take a multifaceted approach to ground-based, airborne, and space-based applications. Current efforts are concentrated on signal processing, carbon dioxide laser development, target and detector calibration, system simulation, and field measurements.

Pulsed lidar work has involved extensive tests of the signal processing system to obtain a better understanding of the errors associated with the algorithms used in estimating lidar signal parameters. The electro-optic modulator has been redesigned to obtain improved performance, and the scan control system has been completely reworked to enhance ground operation. Two new laser configurations are being procured for evaluation. In addition, a program to develop a breadboard laser for space applications is being proposed. Initial simulation studies demonstrating the feasibility of performing tropospheric wind measurements with a coherent lidar operating on the Space Station have been completed and development of a comprehensive simulation program is continuing.

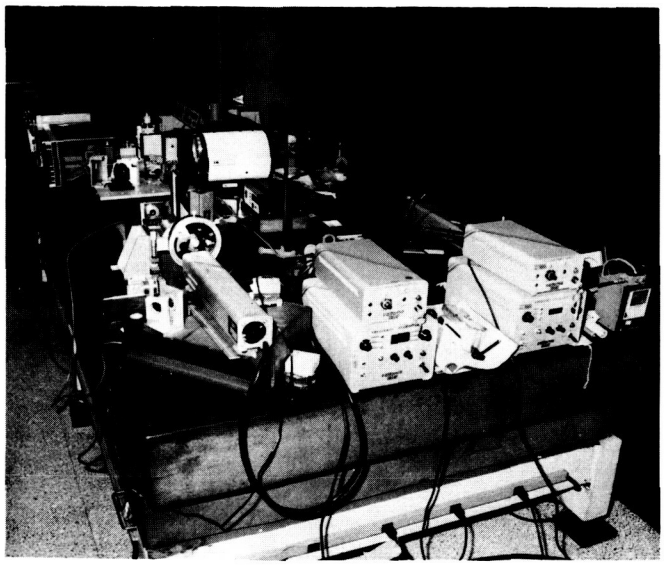

Figure 65. Coherent Lidar Calibration Laboratory.

Continuous wave lidar development has focused on the construction of a 9.11-μm system for backscatter measurement. In the first coherent lidar measurements in the southern hemisphere, the 10.6-μm system was flown in Australia as part of a cooperative experiment to measure backscatter. An additional experiment is planned with both systems in Mauna Loa, Hawaii, to obtain measurements of the backscatter in the mid-Pacific region. These field experiments are designed to provide design data for a space-based coherent lidar.

Laboratory facilities are being upgraded with efforts concentrated on research into the lifetime of mercury-cadmium-tellurium detectors for heterodyne applications. Facilities for research into coherent lidar target material reflectivity, such as the Coherent Lidar Calibration Laboratory shown in Figure 65, are also being upgraded.

Bilbro, J. W.: Airborne Doppler Lidar Measurements: An Overview. 3rd Topical Meeting Coherent Lidar Radar - Technology and Applications, July 7-11, 1985.

Rothermel, J.; and Jones, William D.: Ground-Based Measurements of Atmospheric Backscatter and Absorption Using Coherent CO_2 Lidar. Applied Optics, 24 (21), 1985.

Bilbro, J.; DiMarzio, C.; Fitzjarrald, D.; Johnson, S.; and Jones, W.: Airborne Doppler Lidar Measurements. Applied Optics, submitted, 1986.

J. W. Bilbro/EB23
(205) 544-3467
Sponsor: Office of Space Science and Applications

Doppler Radar Wind Profiler

Two 50-mHz Doppler radar wind profilers were placed in operation at the Kennedy Space Center (KSC) with an immediate objective of comparing Doppler wind profiles with balloon data. The long-range purpose of the study was to determine if and how Doppler wind profiling systems could be used in Shuttle launch and landing decisions, and in the determination of pre-launch wind load calculations. At present, quantitative wind measurements used in the pre-launch wind load calculations are provided by wind profiles obtained with the Jimsphere/FPS-16 radar system.

The two Doppler radar wind profilers were located at KSC approximately 8 mi (12 km) south of the Shuttle launch complex, and approximately 12 km apart. In addition, a NASA/National Oceanic and Atmospheric Administration (NOAA) profiler was located in the KSC industrial area, and a Radian/SOUSY profiler was located at the Pan American weather station and balloon release point near the Cape Canaveral Air Force Station industrial

area. The NASA/NOAA system went into operation on January 24, 1985, and ran until mid-April. Data are available in the form of 1-hour averages during most of the operational period. The Radian/SOUSY system was brought into operation in mid-March and collected data from mid-March to mid-April. There are approximately 80 hours of SOUSY radar data available for analysis during the 1 month of operation.

The comparison between Jimsphere and profiler data for April 12 illustrates similarities and differences between the data sets. Both profiler systems were capable of producing wind profiles which matched in shape, if not in speed and direction, those profiles taken with balloon/ground tracking systems. This was true for the high resolution Radian/SOUSY system as well as for the NASA/NOAA system (Fig. 66).

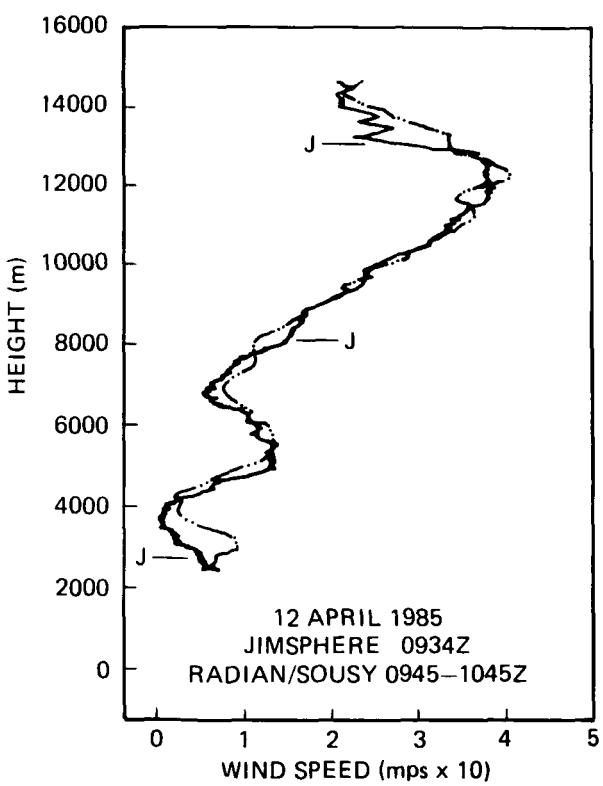

Figure 66. Wind Profiles for the Jimsphere and the Radian/SOUSY Systems.

Although the better Doppler wind profiles (either system) appeared to be as good as the rawinsonde profiles of speed, profiles of direction from the NASA/NOAA system frequently differed by 10 to 30 deg. In the higher resolution Radian/SOUSY profiles, however, much of the higher frequency wind profile changes observed with altitude did not seem to correlate with features in the Jimsphere data.

Based in part on the results of this research study, NASA approved funding for acquisition of a radar wind profiler for use in the Space Shuttle program beginning in 1987.

C. K. Hill/ED44
(205) 544-1664
Sponsor: Office of Space Flight

Precipitation Measurements

Precipitation measurement over the Earth is an important component of the planned Earth Observing System's focus on the global hydrologic cycle and climate processes. The measurement of precipitation over the Earth is presently not possible from the ground because of the lack of coverage by radar and rain gauges. Earth-orbiting satellites are the best platforms from which to make these measurements. Passive microwave radiometers carried on satellites can probe through clouds and measure the attenuation of the very weak microwave radiation that is emitted by the Earth's surface by precipitation.

Satellite data analysis has been fundamental to understanding how to quantitatively relate these attenuation measurements to a precipitation rate. Much has been learned about the way in which radiation is absorbed and scattered from analysis of the Nimbus 7 Scanning Multichannel Microwave Radiometer (SMMR) data. The SMMR measures brightness temperatures at 6, 10, 18, 21, and 37 GHz at both vertical and horizontal polarizations. MSFC's most recent advance in this area is the determination that the dual-polarized, 37-GHz data can be utilized to measure the scattering signal over the ocean. Rain rates derived with this method over the Gulf of Mexico coastal waters have compared very well with radar-derived rain rates. Figure 67 shows an example of this satellite-ground radar comparison off the Florida coast. Unfortunately, these satellite measurements have very poor spatial resolution compared to the structures found in rain systems. Therefore, it has been difficult to determine simultaneously just what the true signal of rain systems is at a number of frequencies.

Experiments are now being performed onboard the NASA high altitude ER-2 aircraft using these frequencies to measure the signatures of rain systems at high spatial resolution from above all

clouds. This is crucial to understanding the measurements received from satellites. During June and July 1986, a microwave precipitation radiometer was flown in cooperation with Goddard Space Flight Center to take these measurements for the first time. This was part of the Cooperative Huntsville Meteorological Experiment, an extensive ground-based, airborne, and satellite atmospheric science experiment in northern Alabama and central Tennessee.

SATELLITE

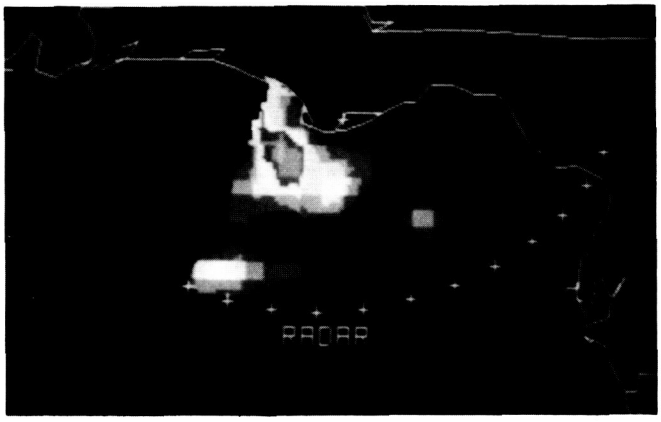

GROUND

Figure 67. Satellite Microwave and Radar Images of Rain off the Florida Coast.

Radiative transfer modeling is supporting these efforts to better understand how radiation is affected by changes in cloud depth, temperature, phase, density of hydrometeors, and hydrometeor size. The most recent development by MSFC in this area has been the modeling of cirrus clouds to determine whether the higher microwave frequencies are significantly contaminated by the scattering from cirrus ice particles. Preliminary indications are that, while many cirrus clouds have negligible impact on passive microwave measurements up to 230 GHz, cirrus emanating from thunderstorms can have a major impact on these measurements, especially above 60 GHz. These results will aid in choosing microwave frequencies for future use in space for precipitation measurement, as well as for atmospheric temperature and moisture sounding. These results also suggest that the higher microwave frequencies can be utilized to measure the microphysical characteristics of cirrus clouds. This is important to global radiation studies due to the importance of cirrus clouds to the Earth's heat budget.

The eventual impact of the passive microwave research will be a well-defined approach to the measurement of precipitation and cloud properties from space.

R. W. Spencer/ED43
(205) 544-1686
Sponsor: Office of Space Science and Applications

Atmospheric Precipitation Systems

A primary focus of atmospheric numerical modeling activities at MSFC is simulation and diagnosis of physical processes leading to precipitation at the mesoscale. The Limited Area Mesoscale Prediction System model is a sophisticated hydrostatic predictive model designed to simulate the evolution of precipitation from atmospheric systems 50 km and larger (Fig. 68). The past

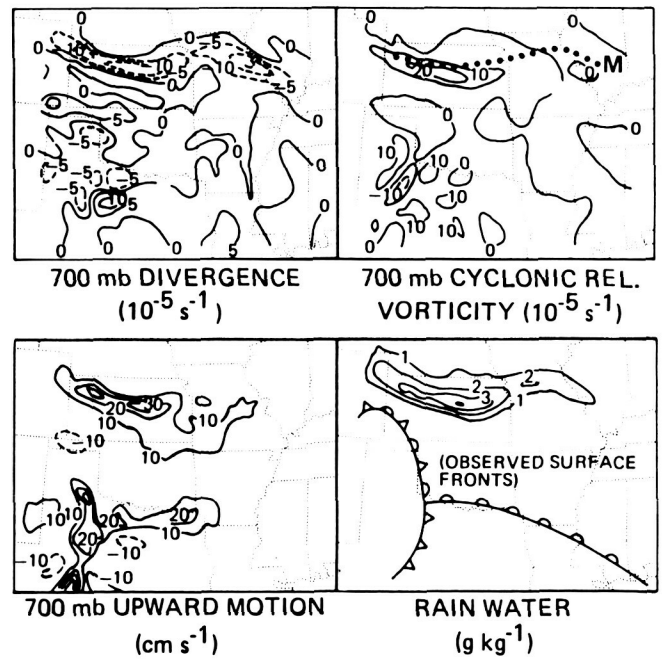

Figure 68. Maps at 0300 GMT Showing the Correspondence of Atmospheric System Parameters (700 mb Short Wave Trough Axis Indicated in Upper Right Panel by Dotted Line).

2 years have been devoted to model implementation and testing on existing MSFC computer systems. Studies have been performed that examine the model's ability to accurately simulate the life cycle of mesoscale convective systems. The sensitivity of the model to the scale of structure has also been studied. Such studies are necessary for understanding the limitations of the model and its ability to simulate and retain mesoscale structures, as well as for understanding the type and scale of atmospheric observations which might be necessary for maximum predictive accuracy.

These efforts are background studies leading up to a more comprehensive research program to use the numerical model as a tool to evaluate the ability of meteorological satellite sensors to observe mesoscale structures in the atmosphere. In the experimental design, a control model run will be made with a high horizontal resolution to generate atmospheric structures which are not easily measured with the operational 12-hour rawinsonde observation network. The advantage of a model mesoscale atmosphere is that the internal dynamical processes in the simulated structures can be diagnosed from the model output, giving a degree of experimental control not achievable with real atmospheric observations.

MSFC will simulate what a satellite system would see if observing the model mesoscale structures, using new initial states derived from these model-based satellite "observations." Comparing model simulations to the known, control model atmosphere solution will provide very important guidelines for how well a proposed space-based system can depict mesoscale atmospheric structure and retain or regenerate those structures.

M. W. Kalb/ED43
(205) 544-1684
Sponsor: Office of Space Science and Applications

Multispectral Mapping

The Multispectral Atmospheric Mapping Sensor (MAMS) was developed during FY85 as part of the MSFC effort to obtain a complement of aircraft instruments to support research and technology activities. The MAMS, through its cross-track scanning capabilities over a 40-km region, provides radiometric data of the surface reflectance from terrain/vegetation features, the temperature structure of the surface, and atmospheric water vapor variations (Fig. 69). Small-scale variability of these parameters will provide critical information needed to better understand and model the atmospheric conditions under which clouds and thunderstorms develop.

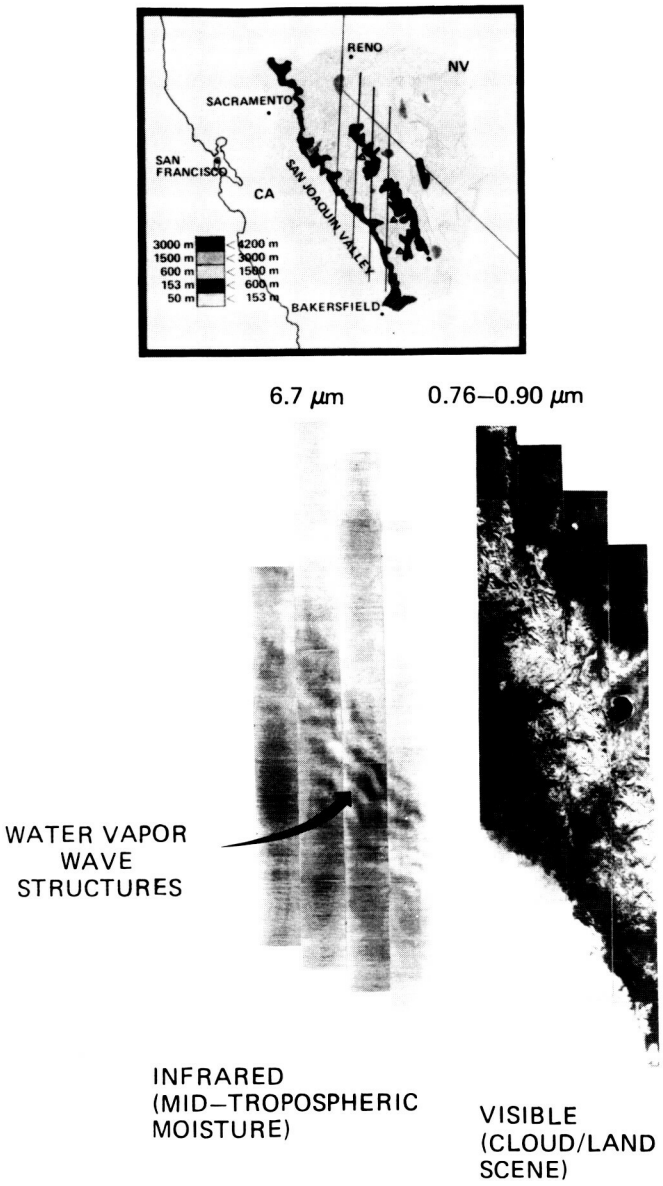

Figure 69. MAMS High Resolution Aircraft Composite Imagery.

Since its development, engineering and science flights have provided crucial information about the MAMS limitations and capabilities, and a much improved instrument configuration is now available. Preliminary analysis of flight data indicates that much variability in atmospheric moisture exists at fine scales. In addition, the thermal character of the surface of the Earth, which is governed by the land cover class (bare soil, type

of vegetation, etc.), is highly variable down to the resolution limits of the sensor, and may significantly affect the temperature structure of the lowest 1500 m of the atmosphere. These two aspects combine with wind to control cloud development and the production of thunderstorms. These hypotheses are currently being tested with data from the Satellite Precipitation and Cloud Experiment (SPACE), a NASA-sponsored activity to collect special atmospheric measurements. The MAMS efforts during SPACE will also help define the requirements for space-borne surface and atmospheric remote sensing instruments in the years to come.

G. J. Jedlovec/ED43
(205) 544-1688
Sponsor: Office of Space Science and Applications

Satellite Infrared Precipitation Measurements

Remotely-sensed precipitation measurements are crucial to many Earth science disciplines, including atmospheric dynamics. The release of latent heat that accompanies precipitation is thought to be a significant source of energy for atmospheric flows ranging in size from thunderstorms to planetary-scale waves. Satisfactory techniques for obtaining rain measurements from space have yet to be fully realized. In addition to passive microwave techniques, there exists a need to fully utilize the existing infrared (IR) information from geostationary satellites because of its unique temporal resolution and a long historical data base. Algorithm development at MSFC has focused on an approach which yields large-scale estimates suitable for use in diagnostic studies of synoptic-scale dynamics.

The methodology involves deriving a simple statistical relationship (quadratic polynominal fit) between individual IR blackbody temperatures and colocated point measurements of precipitation at the ground. The resulting algorithm, if applied at this pixel scale, generates substantial scatter, as IR measurements primarily yield information about suspended hydrometeors and relate only indirectly to precipitation. Averaging of these pixel rain rates over areas ~10^5 km^2 for 12-hour periods yields estimated root mean square errors of 30 to 50 percent. This level of accuracy is comparable to that obtained when deriving precipitation estimates as a residual in moisture balance equations using conventional rawinsonde observations.

Application of this algorithm to IR data taken during the Global Weather Experiment (GWE) has facilitated an analysis of the role of latent heat release in driving the tropospheric flow over the data-poor South Pacific region. Precipitation diagnosed from the Geosynchronous Operational Environmental Satellite (GOES) W IR imagery (Fig. 70) has been used as a constraint in diagnosing vertical profiles of diabatic heating. These heating fields show a middle- to upper-tropospheric maximum which implies vertical circulations consistent with those diagnosed from other independent GWE analyses. Kinetic and potential energy budgets which incorporate these inferred diabatically-forced circulations show heating to be a major source of energy in maintaining the wind fields in the southern tropical Pacific.

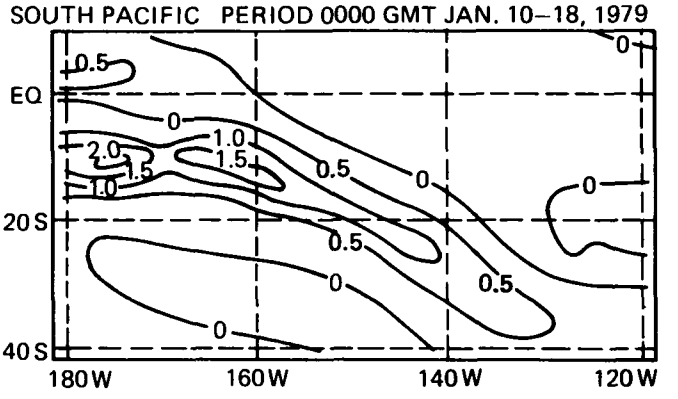

Figure 70. Average Rainfall Rate (mm/h) Estimated from GOES IR Imagery.

Research has recently focused on examining the variability of the algorithm when derived and applied in other climatic regions. This work should contribute to a better understanding of the problems in using satellite IR measurements in estimating global precipitation.

Robertson, F. R.: Use of IR Satellite Rainfall Estimates in Diagnosing Thermally-Forced Circulations in the Pacific During FGGE SOP-1. Conference on The Scientific Results from FGGE, January 14-17, 1986, Miami FL. American Meteorological Society, Boston MA.

Robertson, F. R.: Use of GOES IR Data in Estimating Synoptic-Scale Rainfall: Algorithm Development and Transferability. J. Climate and Applied Meteor.,1986.

F. R. Robertson/ED43
(205) 544-1655
Sponsor: Office of Space Science and Applications

Cloud Top Lightning

Lightning has been studied from above cloud tops using a wide variety of platforms and sensing techniques. Each approach has offered a different perspective and revealed new features of the lightning phenomenon. Observations from space have produced maps of global flash frequency by season and location, and recently, information on the diurnal variation of lightning has been generated from Ionospheric Sounder Satellite-b measurements. Another unique capability that the space perspective provides is the ability to see the big picture. Large storm systems can be imaged in their entirety, making it possible to relate lightning activity to specific storm features.

While space provides an excellent perspective for studies on a large scale and on temporal variability, detailed measurements of lightning characteristics are best made in closer proximity to the event. Extensive optical observations of lightning made from U-2 aircraft flying over the tops of thunderstorms have revealed a great deal of information about the optical characteristics of lightning and of the clouds. A typical set of electronic signatures is shown in Figure 71.

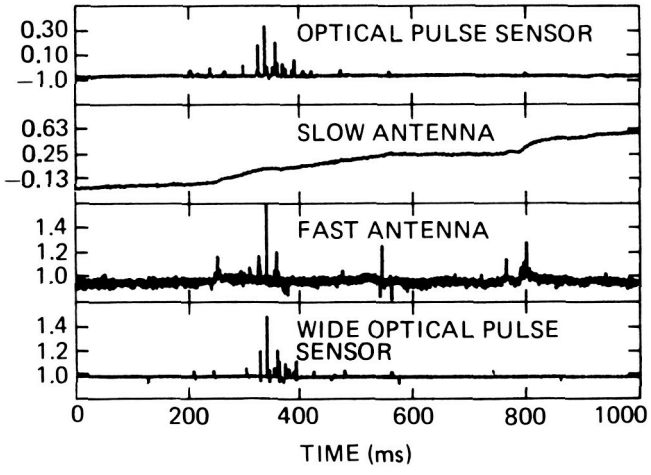

Figure 71. Typical Electronic Signatures Recorded by the U-2 Aircraft.

During 1984, cloud top lightning spectra were measured from a high-flying U-2 aircraft in the wavelength region from 380 nm to 900 nm with a temporal resolution of 5 ms (Fig. 72). With this capability, both visible and near-infrared lightning spectra were acquired on a pulse-to-pulse basis, so that the spectral variability within a flash, as well as flash-to-flash variations, can be studied. The measurements show that important variations do occur, particularly in the strengths of the hydrogen and singly-ionized nitrogen emission lines. Also, the results have revealed significant differences in the integrated energy distributions between the lightning spectra measured above clouds and the spectral measurements of cloud-to-ground lightning made at the ground. In particular, the ratio of energy in the near-infrared to that in the visible is around 1 to 2 for cloud top spectra, compared to about 0.3 for the surface

Figure 72. Above Cloud Top Photo of Lightning Spectra Obtained by Broad Band Spectrometer.

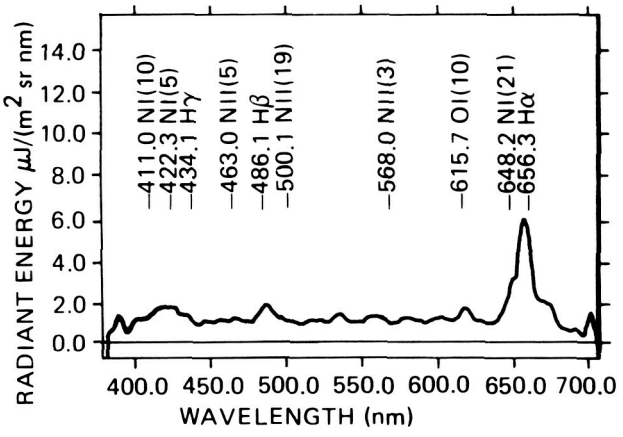

Figure 73. Optical Spectra from 400 to 700 nm.

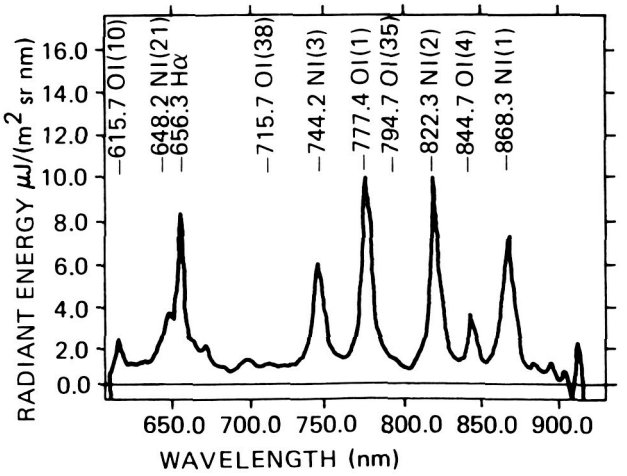

Figure 74. Optical Spectra from 650 to 900 nm.

observations. Figures 73 and 74 show optical spectra from 400 to 700 nm and 650 to 900 nm, respectively.

MSFC is now planning to continue research work in conjunction with the Cooperative Huntsville Meteorological Experiment (COHMEX). The lightning research program for COHMEX, the Lightning and Precipitation Experiment, has obtained lightning data in terms of overall storm physics with a goal of understanding lightning activity and its relation to precipitation and convective processes.

R. J. Blakeslee/ED43
(205) 544-1652
Sponsor: Office of Space Science and Applications

Geostationary Lightning Mapper

The occurrence of lightning is accompanied by the sudden release of electrical energy which is converted into rapid heating in the vicinity of the channel, the generation of a shock wave, and electromagnetic radiation ranging from extremely low-frequency radio waves to x rays. One of the strongest radiation regions is at visible wavelengths, which accounts for almost 1 percent of the total energy release: 100 to 1000 MW of light. These optical emissions result from the dissociation, excitation, and subsequent recombination of atmospheric constituents which are primarily affected by electron bombardment and the sudden heating of the lightning channel. The heating is so intense that the emissions occur primarily at discrete atomic lines, with some continuum at shorter wavelengths. The strongest emission lines are produced by neutral oxygen and neutral nitrogen, and occur in the near-infrared from 7774 to 8683 A.

With present technology, the two viable approaches for the detection and location of lightning events are either optical or radio frequency (RF) techniques. For ground-based operations, RF approaches have been preferred because optical systems suffer from obscuration, attenuation, and limited range (line of sight). Conversely, for remote sensing from space, optical techniques offer many advantages. Light is not affected by the ionosphere or magnetosphere. The relatively short wavelengths of light permit accurate direction-finding with small detectors. The large signal strength of the lightning event at optical wavelengths provides usable signals from a geostationary orbit. On the other hand, radio signals, at longer wavelengths, are strongly attenuated or refracted by the ionosphere, and thus are unsatisfactory for accurate lightning direction-finding from orbit. At higher RF frequencies the lightning source strength is weaker than the cosmic ray background noise at geostationary altitudes, and thus lightning detection would be extremely difficult.

A space-based sensor for the optical detection of lightning is conceptually a very simple device (Fig. 75). It is basically a staring imager that is optimized to detect and locate lightning events. The lightning mapper sensor images a scene in much the same manner as a television camera; however, because of the transient nature of lightning, its spectral characteristics, and the difficulty of daytime detection of lightning against the brightly lit cloud background, actual data handling and processing differs vastly from that required by simple imagers.

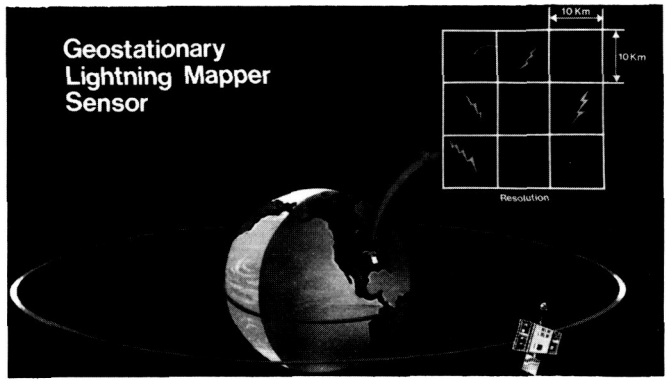

Figure 75. Geostationary Lightning Mapper Sensor.

H. J. Christian/ED43
(205) 544-1649
Sponsor: Office of Space Science and Applications

The Cooperative Huntsville Meteorological Experiment

The Cooperative Huntsville Meteorological Experiment (COHMEX) is a unique field experiment that was conducted from March through July 1986, with a core period of operation in June and July. It took place in the region covering northern Alabama and the adjoining portion of central Tennessee. The experiment's uniqueness derives from the fact that it was actually composed of three distinct experiments sponsored by NASA, the National Science Foundation (NSF),

and the Federal Aviation Administration (FAA), with extensive sharing of resources and data. The Satellite Precipitation and Cloud Experiment (SPACE) comprised the NASA component of the COHMEX experiment during the pre-storm period, and focused on observations of the physical processes leading to the formation of small convective systems.

The sounding stations of the meso-beta SPACE rawinsonde domain were centered over an extensive rain gauge network operated by the Tennessee Valley Authority (TVA) (Fig. 76). After convection developed, emphasis was placed upon observations of precipitation and hydrometeor evolution, using remotely-sensed observables, and upon the influence of moisture sources in the storm environment for the development and maintenance of the precipitation process. During the mature phases of the storms, studies were conducted to relate electrical activity to precipitation and dynamical processes. Before, during, and after the development of convection, detailed sets of atmospheric-state variable data were collected to enable numerical modeling of the boundary layer, tropospheric and cloud-scale thermodynamics, and environmental variability related to the life cycle of small convective systems.

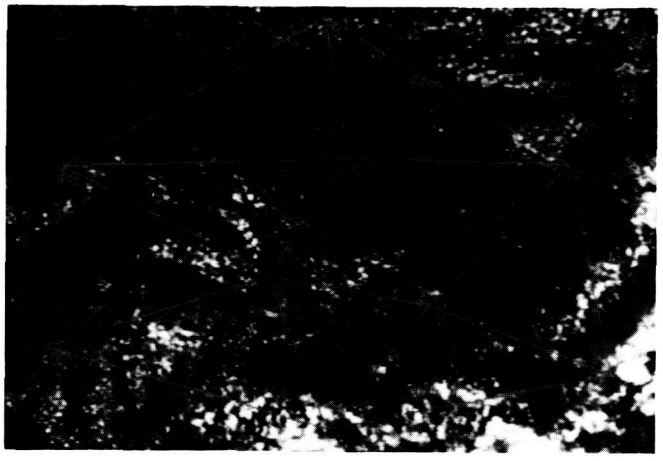

Figure 76. High-Density Atmospheric Sounding Network Centered over the Tennessee Valley.

Crucial observations for NASA's SPACE experiment were obtained from numerous flights of two high-altitude aircraft (a NASA U-2 and an ER-2), with a total complement of ten experimental remote sensing systems measuring visible, infrared, and microwave radiation for determination of various storm/environment characteristics. The systems measured cloud top structure, cloud microphysics, precipitation, cloud and environmental temperature and moisture soundings, lightning characteristics, and high-resolution cloud, water vapor, and surface features. The South Dakota School of Mines and Technology T-28 storm penetrating aircraft was employed for conventional observations of liquid water and hail-size concentrations, hydrometeor size distributions, internal cloud temperature, and electric field structure. In addition, a network of 70 TVA computerized rain gauges, 10 NASA upper air stations, 9 Portable Automated Meteorological Observing System (PAM II) sites (operated by the National Center for Atmospheric Research), 10 special NASA surface stations, and a four-station NASA/AF lightning location were operated at high time resolutions to define the prestorm and storm environments.

J. E. Arnold/ED43
(205) 544-1646
Sponsor: Office of Space Science and Applications

Space Station Geostationary Platform

The geosynchronous platform offers the possibility of observing broad regions of the Earth at half-hour intervals or better. The only limitation on this temporal resolution is the capability of the instrumentation involved. Such temporal resolution is of scientific value in observing processes on the Earth's surface or atmosphere which change significantly over the period of an hour. Events having this characteristic time scale are primarily atmospheric processes and other highly transient geophysical phenomena.

For the past 10 years or more, the Geosynchronous Operational Environmental Satellite (GOES) has been used to monitor such phenomena as tropical depressions and hurricanes, atmospheric fronts, and severe squalls and storms. The operational agencies have used the Visible and Infrared Spin Scan Radiometer (VISSR) on GOES to form sequential images of these phenomena. These "time lapsed" images have then been used to predict the most probable future position of these meteorological phenomena. Although the instruments placed on GOES were used to make quantitative predictions, the imagery has traditionally been used in a more qualitative, picture

mode. The most recent GOES has carried the added capability of quantitative temperature and moisture sounding of the Earth's atmosphere. Although the instrument involved in this observation is in many ways limited, it has identified the scientific usefulness of sounding the atmosphere with high temporal frequency and reasonable horizontal spatial resolution.

The goal for the next generation of geosynchronous observations of the Earth from the Space Station Geostationary Platform would be to improve upon the atmospheric sounding capabilities already demonstrated in low Earth orbit (LEO), as well as to provide new observations of lightning and atmospheric, oceanic, and land phenomena best observed from geosynchronous altitudes (Fig. 77). These observations would be used in the research mode to better understand physical processes in the Earth's atmosphere. This understanding would subsequently be applied to develop techniques useful in operational monitoring, and form a key element of NASA's Earth Observing System capability.

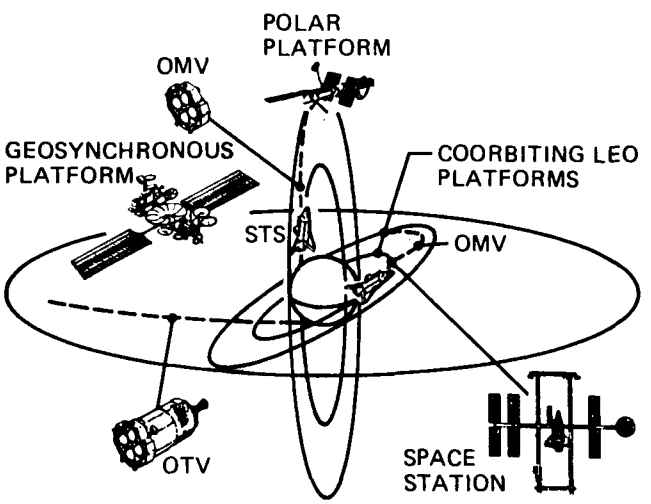

Figure 77. Space Station and Geosynchronous Platform Complex.

G. S. Wilson/ED43
(205) 544-1646
Sponsor: Office of Space Science and Applications

Storm Physics of Convection

The objective of this research is to study the relationship between thunderstorm processes and the characteristics of convection throughout the thunderstorm life cycle. Multiple-parameter radar measurements are used in conjunction with numerical models to determine the kinematic, thermodynamic, and microphysical properties of the observed thunderstorms. The rainfall rates, lightning activity, and storm intensity are being examined in conjunction with factors in the environment which strongly influence the evolution of the thunderstorms. These include the available buoyant energy feeding the storm, wind shear, boundary layer forcing, and low level moisture convergence.

Observations of lightning activity in large storm systems called mesoscale convective complexes (MCCs) show that a single MCC event can produce one-fourth of the mean annual lightning discharges to ground for any site passed over during the most intense phase of its life cycle (Fig. 78). An important implication of this result is that a given location may be well above or below

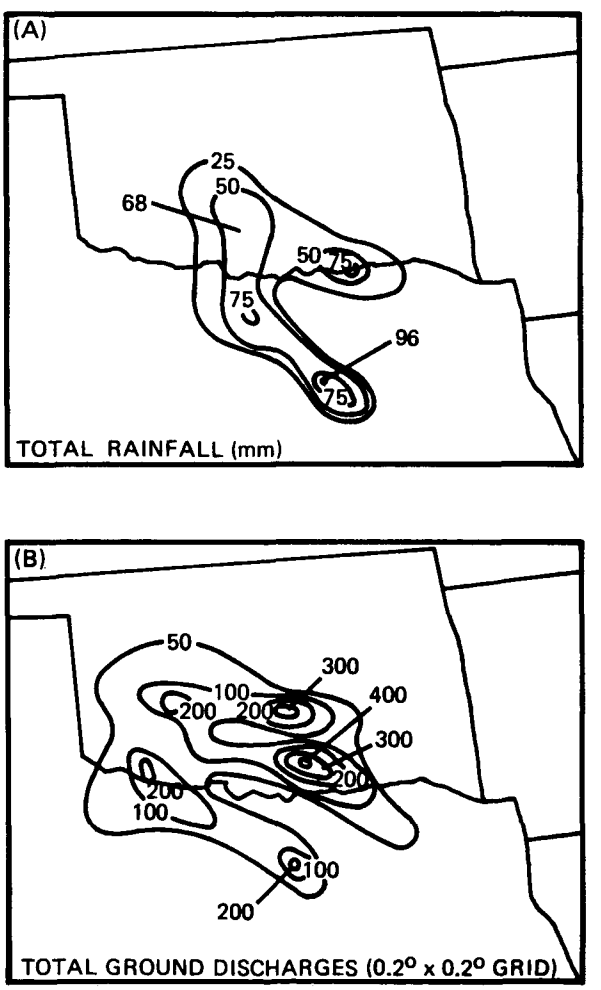

Figure 78. Precipitation and Lightning Discharges to Ground, June 13, 1983 Mesoscale Convective Complex over Oklahoma.

its mean annual lightning total as a result of an MCC either passing directly overhead or circumventing the station when the MCC is most intense. MCCs are of great scientific interest to meteorologists because they are also responsible for much of the beneficial precipitation and most of the severe weather that occurs in the United States in the spring and summer months.

Goodman, S. J.; and MacGorman, D. R.: Cloud-to-Ground Lightning Activity in Mesoscale Convective Complexes. Monthly Weather Review, October, 1986.

S. J. Goodman/ED43
(205) 544-1683
Sponsor: Office of Space Science and Applications

Atmospheric Turbulence Modeling

Predictability of the atmosphere is a research area in the NASA/MSFC Global Scale Processes Program. Advancement must come from concerted effort on general circulation models of the atmosphere, empirical studies, and statistical theories of turbulence. Numerical models and super computers have the capability to include all pertinent, large-scale, dynamic, and geometric characteristics with increasing resolutions. It is evident that a theoretical turbulent predictability model is needed to better determine the general circulation of the atmosphere.

A new analytical statistical theory, the group-kinetic theory, has been developed and may be a powerful method for investigation of atmospheric turbulence. Significant areas in the theory being researched include: generalizing for application to a stratified atmosphere with a Coriolis force; deriving the eddy transport coefficients of momentum, temperature, and humidity; investigating the pressure-strain correlation with shear, stratification, and Coriolis force; analyzing spectral distinctions of temperature and humidity fluctuations and of entropy and energy transfers; investigating turbulence characteristics in the inversion layer; and developing an analytical theory of prediction for the boundary layer.

Previous work in atmospheric turbulence has used the Navier-Stokes fluid equations exclusively for describing large-scale motions. Controversy over the existence of an average temperature gradient for very large atmospheric eddies suggested that a new theory describing large-scale turbulence was necessary. A new soliton formalism as a fluid analogue that generalizes the Schrödinger equation and the Zakharov equations has been developed. This formalism possesses all the nonlinearities, including those from modulation provided by density fluctuations and convection due to the emission of finite sound waves by velocity fluctuations, and treats large-scale turbulence as coalescing and colliding solitons. The new system describes large-scale instabilities more explicitly than the Navier-Stokes system because it has a nonlinearity of the gradient type, while the Navier-Stokes system has a nonlinearity of the non-gradient type. The forced Schrödinger equation for strong fluctuations describes the micro-hydrodynamic state of soliton turbulence and is valid for large-scale turbulence in fluids and plasmas where internal waves can interact with velocity fluctuations.

A nonlinear system of equations has been developed to describe the microdynamic state of turbulence excited by density waves. A kinetic equation was derived to calculate eddy viscosity and to formulate the coupling mechanism for the intensification of turbulent energy and the transfer mechanism for the cascade.

Tchen, C. M.: Excitation of Turbulence by Density Waves. NASA CR-3905, June 1985.

Tchen, C. M.: Soliton Turbulence. NASA CR-3969, March 1986.

M. B. Alexander/ED42
(205) 544-1640
Sponsor: Office of Space Science and Applications

Dynamical Studies of the Earth's Atmosphere

Remote sensing is one of the most important roles of satellites with respect to Earth science. The measurement of atmospheric variables such as temperature, humidity, cloudiness, lightning, and winds is an invaluable addition to "conventional" data acquired from weather balloons, ships, aircraft, buoys, and ground stations. These data are used for operational forecasting, as input to computer models, and to construct data sets which can be studied by researchers in order to obtain a better understanding of basic processes that occur in the atmosphere and oceans. The determination of the requirements for the

space-based sensors, the variables measured, and the spatial and temporal resolution required is often assisted by making theoretical considerations in terms of the dynamical behavior of the atmosphere or ocean as a physical system. That is, given the present understanding of the physical/dynamical processes, what atmospheric or oceanic measurements need to be made in order to further that understanding?

One of the most important problems of atmospheric dynamics is to predict and understand the event known as "blocking." Blocking refers to a shift in the planetary scale flow which ordinarily steers mid-latitude storm systems. When a blocking event occurs, the paths of storms that ordinarily would pass over a particular geographical area are diverted. It is not clear what the physical mechanism for this phenomenon is, nor how to consistently forecast its occurrence.

Since the blocking phenomenon involves atmospheric motion on both planetary and smaller "synoptic" scales, an approach to the problem is to examine the interaction between these two scales. Because the long waves are generally stationary with respect to longitude and tend to have a preferred orientation, they are evidently forced by the presence of the continents and oceans. Synoptic scale cyclones, on the other hand, are apparently the result of a dynamical (baroclinic) instability. The planetary scale waves result in a flow which causes preferred regions for this instability and which then guides the propagation of the short waves. Feedback to the planetary scale waves, due to the large amount of latent heat released and to horizontal heat and momentum fluxes associated with the cyclones, may cause sudden changes in the planetary scale wave pattern.

The "mesoscale" atmospheric processes occur on a slightly smaller scale than the synoptic scale processes, with mesoscale spatial scales ranging from 1 to 1000 km (0.6 to 600 mi). The research described here is in the range of about 100 to 1000 km. It is on this scale that a large fraction of the precipitation in the mid-latitude weather systems is organized. Accurate modeling will not occur unless the mesoscale processes are accurately modeled, either explicitly or by parameterization. Currently, neither of these approaches is being successfully used, and it appears that progress in large-scale modeling is awaiting further developments in the understanding of mesoscale processes.

One of the dynamic phenomena most likely to be of relevance to precipitation on the mesoscale is symmetric instability, which is the result of a combination of buoyant and inertial restoring forces acting on a balanced fluid system. As shown in Figure 79, view A, when the surfaces of constant potential temperature (T) are more nearly vertical than those of constant total momentum (M), the vertical (buoyant) and horizontal (inertial) restoring forces act together to cause a fluid particle to continue an initial displacement. The result is a circulation which is slanted (rather than being either vertical or horizontal) and which lies approximately along surfaces of constant potential temperature or absolute momentum (view B). The circulations lie in the vertical plane containing the mean temperature and momentum gradients, and they

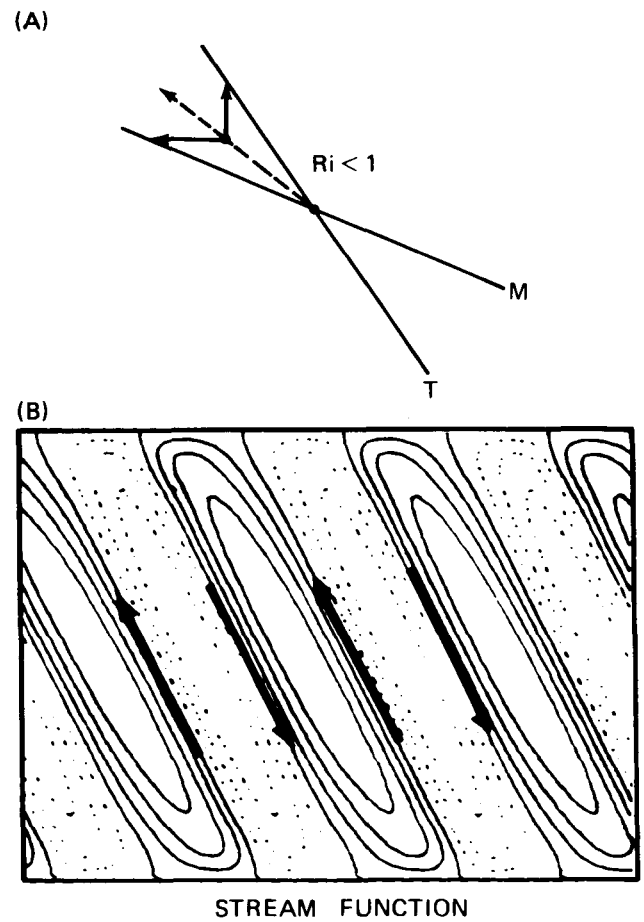

Figure 79. Symmetric Instability Mechanism: (A) Buoyant and Inertial Forces Acting to Continue an Initial Displacement; (B) Resultant Instability.

transport heat and momentum as they extract energy from the mean field. Their effect upon the weather is shown in Figure 80; the circulations due to the symmetric instability organize cumulus through the convergence of heat and moisture in the boundary layer, and through lifting of saturated air in the updrafts. Thus convergence in the lower boundary layer brings heat and moisture into preferred regions, giving rise to an instability, which is indicated by cloud and precipitation bands spaced at about 100 to 300 km (60 to 180 mi).

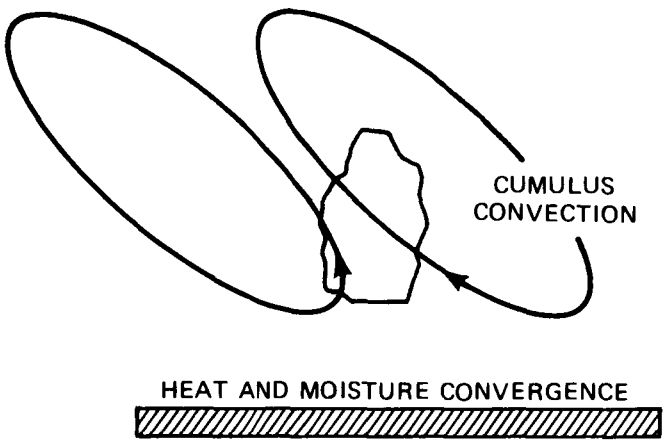

Figure 80. Effect of Symmetrical Instability Circulations upon the Weather.

In the past, the approach to atmospheric modeling has been to analyze the stability of a basic wind which is horizontally uniform and has linear vertical shear. An approach which will be attempted at MSFC will be to use a detailed, numerical weather prediction model to simultaneously model the synoptic scale and mesoscale phenomena. The early work will be of idealized cases with simple initial conditions, no ground topography, and no moisture. Complicating factors will gradually be added until actual atmospheric case studies will be performed. The work is expected to indicate directions for improvement of atmospheric modeling, as well as shed light on which physical processes and observational strategies to use.

Miller, T. L.; and Antar, B. N.: Viscous Non-Geostrophic Baroclinic Instability. J. Atmos. Sci., 43, 329-338, 1986.

T. L. Miller/ED42
(205) 544-1641
Sponsor: Office of Space Science and Applications

Natural Environment Criteria for Shuttle II Design

The Shuttle II is to be a second generation manned space transportation system capable of performing routine, low-cost access to and from space to meet post-year 2000 space transportation needs. The Shuttle II is a space vehicle architecture designed to meet changing mission requirements. This is to be a new system rather than an extrapolation or modification of the current space transportation system. Emphasis is placed on a small- to mid-size payload capability with frequent flights rather than a large payload capability.

This concept of frequent flights having brief space operations of 2 to 3 days emphasizes the importance of a system designed to minimize launch, landing, and ground operational delays due to the natural environment. A design goal is an all-weather aerospace system. Launching on time and within brief launch windows are considered to be critical for many missions. Polar orbits are required; therefore, launch operations from both Kennedy Space Center and Vandenberg Air Force Base are baselined. Atmospheric criteria from both sites are being developed for this program.

It is important to the success of the Shuttle II program that consideration be given to all facets of the natural environment for the systems design and operations. It is also important that the natural environment requirements be defined for the design and operations at the beginning of the program. This is not an easy task in the presence of advancing technologies and the prediction of new technologies 15 years into the future.

As with any new aerospace program, a long list of natural environment requirements has been specified. These requirements are needed to establish the feasibility of new engineering concepts. The natural environment definitions required for the Shuttle II program may be classified into the ten categories shown in Table 7. In all of the categories, the approach being used is to either design for the natural environment effects on the aerospace system, or protect it from the natural environment. In cases where it is not feasible to do either, the approach has been to assess the impact on the operations and establish

definitive operational constraints, determine the chances that the operational constraints will occur, and establish the risk to the operations and consequences to the program if one or more of the operational constraints are violated.

Table 7. Natural Environment Definitions Required for the Shuttle II Program.

- EARTHBOUND OPERATIONS - GROUND FACILITIES DESIGN, LAUNCH COMPLEX, GROUND SUPPORT EQUIPMENT, AND STORAGE.
- TRANSPORT - INCLUDES ATMOSPHERIC FERRY FLIGHT AND SURFACE TRANSPORTATION
- ON-PAD OPERATIONS - PAD STAY TIME AND EXPOSURE PERIODS.
- LAUNCH OPERATIONS.
- ASCENT FLIGHT.
- RECOVERY FROM ASCENT FLIGHT, FLYBACK, AND LANDING.
- ON-ORBIT OPERATIONS.
- RETURN FLIGHT FROM ORBIT AND LANDING.
- MISSION ANALYSIS - INCLUDES ATMOSPHERIC CONTRIBUTIONS FOR LAUNCH DELAY RISK, OPERATIONS DELAY, TRADE STUDIES FOR DESIGN AND FLEET SIZE.
- SPECIAL AREAS - INCLUDES ADVANCED ATMOSPHERIC TECHNOLOGIES IN EQUIPMENT, CONCEPTS, OBSERVATIONS (MONITORING), AND SITE-SPECIFIC WEATHER PREDICTABILITY.

C. K. Hill/ED44
(205) 544-1664
Sponsor: Office of Space Flight

Global Cloud Cover Data Base

A global cloud cover data set has been developed for use in climate studies and for Earth-viewing applications. This data set contains a single parameter, total sky cover, separated in time by 3- or 6-hour intervals, and in space by approximately 50 nautical miles. Cloud cover amount is recorded for each square grid point by an alphanumeric character representing a 5-percent increment of sky cover. The data are arranged in both quarterly and monthly formats. A quarterly format usually contains 3 months of data for one hemisphere, while a monthly format contains up to 5 years of monthly data for one hemisphere.

Although there are gaps in the data (notably all of 1976 for the Northern Hemisphere), the data base currently provides daily, 3-hour observed total sky cover for the Northern Hemisphere from 1972 through 1977, excluding 1976. For the Southern Hemisphere there are data at 6-hour intervals for 1976 through 1978 and at 3-hour intervals for 1979 and 1980. More annual data are being added in both hemispheres. To validate the data base, the percent frequency of ≤ 0.3 and ≥ 0.8 cloud cover was compared with ground-observed cloud amounts at several locations, with generally good agreement.

Mean or other desired cloud amounts can be calculated for any time period and any size area, from a single grid point to a hemisphere. The data base is especially useful in evaluating the consequence of cloud cover on Earth-viewing space missions. The temporal and spatial frequency of the data allows simulations that closely approximate any projected viewing mission. The greatest attribute is that no adjustments are required to account for cloud continuity.

C. K. Hill/ED44
(205) 544-1664
Sponsor: Office of Space Flight

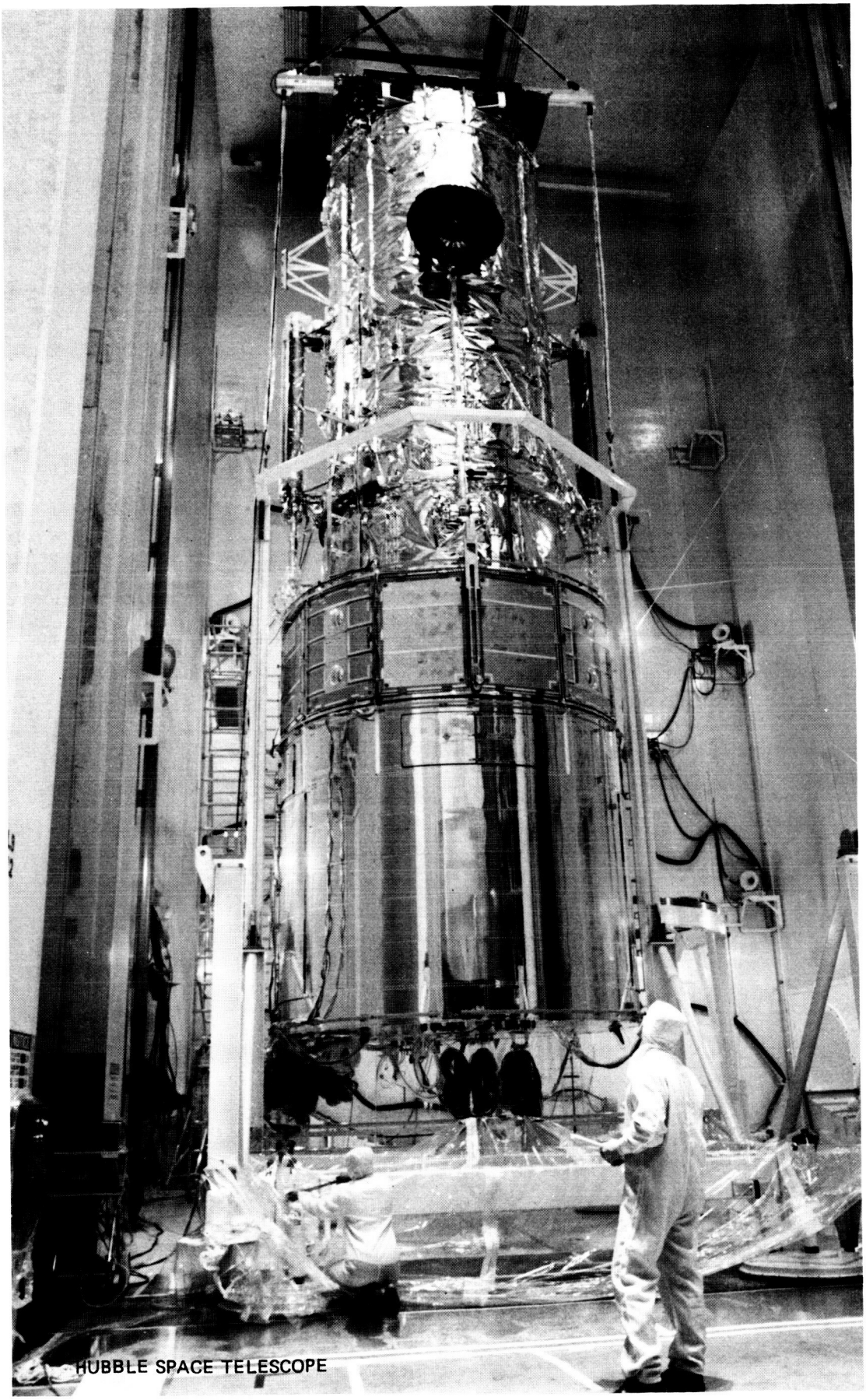

HUBBLE SPACE TELESCOPE

Technology Programs

Innovative engineering solutions to the challenges inherent in the design and development of advanced systems require a vigorous technology program. The Marshall Space Flight Center's design and development assignments range from launch vehicles and associated propulsion systems to complex long-duration spaceflight systems developed to support research and scientific investigations. The many and varied engineering activities required by these assignments have fostered the development of a diverse technology program supported by a highly capable and talented engineering team. Current technology initiatives include advanced design and analysis techniques for propulsion systems, fluid dynamics and heat transfer, structures and dynamics, space power, and information systems. Work is also proceeding on tasks to expand the materials data base, to improve materials, to develop improved material processes, and to expand the range of options available for manned space systems by augmenting the technology base for candidate life support subsystems.

Propulsion

Preburner Combustion Modeling

Analytical and computational modeling of the combustion and flow processes in the SSME fuel preburner were approached using a two-fluid mixing model. This model assumes that the combustion process in the preburner is controlled by details of the mixing of the reacting fluids rather than by the chemical reaction rates. Interaction parameters between the two fluids were calculated using arguments considering the microscale physics of the diffusive and turbulent mixing. Both evaporative and supercritical droplet models were used, with the droplet diameter d_0 serving as a varying parameter. The models were applied to the fuel preburner to obtain flow fields and temperature distributions. Figure 81 shows a multi-fluid analysis with contours of temperature (T), and oxygen volume fraction r_2 for d_0 = 127 μm at injection. It was possible to obtain results which indicated the presence of unreacted oxygen at the preburner dome and at the entrance to the turbine. This results in relatively high temperatures in those regions; that is, higher than expected if the reactions are completed higher in the preburner.

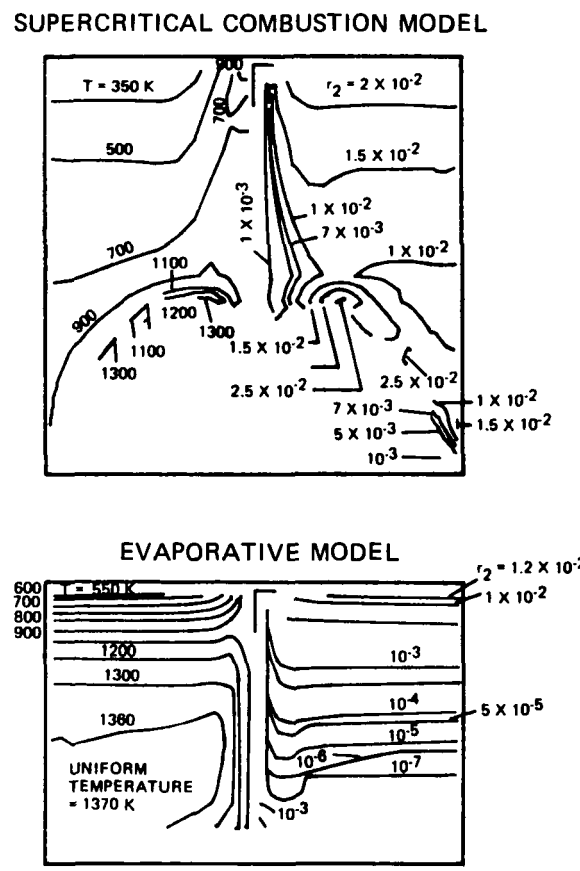

Figure 81. Multi-Fluid Analysis of the SSME Preburner.

Prakash, C.; Singhal, A.; and Schafer, C. F.: SSME Fuelside Preburner Analysis Using a Gas-Gas Diffusion Model for the Mixing of Oxygen and Hydrogen at Supercritical Pressures. SSME Fourth Working Group Meeting, April 8-11, 1986.

C. F. Schafer/ED42
(205) 544-1642
Sponsor: Office of Aeronautics and Space Technology

Liquid Rocket Combustor Code

An Advanced Rocket Injector/Combustor Code (ARICC) has been developed to model the complete chemical/fluid/thermal processes occurring inside rocket combustion chambers. Combustion processes occurring in a fluid medium are probably among the most complex of all flow phenomena. The complexity stems from the so-called "combustion" process, which is actually many physical processes of different types that are strongly linked together. Modeling attempts must carefully select the most important driving processes, while also including the proper secondary process models.

The ARICC code is an attempt to build a modular model to describe the complete combustion process inside a liquid rocket engine using finite difference techniques. The process starts with injection of propellants into the combustion chamber in both liquid and gaseous states at high pressure and under conditions to encourage rapid atomization of the liquid component. The flow created by such injection is highly turbulent and rotational. Furthermore, in the case of liquid oxygen/hydrogen engines (which ARICC emphasizes), the propellant temperatures range from cryogenic (70 K) to superhot (3000+ K) before combustion. The inception of combustion magnifies the local temperature, pressure, and species concentration gradients. A list of requirements deemed necessary for the numerical modeling of the combustion process is given in Table 8.

An adequate numerical model must have the capability to fully describe the following types of phenomena: viscous flow as described by the full Navier-Stokes equation with turbulence modeling; multiple species chemical kinetics, liquid jet injection, atomization, and subsequent vaporization and transport of the droplets; and fine grid resolution near boundaries and corners of particular interest. All of these capabilities have been built into the ARICC. Table 9 lists the mathematical model used for each phenomena.

Table 8. Code Features Required for Liquid Rocket Engine Modeling.

NECESSARY FEATURES	FEATURES INCORPORATED INTO ARICC
• VISCOUS ELLIPTIC FLOW	• FULL NAVIER-STOKES EQN. – SGS TURBULENCE MODEL, ALL FLOW SPEEDS
• FULL CHEMISTRY	• MULTIPLE SPECIES KINETIC AND EQUILIBRIUM REACTIONS
• LIQUID JET INJECTION/ TWO-PHASE FLOW	• VOF TWO-PHASE, FREE SURFACE DESCRIPTION
• DROPLET DYNAMICS	• MONTE CARLO SCHEME/ LAGRANGIAN DROPLET TRACKING, DROPLET HEATUP AND VAPORIZATION, SUPERCRITICAL PROPERTIES, VARIBLE DRAG AND DENSITY
• ATOMIZATION	• CICM ATOMIZATION MODEL, SECONDARY DROP BREAKUP
• FINE RESOLUTION IN CRITICAL AREAS	• ARBIT. GRID WITH CLUSTERING

Table 9. Mathematical Formulations Used for Various Physical Processes.

I. FLUID THERMODYNAMICS:	
• MASS CONSERVATION (CONTINUITY)	PD
• MOMENTUM CONSERVATION (NAVIER-STOKES)	PD
• ENERGY CONSERVATION	PD
II. PHYSICAL MODELS:	
• EQN. OF STATE (CONSTITUTIVE)	AL/TA
• TURBULENCE	AL/PD
• CHEMISTRY	
RATE EQUATIONS	AL
EQUILIBRIUM EQUATIONS	AL/TA
• RADIATION	PD
III. DROPLET DYNAMICS:	OD
• DISCRETE FORMULATION	OD
• CONTINUUM FORMULATION	PD

TYPE OF GOVERNING EQN.

PD = PARTIAL DIFFERENTIAL
AL = ALGEBRAIC
TA = TABULAR
OD = ORDINARY DIFFERENTIAL

D. E. Pryor/EP23
(205) 544-7080
Sponsor: Office of Aeronautics and Space Technology

Dual-Throat Thruster Thermal Model

Future launch vehicles can benefit from employing a dual mode propulsion approach in which high density, moderate performance propellants are used in combination with low density, high performance propellants. Payload benefits can be realized by employing the propellants in parallel at lift-off and switching to the low density, high performance propellants at an appropriate time. One method of burning these propellants is to employ a dual-chambered thruster. One such thruster is the dual-throat thruster (Figure 82).

The dual-throat thruster consists of two concentric combustion chambers; the outer combustor burning the high density propellant and the inner combustor burning the low density propellant. Initially, both chambers burn propellant, and both exhaust gas streams flow through a common nozzle throat. This mode (Mode 1 in Fig. 82) is characterized as having high thrust and low nozzle area ratio (low performance). Later, only the inner chamber operates (shown as Mode 2 in Fig. 82). The expansion of the thruster's exhaust gas is controlled by a small bleed flow so that the flow attaches to the outer chamber nozzle throat surface. This operation results in a high effective nozzle area ratio (high performance), although at a lower thrust.

In providing this dual-mode operation, the dual-throat thruster experiences thermal environments not found in conventional thrusters. A mathematical thermal model describing this heating was constructed. Experimental data were acquired to characterize the heating in these regions for use in calibrating the thermal model. A small dual-throat thruster was constructed for testing to acquire the data. Both combustion chambers contained specially designed water-cooled calorimeter passages to measure the heat flux in the nozzle regions. To provide a combustion environment, oxygen and hydrogen propellants were used in each chamber. Heat flux measurements were taken over a range of chamber pressures, propellant mixture ratios, and nozzle spacing.

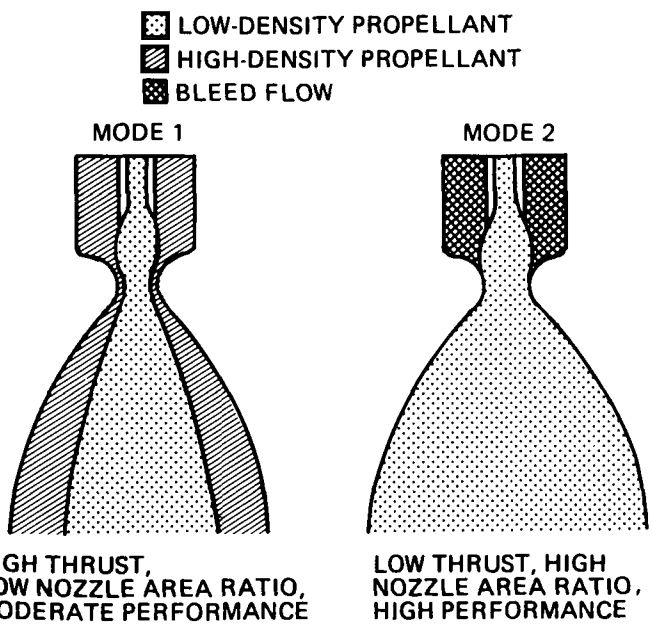

Figure 82. Dual-Throat Thruster.

Analysis of the data substantiated predictions of flow separation in the inner nozzle during the high thrust mode and indicated that the local heat flux values increased by a factor of greater than two in the flow separation areas. The heat flux around the inner nozzle lip area was equal to or lower than that found at the inner nozzle exit surface. During the low thrust mode, heat flux values observed in the outer nozzle throat region where the inner chamber exhaust stream attaches to the outer nozzle surface were well below the values observed during high thrust mode.

The conclusions from these test results are threefold: The inner nozzle exit surface should be designed to accommodate heat flux values greater than twice the value normally expected in nozzles with full flow (i.e., non-separated flow); the inner nozzle exit lip region cooling design should be keyed to that expected at the nozzle exit surface; and the inner nozzle exhaust flow attachment to the outer nozzle throat region in low thrust mode is not a driving thermal design issue.

O'Brien, C.; and Ewin, R.: Dual-Throat Thruster Thermal Model. Aerojet TechSystems Company, Final Report (Contract NAS8-34136).

F. W. Braam/EP22
(205) 544-7055
Sponsor: Office of Aeronautics and Space Technology

Rotordynamics of Reduced Models

This study to develop advanced methods for rotordynamic analysis of large systems entailed the development of methods to accurately reduce models; preparation of effective procedures for

analyzing the transient response of the Space Shuttle Main Engine (SSME) in the presence of rotor rubbing, imbalance, and bearing clearances; and the implementation of substructuring techniques for transient analysis.

During FY86, efforts to improve modeling have resulted in the development of three methods. One method incorporates subsystem base procedures utilizing alternate forms of transition matrices instead of direct numerical integration. This method shows promise for reduced run time. Another semi-analytic method, called incremental harmonic balance/Fast Fourier Transform, is being used to study a single disk model with bearing clearance, side forces, and rubbing. This method is being extended to general multi-degree dynamic systems with large local nonlinearities and physical coordinates at the points of interaction between rotor and housing, such as that shown in Figure 83. The third method employs a formulation of the Duhamel Convolution Integral on the SSME turbopump housing (Fig. 84) to allow the use of model transformation to reduce the housing model to physical coordinates at only the coupling points to the rotor.

This study has resulted in the selection and development of several excellent methods of analyzing multi-degree-of-freedom dynamic systems. This was accomplished by reducing the models to a low degree of freedom while maintaining model accuracy and treating the models that contain large local nonlinearities in an analytic fashion.

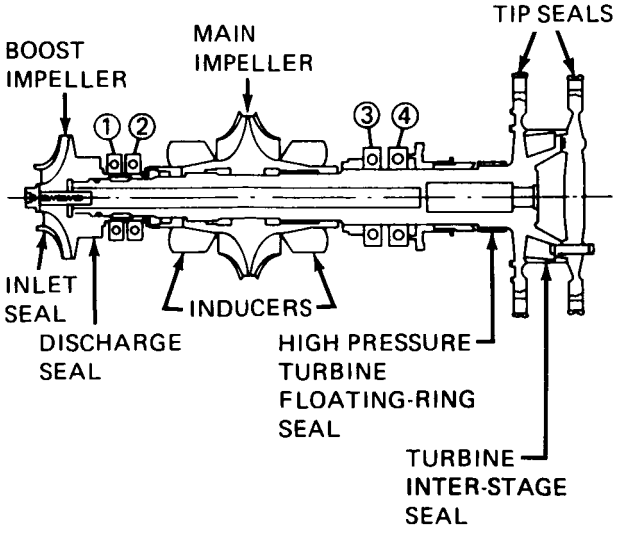

Figure 83. SSME Powerhead Component Arrangement and Local Rotor Coordinate Systems.

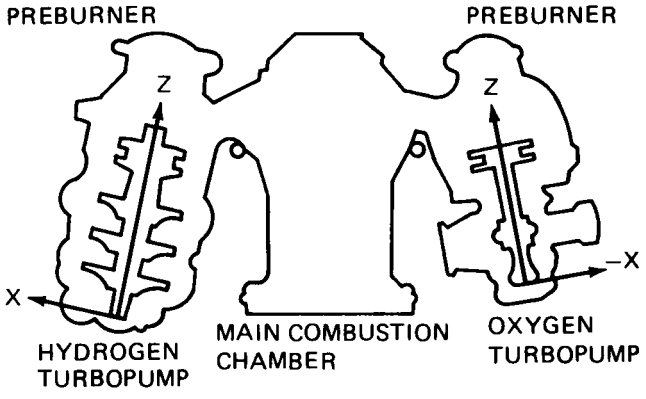

Figure 84. SSME High Pressure Oxidizer Turbopump Rotating Assembly.

Choi, Y. S.; and Noah, S. T.: Forced Periodic Vibration of Unsymmetric Piece-Wise Linear Systems. Journal of Sound and Vibration, submitted, 1986.

Choi, Y. S.; and Noah, S. T.: Nonlinear Steady-State Response of a Rotor-Support System. ASME, Journal of Vibration, Acoustics, Stress, and Reliability in Design, submitted, 1986.

Noah, S. T.; Fan, U. J.; Choi, Y. S.; and Fox, T. H.: Efficient Transient Analysis Methods for the Space Shuttle Main Engine (SSME) Turbopumps. Presented at the Advanced Earth-To-Orbit Propulsion Technology Conference, NASA, MSFC, May 13-15, 1986.

T. H. Fox/ED14
(205) 544-1462
Sponsor: Office of Aeronautics and Space Technology

Hyper-Coherence Functions

The harmonic content in dynamic measurements from rotating machinery contains much subtle information concerning equipment operational condition and component degradation. For this reason, the power spectral density (PSD) has long been employed to assess the relative magnitude of fault-related spectral contributions. Measurements on high-performance rocket engine turbomachinery suffer from severe noise contamination from numerous extraneous sources, which impedes diagnostic evaluation of rotating elements. Thus it is difficult to determine whether an apparent high-level harmonic contribution is related to the fundamental rotational frequency or is possibly due to an independent source. The ordinary PSD, being an absolute value, is of no assistance to this problem. In an effort to relate synchronous speed characteristics with an arbitrary harmonic component, a unique coherence spectrum was devised and termed the hyper-coherence function. The hyper-coherence

function defines the nonlinear correlation between waves at the fundamental frequency and harmonics. The computation is made by Fast Fourier Transform methods and results in a line spectrum of correlation coefficients as a function of harmonic number. Although developed specifically for the Space Shuttle Main Engine, the technique should find wide application in the diagnostic assessment of turbomachinery.

The technique was applied to Space Shuttle Main Engine turbopump measurements. The linear spectra of two different tests appear virtually identical, other than the background noise (Fig. 85, views A and B). The PSD amplitudes at 3N frequency are very high for both tests. In Figure 86, views A and B depict the hyper-coherence functions computed for the same two test measurements. View A indicates that almost all the power at 3N is correlated with the rotational frequency component. On the other hand, the 3N component of the second test shown in view B is due to a differing physical phenomena not related to the rotational frequency.

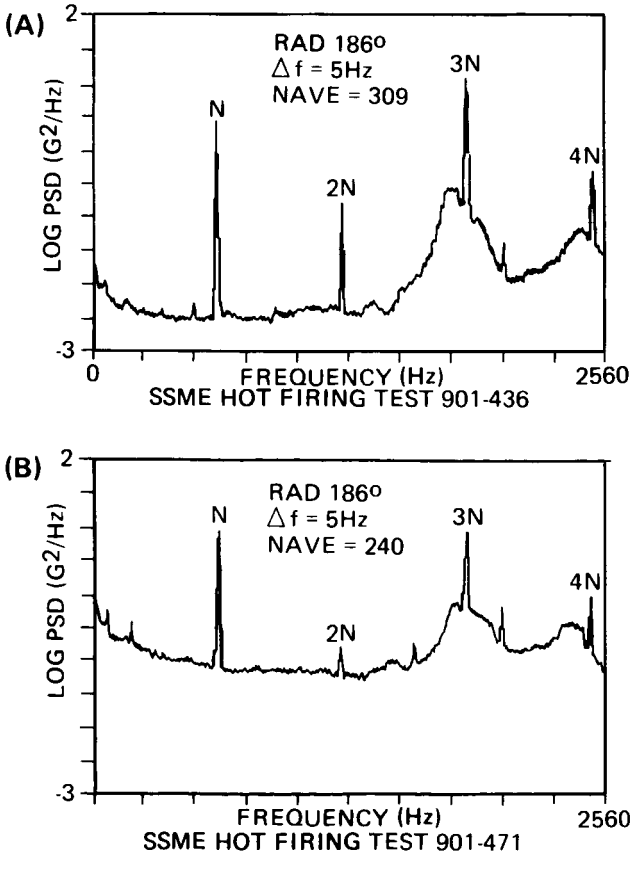

Figure 85. Power Spectra from High Pressure Fuel Pump Measurements.

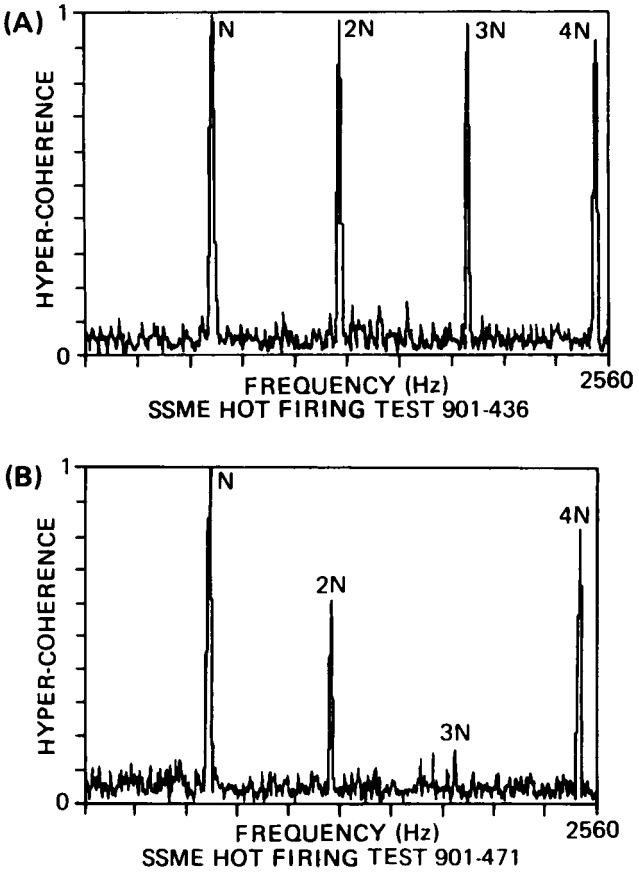

Figure 86. Hyper-Coherence Spectra.

The hyper-coherence function defines the nonlinear correlation between a reference frequency component in a vibratory signal and its harmonics. The formulation provides a concise summary of a succession of higher order coherence functions in only two dimensions. A major benefit is determination of whether an apparent harmonic in a complex vibration signal is correlated with the fundamental or independent source of extraneous noise. The technique is computationally easy to implement. The method is limited to assessment of integer multiple frequency components in a signal, and thus is not applicable to signals involving modulation or more general nonlinear dependence.

J. H. Jones/ED24
(205) 544-1543
Sponsor: Office of Aeronautics and Space Technology

Statistical Modeling of Persistence Time

The Flight Accelerometer Safety Cutoff System (FASCOS) is a vibration-based engine condition

monitor. The system continuously monitors accelerations measured on the Space Shuttle Main Engine (SSME) turbopumps during engine operation. Based on these measurements and assigned vibration "redlines," the FASCOS and engine control computer determine the operational health of each engine through a series of nonlinear operations on the vibration signals and a voting protocol. The outcome of the decision process (run/cutoff) is highly dependent on the redline values assigned to the FASCOS comparator and on the statistical behavior of the monitored signals. For this reason, an intensive analysis/simulation effort was initiated to define the FASCOS decision process as a guide to the assessment of redlines with respect to mission success and safety. Major elements of the FASCOS are a filter/detector stage, a comparator with time delay, and a voting protocol based on the simultaneous output state of the three comparators. Key issues addressed in system modeling, simulation, and performance assessment are shown in Table 10.

Table 10. Key Issues in Statistical Modeling.

• STATISTICAL CHARACTERIZATION OF THE CLASS OF RANDOM FUNCTIONS REPRESENTATIVE OF OPERATIONAL VIBRATION SIGNALS.
• MODELING OF THE NONLINEAR DETECTOR OUTPUT TO REPRESENTATIVE STOCHASTIC INPUT.
• DERIVATION OF THRESHOLD EXCEEDANCE PERSISTENCE TIME PROBABILITIES REPRESENTATIVE OF THE COMPARATOR OPERATION.
• ESTIMATION OF JOINT STATISTICAL PROPERTIES REQUIRED TO MODEL THE PROBABILITY OF COMBINED LEVEL EXCEEDANCE AS UTILIZED IN THE CONTROLLER VOTING PROCESS.

The band-passed vibration signals were considered representative of a random sine wave plus independent Gaussian noise process. Under this assumption, a mathematical description of the filter/detection stage output (power spectrum and covariance function) was derived as a function of input, filter, and averaging characteristics. This model admits a wide range of spectrum shapes and signal-to-noise level, yet is mathematically tractable. Computer results have demonstrated excellent agreement with simulations developed by MSFC. The definition of threshold exceedance time persistence probabilities, to model the comparator output, represents a formidable theoretical problem. Several approximate formulations were implemented for evaluation. These are called the Rice method, the method of non-correlated pulses, and the quadratic approximation method. The estimation of joint properties between vibration signals appears best approached through empirical simulation. In the absence of such information, however, bounds on system behavior may be obtained by assuming joint properties.

A computer program was developed to define the probability of engine cutoff as a function of assigned redline values, turbopump vibration characteristics, and FASCOS logic operation. The modeling techniques developed should find application in the design and evaluation of monitoring and control systems.

J. H. Jones/ED24
(205) 544-1543
Sponsor: Office of Aeronautics and Space Technology

Space Shuttle Main Engine Turbine Blade Analysis

During extended operation of Space Shuttle Main Engine (SSME) high pressure oxidizer turbopumps, individual blades are developing cracks near the area where they begin contact with the blade mounting disc. Previous investigations have shown these blades to have natural frequencies which are close to both the input forcing function frequencies and the higher order disc frequencies and which are located at points on the disc which deflect in these higher order modes.

Previous work has included dynamic math model analyses of a complete blade/disc system with both tuned and mistuned blade frequency distributions. A tuned system is one in which all blades are similar and have identical first and second natural frequencies, while a mistuned system has a distribution of first and second natural frequencies over a range of values. These analyses were difficult to handle, but an understanding of the system was developed to allow the problem to be broken down into a smaller one for utilizing a different approach. A simplified dynamic math model (with limited degrees of freedom) of a portion of the disc/blade system was

developed for determining and comparing the responses of a tuned system to that of a mistuned system.

This investigation will proceed to determine tuned disc/blade system response, mistuned disc/blade system response, and the comparison between the results of the two disc/blade configurations (Fig. 87). This will be done with a loads program that has been developed and has been applied in similar situations for determining loads and response. The simplified model will continue to be improved as disc/blade systems are better understood. The response will be due to both the input jet forces and the higher disc modes. The input jet force drives the higher disc frequency because at operating speed both occur at similar frequencies.

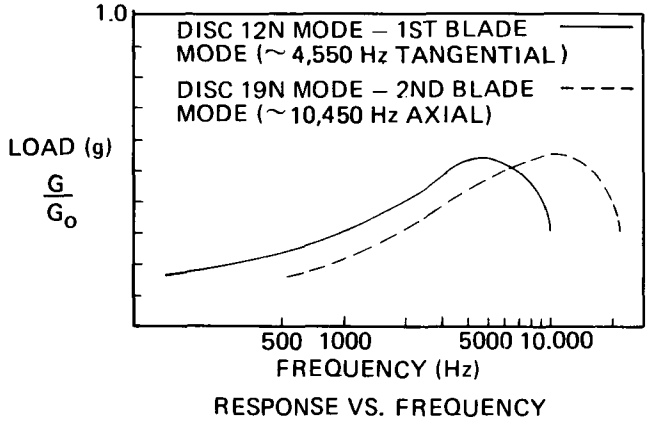

Figure 87. Comparison Between Results of Two Disk/Blade Configurations.

L. D. Kos/ED23
(205) 544-1522
Sponsor: Office of Space Flight

Non-Intrusive Speed Sensor

Early in the Space Shuttle program, the Space Shuttle Main Engine High Pressure Oxidizer Turbopump (HPOTP) had a speed sensor. But this sensor encountered frequent failures due to structural problems, and was removed. The only HPOTP speed measurement presently made is its synchronous speed determined from the pump accelerometers. This accelerometer data is deficient in that start and shutdown transient data cannot be obtained, pump breakaway cannot be measured, and the data is inadequate for anomaly investigations. Therefore, a research effort was initiated to provide a non-intrusive speed sensor for this measurement.

Fourteen technologies were identified as having potential application to the HPOTP. These technologies were narrowed to three for experimental evaluation: variable source magnetic, infrared, and microwave. Of these, the variable source magnetic approach was chosen for further development, since the turbopump housing, Inconel 718, is a non-magnetic material. Additional advantages were that no controller or software changes would have to be made.

A model sensor design has been approved (Fig. 88) and has been fabricated and tested to 40,000 rpm in a spin test facility. These tests indicated that the controller 75 mV input requirement was accomplished using a solid Inconel plate 1-in. thick. However, the HPOTP configuration has a 3/8-in. hole drilled through the pump housing at the location the speed sensor would be installed. Additional spin tests will be conducted to determine how much the sensor output will be increased by the presence of this hole, potentially exceeding the 75 mV requirement. Recommendations have been made to incorporate this sensor into the Technology Test Bed Engine.

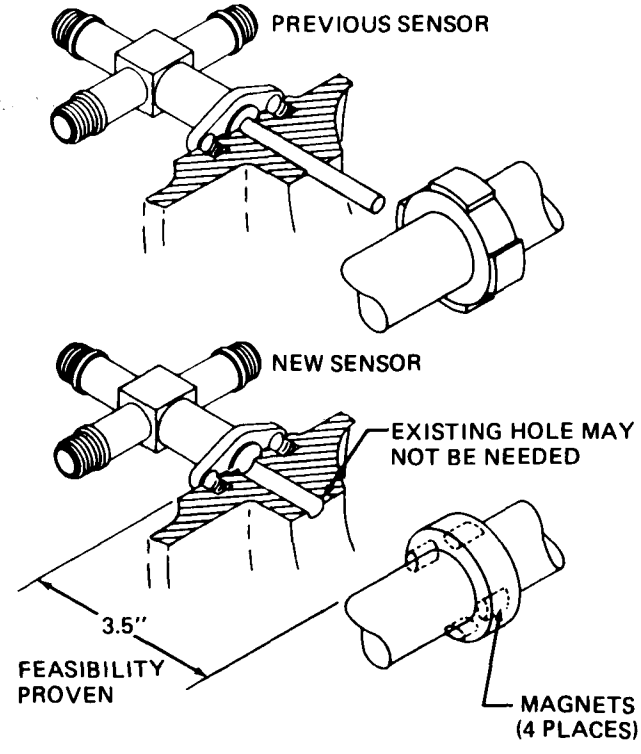

Figure 88. Non-Intrusive Speed Sensor.

This research has resulted in a method of measuring the speed of the HPOTP without inserting probes inside the pump. In addition, it can be implemented with no changes to the engine controller or electrical harness.

T. N. Marshall/EB22
(205) 544-3448
Sponsor: Office of Aeronautics and Space Technology

Low Cycle Fatigue Life

Low cycle fatigue failures are a severe problem in liquid oxygen (LOX)/hydrogen rocket engine turbines. Startup and shutdown transients produce extreme thermal gradients within the components which, when coupled with high heat transfer coefficients, cause very high thermal strains. The low cycle fatigue (LCF) life of most materials is only a few cycles. This results in frequent cracking and replacement of turbine hardware.

The Space Shuttle Main Engine (SSME) high pressure fuel turbopump is a typical example of this severe environment and the resulting hardware failures. Turbine blades experience airfoil leading edge cracks, airfoil radial cracks, and platform cracks, and thus require "infield" inspections of the blades after every three starts. This necessitates removal of the turbopump from the engine and a likely replacement of cracked blades, significantly increasing Shuttle maintenance and operation costs and turnaround time.

To alleviate the LCF problem, turbine airfoils should be designed to minimize startup and shutdown thermal gradients. Two techniques proposed to minimize thermal gradients are hollow core airfoils and circulation of turbine drive gas through the hollow core. In FY86 these design techniques were evaluated in a series of tests in the MSFC turbine blade tester. The thermal cycle of the blade test rig does not exactly simulate that of the SSME, but produces more accelerated cracking than the engine environment. Because the test environment is more severe than the SSME, the results can be used for a relative comparison of LCF life for different designs, while minimizing test cost and time. During startup the blade is exposed to a maximum temperature gradient of 1055 K/s for 0.12 s. Burning lasts approximately 8 s and then the igniter and oxygen flow are turned off. The liquid hydrogen flow then quenches the blades to 60 K at a rate of -1720 K/s over 0.12 s. The quench lasts approximately 8 s and then the process is repeated. At designated inspection points the blades are removed and metallurgically inspected under magnification to 25X and dye-penetrant photographs are taken.

A simple airfoil shape was chosen to minimize fabrication costs. The blades were made from PWA-1480SC and from MAR-M246(Hf) DS, which is the current SSME material. Five variations of the simple airfoil were made. The baseline blade for comparison was the solid airfoil, made of either MAR-M246 or PWA-1480. The other airfoil variations were hollow wall thicknesses of 0.140 cm and 0.089 cm. In addition, two of the designs had a 0.140-cm hollow wall thickness with either a 0.127-cm or 0.254-cm vent hole to allow hot gas to enter the center of the blade, and were made from PWA-1480SC only. The vent hole represents an alternative for cases when the blade stresses are too high to use the optimum wall thickness for thermal response. The internal flow added with the vent hole reduces the thermal gradient through the wall to an acceptable level.

Table 11. Relative Benefits of Geometry Demonstrated by LCF Life Ratios.

GEOMETRY	LCF LIFE RATIOS: MAR-M246	PWA-1480
SOLID/ SOLID	1	1 TO 2
0.140 cm/ SOLID	1	2 TO 4.8
0.089 cm/ SOLID	15	>17 TO 20
0.140 cm*/ SOLID	N/A	12
0.140 cm**/ SOLID	N/A	>10

*WITH 0.127-cm VENT HOLE
**WITH 0.254-cm VENT HOLE

The relative benefit of each blade was judged against the baseline (solid) blade. The ratio of cycles-to-cracking for the test blade over cycles-to-cracking for the baseline blade was used to determine the relative benefit of each blade design. Conservatism was added to the analysis because cycles-to-cracking for the baseline blade was assumed to be when cracking was first observed, and for the comparison blade it was assumed to be the last time the blade was inspected and shown to be crack free. The baseline life was

C-2

three cycles for the MAR-M246(Hf) DS blades and five cycles for the PWA-1480SC. The test results shown in Table 11 indicate that thin-wall hollow core geometry yielded a life improvement of up to 20 times over the baseline blade.

L. A. Gross/EP23
(205) 544-7067
Sponsor: Office of Space Science and Applications

Global Model of the Space Shuttle Main Engine

A two-dimensional/three-dimensional Global Model of the SSME flow regions for the oxygen, hydrogen, and mixed hot gas is necessary in order to understand the upstream/downstream effects.

This year a three-region model of the turnaround duct of the SSME was developed and tested. This model is being extended to five domains to include the preburner and high pressure fuel turbine. The existing one-dimensional system model was reviewed, with test cases run and reported to the Computational Fluid Dynamics workshop April 11, 1986. Comparisons between the contents of this program and the new global model are continuing. Some of the features of this program will be adopted in the global model.

Mukerjee, T.; Przekwas, Tam, L. T.; and Holland, R. L.: One Dimensional Global-System Computer Programs for Internal Flows. SSME Computational Fluid Dynamics Fourth Working Group Meeting, MSFC, April 8-11, 1986.

Carrasquillo, R.; and Holland, R. L.: One Dimensional Global-System Computer Programs for Internal Flows. SSME Computational Fluid Dynamics Fourth Working Group Meeting, MSFC, April 8-11, 1986.

R. L. Holland/ED42
(205) 544-1635
Sponsor: Office of Aeronautics and Space Technology

Damping Seals and Flexible Rotor Balancing

The high pressure turbopumps for oxygen (HPOTP) and fuel (HPFTP) of the Space Shuttle Main Engine (SSME) run at supercritical speeds. Thus the pumps become susceptible to balancing inaccuracies and subsynchronous whirl instability. Balancing inaccuracies are mainly due to balancing the rotor like a rigid rotor at low speeds, and the unavoidable reassembly of the previously balanced rotor during pump assembly. A new balancing method was developed for low-speed balancing in several planes by considering the rotor bending. The new method will eventually replace rigid rotor balancing in supercritical rotor cases.

As seen in Figure 89, damping seals have been installed in the HPOTP next to the preburner pump (PBP) bearing to suppress a 90-percent subsynchronous whirl which limited SSME power. The seal is certified, and is part of the phase II design. The tests also showed a PBP ball bearing load reduction due to load sharing by the damping seal. Thus the rotor became less sensitive to unbalance at full speed. Other damping seals were fabricated for the HPFTP to prevent a 50-percent subsynchronous whirl when sideloads are reduced in future pumps.

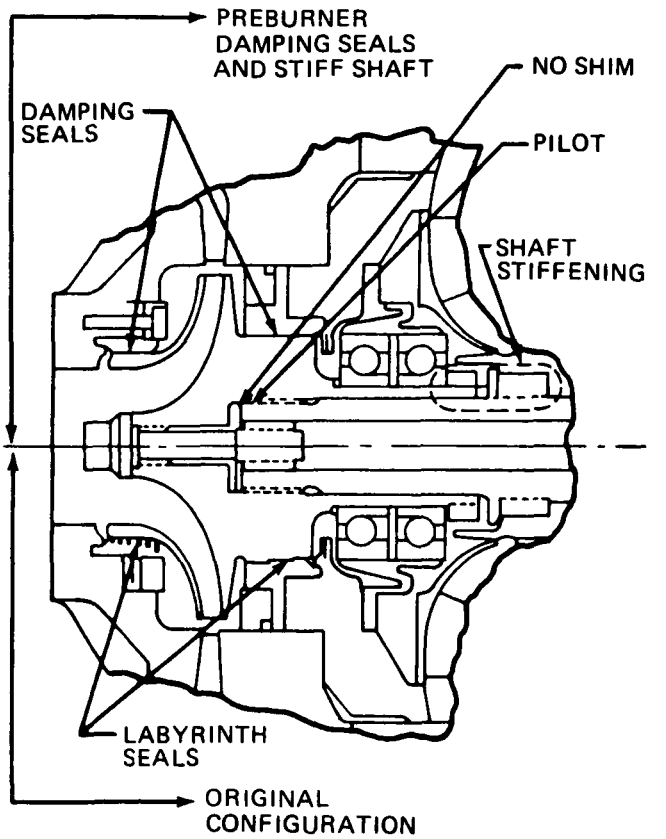

Figure 89. High Pressure Oxygen Turbopump Damping Seals.

The damping seals, analytically formulated in 1982, are being tested in the seal tester shown in Figure 90. Damping and leakage were well predicted, but values for stiffness and cross-coupling

of the seal's fluid film are only one-half of those predicted. The findings were reported at the 1986 Conference on Advanced Earth-to-Orbit Propulsion Technology in May, 1986.

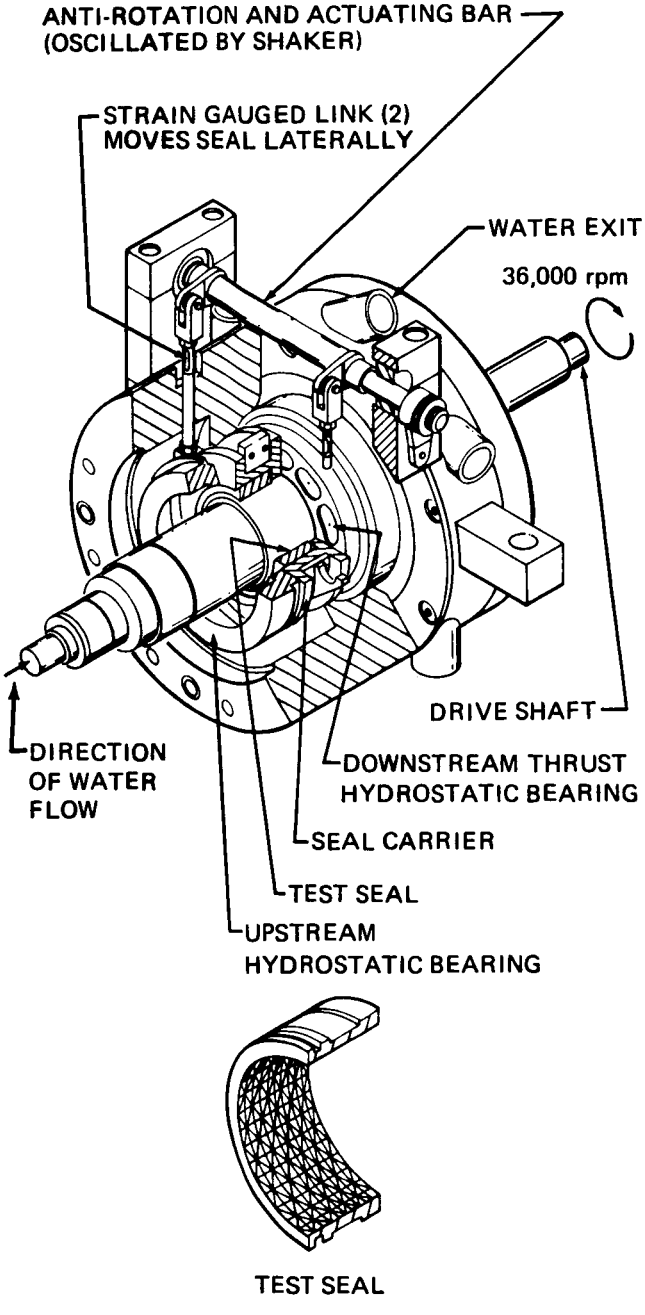

Figure 90. Damping Seal Tester.

The seal tester is being repaired after two misaligned bearings failed at 20,000 rpm. Improvements to avoid such failures and to obtain better data are being incorporated, and the initial results are encouraging. Further tests are expected to contribute much to damping seal development and the formulation of analytical predictions.

Cappel, K. L.; and von Pragenau, G. L.: Damping Seal Tester Progress and Initial Test Results. 1986 Conference on Advanced Earth-To-Orbit Propulsion Technology, May 13-15, 1986.

von Pragenau, G. L.: Damping Seals for Turbomachinery. NASA Technical Paper 1987, March 1982.

Zorzi, E.; Giordano, J.; and von Pragenau, G. L.: High-Pressure Oxidizer Turbopump Low-Speed Flexible Rotor Balancing for Smooth, High-Speed Operation. 1986 Conference on Advanced Earth-To-Orbit Propulsion Technology, May 13-15, 1986.

G. L. von Pragenau/ED14
(205) 544-1469
Sponsor: Office of Aeronautics and Space Technology

Carbon Phenolic and Carbon-Carbon Nozzle Technology

MSFC is conducting an investigation of the materials technology associated with carbon phenolic and carbon-carbon Solid Rocket Motor (SRM) nozzles. It is the intent of this program to improve the phenolic pre-impregnated carbon ("prepreg") materials and processes utilized to produce this hardware and to determine statistically significant materials properties for use in thermostructural models.

Several lots of carbon phenolic prepreg have been produced at U. S. Polymeric Inc. for use on this program. Each lot of carbon or graphite cloths, filler, and resin is being fully characterized under a "fingerprint" test approach. Some of the material produced is being used to manufacture carbon phenolic and carbon-carbon flat panels, cylinders, and cones as test components. These components will be tested in statistically significant quantities to determine the materials' high temperature properties. An intense review and documentation of available materials properties of carbon phenolic and carbon-carbon has been completed. Based on this survey a test matrix has been formulated for the generation of additional required materials property data.

An investigation of the chemical reactions associated with carbon phenolic materials processing is underway. The investigation is providing insight into the reaction rates, exotherms, and resin advancement at specific periods during curing. These data are being utilized to custom-cure carbon phenolic material in-house at MSFC. Flat panels and cylinders are being fabricated

utilizing tailored cure cycles to eliminate delaminations and porosity that are often the cause for rejection of carbon phenolic nozzle components.

An activity has also been initiated to develop improved test methods for evaluating carbon phenolic materials. Improved methods for determining filler content and volatile content in prepreg materials have been developed. This effort will continue to evaluate test techniques and acceptance/rejection criteria for resin, filler, cloth, prepreg, and finished products.

R. L. Nichols/EH34
(205) 544-2686
Sponsor: Office of Space Flight

Solid Rocket Motor Nozzle Instrumentation

The objective of this research task is to improve instrumentation used in analytical model validation and performance evaluation tests of solid rocket motor nozzles. A study program was begun in May 1985 with a compilation of test data from previous nozzle tests. A total of 32 test firings of solid rocket motors, as well as simulated firings, were found with both analytical predictions and instrumented test data available. Test durations ranged from 5 to 120 seconds, and were conducted from January 1982 to August 1985.

The most common temperature sensors used on the test articles were thermocouples. Analysis of temperature instrumentation data and model predictions indicates that the test data lags the predicted temperature, especially for surface temperature measurements. The lag is attributable to the thermal coupling between the surface and the measuring sensor, and thus is a direct result of the bonding technique used to mount the sensor.

Strain gauges on the test nozzles were found to be limited in scope and success, due to the extreme thermal environment and lack of adhesion to the carbon composite nozzle materials. The wire-based strain gauges used have very large apparent strain errors due to temperature effects and mismatch of thermal coefficients of expansion between the gauge and the nozzle component. These large temperature-induced errors can be eliminated in data reduction if the exact temperature is known. Unfortunately, the temperature measurement time lag, mentioned above, is prevalent and the resultant temperature-corrected data is very questionable.

The research program includes a hardware phase to develop strain gauge and temperature sensing technology for application on nozzle materials. Operational goals are for strain measurements to 1093 °C (2000 °F) and temperature measurements to 2204 °C (4000 °F) during the first 20 seconds of firing. Initial development efforts will concentrate on strain gauge technology with emphasis on adhesive/attachment techniques, lead wire attachment, and elimination or compensation of temperature-induced strain. Development activities are to be completed by December, 1986.

J. E. Zimmerman/EB22
(205) 544-3458
Sponsor: Office of Space Transportation Systems

Main Chamber Combustion and Cooling

In the development of combustion chamber design for the existing Space Shuttle Main Engine (SSME) and for future high pressure oxygen/hydrogen engines, a controlling factor in predicting chamber life is the onset of "blanching." Blanching is the deterioration of the copper alloy chamber wall, characterized by a bright silver-copper appearance and local wall roughness. In blanched areas of the SSME, combustion chamber liner cracks occur in only 2 to 10 cycles, while the predicted design life, excluding these effects, is 80 to 100 cycles.

To understand this phenomenon and define the conditions under which it occurs, a major program to conduct a metallurgical examination of hot-fired samples and to duplicate blanching under laboratory conditions was initiated. A metallurgical analysis was conducted on samples of the copper alloy NARloy-Z, which had undergone blanching in the SSME and in the "40k" SSME chamber. It was concluded that a blanched surface is a network of interconnected porosity which results in reduced effective liner wall thermal conductivity and a surface roughness of 200 to 400 micro-inches, which increases the heat

transfer coefficient. This results in wall temperatures greater than 1200 K (1700 °F) (the design temperature is 783 K, or 950 °F), surface distress, and longitudinal cracking of the wall.

An abrupt change in roughness between the over-channel and over-land areas was also observed. This suggests that some geometrical effect may contribute to the roughening. One theory is that high compressive stresses in the blanched areas are a contributing factor. Therefore, it would seem that blanching involves high wall temperatures, high compressive stresses, and an environment which induces surface porosity.

A thermogravimetric analysis (TGA) was conducted on samples of NARloy-Z, NARloy-A, oxygen-free high conductivity copper, and zirconium copper alloys. TGA involves precise measurement of the weight change of a material specimen as a function of time and/or temperature in a controlled gas environment. Samples were subjected to five different atmospheres, including inert, reducing, and oxidizing gases, and oxidation and reduction environments. A temperature range from 588 K (600 °F) to 1255 K (1800 °F) was explored. It was concluded that blanching is caused by an oxidation-reduction reaction which occurs at temperatures as low as 588 K (600 °F), with oxidation increasing at an exponential rate with temperature. Thus blanching will occur whenever free oxygen is present in the combustion gas adjacent to the wall and the wall is subsequently exposed to a fuel-rich gas. It is possibly associated with local fluctuations in the combustion gas composition, which represent alternating oxidizing and reducing conditions. The rate of blanching is believed to increase with increased high compressive stresses and, although it occurs at wall temperatures as low as 588 K (600 °F), the rate increases with temperature.

From this investigation it has been concluded that avoidance of blanching is an important design consideration for high pressure oxygen/hydrogen engines, as blanching degrades chamber life significantly. To prevent or reduce blanching it is necessary to reduce wall temperatures and compressive stresses, or to protect the wall from free oxygen either by reducing the wall mixture ratio or by using an oxidation-resistant coating.

R. H. Counts/EP23
(205) 544-7081
Sponsor: Office of Aeronautics and Space Technology

Fluid Dynamics

Two-Phase Flow Over a Cavity

The problem of flow over a cavity of a gas containing a fine, dispersed particulate phase was addressed computationally. The purpose of the study was to obtain an indication of whether a cavity existing at the wall containing such a two-phase flow would tend to grow under the influence of the flow.

Single-phase computations of the gas flow velocities show that a recirculation zone is produced in the cavity with velocities in the recirculating region on the order of 10 percent of the free stream velocities. For low aspect ratios (length-to-depth) of about 1, the recirculation cell fills the cavity. For higher aspect ratios (up to 10), the recirculating cell is concentrated near the leading edge of the cavity, with the streamlines from the flow outside the cavity dipping into the downstream region of the cavity (Fig. 91). It might be possible that the cavity could be further eroded by the flow if the particulate phase does not follow the gas phase in the highly curved flows of the recirculating flow. It was seen from initial two-phase results, however, that for particles on the order of 10 μm in diameter, the particle phase streamlines closely followed the gas phase streamlines (Fig. 92). It appears unlikely, then, that the cavities would tend to be deepened by the effect examined here. Gas properties and particle sizes selected for this study were appropriate for comparison to flow in solid propellant rocket motors.

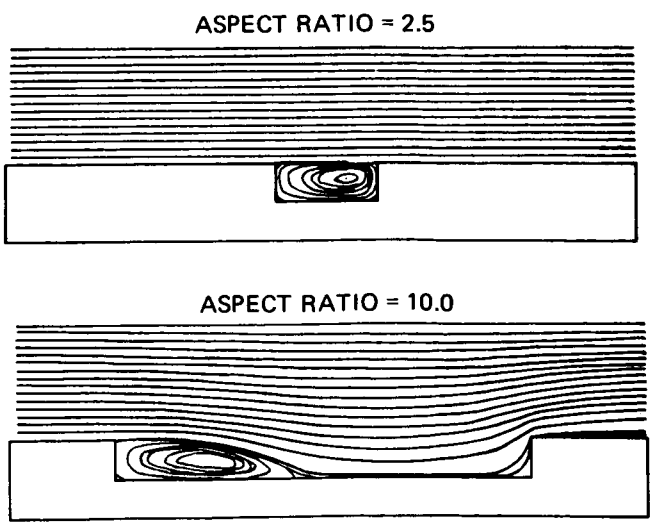

Figure 91. Flow Over a Cavity (Single-Phase).

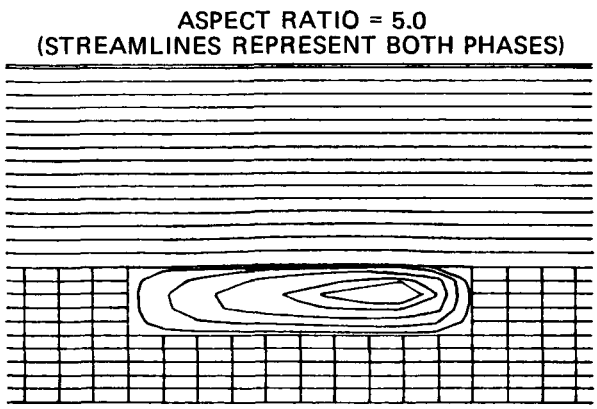

Figure 92. Flow Over a Cavity (Two-Phase).

C. F. Schafer/ED42
(205) 544-1642
Sponsor: Office of Aeronautics and Space Technology

Development of Turbulence Models

The current widely used two-equation and Reynolds stress turbulence closure models for complex turbulent flows suffer a serious drawback: a single set of scales is used to characterize the entire spectrum of turbulent motion. Under this simplification, the use of this level model should be limited to cases where the mean flows are slowly evolving. This is almost never the case for flows in complex geometry where the energy spectrum is not in equilibrium and the mean flow is changing rapidly.

Over the past few years several proposals, including full spectral modeling, have been devised to take into account the non-equilibrium spectral energy transfer of turbulent flows. A so-called multiple-scale turbulence model based on the multiple-time-scale concepts of Launder and coworkers has been developed to characterize the different scales in turbulent flows. The key feature of the multiple-scale model is the partition of the energy spectrum. This allows the energy transfer rate of large-scale eddies to be related directly to the mean strain and the mean flow field characteristics such as degree of swirl and curvature, while the energy transfer rate of small eddies is modeled to its own action rather than to the large eddy motion in the low wave number region of the spectrum. The partition between the production and transfer region of the spectrum is characterized by the model coefficients introduced in the model transport equations.

This multiple-scale model has been tested in various free shear flows, recirculating flows, swirling flows, and geophysical flows, and shows significant improvement of predictive capability over the conventional single-scale turbulence model. This model, in the current status, does not take into account the non-isotropy of the turbulence. With incorporation of the Algebraic Stress Model into the multiple-scale model scheme, reasonable predictions of the turbulence field of complex flows may soon be possible.

Chen, C. P.: Multiple-Scale Turbulence Closure Modeling of Confined Recirculating Flows. NASA CR-178536.

Chen, C. P.: Application of a Multiple-Scale Turbulence Model in Confined Swirling Jet Predictions, submitted, 1986.

C. P. Chen/ED42
(205) 544-1678
Sponsor: Office of Space Science and Applications

Two-Phase Flow Processes

In designing industrial gas-solid devices such as pulverized coal gasifiers and combustors, solid-fired gas turbine engines, solid-fueled ramjet engines, and fluidized bed combustors, fundamental questions concerning how the particles affect the entrainment of hot gases, and how the fuel particles are dispersed in a gas stream need to be addressed. Two-phase flows are too complicated to be treated in a complete way. For numerical modeling, there are basically two approaches commonly used to predict two-phase flows. The first, called the Lagrangian or "tracking" approach, starts with equations of motion for dispersed particles in a turbulent flow field and calculates their trajectories.

The other approach, which is undertaken here, is the "two-fluid" model or Enlerian approach. In this approach, the cloud of particles is regarded as a continuum and the governing equations are obtained by properly averaging the conservation equations over a control volume and expressing the equations in differential forms. The present modeling scheme accounts for the combined effects of interphase slip and turbulent dispersion of particles. The effects of two-way coupling are incorporated into the Enlerian governing equations and the turbulent dispersion of particulates is represented via the ratios of the particle response time scale and various time scales of underlying

turbulent flows. The multiple-scale turbulence model which is utilized for the turbulence field modeling of the primary phase has been modified to account for the added dissipative mechanism caused by the particles. A numerical code has also been developed to solve the governing equations on a staggered interconnected calculation grid. This mathematical model has been used to predict several confined, recirculating, turbulent gas-solid flows.

Chen, C. P.: Numerical Analysis of Confined Recirculating Gas-Solid Turbulent Flows. Gas-Solid Flows, J. Jurewicz Ed., ASME, 1986.

Chen, C. P.: Particle Dispersion in Confined Turbulent Swirling Flows. AIAA Paper 86-1450, 1986.

C. P. Chen/ED42
(205) 544-1678
Sponsor: Office of Space Science and Applications

CAD/CAM Applications

This year has been devoted to applying the new technology which has been developed in the computer-aided design/computer-aided manufacturing (CAD/CAM) industry to computational fluid dynamics (CFD) preprocessing and postprocessing. In preprocessing, it is necessary to create, store, retrieve, and transfer engineering design drawings, data files, and color three-dimensional images and plots. This information is then used to generate boundary geometry for the fluid flow region. With the boundary geometry defined, it is then necessary to discretize the region within the boundary. This grid generation process is most important in determining the correct solution to the flow field.

The CAD/CAM industry has already developed a base set of computer commands and instructions which builds designs of three-dimensional objects of arbitrary shape, as well as a limited set to discretize the objects and obtain grid coordinates within the object. This is especially true for finite element analysis of structures. There also exists a limited instruction set to obtain a boundary-fitted mesh. The thrust of this effort has been to take the existing instruction set available in the CAD/CAM industry and apply it to CFD, and to develop interfaces with CFD codes. Work is also continuing on improving the preprocessing software.

The CAD/CAM hardware and software can also be utilized very effectively for postprocessing and displaying the results of flow field solutions in the form of contours and vector plots in color. During the past year, it has been demonstrated that grids can be generated quickly and effectively on CAD/CAM hardware and software and the coordinates used as input to CFD flow solvers. Specific solvers used included the Parabolic Hyperbolic or Elliptic Numerical Integration Code Series (PHOENICS), and the Incompressible Navier-Stokes BD (INS3D) code.

This study was performed using the IBM 5080 terminal with the Engineering Analysis Data System (EADS) CPU and CAEDS software. The engineering design drawings developed for the Phase II+ air flow model of the Space Shuttle Main Engine were transferred by tape from Rocketdyne to Marshall Space Flight Center and read by an Intergraph CAD/CAM system.

R. L. Holland/ED42
(205) 544-1635
Sponsor: Office of Aeronautics and Space Technology

Navier-Stokes Solver

During FY85 a three-dimensional incompressible/compressible Navier-Stokes equation solver was developed and evaluated for external and internal flow problems.The main purpose of this development was to provide a numerical tool for internal flow simulations and analyses of the Space Shuttle Main Engine (SSME). Applications of this code to the SSME internal flow analyses include turbulent flow computation inside the 180-degree turnaround duct of the fuel-side turbopump; fully three-dimensional turbulent flow analyses for the high-speed bearing assembly of the oxydizer-side turbopump; and numerical simulations of turbulent flow inside the turbine blade cascades of the fuel-side turbopump.

The code employed generalized curvilinear coordinate transformation to handle complex geometry flow problems. Finite difference methods are used to solve the governing equations. Second order finite difference discretizations were used to reduce numerical diffusion so that more accurate results can be predicted. Turbulence models embedded in the present code are the widely used two-equation turbulence model, a

two-scale turbulence model, and a root-mean-square pressure fluctuation model. Also, for turbulent flow computations, wall functions are commonly used. Due to the fact that conventional wall functions break down for boundary layers subject to strong adverse gradient, a set of wall functions that includes the effects of adverse gradient up to the flow separation point has also been developed and evaluated successfully.

Chen, Y. S.: A Pressure Fluctuations Model for Internal Flow Applications. NASA CR-3928, 1985.

Chen, Y. S.: Applications of a New Wall Function to Turbulent Flow Computations. AIAA Paper 86-0438.

Chen, Y. S.: A Computer Code for Three-Dimensional Incompressible Flows using Nonorthogonal Body-Fitted Coordinate Systems. NASA CR-17818, 1986.

Chen, Y. S.: A Three-Dimensional Navier-Stokes Equation Solver using Nonorthogonal Body-Fitted Coordinate Systems. SSME Computational Fluid Dynamics Fourth Working Group Meeting, April 8-11, 1986.

Y. S. Chen/ED42
(205) 544-1680
Sponsor: Office of Aeronautics and Space Technology

Flow-Solid Interactions

In the Space Shuttle Main Engine (SSME), the liquid oxygen posts are subjected to severe cross-flow. In order to enhance the design capability of the SSME, a flow-solid interaction analysis is required. Solving flow-solid interaction problems requires solving turbulent flow problems and materially and/or geometrically nonlinear structural vibration problems, and coupling the flow-solid interface. Primarily, the structural analysis methods are based on the finite element method, and the turbulent flow analysis methods are based on the finite difference method. At this time, there exist only a few publications on the finite element analysis of turbulent flows. The finite element method was chosen for the flow-solid interaction analysis for several reasons: The flow passage in tube banks is quite complicated, and the finite element method can model the geometry more adequately. In flow-solid interactions, capability to predict the structural response is more critical than the capability to predict the flow field precisely. A few flow-solid interaction analyses have already successfully been made using the finite element method.

Since the finite element method is still in its development stage for turbulent flows, a commercial finite element code for turbulent flows is not yet available. Development of a finite element flow analysis code is in progress at this time. In order to select and/or develop a turbulence model to be used in the three-dimensional flow-solid interaction analysis code, a finite element boundary layer analysis code (BLFLOW) has been developed. A number of turbulence models, such as the standard k-ε turbulence model, the extended k-ε turbulence models, the algebraic Reynolds stress models, and the multiple-scale turbulence models, have been tested using the BLFLOW. Improvement of the turbulence model which performed the best (the algebraic Reynolds stress model due to Rodi) is in progress and the model development will be presented in the near future. Based on the boundary layer analysis code, a parabolic Navier-Stokes equation solver is also in progress to further test and develop the turbulence model.

S. W. Kim/ED42
(205) 544-1679
Sponsor: Office of Space Flight

Materials and Processes

Powder Metallurgy Bearings

Advanced powder metallurgy techniques have the potential to develop materials that are resistant to corrosion, wear, and rolling contact fatigue, and thus afford a viable solution to extending the service life of the cryogenic turbopump bearings of advanced rocket engines. Several powder metallurgy alloys continue to be studied, and six promising candidates were identified for further evaluation (D-5, MRC-2001, T-440V, WD-65, X-405, and 14-416V). The purpose of the evaluation program is to select the top two or three candidate bearing alloys which will be tested at the MSFC Bearing Materials Tester, with the best material recommended for application in the turbopumps.

Stress corrosion cracking (SCC) tests were conducted as a part of the evaluation program. These tests were run with 0.125-in. diameter tensile specimens, hardened and tempered.

The specimens were placed in small stressing frames to give the desired stress (345 MPa, or 50,000 psi). The specimens were then placed in a humidity cabinet at 100 °F and 100 percent relative humidity. The results of a series of tests, based on 3 months exposure to high humidity, are shown graphically in Figure 93, along with results for 440C, the current bearing material. The results show that stress corrosion cracking resistance of these alloys is as good or better than that of 440C, and therefore is acceptable for turbopump bearing applications.

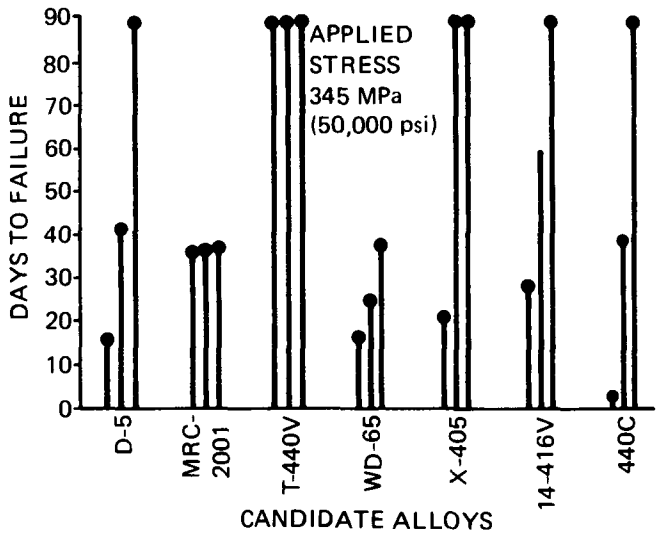

Figure 93. Stress Corrosion Cracking Test Results.

B. N. Bhat/EH23
(205) 544-2596
Sponsor: Office of Aeronautics and Space Technology

Turbine Disk Powder Metallurgy Alloys in Hydrogen

The turbine disks are probably the most critical and highly stressed component in the Space Shuttle Main Engine (SSME). They are produced from Waspaloy, a complex nickel-base superalloy. All nickel-base alloys evaluated in high pressure hydrogen have shown marked reduction in strength, low-cycle fatigue (LCF) life, and increased crack growth rate. To counter this, the SSME turbine disks are gold-plated. The gold plating is costly, time consuming to apply, easily scratched, of questionable integrity, and occasionally spalls in service.

Powder metallurgy (PM) disks have become predominant in commercial jet engines because their uniform fine grain size enhances LCF life. MSFC is evaluating PM alloys in hydrogen in a search for an alloy that is more resistant to hydrogen degradation. The PM alloys selected for screening in hydrogen were Astroloy, AF-115, MERL 76, Rene' 95, IN-100, and Waspaloy, with several of the alloys in two different heat-treated conditions. The base for comparison was forged Waspaloy as used in the SSME turbine disks.

The screening tests consisted of testing notched tensile specimens at room temperature in 34.5 MPa (5,000 psi) hydrogen (H_2), and in air at ambient pressure. The notch stress concentration factor was 8 ($K_t = 8$). The notch H_2/air ratio was used as the selection/rejection criteria to select the best three PM alloys for more detailed evaluation. The results are shown in Table 12.

Table 12. Results for PM Alloys Screened in Hydrogen.

	ALLOY	NOTCH H_2/AIR
LEAST AFFECTED	ASTROLOY PM MATE HEAT TREAT.	0.98
	ASTROLOY PM STD.	0.97
	IN-100 PM STD.	0.96
	WASPALOY FORGED	0.94
	WASPALOY PM SUPER	0.94
	MERL 76 PM	0.91
	IN-100 PM PWA HEAT TREAT.	0.90
	WASPALOY PM SUB-SOLVUS	0.89
	AF-115 PM	0.80
MOST AFFECTED	RENE' 95 PM	0.63

The three best alloy/condition combinations were the two conditions of Astroloy, and IN-100. Detailed evaluation will include tensile, LCF, and crack growth tests at elevated temperatures of 538, 649, and 760 °C (1000, 1200, and 1400 °F), as well as at room temperature.

W. B. McPherson/EH23
(205) 544-2601
Sponsor: Office of Aeronautics and Space Technology

Vacuum Plasma Spray Coating

Currently, protective plasma coatings are applied to SSME turbine blades made of MAR-M246(Hf), which are then diffusion-bonded in vacuum for 4 hours at 1975 °F before applying the standard blade-aging treatment of 1600 °F for 24 hours. In this study of vacuum plasma spray coating, plasma coatings of nickel-chromium-aluminum-yttrium (NiCrAlY) applied in a reduced pressure atmosphere of argon/helium were further enhanced by diffusion bonding. Enhanced coatings showed no spalling after 40 MSFC burner rig tests cycling between 1700 °F and -423 °F, while current SSME coatings spalled during 25 test cycles.

This work is a joint development effort with Rocketdyne, and utilizes the new Vacuum Plasma Coating Development Cell at MSFC (Fig. 94). The new process is directly applicable to single crystal PWA 1480 turbine blades which incorporate the 1975 °F diffusion bonding into the blade manufacturing process. Single crystal PWA 1480 turbine blades are being manufactured and will be run in Rainbow Wheel Engine Tests and Certification Engine Tests, simultaneously with tests planned for the MAR-M246(Hf) blades.

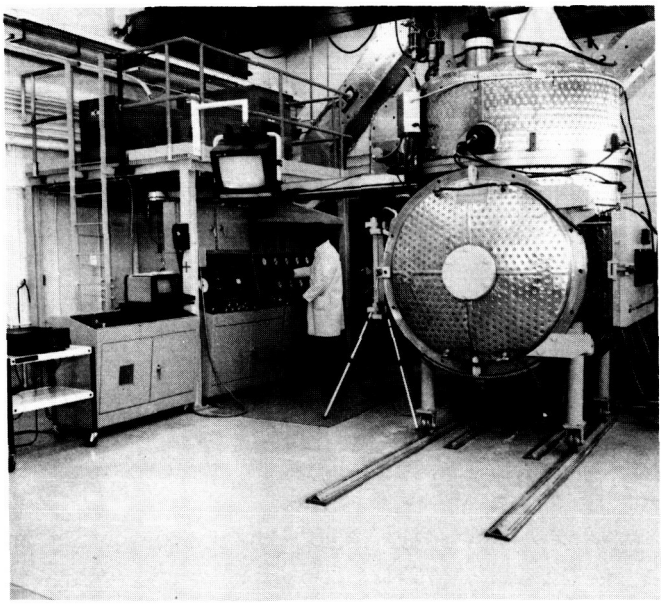

Figure 94. Vacuum Plasma Coating Development Cell.

Development work is in progress for applying durable thermal barrier coatings of zirconia to SSME first stage high pressure fuel turbopump turbine blades, utilizing the enhanced NiCrAlY bond coating process. Of equal importance is the application of a vacuum plasma coating of copper onto the SSME titanium main fuel valve housing (MFVH). Vacuum plasma copper coatings sprayed on titanium sample coupons not only passed the standard adhesion test of bending 90 degrees around a 0.8-inch mandrel, but also showed excellent adhesion when bent around the 0.4-inch mandrel used for testing the ductility of the titanium coupon. Conversely, standard atmospheric plasma-sprayed copper flaked off and failed the 0.8-inch mandrel bending test. Tooling fabrication is in progress at MSFC for plasma-spraying a test SSME titanium MFVH to assess any differences in the effects of heat sink properties on coating adhesion.

R. R. Holmes/EH43
(205) 544-2722
Sponsor: Office of Space Flight

Advanced Coating Techniques

Due to rapid startup and shutdown procedures used in the Space Shuttle Main Engine (SSME), components such as turbine blades and nozzles are subjected to severe thermal shock, which results in reduced component life. To extend the life of these components, thermal barrier coatings are generally used. Conventional plasma-sprayed yttria-stabilized zirconia (ZrO_2/Y_2O_3) is applied to turbine blades by spraying ZrO_2/Y_2O_3 on top of a nickle-chromium-aluminum-yttrium (NiCrAlY) bond coating. However, both ZrO_2/Y_2O_3 and NiCrAlY coatings spall in service, thus offering little protection from thermal shock.

A study was conducted to identify advanced coatings and coating techniques that have potential for application in rocket engines. Several candidate coatings were identified. The example shown in Figure 95 is a multilayer coating with a MCrAlY bond coat (where M stands for metal), a graded ZrO_2/Y_2O_3 metal coat with metal concentration decreasing from bottom to top, and a 100-percent ZrO_2/Y_2O_3 coat on top. Vacuum plasma spraying will be employed instead of conventional air plasma spraying for better adhesion. Candidate coatings will be tested in a special oxygen/hydrogen burner rig which simulates SSME thermal cycles, and the best candidate coating selected for further testing.

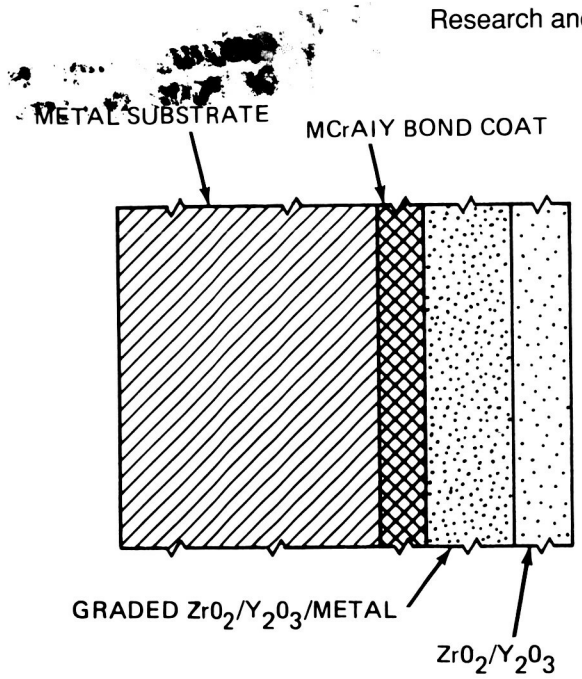

Figure 95. Graded Coating for Turbine Blades.

B. N. Bhat/EH23
(205) 544-2596
Sponsor: Office of Aeronautics and Space Technology

Sprayable Ablator for Solid Rocket Booster Structures

An intensive processing parameter sensitivity analysis has been executed for the sprayable ablator MSA-2, developed as a Thermal Protection System (TPS) for Solid Rocket Booster (SRB) forward and aft structures. MSA-2, which can be applied in thicknesses of up to 1.47 cm (0.50 in.), is required to protect against overall thermal loads of 1.249×10^3 to 1.367×10^3 J/cm^2 (1100 to 1200 Btu/ft^2). Automated sprayed-on coatings of MSA-2 will now replace labor-intensive, hand-bonded applications of sheet cork on the SRB aft skirt and applications of the sprayable ablator MSA-1, currently used on SRB forward structures. The sensitivity analysis identified the maximum high and low limits for each of 19 processing parameters, thereby defining an acceptable operating range centered around a baselined value for each parameter.

MSA-2 is formulated from epoxy resin filled with phenolic microballoons, glass microspheres, and cork and glass fibers, and is processed through a highly automated spray system. Thus parameters designated for attention included formulation variables and key procedural variables descriptive of the entire process, from mixing through spray, pre-cure, and cure activities. Tests included automated spray runs onto test panel substrates and large test configurations (Figure 96). Each completed test article was subject to acceptance criteria of 52×10^5 dynes/cm^2 (75 psi) average flatwise tensile strength, and a volume displacement density of 0.27 to 0.35 gm/cm^3 (17.0 to 22.0 lb/ft^3).

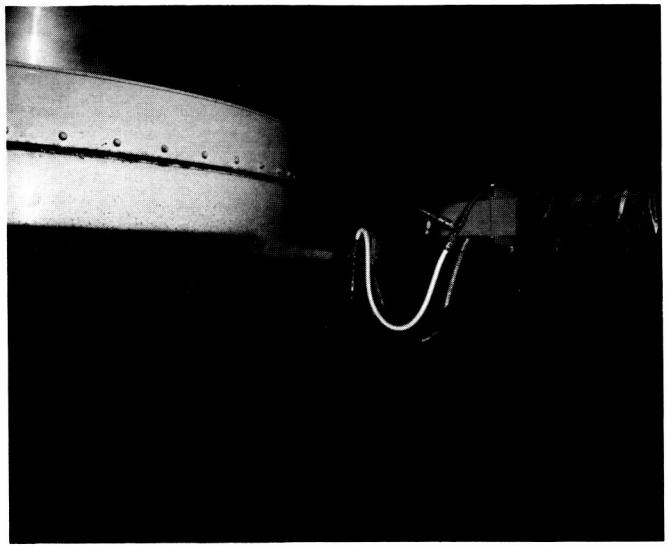

Figure 96. Robot Applying MSA-2 Sprayable Ablator.

The sensitivity analysis met the objective of facilitating transfer of advanced TPS technology into flight hardware production lines through development of a detailed data base. Experience has shown that production startup problems are inversely proportional to the scope of processing information that can be transferred from the preceding R&D activity. The data base generated by the MSA-2 processing sensitivity analysis is expected to provide a significant boost to online productivity for flight hardware refurbishment activities.

W. E. Hill/EH43
(205) 544-2716
Sponsor: Office of Space Flight

Cure Cycle Development

Composite cure behavior is a factor of both the resin's polymerization characteristics and the physical flow/compaction properties of the composite system. Polymerization of the resinous matrix material forms a permanent bond between

fibers and laminae. The curing process may occur unaided or be accomplished by the addition of heat and/or pressure.

Mechanical properties of composite structures are significantly affected by the vacuum bagging technique and curing profile. A joint research effort conducted by MSFC and Martin Marietta to investigate composite application on the External Tank (ET) has led to the optimization of cure cycles for composite materials such as graphite/epoxy, graphite/bismaleimide, graphite/polyimide, glass/phenolic, glass/epoxy, silica/phenolic, and Kevlar/epoxy. Vendor-supplied cure cycles have been modified to consistently produce high quality components. A typical cure analysis involves a detailed review of vendor-supplied data on the properties of pre-impregnated fibers ("prepreg") and cure. A microdielectrometer test is then performed on 6- by 6-in. six-ply prepreg samples to determine the basic characteristics of the resin system.

Data from these tests describe the behavior of viscosity in relation to time and temperature. A preliminary cure cycle is then established for hardware cure. These cure cycles minimize or eliminate common problems such as voids, porosity, and non-uniform thickness in cured parts.

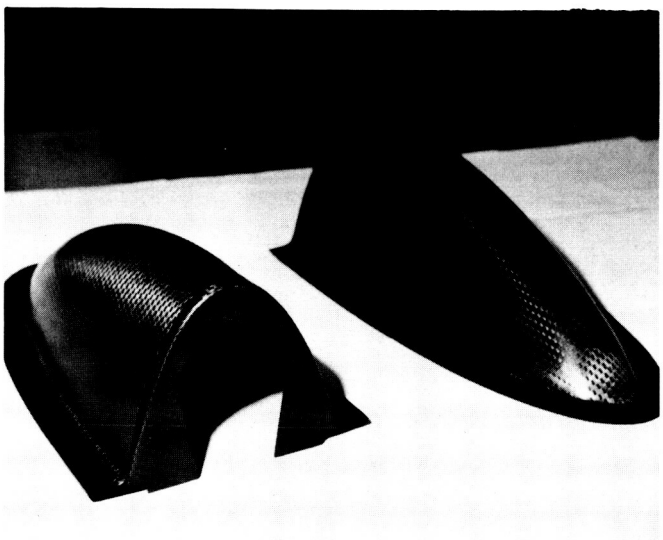

Figure 97. Graphite Epoxy, Forward GH_2 Pressure Line Fairings.

ET components which are candidates for composite structures utilizing these analytically developed cure cycles include the forward gaseous hydrogen (GH_2) pressure line fairing (Fig. 97), the aft GH_2 pressure line fairing, cable trays, and cable tray covers.

G. H. Gordon/EH43
(205) 544-2726
Sponsor: Office of Space Flight

Composite Curing Control System

The Composite Curing Control System is a computer-based system designed and developed to precisely control the curing of composite materials in autoclaves and ovens. The system provides complete cure cycle control, cure cycle management, monitoring and reporting, and other functions important to proper operation of curing equipment (Fig. 98).

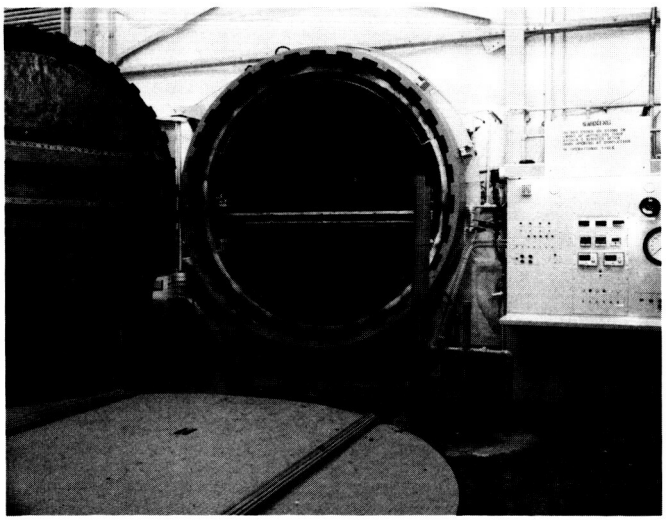

Figure 98. Composite Curing Control System Autoclave.

Accurate temperature control for a 2.74- by 3.66-m (9- by 12-ft) autoclave is made possible by the use of Silicon Control Rectifier (SCR) power controllers driven by a computer in conjunction with a specially written application program. The interior of the autoclave is heated to 343 °C (650 °F) by 24 heaters controlled by the SCR power controllers. There is a long time delay between changes of power to the heaters and changes in temperature inside the autoclave. In turn, when a composite part in the autoclave is large, its temperature lags far behind autoclave temperature. To alleviate this effect, the process

variable temperature used in the Proportional-Integral-Derivative (PID) control equation is set equal to a percentage of the desired temperatures of both the autoclave and composite part.

The system is controlled by a Digital Equipment Corporation PDP 11 host computer and the specially written application program. The system is designed to automatically start up, maintain the preprogramed temperature and pressure profiles, detect abnormal conditions, and perform emergency shutdowns or normal orderly shutdowns when the curing cycle is completed.

E. Martinez/EH43
(205) 544-2724
Sponsor: Office of Space Flight

Protective Coatings

Fifteen materials consisting of metallizations and silicones were applied as protective coatings to selected spacecraft material surfaces and exposed on Shuttle flight STS-41G to the low Earth orbit atomic oxygen environment (Fig. 99). Evaluations of the protective effectiveness of the coatings were made by assessing their mass loss/gain characteristics, maintenance of base material optical properties, and imperviousness to atomic oxygen attack. The candidate overcoats were chosen based on their known stability in an oxidizing environment, prior experience using them as an overcoat, and the availability, ease, and convenience of application. The data generated from this investigation were utilized to address pressing atomic oxygen issues for spacecraft hardware currently in fabrication. In several cases, materials were utilized in unique applications as overcoats.

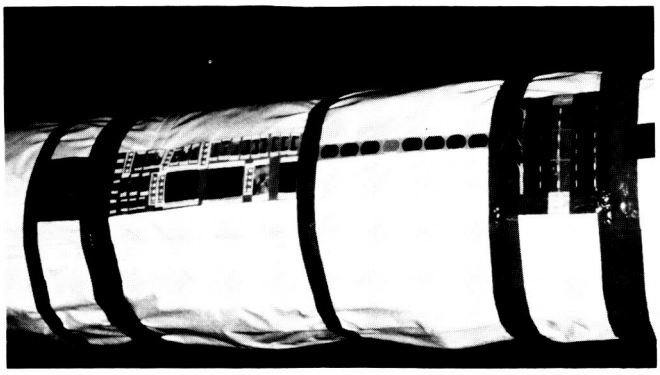

Figure 99. Material Specimens Shown Mounted on the Shuttle Cargo Bay Arm.

As expected, no mass loss was evident with silicone overcoats. Those silicones termed glass resins, such as the OI 651, showed a minimal surface reactivity as overcoats for specular paints, maintaining the very stringent requirements of limited diffuse reflectance. Optical data showed an increase in the diffuse reflectance of paint surfaces coated with RTV-602 and MN41-1104-0 silicone.

The DC 1104 silicone, while relatively thick (~0.5 mil) and nonporous, provided good protection for silver, as expected. No oxygen diffused through this coating to the silver substrate during this short exposure of the Shuttle flight. The DC 1200 primer system, because of its poor cohesion and easy transferability, failed to protect the silver.

The applied thin metallizations of aluminum, palladium, and gold in thicknesses to 5000 Å were inadequate for protecting silver under the combined conditions of atomic oxygen and thermal vacuum. Once the atomic oxygen appeared to diffuse through these coatings to the silver, the oxidation of the silver was initiated. Some intermetallic diffusion accompanied this process to accelerate the result. The thicker films seem to retard the onset of oxidation, as expected. However, post-flight evaluation indicated that the metallic film thicknesses to 5000Å would not be expected to provide long-term protection.

A. F. Whitaker/EH11
(205) 544-2511
Sponsor: Office of Space Science and Applications

Candidate Solar Reflector Materials

A test program to determine the effects of the space environment on candidate materials for Earth orbital solar arrays is under way which includes exposures to particle and ultraviolet irradiation, thermal vacuum, and atomic oxygen environments. The study focuses on the effects of thermal vacuum cycling on eight materials with atomic oxygen-resistant coatings which have been identified as candidate solar reflector materials.

Five test specimens of each of the eight identified candidates were exposed to a thermal vacuum cycling environment and examined for microcracking. Specimens from each group were then

exposed to an active oxygen environment to determine if their protective coatings had been penetrated. Examinations were made before and after each environmental exposure to determine the presence and severity of microcracking.

Materials selected for this initial testing varied with respect to the substrate material used (aluminum or beryllium copper), the substrate surface finish applied (burnished or optically polished), and the overcoat material applied to the coated substrate surfaces (magnesium fluoride or silicon dioxide). Both the magnesium fluoride and the silicon dioxide provided some protection for the underlying materials, although some microcracking was observed for all materials tested. The substrates with optically polished surfaces and thinner applications of protective coatings sustained the most severe microcracking. Relative changes in reflectance values due to the environmental effects are being examined and their significance to the material requirements for the given application is being assessed. Additional thermal vacuum testing and active oxygen exposure are planned.

S. A. Little/EH12
(205) 544-5960
Sponsor: Office of Aeronautics and Space Technology

Mobile Hydrogen in Metals

Alloys used to make Space Shuttle Main Engine components such as the turbine blades and disks are subject to embrittlement due to absorption of hydrogen into the metal. This study developed and applied a method of analyzing hydrogen absorption data. The data consist of quantitative determinations of the amount of hydrogen absorbed in the metal, and the effective state of that hydrogen (i.e., whether it is mobile or trapped).

Hydrogen desorption data, expressed as coulombs (C) desorbed vs. time, have been obtained for Waspaloy, Rene' 41, and 4340 steel using electrochemical methods, and a more general method of data analysis, using diffusion theory, has been developed and applied. The method may assume either an initial hydrogen distribution which conforms to that predicted by diffusion theory, or a uniform initial distribution. The hydrogen desorption data are interpreted in terms of either of these initial distributions, or a combination thereof.

The desorption curves for Rene' 41, charged electrolytically for 4 h at 1 mA/cm^2, are shown in Figure 100. As shown in the figure, the fit of the experimental curve indicates that desorption is completely explained by a 100 percent non-uniform initial distribution (that which would be predicted by diffusion theory). Thus the "fast" hydrogen is not necessarily due to surface and sub-surface hydride formation as has been previously proposed (based on the assumption of a uniform initial distribution), although at least partial electron transfer, or bond formation, is necessary in order for the hydrogen atoms to fit into the octahedral holes of the face-centered cubic metal lattice. This occurs not only at the surface, but to whatever depth the hydrogen is able to penetrate. A similar result was also obtained for Rene' 41 at the faster charge rate of 1 h at 60 mA/cm^2. Almost identical results were obtained for Waspaloy using both the electrolytic charging and high pressure (5,000 psi) charging with gaseous hydrogen.

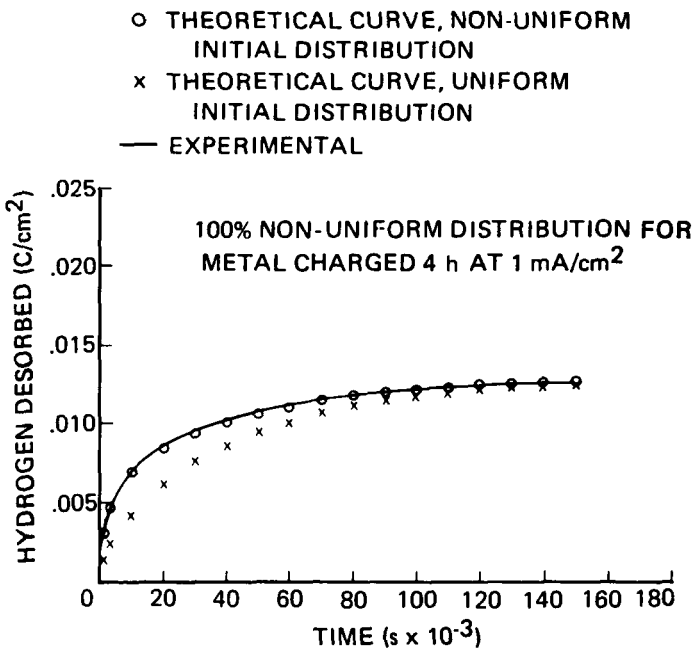

Figure 100. H_2 Desorption Curve for Electrolytically Charged Rene' 41, Slow Charge.

In contrast, the experimental desorption curve for 4340 steel (Fig. 101), charged 4 h at 1 mA/cm^2, is completely explained by a 100 percent uniform distribution. A similar result was obtained at a higher charge rate (1 h at 60 mA/cm^2), where a 59.2 percent uniform distribution was observed. In this case, the diffusion coefficient for the absorption is an order of magnitude greater than that

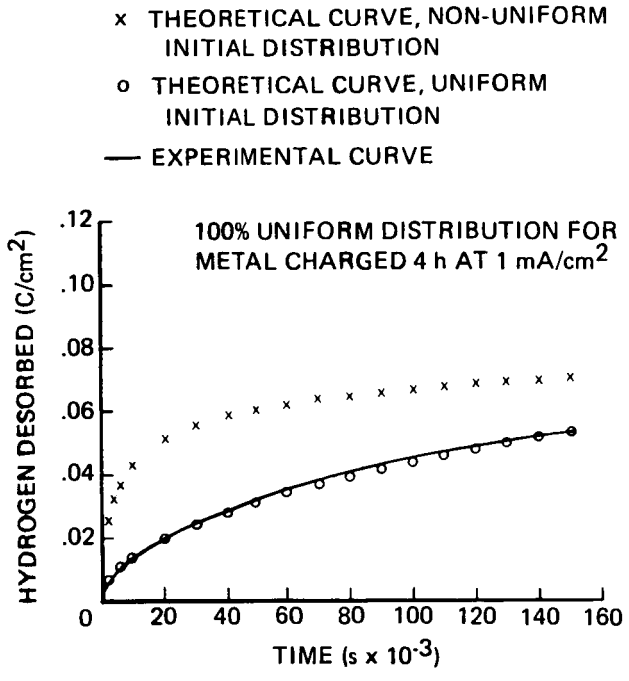

Figure 101. H_2 Desorption Curve for Electrolytically Charged 4340 Steel, Slow Charge.

for the desorption, indicating that 4340 steel has a high affinity for hydrogen (4340 steel is body-centered cubic). This is also reflected in the observed solubilities, as shown in Table 13.

Table 13. Observed Solubilities for Hydrogen in Metals.

MATERIAL	METHOD	CHARGE RATE	TEMP. (°C)	SOLUBILITY (ppm)
WASPALOY	ELECTRO.	FAST[a]	25	1.28
	ELECTRO.	SLOW[b]	25	0.75
	ELECTRO.	FAST	150	3.64
	HP (5,000 psi)	–	–	1.28
RENE' 41	ELECTRO.	FAST	25	1.17
	ELECTRO.	SLOW	25	0.29
4340 STEEL	ELECTRO.	FAST	25	4.97
	ELECTRO.	SLOW	25	2.30

(a) 60 mA/cm^2 (b) 1 mA/cm^2

These results will be correlated with grain size, crystallographic data, mechanical properties, etc., in order to gain further insight into the hydrogen embrittlement problem.

Danford, M. D.: The Application of Diffusion Theory to the Analysis of Hydrogen Desorption Data at 24 °C. NASA TM-86531, October, 1985.

M. D. Danford/EH24
(205) 544-2612
Sponsor: Office of Space Flight

Work-Strengthened Inconel 718 Bar Material

Inconel 718 bar material has been developed for use in the tensioner for the Space Shuttle Solid Rocket Booster (SRB) holddown studs. A work-strengthening process developed by Wyman Gordon using triple-melted material and direct double-aging produced bars with diameters of 10.16 cm (4.00 in.) and 14.60 cm (5.75 in.) with ultimate tensile and yield strengths in excess of 1447.9 MPa (210.0 ksi) and 1344.5 MPa (195.0 ksi), respectively. The mechanical properties and stress corrosion resistance of the bars were determined and evaluated by MSFC.

Fracture toughness and Charpy V-notched strengths are shown in Figures 102 and 103, respectively. There appears to be very little, if any, degradation in the material's toughness with decreasing temperature, within the limits of the testing program. In addition, the work-strengthened Inconel 718 alloy showed excellent resistance to stress corrosion, as evidenced by the mechanical properties of stressed specimens after 180 days of exposure to a salt fog environment.

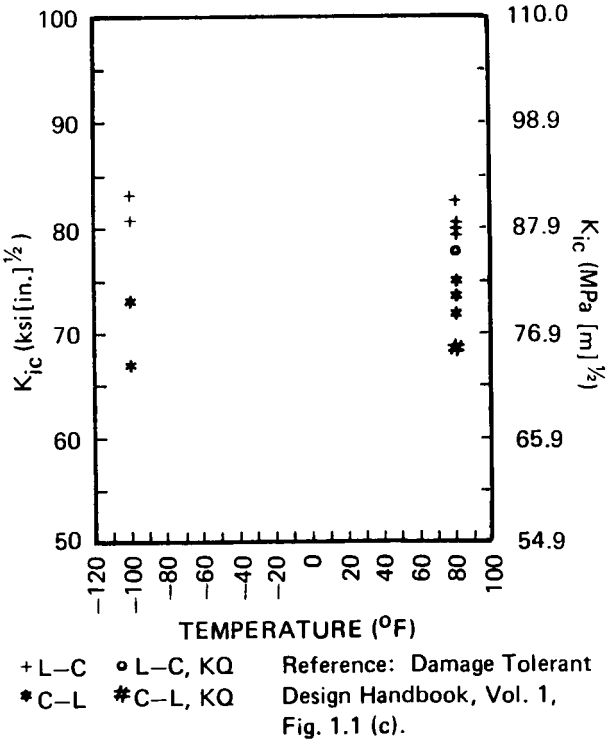

Figure 102. Fracture Toughness of Work-Strengthened Inconel 718 Alloy Bars.

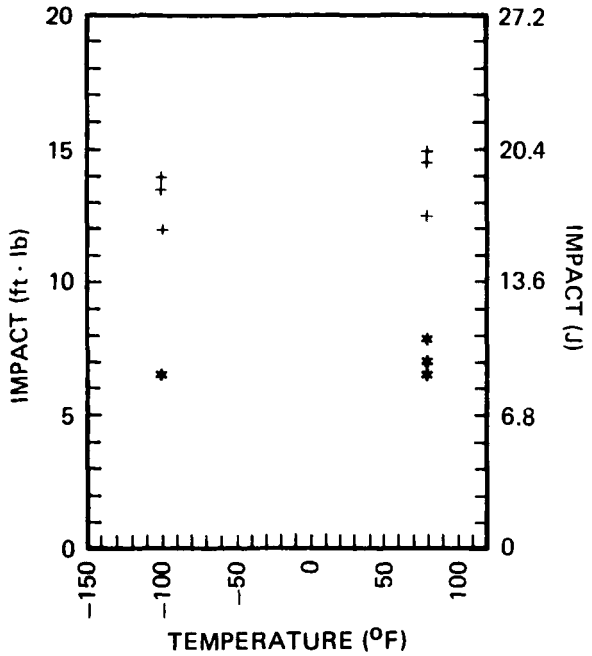

DATA:	−100°F (−73°C)	80°F (26.7°C)
+ LONGITUDINAL	12, 13.5, 14	12.5, 14.5, 14.5, 15
* TRANSVERSE	6.5, 6.5	6.5, 7, 8, 8

Figure 103. Charpy V-Notched Impact Strength of Work-Strengthened Inconel 718 Alloy Bars.

Based on the test data generated, the solution-treated, work-strengthened, and direct-aged material is now being used at Kennedy Space Center in the Biach Industries tensioner which applies the tension load to the SRB holddown studs. Vandenberg Air Force Base has also been supplied with tensioners using this work-strengthened Inconel 718 alloy.

J. W. Montano/EH22
(205) 544-2581
Sponsor: Office of Space Flight

Corrosion Fatigue

Corrosion fatigue tests were conducted on bare, chemical conversion coated, and anodized 2219-T87 aluminum. These tests were performed using a rotating beam machine running at a velocity of 2500 rpm. The corrosive environments were distilled water, 100 parts per million sodium chloride (100 ppm NaCl), and 3.5 percent NaCl.

The results of these tests are shown in Figure 104 and clearly indicate the adverse effect of corrosive environments on the fatigue life of this alloy. In all cases the effects were related to the general corrosivity of the test solution; i.e., the effect of 3.5 percent NaCl was greater than that of 100 ppm NaCl, which was greater than that of distilled water. The corrosion fatigue strength (CFS) of bare 2219-T87 aluminum ranged from 104 MPa in distilled water (a ratio to the endurance limit of 0.76) to 20 MPa in 3.5 percent NaCl (a ratio of 0.15).

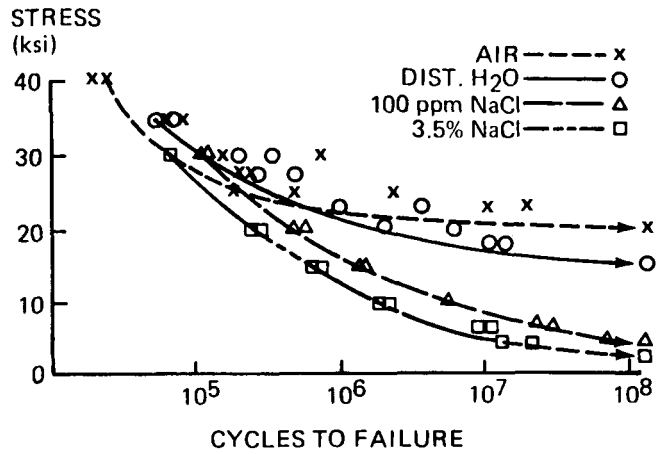

Figure 104. Corrosion Fatigue Strength of Bare 2219-T87 Al.

The effect of the protective coatings is evident, as shown in Figures 105, 106, and Table 14. The CFS of the conversion-coated sample in a 100 ppm NaCl environment was 45 MPa (a ratio of 0.34 to the endurance limit in air). This represents an increase in CFS of 15 MPa over values for bare aluminum samples in equivalent environments. Even further improvements were obtained with the use of anodized coatings, which yielded a CFS of 69 MPa in 100 ppm NaCl. This value represents an increase of 38 MPa in CFS

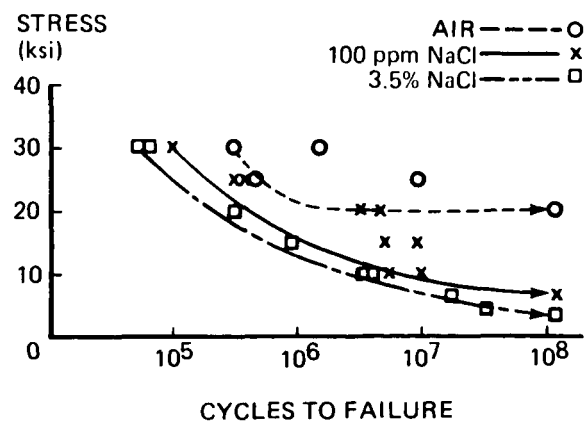

Figure 105. Corrosion Fatigue Strength of Conversion-Coated 2219-T87 Al.

Table 14. Estimated Corrosion Fatigue Strength (CFS) of 2219-87 Al.

ENVIRONMENT	BARE ALUMINUM			CONVERSION COATED ALUMINUM			ANODIZED ALUMINUM		
	MPa	(ksi)	CFS/E.L. (a)	MPa	(ksi)	CFS/E.L. (a)	MPa	(ksi)	CFS/E.L. (a)
AIR	137.8	(20)	–	137.8	(20)	1.00	103.29	(15)	0.749
DISTILLED H_2O	104.0	(15.1)	0.755	–	–	–	–	–	–
100 ppm NaCl	31.0	(4.5)	0.225	46.14	(6.7)	0.335	68.9	(10.0)	0.500
3.5% NaCl	19.97	(2.9)	0.145	24.10	(3.5)	0.175	30.29	(4.4)	0.220

(a) RATIO OF CFS TO THE ENDURANCE LIMIT OF BARE Al IN AIR

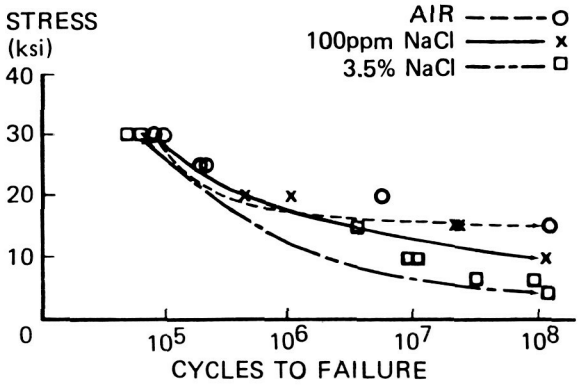

Figure 106. Corrosion Fatigue Strength of Anodized 2219-T87 Al.

over bare aluminum samples. Similar results were obtained in the 3.5 percent NaCl environments, with CFS values of 20 MPa for bare, 24 MPa for conversion-coated, and 30 MPa for anodized samples.

The results of this series of tests indicate that a significant reduction in fatigue strength can be expected when components are exposed to corrosive atmospheres. It has been determined that the effectiveness of protective coatings in prolonging corrosion fatigue life depends upon the type of coating used and the corrosiveness of the atmosphere.

V. C. McMillan/EH24
(205) 544-2615
Sponsor: Office of Space Flight

Space Station Common Module Assembly

Space Station technology development at MSFC includes full-scale assessment of the two assembly methods for the Common Module developed by Boeing Aerospace Corp. and Martin Marietta Michoud Aerospace (MMMA).

The Martin Marietta development structure is a skin and stringer design that utilizes excess External Tank (ET) panels for the four barrel sections. To construct each of these barrels, the large ET vertical weld fixture was modified to hold the smaller-diameter components for longitudinal welding. A girth weld fixture was fabricated to weld T-ring flanges to each barrel. All welds utilize the Variable Polarity Plasma Arc (VPPA) weld process perfected by MSFC for use on the ET. After each barrel segment is welded, a T-ring is attached, the barrels are bolted together, and bulkheads are attached (Fig. 107).

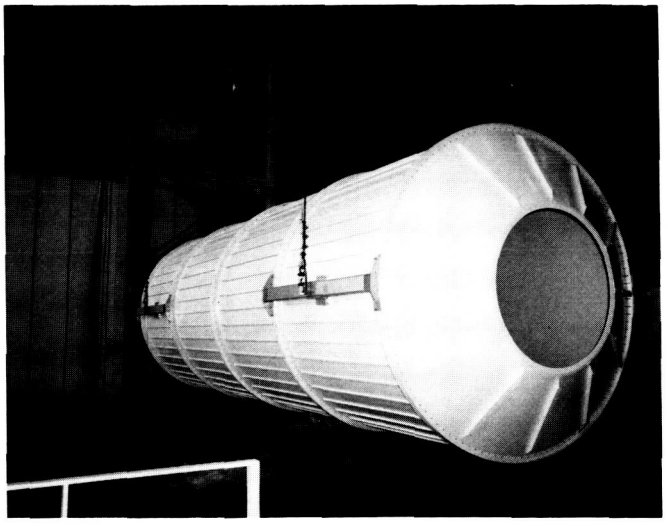

Figure 107. MMMA Common Module Integration Simulator.

The Boeing development structure is a waffle-grid design with external ribs on the three barrel sections that make up the module. These barrels will be made on development tooling installed in the MSFC Productivity Enhancement Facility. This tooling includes a vertical weld station for the

longitudinal welds on each barrel and a girth weld and assembly fixture for the circumferential welds. A single VPPA weld process system supports both fixtures. The completed barrel sections are welded together with an interfacing T-ring. Attachment of conical bulkheads to each end completes the structure. The module also incorporates a 20-inch window. This unit closely simulates the proposed flight configuration.

The efforts under way with Boeing and Martin Marietta will serve to optimize tooling concepts, welding parameters, and process controls for fabricating flight hardware. The completed development structures will be used further as test beds for the environmental control systems and for optimizing design and placement of internal equipment.

C. J. Bramon/EH44
(205) 544-2800
Sponsor: Office of Space Station

Space Shuttle Main Engine Robotic Weld System

Robotic welding of Space Shuttle Main Engine (SSME) components has begun at the Rocketdyne Canoga Park production facility. This highly successful automation program has its roots in the robotic welding development cell at MSFC. NASA and Rocketdyne engineers have worked closely to implement robotic automation in SSME production. This new approach promises to reduce defect rates compared to the manual welding which it replaces.

Fabrication of a SSME requires approximately 584 m (23,000 in.) of welding, 60 percent of which is performed by automatic equipment. The remainder of the welds are made manually, at a defect rate greater than that of the automated welds. Application of conventional automatic welding equipment is not practical for these welds because of the complex geometry of the joints and the need for adaptation during the weld.

The SSME robotic welding system being developed by MSFC represents a distinct improvement over conventional (non-robotic) automatic welding. This is because of the extensive positioning capability of its five-axis torch manipulator, which allows one machine to be programmed for a variety of parts. A two-axis part positioner moves the part as it is welded, maintaining a preferred orientation of the weld joint at all times for consistent weld properties. The robot controller also programs the operation of all the welding process equipment to a degree of repeatability unattainable by human counterparts. The system is equipped with a computer interfaced to a vision-based welding sensor that can compensate for variations in seam alignment and puddle size as the weld is being made.

Engineers from Rocketdyne's facility are working with NASA engineers to characterize the parameters necessary to develop equipment and processes for welding SSME hardware. Representative parts are being welded to develop sensors and tooling that will be used in production, and candidate welds for robotics are being demonstrated on fixtures developed at MSFC. Two tools have been designed, built, tested, and sent to the production facility to be used on the manufacturing robots. One is a tool for welding joints on the main combustion chamber, and the other welds joints on a main injector manifold.

The vision-based welding sensor developed by Ohio State University has demonstrated its ability to track the weld joint on a variety of welds. Tests have been made to determine the critical sensor control parameters for tracking joints on SSME hardware. Computer programs have been developed to allow an operator to generate the robot programs from a graphic representation on a computer terminal. This will permit more accurate programs to be written for the robot than can be done by hand, and eliminate the need to remove robot hardware from production to program it for new applications. An initial demonstration of this capability has been performed at MSFC.

C. S. Jones/EH42
(205) 544-2701
Sponsor: Office of Space Flight

Simulation and Programming of Manufacturing Processes

The development of new manufacturing processes often requires the use of new, complex, sensitive, and expensive equipment and raw materials. For instance, a robot welding workcell

for Space Shuttle hardware uses a multi-axis robot in conjunction with special welding, sensor, and operator control equipment to perform a weld on expensive, one-of-a-kind parts. When specifying equipment to process these parts or when testing existing equipment for use with new and different parts, the applicability of a particular equipment setup to a certain piece of Shuttle hardware can be determined by simulating the system concept before any hardware is bought or delivered.

A development program is under way to simulate new and existing manufacturing processes for the Shuttle on a commercial computer-aided design/computer-aided manufacturing (CAD/CAM) system. Applications developed during FY86 include composite filament winding and robotic welding. In these applications, the motions of the equipment can be simulated in graphics to determine feasibility (Fig. 108). Once a process development program is under way and hardware is operational, the system can be used to generate computer commands to execute the simulated task on actual hardware. This method avoids tying up the target system for program development. Programs developed in the simulator or on the hardware can be stored on a data base for analysis by other NASA groups or contractors doing similar work. The system can serve as a focal point for the scheduling, testing, and analysis of a development program.

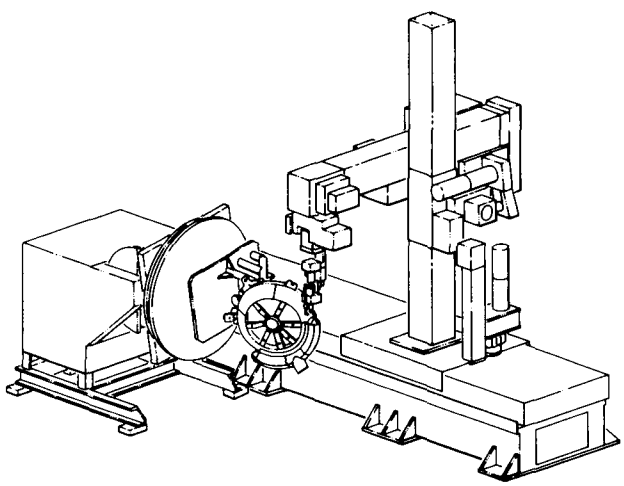

Figure 108. Example of Graphic Simulation for Robotic Welding.

Robotic welding for the Space Shuttle Main Engine and filament winding patterns for the solid rocket motor cases have been simulated. Commands for programming the development systems have been downloaded from the computer to the actual workcell and executed. An interactive program to inject the applicable welding parameters for integration with robot motion has been developed.

While only in its early development stages, the system promises to provide keen insight into the behavior of complex processes without the need to involve expensive hardware and raw materials.

C. S. Jones/EH42
(205) 544-2701
Sponsor: Office of Space Flight

Software Development for Stripping Large Space Structures

The MSFC Thermal Protection System (TPS) Removal Facility was fully automated in FY86, via a DEC PDP 11/23 Plus host computer that integrates and controls all subsystems while permitting operator intervention when required. The objective of this project was to create a user-friendly system to automate the TPS Removal Facility. The software that was developed provides a way to centralize control of all subsystems, standardize a variety of processes without sacrificing process flexibility, improve process reliability, and simplify computer control of each task, particularly for operators with minimal computer experience.

A milestone for software development was reached with the fully automated waterblasting of a Solid Rocket Booster (SRB) frustum model generated by the newly-completed TPS removal software. This innovative system is capable of teaching, verifying/editing, and running models for stripping procedures specific to a SRB structure (frustum, forward skirt, nose cone, aft skirt). As shown on Figure 109, the host computer integrates and controls all subsystems (six-axis robot, robot lift table, turntable, and dual pump system), requiring only that an operator identify the correct RUN software for stripping a given material from a specific structure, and monitor the operation. By means of the TEACH and VERIFY/EDIT software, the technician can create new models (a set of commands comprising a given process) or easily alter existing ones.

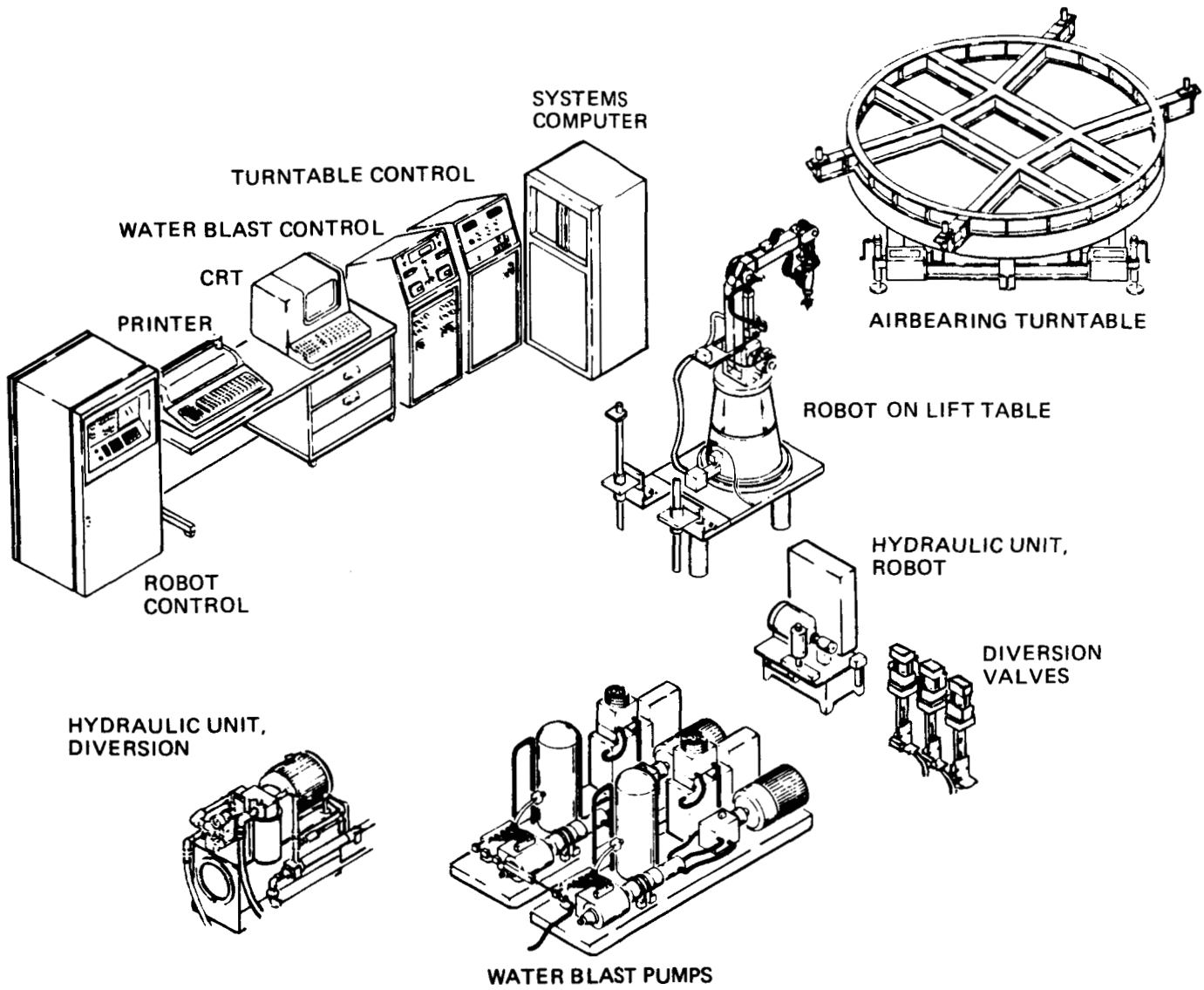

Figure 109. SRB Automated TPS Removal System.

All parameters for the existing system have been automated, with the majority of the software verified and documented by the publication of a preliminary user's guide. Computer control of the basic processes offers the means to pursue developmental research of an increasingly sophisticated nature. The automation of this formerly manual stripping system offers process reliability, expeditious hardware flow, and greatly improved conditions for personnel, who can now be removed from the waterblast area to the control room. The user-friendly menus and creative capabilities of the system enable a process technician with no programming experience to customize automated procedures as needed. In short, this software permits the building of a process library suited to a particular TPS removal site, such as Kennedy Space Center's (KSC's) High Pressure Wash Facility.

As part of the ongoing effort to optimize the TPS Removal System, several enhancements are planned. A new DEC PDP 11/73 Plus central processing unit will be installed that enables processing of a computer program in one-fifth of the time now required. The Allen Bradley data highway software will be modified to permit a multi-station communications link that will be transferable to the Marshall Sprayable Ablator-2 spray cell, allowing computer control of the turntable and process switches in that facility. The current software will also be modified for KSC purposes, concentrating on pump drive control and robotic manipulation programming.

Optical scanning will be introduced with a camera that views segments of a stripped structure to evaluate stripping coverage prior to touchup work. It will provide x-y coordinates for locating each flaw, resulting in a model file by which precision touchup work can be automated. The camera system will be implemented after the optical scanner software is verified.

Off-line programming for stripping models will be possible with the newly installed kinetic graphics simulator. This system will enable multi-directional manipulation of three-dimensional images of the facility's turntable and robot, and will permit the operator to visualize a run sequence in real time prior to its verification and use in the blast room. As a prerequisite, a subsystem will be developed to define individual configurations of SRB hardware as a feeder for the graphics simulator.

M. L. Roberts/EH43
(205) 544-2717
Sponsor: Office of Space Flight

Foam Application Development

An investigation is under way to develop and qualify a spray-on foam insulation (SOFI) to be used as a backup/replacement for the CPR-488 foam presently used on the Space Shuttle External Tank (ET) sidewall. The CPR-488 foam has a density of 2.3 to 2.6 lb/ft^3. The NCFI 22-65 foam presently used on the ET liquid hydrogen tank aft dome has a density of 2.6 to 3.1 lb/ft^3. The major thrust of the project is to develop a less expensive formulation of NCFI foam (NCFI 23-66) with lower density than CPR-488, but equivalent performance.

The nominal density of the NCFI 23-66 under development is 2.1 lb/ft^3. Preliminary test results from process definition spray runs are promising. The new NCFI 23-66 foam, when fully developed and used on the ET, can result in a weight savings of approximately 400 pounds. The materials cost savings will be significant since there is a difference of $5.22/lb between CPR-488 and NCFI 23-66.

A second project is under way to develop kinematic simulation of SOFI spray application for off-line programming of the MSFC Productivity Enhancement Facility SOFI Development Cell. An Evans & Sutherland (E&S) kinematic simulation Computer system is used for this activity (Fig. 110). The E&S system is utilized to graphically model the Cincinnati Milacron T3 robot, the airbearing turntable, etc., used in the SOFI Development Cell. Each of the graphic models is dimensionally scaled to the physical equipment in the spray cell. The robot is taught in straight line jog movement along the major axes x, y, z, and vector rotations about each of the major axes. The robot controller displays rectangular coordinates on a CRT at the end of each jog move. Point locations can be edited by entering relative incremental changes via the keyboard along or about the major axes. The graphical model is manipulated by moving each of the robot's six joints independently with the E&S system. No provision is made for the incremental editing of the point locations.

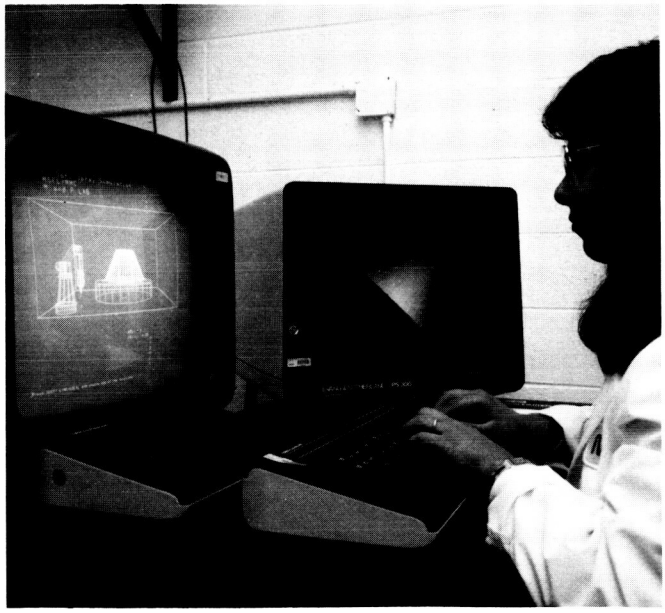

Figure 110. E&S Graphic Simulation System.

To make the simulation system useful at the SOFI cell technician level, the manipulation of the graphic model must be made similar to the teach pendant operation of the robot in the teach mode. To do this, a function describing the robot's joint angles in terms of work coordinates must be used. This inverse kinematic solution will have to be derived. At the present level of capability, the E&S system is being used to graphically simulate the ET liquid oxygen ogive segment and environmental test panel(s) configurations for future spray development programs.

The off-line simulation of these activities precludes disruption of present or on-going SOFI cell development activities, resulting in a more productive R&D effort.

C. H. Jackson/EH43
(205) 544-2723
Sponsor: Office of Space Flight

Abrasive Water Jet Cutting

Welding and refurbishment process development for the Space Shuttle Main Engine (SSME) have been enhanced through introduction of a system for effectively cutting superalloy materials. The system, which consists of an abrasive water jet cutting station and a tracer mill, has been installed in MSFC's Productivity Enhancement Facility (Fig. 111).

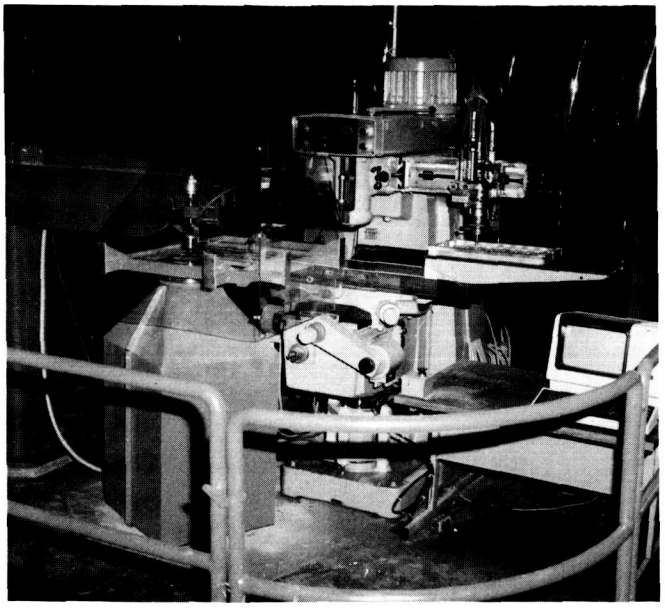

Figure 111. Abrasive Water Jet Cutting Station.

The abrasive water jet system utilizes a 1.24-gpm flow of 60,000-psi deionized water constricted through a 0.025-cm (0.010-in.) diameter orifice. Garnet abrasive is injected into the nozzle assembly below the orifice and carried by the water to the cutting area. The tracer mill manipulates the part to be cut in a plane under the stationary cutting head, while a catcher tube assembly under the part to be cut collects the abrasive/water mixture.

This system has been used to cut Inconel 718 weld test specimens to within 0.051 cm (0.020 in.) of finished dimensions, as well as SSME weld joint simulation samples of the same material for robotic welding development. Other applications include dismantling of welded component assemblies and cutting of raw stock. A maximum thickness of 2.54 cm (1.00 in.) of Inconel 718 has been cut with a kerf angle of 0.16 cm (0.063 in.).

The abrasive water jet cutting station has proven to be a versatile system for cutting SSME materials, with appreciable savings in cost, time, and quality.

C. Kurgan/EH42
(205) 544-2705
Sponsor: Office of Space Flight

Structures and Dynamics

Inter-Stability Approach to Complex Control Problems

The attitude control of the space station is an example of a complex control system. The feedback loop pervades the total system from attitude sensing, over a structure with many uncertain resonances, to the control force (or moment) actuators. Stability is of great concern. Therefore, much effort is extended in analyses, system identification, and ground vibration testing. Lead times are long and costs are high to accomplish the task, and system changes impact the total system, often requiring that the costly effort be repeated. These difficulties prompted the concept of inter-stability. Inter-stable systems are decomposed into stable subsystems so that stability can be ascertained by analysis of low-order subsystems. Inter-stability is defined by compatibility criteria and allowable connections for subsystems. Compatible systems have frequency responses in the same complex half-plane. Three types are identified by the half-planes: positive imaginary, positive real, and negative imaginary. Inter-stable connections preserve the half-plane property of the subsystems such that the total system response occupies the same half-plane. Connections such as parallel, series, and vector coupling are algebraically defined by addition, reduction (symbol x), and coupling matrices.

Figure 112 shows a control loop with a controller H feeding back into a resonant structure, the negative imaginary plant G. The controller is compatible when the inverse 1/H is also a negative imaginary system. G and 1/H are connected by a reduction (symbol x). The low order of the subsystems yield simple criteria for inter-stability, e.g., inequalities. Frequency response criteria are also available. Inter-stability helps to divide a complex control problem into low-order problems. Docking, undocking, or other changes are readily assessed with respect to stability. Inter-stability was applied to the Space Shuttle ground vibration tests. The half-plane criteria make interstability insensitive to structural resonances. Inter-stability seems to meet the objective, aid scheduling, resolve many analytical difficulties, and save cost.

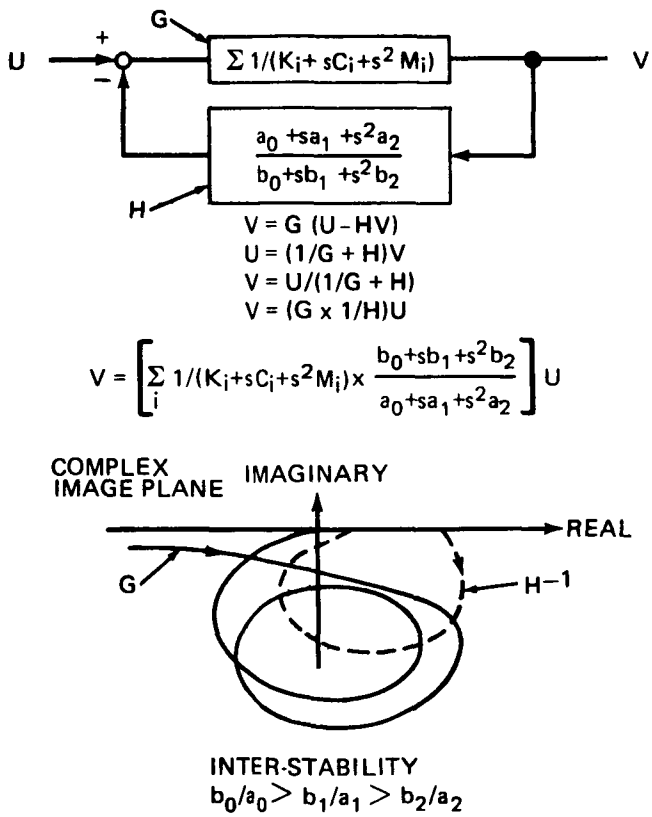

Figure 112. Inter-Stability Example.

von Pragenau, G. L.: Inter-Stable Control Systems. Workshop on Structural Dynamics and Control Interaction of Flexible Structures, April 22-24, 1986.

von Pragenau, G. L.: Resonance-Inert Stabilization for Space Stations. NASA TN D-6731, June 1972.

G. L. von Pragenau/ED14
(205) 544-1469
Sponsor: Office of Aeronautics and Space Technology

Control System Design

Several control system design strategies have been proposed in recent years. Many of these are theoretically sound, but practical problems are encountered in their implementation. The Design to Performance Concept provides for the "tuning" of the control system on-orbit using measured data from the control system sensors themselves (Fig. 113). From this data a frequency response description of the plant is derived and used to redesign the controller. This systematic approach enables better performance to be extracted from the same control system hardware, and partially eliminates the need for large-scale vibration testing of the structure.

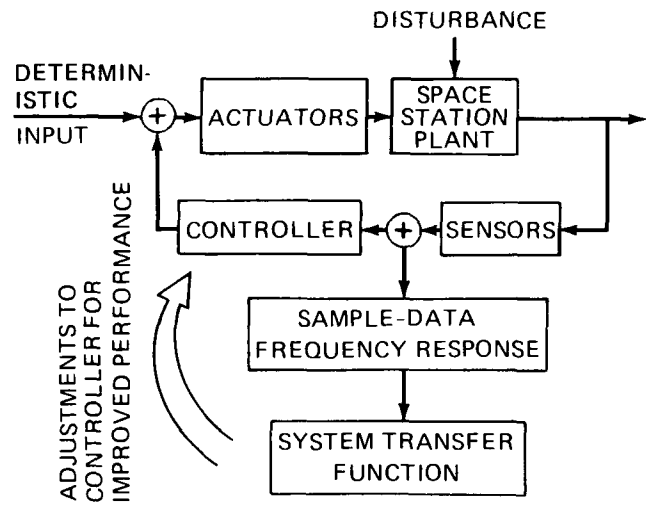

Figure 113. Control System Design to Performance Approach.

A 12-month study of the Design to Performance Concept has recently been concluded. It showed the concept to be feasible and included the application of the technique to two design problems: a single-input/single-output Space Station example, and a multiple-input/multiple-output generic space structure problem. Recommendations for future research in this area include the application of this concept to an actual control experiment which includes both structure and control hardware.

H. J. Buchanan/ED15
(205) 544-1470
Sponsor: Office of Aeronautics and Space Technology

Solar Array Flight Experiment/Dynamic Augmentation Experiment

The Solar Array Flight Experiment (SAFE) Dynamic Augmentation Experiment (DAE) was conceived in 1981 to demonstrate the feasibility of on-orbit measurement and ground processing of large space structure dynamic characteristics such as frequency, damping, and mode shapes. Test definition or analysis verification provides the dynamic characteristic accuracy required for control systems use. In earlier space vehicles, including the Shuttle, the control system natural frequency could be placed well below the lowest structural natural frequency to prevent control system/structural interaction and maintain adequate control authority. Large space structures (LSSs), however, have such low natural frequencies that the control system natural frequency will have to be "nested" among the structural natural frequencies in order to have adequate control authority. This problem, coupled with the dense rate of LSS structural frequencies, requires a very accurate definition of the structural characteristics. LSS-type structures cannot be tested in 1-g Earth environment, leaving on-orbit tests as the remaining alternative. Fortunately, the SAFE was in development and scheduled for a 1984 launch. The SAFE has all the characteristics of an LSS and was a target of opportunity years ahead of the next structure. This opportunity provided the impetus for the SAFE/DAE.

The SAFE/DAE utilizes a special sensor system which was developed for the experiment. It consists of a retroreflector field tracker (RFT), which is positioned near the base of the solar array. The RFT illuminates 18 to 23 retroreflector targets on the array with 5 laser diodes at 800 nm spectrum. The sensor portion is an adaptation of a multifield star tracker. The sensor optics focus the retroreflector images on a solid state, charge injection device detector. A remotely located microprocessor controls the data acquisition, interrogates the sensor detector, converts the sensor data to engineering units, and provides a digital output. The data are then multiplexed and stored on a digital tape recorder. Post-flight ground data evaluation processes the x and y motions from all targets to determine the dynamic characteristics. Evaluation techniques utilize the free decay and time and frequency domain analysis.

Six SAFE/DAE tests were run and data obtained from all targets. One anomaly was the solar array unexpectedly curving around the mast on the dark portion of the orbit. This curvature was measured and is shown in Figures 114 and 115. In Figure 115, the small bright dots on the mast top enclosure and blanket are the retroreflector targets. The larger circular targets on the array are the photogrammetric targets. Summary results are shown in Table 15.

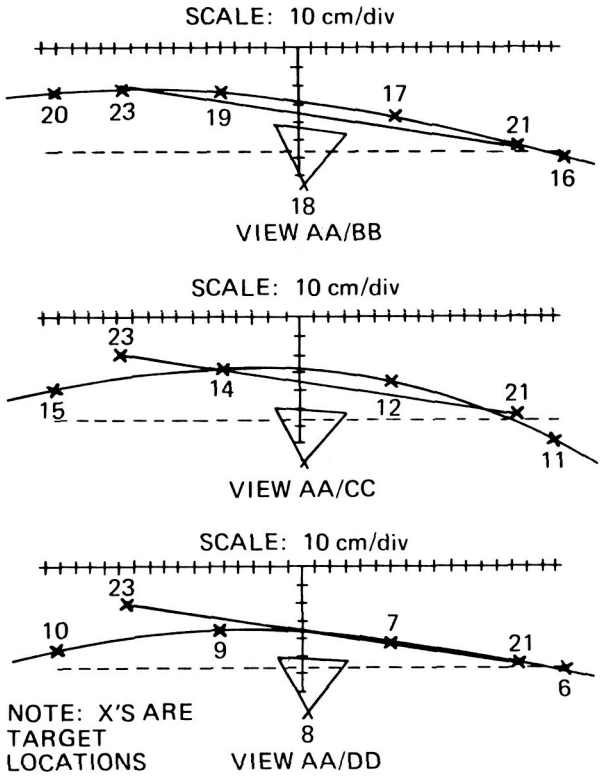

Figure 114. Blanket Curvature, First SAFE/DAE Test.

Figure 115. Solar Array Dark Side Curvature.

Table 15. Solar Array Dynamic Characteristics.

ANALYTICAL FREQUENCY (Hz)	MODE SHAPE	TEST FREQ.	DAMPING (%)
0.064	OUT-OF-PLANE BENDING	0.059–0.072	2–8
0.067	IN-PLANE BENDING	NOT IDENT-IFIED	
0.115	1ST TORSION	0.089–0.092	1–2
0.179	2ND OUT-OF-PLANE BENDING	0.121	2–4
0.213	2ND TORSION	0.172	2

Evaluation of the measured dynamic characteristics indicates that the mode shapes tended to match well, but natural frequencies not only differed from test to test but changed during decay from each individual excitation. Damping also varied in a similar fashion. These phenomena are characteristic of nonlinear structures. The conclusions resulting from the program were: The DAE successfully measured the SAFE solar array dynamic response, even under out-of-design conditions; four of the first five solar array modal characteristics were successfully determined; significant structural nonlinearities are expected in a LSS; and LSS damping is expected to be high.

R. W. Schock/ED24
(205) 544-1537
Sponsor: Office of Aeronautics and Space Technology

Large Space Structure Control Verification

MSFC has developed a facility in which closed-loop control of a large space structure (LSS) can be demonstrated and verified. The main objective of the facility is to verify LSS control system techniques so that on-orbit performance can be ensured. The facility consists of a LSS test article which is connected to a payload mounting system that provides control torque commands. It is

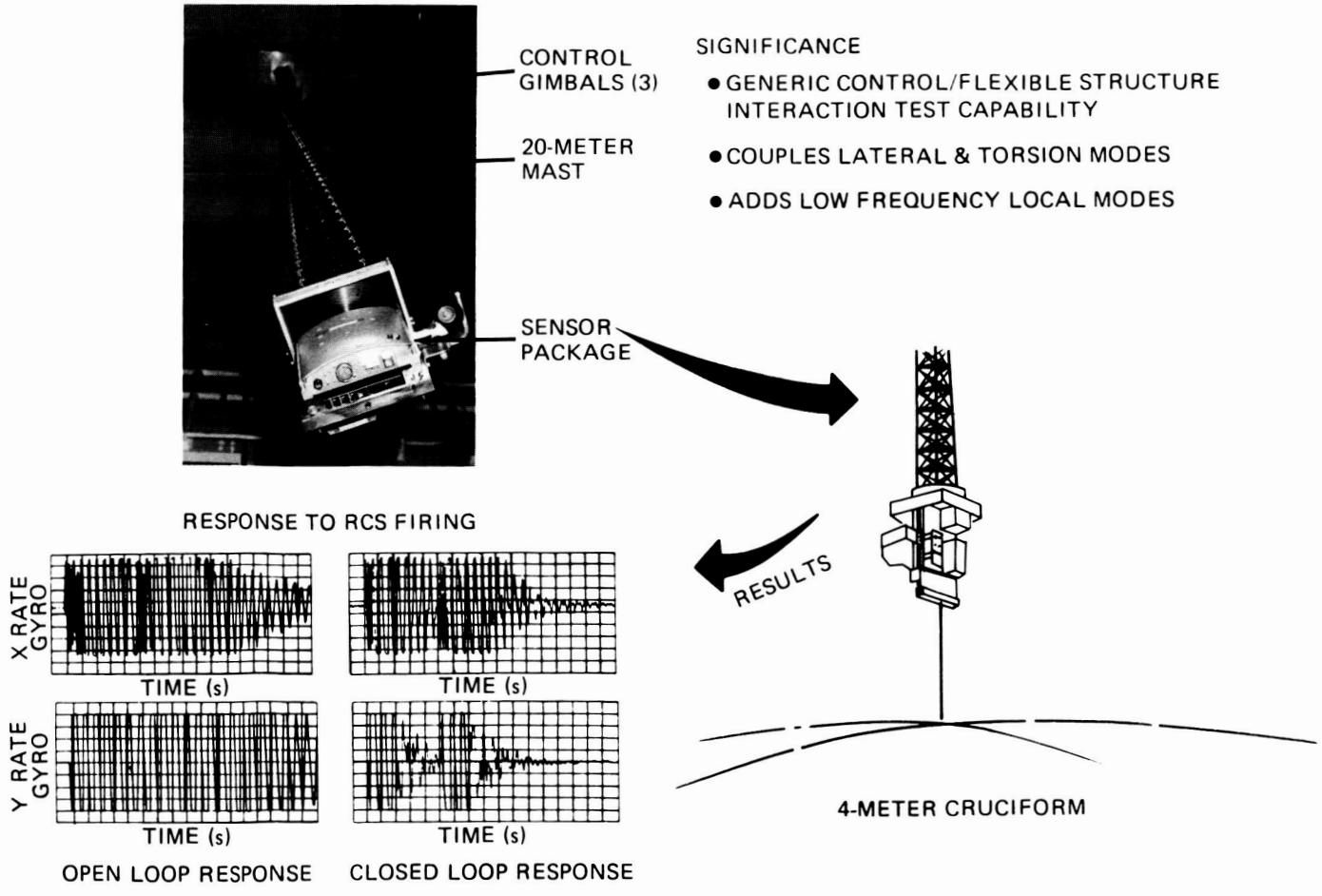

Figure 116. Structures/Controls, Test Facility Configuration 1.

attached to a base excitation system which simulates disturbances most likely to occur with payloads. A control computer contains the calibration software and control algorithms. The total system is suspended in such a fashion that the LSS test article has the characteristics common to all LSSs.

In its present configuration, the LSS test article has attached to its lower end a 4-m cruciform which lowers and compresses the system modes. With the addition of the cruciform, and with the natural twist in the Voyager Magnetometer boom, the vibrational modes of the test article are coupled in the transverse and torsional direction (Fig. 116). The test article has 12 vibrational modes below 2 Hz. The accelerometer/rate gyro packages at both ends of the structure and three gimbal torque motors permit both centralized and decentralized digital control experiments of the following types: classical frequency response methods, pole placement algorithms, observers/estimators, and linear quadratic regulators. An end-to-end system checkout has been performed on the cruciform configuration with a centralized pole placement algorithm which provides direct authority on four system modes, while increasing the damping of the remaining modes. The successful system checkout also verified the analytical modeling and simulation methods, which will become increasingly important in future LSS experiments.

The next planned configuration features a flexible antenna-like structure mounted in place of the cruciform. A two-axis steering mirror, mounted at the other end of the test article, will be used to investigate image motion compensation techniques by redirecting a laser beam from a reflecting mirror at one part of the antenna to a detector at an opposing location (Fig. 117). Vibration suppression will be enhanced with the addition of linear, bi-directional cold gas thrusters at the antenna end of the structure. Distributed control techniques will be investigated with the addition of linear momentum exchange devices (LMEDs) at various locations along the astromast. The LMEDs will be provided by the Air Force as part of their Active Control of Space Structures program. Opportunities for industry participation will be provided in the evaluation of disturbance isolation control

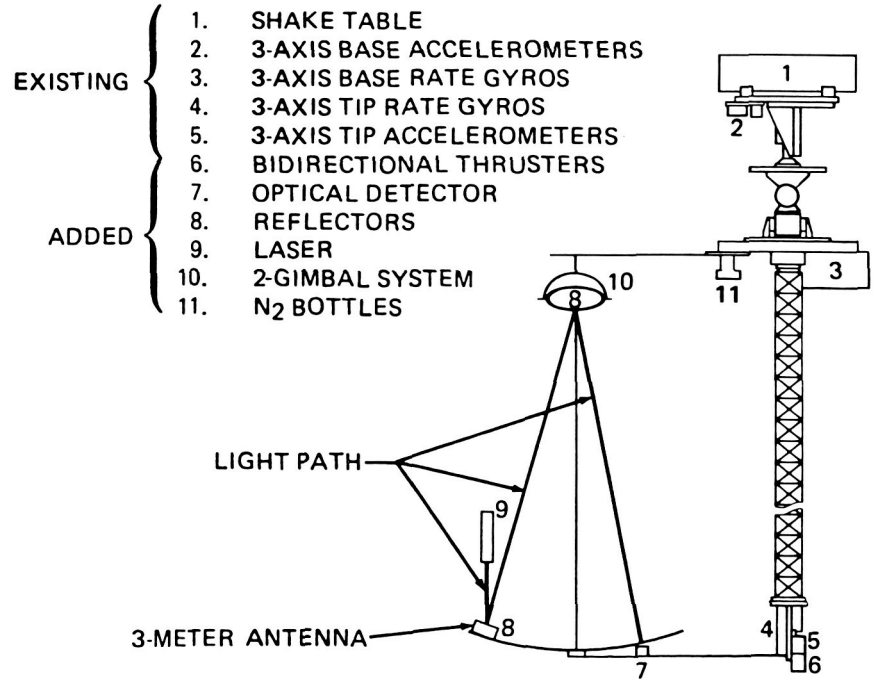

TECHNIQUES TO BE DEMONSTRATED:
- ACTIVE IMAGE MOTION COMPENSATION
- VIBRATION CONTROL VIA LINEAR THRUSTERS
- EVOLUTIONARY CONTROL
- CLOSED LOOP PARAMETER ESTIMATION/CONTROL

Figure 117. Structures/Controls, Test Facility Configuration 2.

techniques such as model error sensitivity suppression, model reference adaptive control, maximum entropy/optimal projection, and high authority/low authority control integration. Future configurations under consideration include use of the SAFE-I boom for preliminary Pinhole Occulter Facility investigations and large-angle, flexible multibody experiments.

H. B. Waites/ED12
(205) 544-1441
Sponsor: Office of Aeronautics and Space Technology

Control System Simulation

Accurate modeling and simulation of complex, flexible spacecraft is a prerequisite for the design and verification of their control systems. The task can become exceedingly difficult in the case of large space structures (LSSs) since the equations of motion are nonlinear and may require months to be generated manually. Also, a control system design for a LSS is an iterative process in which the dynamics must be reformulated for different sensor and actuator locations. Recent analytic developments have enabled digital computer generation of the equations of motion for a wide class of flexible, multibody problems. MSFC realized the advantage of automatically-generated equations of motion, and sponsored a contract to develop such computer software under a program called the Augmented Flexible Body Dynamic Analysis Program (AFBDAP).

Three major computer simulation programs were developed under AFBDAP, each with increasing complexity. Each of the three programs was based upon the Singh-Likins formulation of

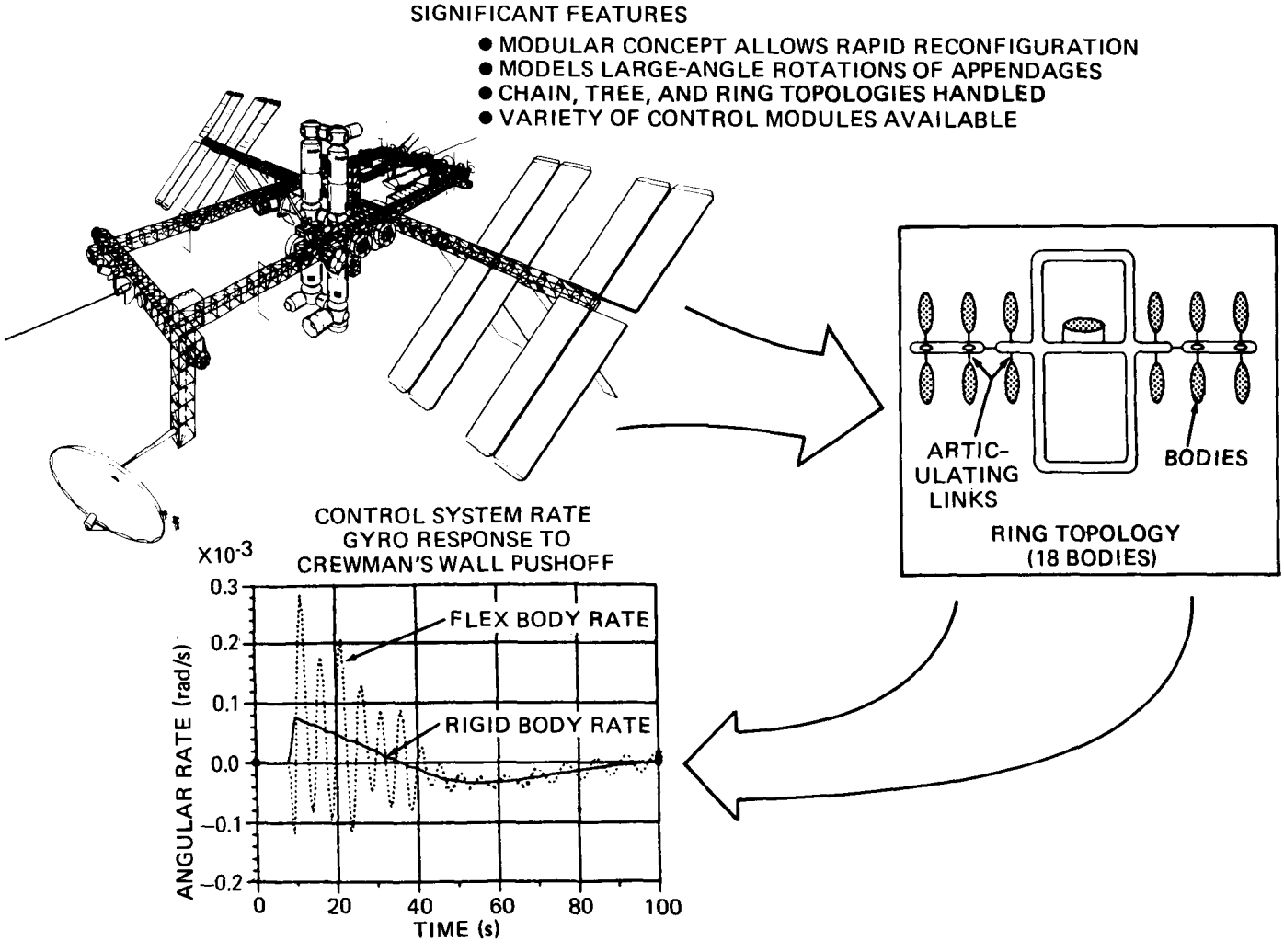

Figure 118. Non-Linear Simulation and Modeling.

Kane's method for generating the equations of motion. This method allows up to 6 degrees-of-freedom between adjacent bodies, but eliminates any constrained motion. Constraint and contact forces and torques can be reconstructed as an option. Bodies are modeled on an individual basis using component modes for flexible bodies, and allowing simple descriptions, rapid reconfiguration, and large angular displacements and velocities. Continuous and discrete control modules are provided which can be arbitrarily connected to user-supplied subroutines to form control systems of any desired complexity. Significant features of non-linear simulation and modeling are shown in Figure 118. Future enhancements, including orbital dynamics and disturbances, will further increase the usefulness of these programs.

Singh, R. P.; VanderVoort, R. J.; and Likins, P. W.: Dynamics of Flexible Bodies in a Tree Topology - A Computer Oriented Approach. Journal of Guidance, Control and Dynamics, Vol. 8, No. 5, September, 1985.

Singh, R. P.; and Likins, P. W.: Singular Value Decomposition for Constrained Dynamical Systems. Journal of Applied Mechanics, Vol. 52, December, 1985.

J. P. Sharkey/ED12
(205) 544-1437
Sponsor: Office of Aeronautics and Space Technology

Satellite Attitude Motion Models

One of the proposed missions for the Orbital Maneuvering Vehicle (OMV) is the retrieval of nonfunctioning satellites. These satellites are generally undergoing some large angular rotations as a result of aerodynamic and gravitational forces. To gain insight into the types of motion to be expected and to provide math models for evaluating OMV performance, a systematic study of natural satellite motion was begun. Categorization based on the dominance of gravity gradient or aerodynamic forces as well as the relative kinetic energy and angular momentum possessed by the body was found to be a very convenient way of generalizing the large number of possible cases. Analytic and semi-analytic solutions for many of these categories have appeared in the literature over the past 25 years. These solutions are being corrected, extended, and validated. When complete, this effort will provide a compilation of relatively simple models which the controls engineer can use to estimate the type of motion a failed satellite can be expected to assume. The same model can also be used in simulations to evaluate the performance of both piloted and automatic docking schemes.

H. J. Buchanan/ED15
(205) 544-1470
Sponsor: Office of Aeronautics and Space Technology

Space Systems

The Hubble Space Telescope Keel Latch

For the Hubble Space Telescope (HST) maintenance mission, a structural latch was required to secure the HST keel fitting during astronaut sleep cycles or orbiter primary reaction control system firings (Fig. 119). The keel latch was to have a capture range of ± 2.54 cm (±1 in.) in the transverse and 3.81 cm (±1.5 in.) in the longitudinal direction.

The flight support system maintenance platform positioning corrects for vertical direction alignment requirements. The keel latch is designed not to impart loads in the longitudinal direction, allowing for the thermal expansion/contraction of the HST. It is also was designed to dampen the impact load of the HST while being tilted to the stowed position at the maximum rate, without damage to the latch device or the HST. The latch was not to apply more than 38.3 kg (85 lb) to the HST keel fitting during latching operations. It must be two-failure tolerant for all crew safety operations. Astronaut extravehicular activity (EVA) may be required after a second failure.

Before the HST is initially launched, a keel spool is mounted to the HST keel fitting by a spring-loaded plunger. The Belleville spring washers dampen any shock load as the keel fitting is placed into the keel latch capture envelope. In operation, the HST keel fitting/keel spool is placed in the keel latch capture envelope (refer to Fig. 120). The spool makes initial contact with a T-bar and depresses it, at which time redundant switches are actuated and give a ready-to-latch indication on the aft flight deck. When a ready-to-latch indication is obtained, jaw 1 motor drive unit

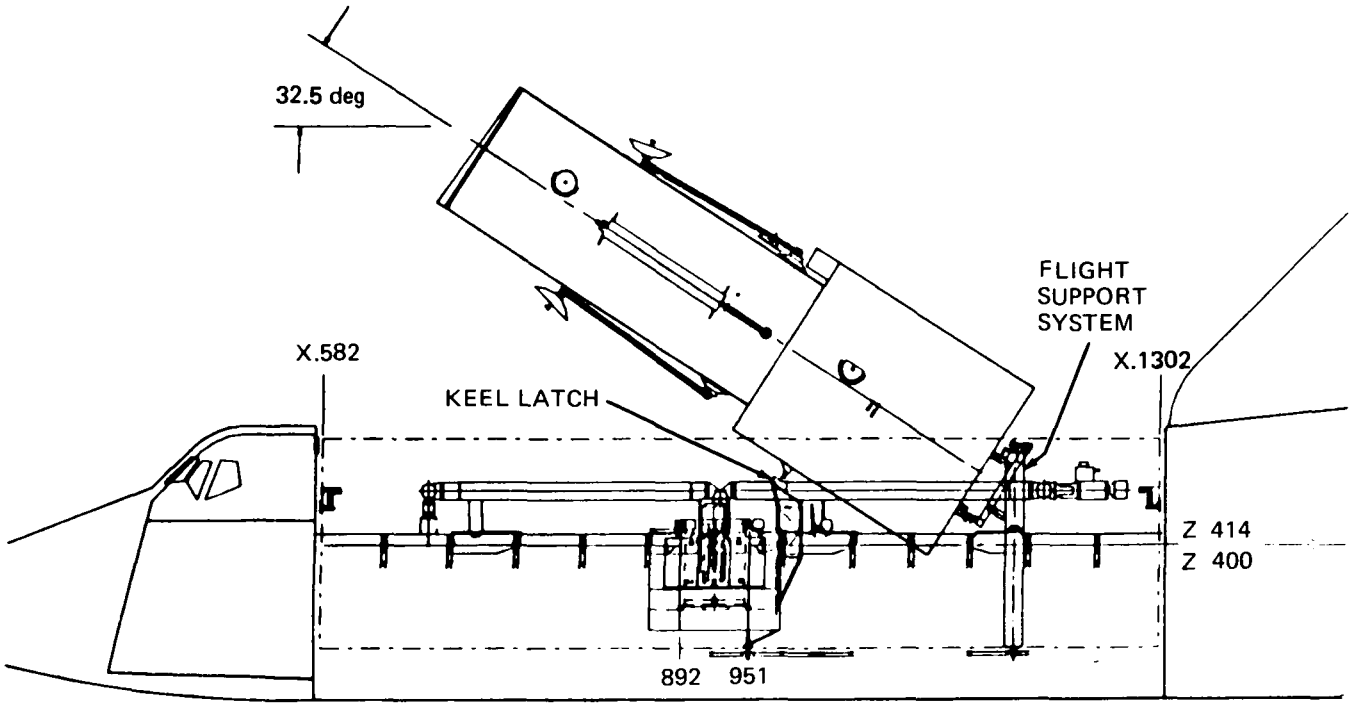

Figure 119. HST Keel Latch Stowed/Reboost Configuration.

(MDU) is turned on. The MDU bevel drive gear drives a bevel gear, with the two bevel gears held in mesh by an EVA nut. By removing the EVA nut from the driven bevel gear, the gear can be disengaged from the MDU bevel gear; this allows the drive screw to be rotated without having to backdrive the MDU. This is a safety feature to allow the jaws to be opened in case the MDU malfunctions.

With the MDU operating, the drive screw rotates and moves jaw 1 away from the stow position. As jaw 1 begins to move, a lever system allows a bumper to be extended from the front of jaw 1 by spring force. Jaw 1 continues to move until the protruding bumper makes contact with the spool. As the bumper is forced back, it actuates switches on the aft flight deck that indicate jaw 1 is in the locked position.

The MDU for jaw 2 will then be turned on. Jaw 2 travels toward the closed position until stops on jaw 2 make contact with stops on jaw 1. The closing force for jaw 2 is reacted by the jaw 1 stops. Thus no force is exerted on the spool. The MDU for jaw 2 continues to drive until a preload is applied between the mating stops. When the predetermined preload is reached, the jaw 2 MDU is cut off by the power nut being moved in relation to the rest of jaw 2. Four Belleville washer spring stacks allow movement between the power nut and jaw 2. This preload between the jaws captures the spool between jaw 1 and jaw 2. The stop lengths are determined at assembly to provide for clearance between the jaws and the keel fitting spool, allowing the jaws to resist keel fitting spool loads in the vertical and transverse directions, but allowing the HST keel fitting to move in the longitudinal direction.

The spool is released from the latch by actuating the jaws in the reverse order from which they are latched. When the jaws are nearing their stowed position, they come in contact with individual preload switches. These switches serve two functions: they cut off the operation of the MDUs when they are operated in the reverse direction and the jaws reach their stowed position, and they provide stability for the jaws during launch and landing vibration.

J. A. Calvert/EP36
(205) 544-7166
Sponsor: Office of Space Science and Applications

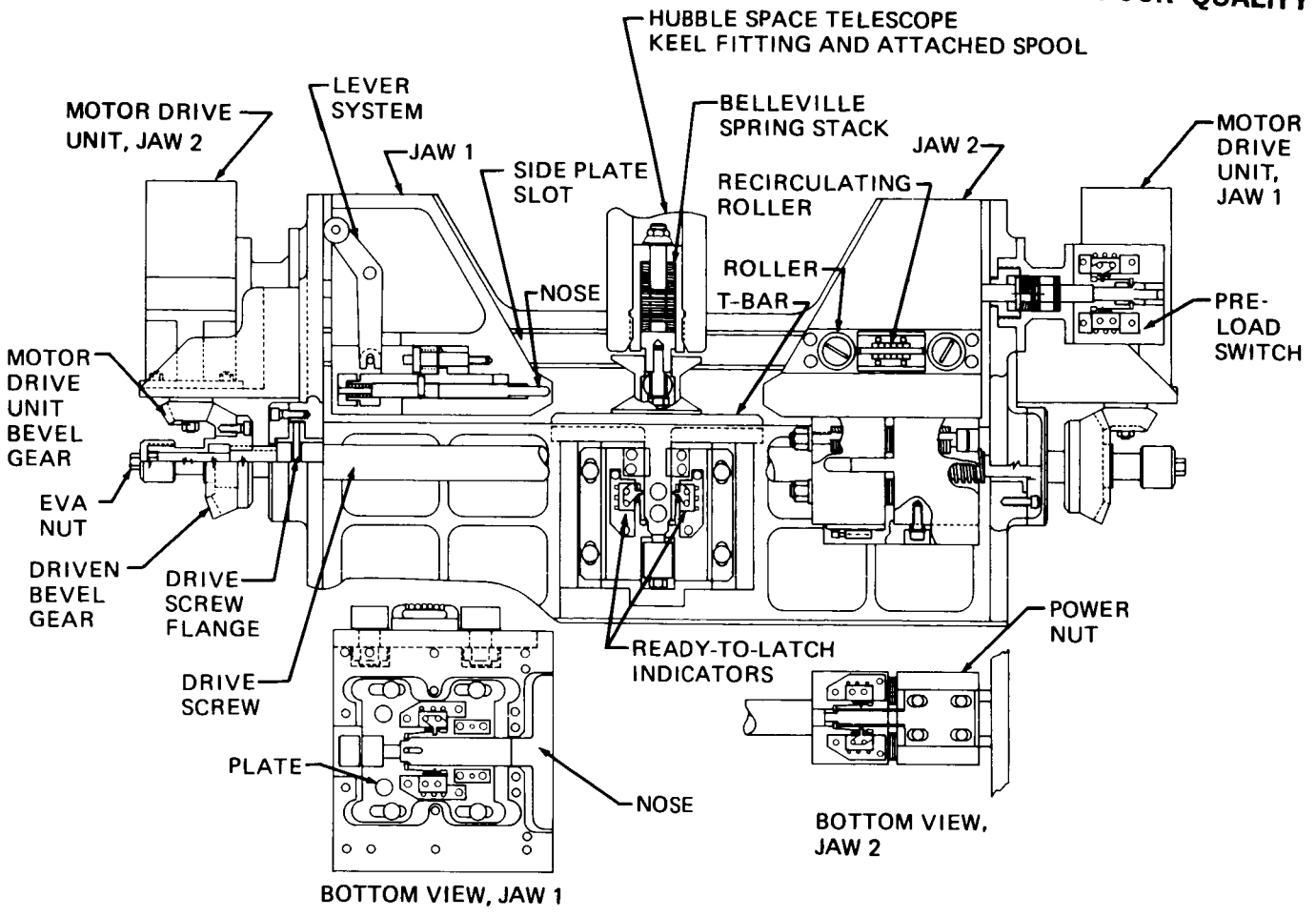

Figure 120. HST Keel Latch Sectional Views.

Telerobotics

With the advent of vehicles that will remain in orbit for many years, on-orbit servicing will be a necessity. Anticipating this, MSFC has been developing realistic ground-based simulations of teleoperators and robotics for remote servicing of satellites in orbit. MSFC has a telerobotic simulation facility with real hardware consisting of an automated servicing demonstration with the integrated orbital servicer system (IOSS), and a teleoperator (man-in-loop) servicing system with the protoflight manipulator arm (PFMA).

During 1985 and 1986, several additions and improvements were made. Multimission modular spacecraft (MMS) modules, or orbital replacement units (ORUs), were installed on the IOSS (Fig. 121). Exchanging or replacing these ORUs requires a modified module servicing tool on the IOSS robotic arm and a new software program. The MMS module operation is an extravehicular

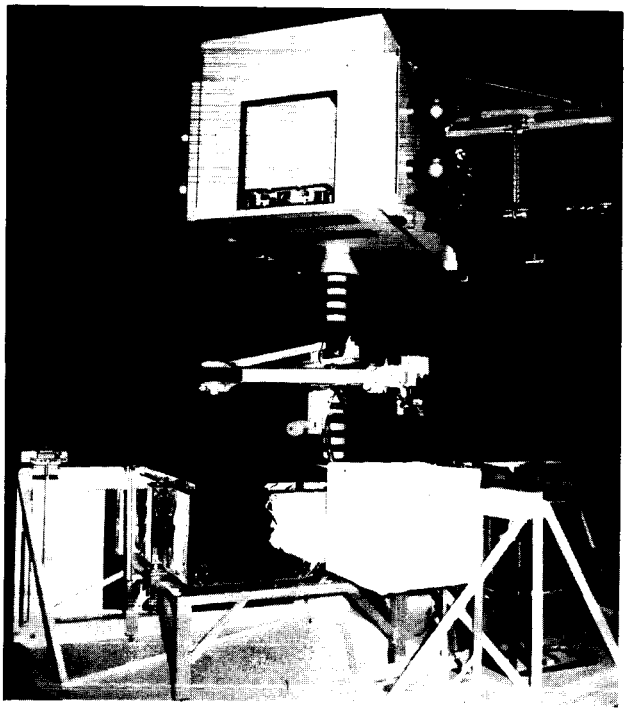

Figure 121. IOSS with MMS Modules.

activity task, but was successfully accomplished with the IOSS robotic arm under computer control, emulating remote satellite servicing. Program flexibility allows the operator to override and make adjustments in case of problems.

A baseline PFMA definition was determined and a number of tests performed to establish a reference data base for comparison to future changes. Further additions and improvements to the PFMA include interchangeable tools that perform tasks such as mating fluid couplings, removing/installing bolts with a rotary power tool, and module exchanges. A task board that simulates a tool storage rack and spacecraft, and improvements to the software control system were also added. A "smart" end effector monitored by the operator and measuring force, torque, and grasp force were added to the PFMA in June, 1986. The objectives for the PFMA are to determine the capabilities and limitations of state-of-the-art, dextrous, remotely-controlled manipulator arms functioning in a remotely-controlled satellite servicing simulation (Fig. 122).

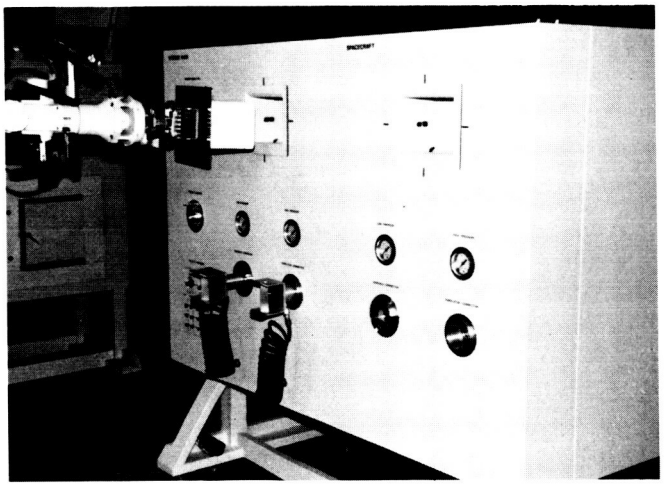

Figure 122. PFMA and Task Board.

D. R. Scott/EB24
(205) 544-3509
Sponsors: Office of Space Transportation Systems
Office of Aeronautics and Space Technology

Innovative Automation Approaches

MSFC is employing both traditional automation and artificial intelligence approaches in developing autonomous systems for spacecraft and ground support. Such autonomous controls are currently being applied to electrical power systems, simulation activities, and Payload Crew Training Complex (PCTC) computer processing functions.

Attention has been focused on automating the electrical power system for future spacecraft. The Fault Isolation Expert System II (FIES II) is a second generation system which identifies faults in a multi-channel electrical power system breadboard (Fig. 123). Fault identification and recovery are important activities in the operation and maintenance of all subsystems on spacecraft. Because such activities are often man-hour intensive, they are excellent candidates for automation. FIES II is implemented on a Symbolics AI workstation.

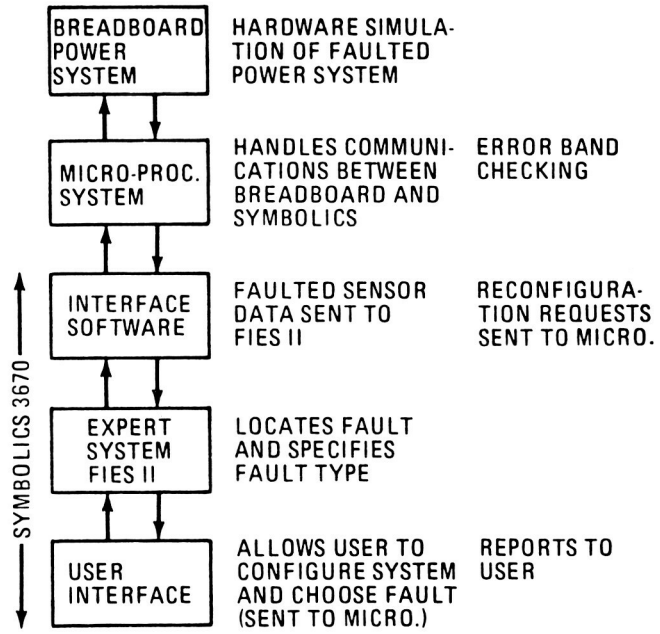

Figure 123. FIES II System Architecture.

The Space Station Experiment Scheduler is a proof-of-concept system designed to reschedule payloads in the event of perturbations to spacecraft power. The system will reschedule loads when breadboard faults occur or available power changes are announced.

The Space Telescope Expert System, illustrated in Figure 124, performs fault diagnosis and analysis on the Hubble Space Telescope electrical power system breadboard.

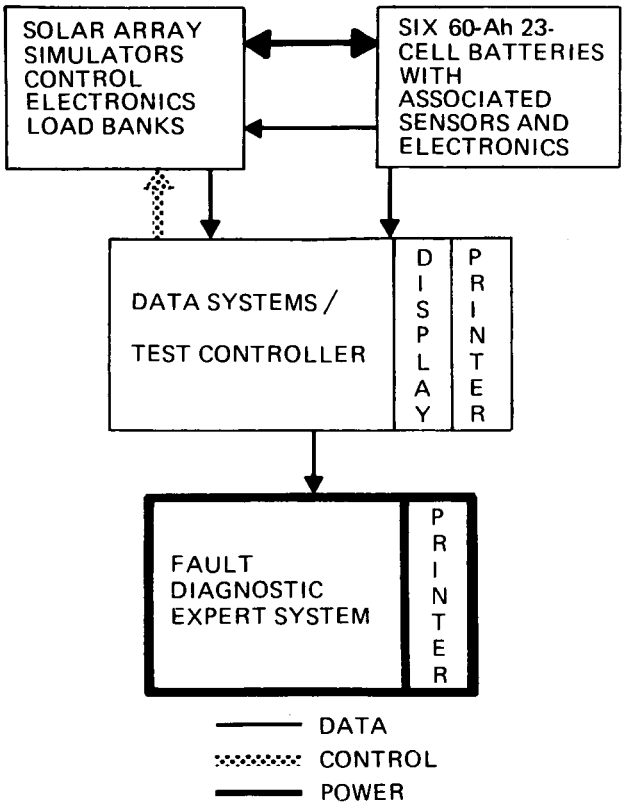

Figure 124. Hubble Space Telescope Electrical Power System Breadboard.

The Autonomously Managed Power System (AMPS) breadboard has reached operational status. Employing conventional algorithms, the AMPS system contains three embedded microprocessor-based controllers which communicate with one another and with the host computer. The AMPS breadboard provides NASA with a test facility to verify and characterize various power system components, including automation approaches.

A Space Station common module power management and distribution system, the Loads Priority List maintenance system, is under development. This system will continually track dynamic priorities of payloads in a common module.

The NASA Expert Simulation System (NESS) couples an expert system with conventional computer simulation techniques. Due to simulation complexity, it has traditionally been necessary for the simulation engineer to remain closely involved during the operational phase. To release the simulation engineer for developing other simulations, the NESS contains the knowledge necessary to run the simulation during the operational phase (Fig. 125).

The Distributed Module Expert System (DMES) analyzes timing, delays, scheduling, and parallelism of multiple processors for utilization in the MSFC Payload Crew Training Complex. The DMES analyzes a multiple processor system using a communications network.

These early steps in applying such advanced automation techniques in conjunction with more traditional approaches are essential to the evolution of autonomous spacecraft systems. Such systems are necessary to minimize operational costs and to assist crew and ground support personnel in achieving greater productivity.

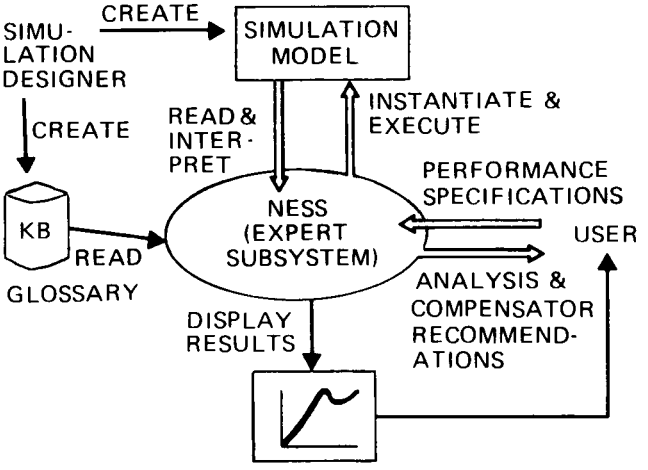

Figure 125. NESS Design Principle.

Weeks, D. J.: Application of Expert Systems in the Common Module Electrical Power System. SPIE Vol. 580 Space Station Automation, 1985.

Weeks, D. J.; and Bechtel, R. T.: Autonomously Managed High Power Systems. Proceedings of the 20th IECEC, 1985.

D. J. Weeks/EB12
(205) 544-3309
Sponsors: Office of Aeronautics and Space Technology
Office of Space Station

Air Evaporation Water Recovery

Projected logistics penalties associated with long-term manned space missions make onboard recovery of wastewater necessary. An air evaporation water recovery subsystem has been developed and successfully demonstrated in 60-day and 90-day manned chamber tests. Currently, efforts are being made to define design improvements intended to enhance the operation without compromising the high reliability demonstrated in previous tests.

A simple form of an air evaporation water recovery system is shown in Figure 126. Hot air exiting an electric resistance heater is passed through a wick evaporator saturated with wastewater. As water evaporates from the wick material, it is removed from the evaporator by the passing air stream, leaving solid contaminants behind. The humidified air is then passed through a condensing heat exchanger. A water separator removes condensed water from the air stream. The dried air is subsequently reheated and recycled, while the condensed water is further treated in a post-treatment unit prior to storage.

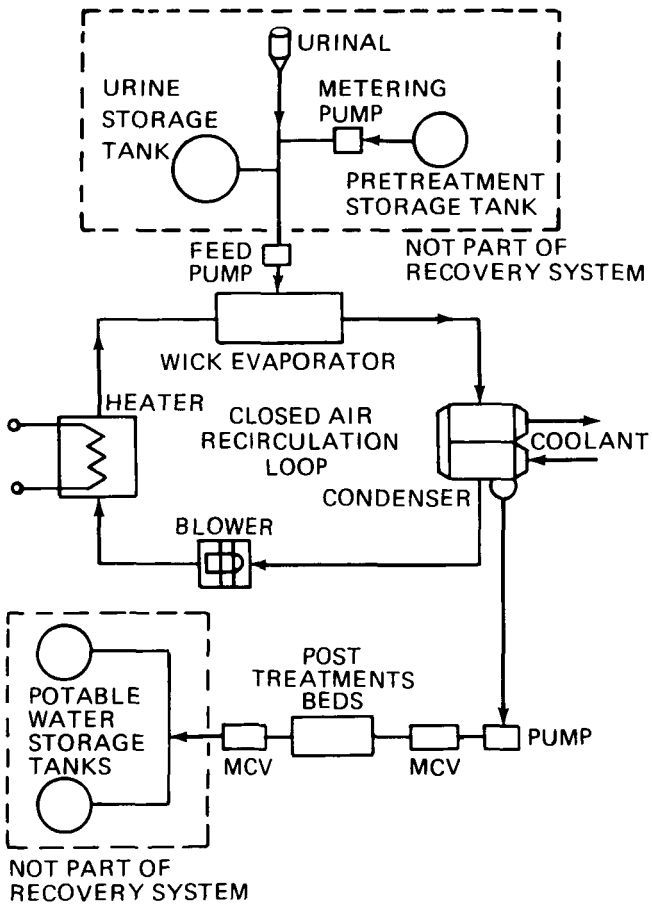

Figure 126. Breadboard Air Evaporation Subsystem Schematic.

Investigations are under way to optimize the feeding of wastewater to the wick evaporator using various wick materials in order to better control the distribution of wastewater and solids. Energy-saving innovations include incorporation of recuperative heat exchangers, heat pumps, and interfaces with solar collectors.

R. M. Bagdigian/EL84
(205) 544-7222
Sponsor: Office of Space Station

Hydrophobic Molecular Sieve

All regenerative carbon dioxide (CO_2) removal subsystems are sensitive to inlet water vapor. Performance degradation can occur unless the inlet moisture level is maintained within certain limits. A development effort was conducted to determine the feasibility of producing carbon molecular sieve sorbent materials which are hydrophobic and still have significant CO_2 adsorption capability.

More than 90 sorbents were carbonized, producing 40 different carbon molecular sieves. Of these, 33 were found to adsorb CO_2 selectively over moisture at a CO_2 partial pressure of 0.4 KPA (3 mmHg). Water adsorption was slow and minimal at relative humidities less than 50 percent. The amount of water adsorption at relative humidities higher than 50 percent was strongly affected by the carbon molecular sieve preparation. Carbon molecular sieves were found to desorb CO_2 at significantly lower temperatures than 5A Zeolite molecular sieve, resulting in lower desorption power requirements. The carbon molecular sieves are chemically and physically stable. Analysis for trace gases at elevated temperatures indicated no detectable contaminants.

Among the polymer precursors investigated, polyvinylidine chloride-polyvinyl chloride (PVDC-PVC) copolymer and PVDC homopolymer yielded carbon molecular sieve sorbents with the best performance in terms of CO_2 capacity. These sieves were determined to have a CO_2 capacity similar to 5A Zeolite sieve. Using PVDC-PVC characterization data (CO_2 capacity isotherms), a preliminary design was developed for a two-bed sieve CO_2 removal system. The resulting preliminary design data indicated a system that is less complex and with lower weight, power, and volume requirements than other techniques under development.

The results of this development effort indicate that carbon molecular sieve material can be produced that is essentially hydrophobic, yet has a CO_2 capacity close to that of 5A Zeolite molecular sieve, and is a viable candidate for Space Station application.

C. D. Ray/EL84
(205) 544-7215
Sponsor: Office of Space Station

Variable Emissivity Surfaces

Heat transfer in the space environment is largely a radiative process. The emissivities of the surfaces linking the payload to the space environment are the key to temperature stabilization and control in orbiting satellites. The purpose of this research effort was to develop surfaces which have variable thermal emissivities and variable solar absorptivities. The development of such surfaces will provide a means of actively controlling heat transfer between orbiting satellites and the space environment. Modulation of the emissivity and absorptivity is achieved by the passage of a small DC electric current through a surface coating and is based on the concept of electrochromism. An oxide of tungsten, WO_3, was chosen as the principal electrochromic element in the coatings investigated.

Several multilayer, thin-film electrochromic coatings that allow control of thermal emissivity or solar absorptivity were designed. Each component of the multilayer coatings was prepared by reactive radio frequency sputtering or vacuum evaporation. The requisite optical properties of each layer (emittance, reflectance, or transmittance) were determined spectroscopically over a wavelength range of 0.4 to 14 μm. Several materials were identified as electrochromic materials whose optical properties could be usefully modulated by lithium insertion. The thermal emittance and solar absorptance of c-Li_xWO_3 and a-Li_xWO_3 were determined as a function of lithium concentration (x). Using appropriate substrate materials, thermal emittance (e) control from 0.06 to 0.75 and solar absorptance (α_s) control from 0.32 to 0.98 were achieved.

A model for radiant heat transfer through a multilayer exterior wall was developed and the thermal emissivity data were used to predict the extent of thermal control. A complete self-contained electrochromic device that demonstrated variable optical modulation was fabricated as a prototype for future development and scale-up. Figure 127 shows the structure of a variable thermal emittance or variable solar absorptance electrochromic coating. In Figure 128, the theoretical modulation of the reflectance edge in a crystalline electrochromic material is shown with respect to the solar and thermal spectral distributions. The reflectance edge may be adjusted to modulate or transmit radiation from the thermal (10μ) to the visible (0.5μ) regions of the spectrum. The theoretical modulation of absorption in an amorphous electrochromic material with respect to the solar and thermal spectral distributions is shown in Figure 129. The wavelength at which absorption occurs is fixed in the visible and near-infrared regions of the solar spectrum.

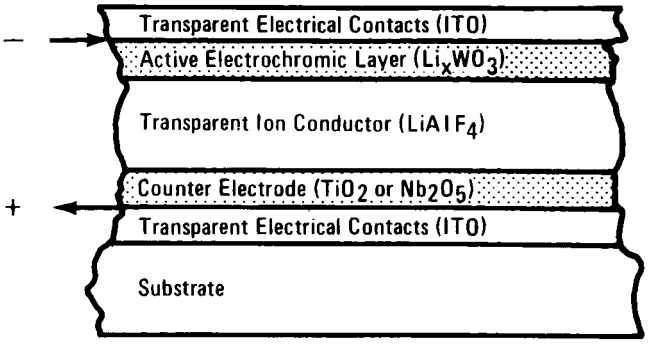

Figure 127. Structure of an Electrochromic Coating.

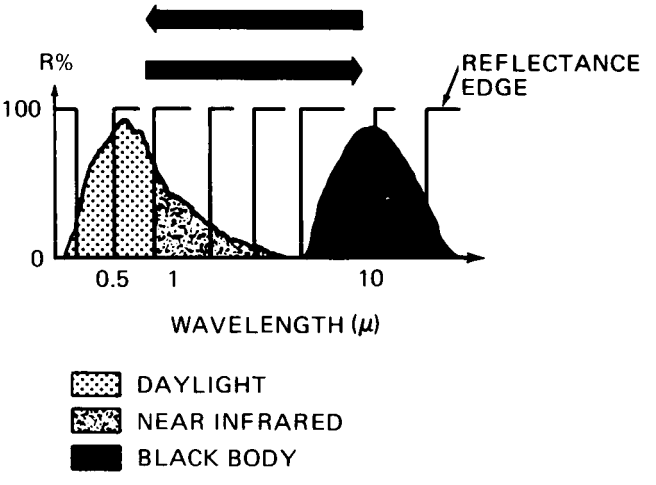

Figure 128. Modulation of the Reflectance Edge in a Crystalline Electrochromic Material.

Variable emissivity and variable absorptivity coatings are applicable to the control of radiant heat transfer in the Space Shuttle, the Hubble Space Telescope, and orbiting satellites with thermally sensitive payloads. The coatings may be used on radiator surfaces, skin surfaces, instrument packages, or for any application that would benefit from modulated radiant heat transfer. Besides spaceborne applications, electrochromic coatings may be commercially useful as variable transmittance windows for energy management in

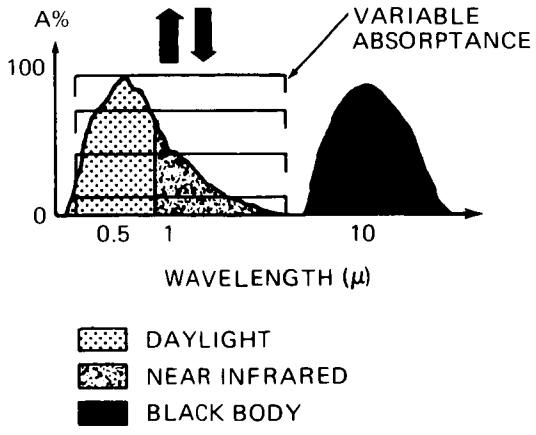

Figure 129. Modulation of Absorptance in an Amorphous Electrochromic Material.

buildings and as electrochromic display devices for superposition of multiple images. Further development of this technology is being pursued.

J. W. Owen/EP44
(205) 544-7213
Sponsor: Small Business Innovation Research Program

High Performance Heat Pipe

Thermal management, which encompasses the acquisition of thermal energy from a heat source, the storage and transport of the heat, and the rejection of unusable thermal energy to space, is emerging as a key technology for space missions. The NASA Space Power Workshop addressed the civil, commercial, and military power requirements for future space applications. One or more primary and secondary power technologies are being studied and proposed for each type of mission. Thermal management is required for all power systems and in some missions is considered the enabling technology.

This project addresses an innovative method in which 5,000 W may be transported over a distance of 1,524 cm with an evaporator load density of 10 W/cm^2, through use of aluminum heat pipe with ammonia as the working fluid. The specific method used to achieve the improvement in heat pipe performance was the design and fabrication of aluminum/ammonia heat pipes using sintered powder aluminum wick structures.

Sintered aluminum wicks have been fabricated with a capillary radius of 0.001 cm, which is 65 times smaller than the capillary radius of a typical axial groove heat pipe. Smaller capillary radii generate a larger capillary pressure when filled with the heat pipe working fluid. Accordingly, higher fluid circulation rates and heat transport rates are achieved. The relatively low permeability or high resistance to liquid flow which is common to small capillary pore structures is offset by innovative wick designs which separate the longitudinal liquid flow path from the circumferential liquid flow path. A second advantage to the use of sintered aluminum wick structures is their ability to accept high evaporator heat fluxes. The high thermal conductivity of the wick structure reduces the change in temperature across the wick. This permits higher heat loading to be achieved before boiling or evaporator dryout occurs.

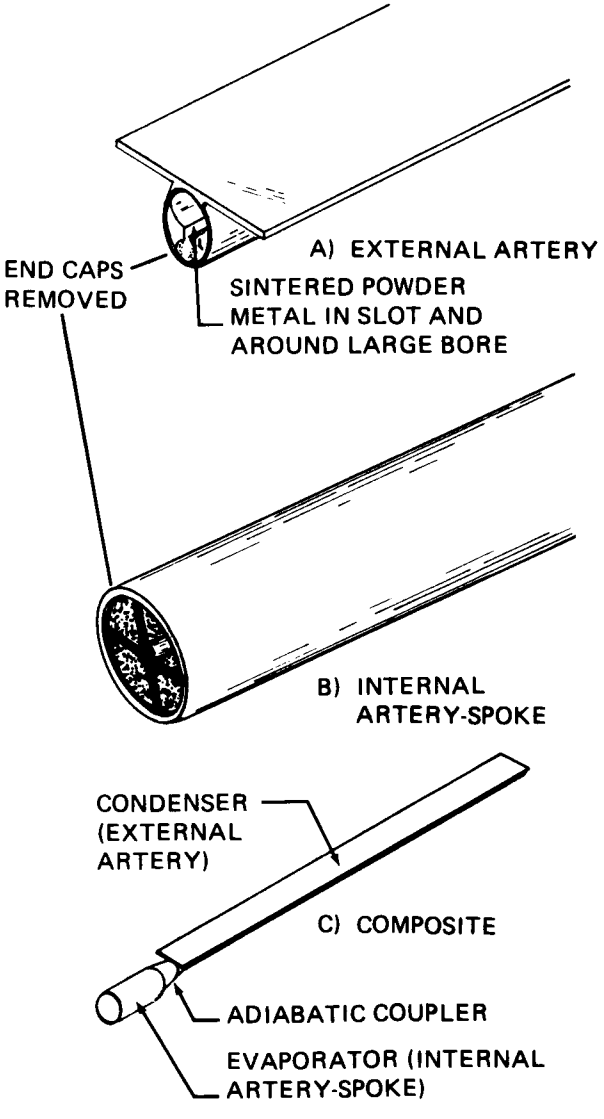

Figure 130. Potential Heat Pipe Designs (Not to Scale).

Figure 130 shows potential design concepts for a high-performance ambient temperature heat pipe and Figures 131 and 132 show the

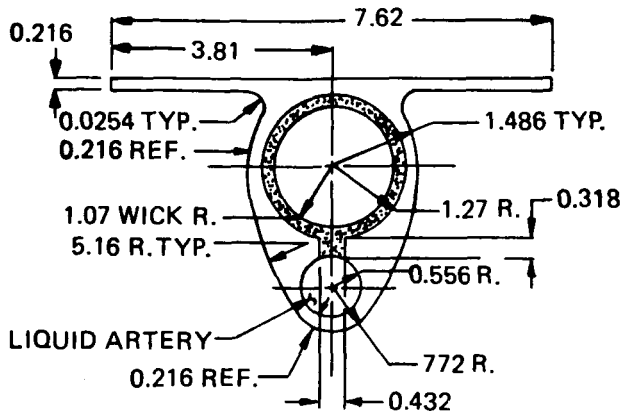

(DIMENSIONS IN cm)

Figure 131. Conceptual Heat Pipe Design, Cross-sectional External Artery.

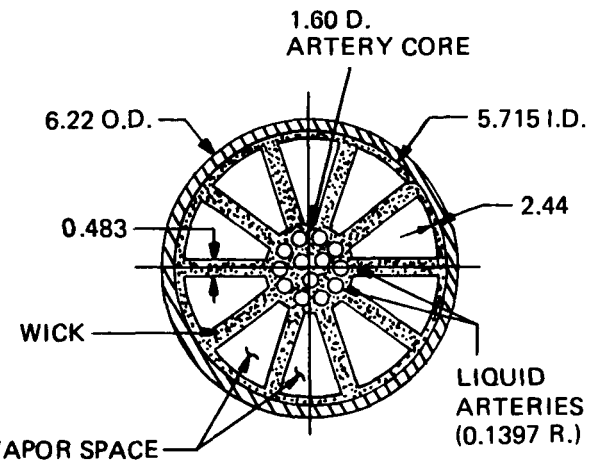

(DIMENSIONS IN cm)

Figure 132. Conceptual Heat Pipe Design, Cross-sectional Internal Artery Spoke.

cross-sectional details. Conclusions from this effort are that complex sintered aluminum powder wick structures in heat pipes are capable of accepting heat flux densities in excess of 10W/cm^2, and that the external artery and composite heat pipe concepts designed and analyzed are capable of transporting 5,000W over 1,524 cm. The second phase of this project will develop this heat pipe technology further.

J. W. Owen/EP44
(205) 544-7213
Sponsor: Small Business Innovation Research Program

Metal Hydrides

Metal hydrides are chemical compounds formed when hydrogen gas (H_2) reacts with metals. Many hydrides absorb and release hydrogen at pressures and temperatures that can be useful in spacecraft systems. Several concepts have been evaluated for potential space applications which make use of metal hydrides to absorb, store, pump, compress, or expand hydrogen gas. The phase changes during formation and decomposition of metal hydrides are also accompanied by a significant flow of heat that may be useful for thermal energy management or propulsion purposes.

The suitability of a hydride device is determined by its mass, size, power, and thermal requirements, relative to alternative methods. The purpose of this project was to develop information about hydride devices specifically designed for use in space, so that realistic comparisons with competing concepts could be made. The objectives of the project were to identify heat sources and sinks suitable for driving metal hydride thermal cycles in space; design hydride subsystems to use the available heating/cooling methods; and form a data base containing estimated size, mass, and performance of realistically designed hydride devices for use in space, such as the long-term hydrogen storage tank described in Table 16.

Table 16. Properties of a Long-Term Hydrogen Storage Tank.

• HYDROGEN CAPACITY		22.5 kg
• HYDRIDE (MgH_2 POWDER)		274 kg
• RATED PRESSURE		1.4 MPa
• SAFETY FACTOR (ON YIELD)		1.5
• CONTAINER		
(368-ℓ CAPACITY, 1-m DIAMETER)		
• PRESSURE VESSEL	33.9 kg SS	
• OUTER SHELL	13 kg ALUM.	
• GIRTH RING	4 kg ALUM.	
• MISC. COMPONENTS	10 kg	
• CONTAINER MASS		60.9 kg
• SYSTEM MASS		357.4 kg

Most of the potential applications studied during this project are promising enough to warrant further consideration. These include heat pumping, thermal storage, hydrogen compression for propulsion, and long-term hydrogen storage

(Fig. 133 and Fig. 134). Further development of these concepts will be pursued in the second phase of this project.

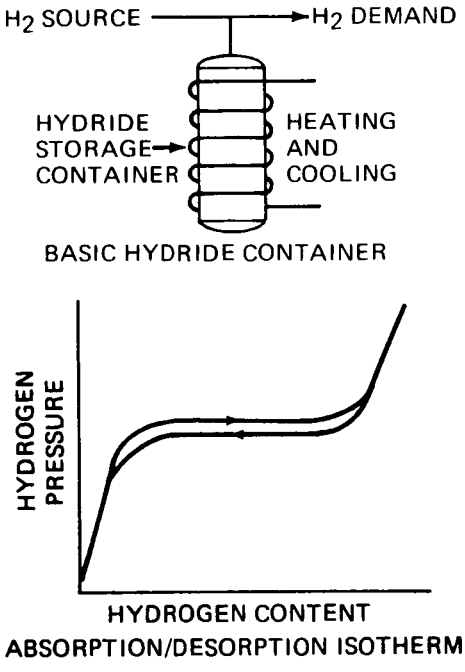

Figure 133. Metal Hydride Hydrogen Storage Concept.

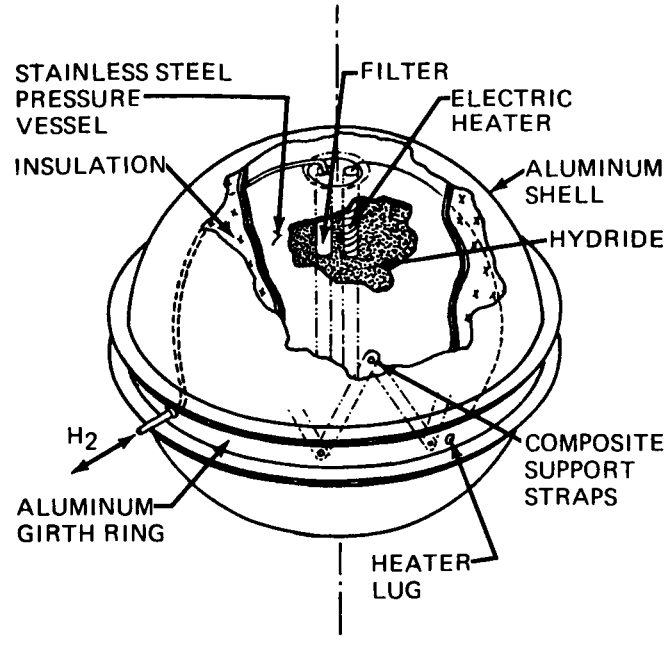

Figure 134. Long-Term Hydrogen Storage Tank with Lightweight Metal Hydrides.

J. W. Owen/EP44
(205) 544-7213
Sponsor: Small Business Innovation Research Program

INDEX OF AUTHORS